SYNTHESIS, CYTOTOXICITY AND APOPTOSIS STUDIES ON NICKEL AND ZINC DERIVATIVES OF TESTOSTERONE-N^4-SUBSTITUTED-THIOSEMICARBAZONES

HENG MOK PIEW

FACULTY OF SCIENCE
UNIVERSITI MALAYA
KUALA LUMPUR

2020

SYNTHESIS, CYTOTOXICITY AND APOPTOSIS STUDIES ON NICKEL AND ZINC DERIVATIVES OF TESTOSTERONE-N^4-SUBSTITUTED-THIOSEMICARBAZONES

HENG MOK PIEW

THESIS SUBMITTED IN FULFILMENT OF THE REQUIREMENTS FOR THE DEGREE OF DOCTOR OF PHILOSOPHY

INSTITUTE OF BIOLOGICAL SCIENCES
FACULTY OF SCIENCE
UNIVERSITI MALAYA
KUALA LUMPUR

2020

UNIVERSITI MALAYA

ORIGINAL LITERARY WORK DECLARATION

Name of Candidate: **HENG MOK PIEW**

Matric No: **SHC160029**

Name of Degree: **DOCTOR OF PHILOSOPHY**

Title of Thesis ("this Work"):

Synthesis, Cytotoxicity and Apoptosis Studies on Nickel and Zinc Derivatives of Testosterone-*N*^{4}-Substituted-Thiosemicarbazones

Field of Study:

BIOCHEMISTRY

I do solemnly and sincerely declare that:

(1) I am the sole author/writer of this Work;
(2) This Work is original;
(3) Any use of any work in which copyright exists was done by way of fair dealing and for permitted purposes and any excerpt or extract from, or reference to or reproduction of any copyright work has been disclosed expressly and sufficiently and the title of the Work and its authorship have been acknowledged in this Work;
(4) I do not have any actual knowledge nor do I ought reasonably to know that the making of this work constitutes an infringement of any copyright work;
(5) I hereby assign all and every rights in the copyright to this Work to the University of Malaya ("UM"), who henceforth shall be owner of the copyright in this Work and that any reproduction or use in any form or by any means whatsoever is prohibited without the written consent of UM having been first had and obtained;
(6) I am fully aware that if in the course of making this Work I have infringed any copyright whether intentionally or otherwise, I may be subject to legal action or any other action as may be determined by UM.

Candidate's Signature Date: 4 Jun 2020

Subscribed and solemnly declared before,

Witness's Signature Date: 4 June 2020

Name:

Designation:

SYNTHESIS, CYTOTOXICITY AND APOPTOSIS STUDIES ON NICKEL AND ZINC DERIVATIVES OF TESTOSTERONE-N^4-SUBSTITUTED-THIOSEMICARBAZONES

ABSTRACT

The side effects of cisplatin such as toxicities are mainly due to the lack of selectivity of this chemotherapeutic agent. In order to increase the selectivity of an anticancer agent, hormone molecule that targets a specific receptor may be utilized. This research aimed to prepare cytotoxic Schiff base compounds (and their nickel and zinc complexes) with testosterone and derivatives of thiosemicarbazide, which are potentially selective towards cancerous cells. Three Schiff base ligands (**TM**, **TF**, and **TP**) were made from the conjugation of testosterone with three derivatives of thiosemicarbazide (N^4= methyl, fluorophenyl, and ethylphenyl) and their respective nickel (**NM**, **NF**, and **NP**) and zinc complexes (**ZM**, **ZF**, and **ZP**). A zinc complex **ZE** (N^4= ethyl) was included as well. Characterizations of these compounds were done by means of FTIR, CHN elemental analyses, ^{1}H-NMR and ^{13}C-NMR, and X-ray crystallography. Mononuclear complexes of **NM** and **NF** adopt a distorted square planar geometry, with two molecules of Schiff base ligand coordinated to the nickel ion *via* two imine nitrogens and two tautomeric thiol sulfurs. The cytotoxicity of these compounds against several human cancerous cell lines (prostate cancer cell line PC-3 and LNCaP, breast cancer cell line MCF7, colorectal carcinoma cell line HCT 116) and their general toxicity against two human normal cell lines (normal prostate RWPE-1 and normal colon CCD-18Co) were investigated, with cisplatin as positive reference standard. Eight out of the nine synthesized compounds were cytotoxic towards the HCT 116 colorectal carcinoma cell line tested, while only two of them were toxic against the CCD-18Co normal colon cell line tested, reflecting high selectivity index of these compounds against the colorectal carcinoma cell line. Morphological changes induced by these compounds were observed and photographed.

Ability of the cytotoxic compounds to induce apoptosis was proven *via* flow cytometry and this study was then focused on colorectal carcinoma cell line due to the high selectivity index. Five of the cytotoxic compounds (**TM**, **NM**, **TF**, **TP**, and **NP**) were able to depolarize the mitochondrial membrane potential, thereby suggesting their capability to induce intrinsic apoptotic pathways. All the cytotoxic compounds successfully arrested cell cycle of HCT 116 at G_0/G_1 phase. Furthermore, all the nine compounds were proven to bind to the DNA surface and they might be DNA minor groove binders. However, the general toxicity of **TF** against all the tested cell lines (IC_{50} values range from 12.03 to 29.37 μM) might be due to its outstanding affinity towards DNA ($K_b = 2.9 \times 10^7\ M^{-1}$), while high selectivity of **ZP** (SI>3.22) might be due to its weak DNA binding strength ($K_b = 3.7 \times 10^5\ M^{-1}$). The three compounds (**TM**, **NM**, and **ZP**) were able to suppress enzymatic reaction of topoisomerase I, thereby suggesting the cytotoxicity of these compounds against the colorectal carcinoma cell was due to their topo I inhibitory properties. Such inhibition might in turn, block the cell from entering S phase of cell cycle, and the cells might then be subjected to programmed cell death.

Keywords: Testosterone Schiff base, metal complexes, colorectal carcinoma cell-targeting, topoisomerase I inhibitor.

SINTESIS, KAJIAN KESITOTOKSIKAN DAN APOPTOSIS DERIVATIF NIKEL DAN ZINK TESTOSTERON-N^4-TERTUKARGANTI-TIOSEMIKARBAZON

ABSTRAK

Kekurangan spesifikasi terhadap sel kanser merupakan punca utama kesan sampingan agen kemoterapeutik cisplatin. Molekul hormon yang menyasarkan reseptor tertentu boleh diguna untuk meningkatkan keupayaan selektiviti agen antikanser. Penyelidikan ini bertujuan untuk menyediakan sebatian-sebatian sitotoksik bes Schiff (serta kompleks nikel dan zink mereka) dengan testosteron dan derivatif tiosemikarbazida (N4= metil, fluorofenil dan etilfenil) yang berpotensi selektif terhadap sel kanser. Tiga ligan bes Schiff (**TM**, **TF**, dan **TP**) telah disediakan melalui konjugasi testosteron dengan tiga derivatif tiosemikarbazida dan kompleks nikel (**NM**, **NF**, dan **NP**) serta kompleks zink (**ZM**, **ZF**, dan **ZP**). Satu kompleks zink **ZE** juga dimasukkan dalam kajian ini (N^4= etil). Ciri-ciri sebatian tersebut telah ditentukan dengan kaedah spektroskopi seperti FTIR, analisis unsur CHN, ^{1}H-NMR dan ^{13}C-NMR, serta kristalografi sinar-X. Kompleks mononuklear **NM** dan **NF** merupakan geometri empat segi sesatah 'terherot', dengan dua molekul ligan bes Schiff yang diselaraskan dengan ion nikel melalui dua nitrogen imina dan dua sulfur tiol tautomerik. Aktiviti sitotoksik sebatian-sebatian tersebut terhadap beberapa sel-sel kanser manusia (kanser prostat PC-3 dan LNCaP, kanser payudara MCF7, dan kanser kolon HCT 116) serta ketoksikan umum mereka terhadap sel-sel normal manusia (prostat RWPE-1 dan kolon CCD-18Co) telah disiasat, dengan cisplatin sebagai rujukan positif standard. Lapan daripada sembilan sebatian yang disintesis adalah sitotoksik ke atas sel-sel kanser kolon yang diuji, di mana hanya dua daripadanya yang toksik terhadap sel-sel kolon biasa yang diuji, ini menggambarkan indeks selektiviti yang tinggi sebatian-sebatian tersebut terhadap sel-sel kanser kolon. Kesan sebatian ke atas perubahan morfologi sel-sel kanser telah diperhatikan dan difoto. Keupayaan sebatian-

sebatian sitotoksik untuk merangsang apoptosis terbukti melalui analisis aliran sitometri dan kajian ini seterusnya memberi tumpuan kepada sel-sel kanser kolon atas sebab indeks selektiviti yang tinggi. Lima sebatian sitotoksik tersebut berupaya mengubahkan potensi membran mitokondria, maka dicadangkan bahawa kematian sel adalah secara apoptosis intrinsik. Semua sebatian sitotosik tersebut berjaya merencatkan kitar sel kanser kolon HCT 116 di fasa G_0/G_1. Selanjutnya, sembilan sebatian terbukti sebagai pengikat permukaan DNA dan berkemungkinan pengikat DNA 'minor groove'. Walau bagaimanapun, ketoksikan umum **TF** terhadap semua sel yang diuji (nilai IC_{50} dari 12.03 ke 29.37 μM) dipercayai disebabkan oleh afiniti yang tinggi terhadap DNA ($K_b = 2.9 \times 10^7\ M^{-1}$), manakala ikatan yang lemah pada DNA mungkin menjelaskan ciri sebatian **ZP** ($K_b = 3.7 \times 10^5\ M^{-1}$) yang tidak toksik terhadap sel-sel kolon normal yang diuji (SI>3.22). Tiga sebatian (**TM**, **NM**, dan **ZP**) berupaya merencatkan tindak balas enzimatik topoisomeras I, maka dicadangkan bahawa kesitotoksikan sebatian tersebut terhadap sel kanser kolon adalah disebabkan oleh keupayaan perencatan enzim topo I. Perencatan enzim topoisomeras mungkin akan menghalang kemasukan sel-sel kanser kolon ke fasa S dalam kitaran sel, dan merangsangkan apoptosis.

Kata kunci: Bes Schiff testosterone, kompleks logam, penyasaran sel kanser kolon, perencat topoisomeras I.

ACKNOWLEDGEMENTS

First of all, I would like to express my appreciation to my supervisors Associate Professor Dr. Sim Kae Shin and Dr Tan Kong Wai for their critical comments, excellent guidance, and continuous support in this research.

Besides my advisors, I am especially grateful to Dato' Professor Dr. Ng Seik Weng for the helps in solving crystal structures and the valuable advice. Also, I would like to thank Dr. Saravana Kumar Sinniah, Dr. Teoh Wuen Yew, and Dr. Suerialoasan Navanesan for their guidance especially in the cell culture-related assays. I am also indebted to my labmates, namely Miss Hazwani Mat Saad and Mr Tan Chun Hoe, for their encouragement and kind hands. Many thanks to the staffs in Universiti Malaya for the help throughout this research.

Finally, I would like to thank my beloved family and life partner for their patience, endless support, concern and encouragement throughout the years.

TABLE OF CONTENTS

LIST OF FIGURES

LIST OF TABLES

LIST OF SYMBOLS AND ABBREVIATIONS

Å	:	Angstrom
ΔΨm	:	Mitochondrial transmembrane potential
BSA	:	Bovine serum albumin
CT-DNA	:	Calf-thymus DNA
DMF	:	N,N-dimethylformamide
DMSO	:	Dimethylsulfoxide
E. coli	:	*Escherichia coli*
IC_{50}	:	Median inhibition concentration
K_b	:	Intrinsic binding constant
NMR	:	Nuclear magnetic resonance
PDB	:	Protein data bank
PI	:	Propidium iodide
Topo	:	Topoisomerase
UV-Vis	:	Ultraviolet-visible

LIST OF APPENDICES

CHAPTER 1: INTRODUCTION

The discovery of cisplatin and its rapid approval by the Food and Drug Administration (FDA) of the USA consolidated this platinum-based drug as the principal anticancer chemical in use worldwide (Sanchez-Cano & Hannon, 2009b). The clinical usefulness of cisplatin is somewhat restricted by setbacks such as drug resistance, along with severe toxic side effects that include hepatotoxicity, nephrotoxicity, and neurotoxicity (Bruijnincx & Sadler, 2008; Ibrahim et al., 2019; Ruiz et al., 2011). The unparalleled success of cisplatin in the treatment of cancer has led to research that extended to the use of coordination complexes, particularly transition metal complexes, in antitumour therapy (Sanchez-Cano & Hannon, 2009a). Some transition metal ions are themselves essential for the normal functioning of living organisms, these being involved as modulators for biological system; in fact, nearly one-third of enzyme-mediated process require metal cofactors for the activity (Maxwell & Bates, 2009). In the human body in particular, the second most abundant transition metal is zinc (while ferum being the most abundant), which is required for cell growth and division. Among research on the anticancer properties of zinc complexes, the zinc derivative of Schiff-base type of thiocarbohydrazone was implicated as a DNA binder by the use of a simple spectroscopic method (Tiwari et al., 2011).

Aside from zinc, nickel is another much-examined metal in the search for the metal-based anticancer therapeutics. Together with palladium and platinum, these transitional metal elements are categorized in the Periodic Table as a triad that behave as close relatives in their chemical as well as possible biological interactions (Stromberg et al., 1997). For example, nickel complexes of 1,2-naphtoquinone-based thiosemicarbazone ligands are more cytotoxic against MCF7 human breast cancer cell line than the

commercial antitumour drug etoposide (Chen et al., 2004). Furthermore, nickel complexes with polypyridyl ligands induce selective growth inhibition towards cancer cells by stabilizing the G-quadruplex of DNA, a feature that is crucial to the potential use of these as metal-based antitumour drugs (Dixon et al., 2005; Le et al., 2013).

Many studies have addressed the delivery of an anticancer agent to the cell or its functional target; such drug targeting strategies may be achieved by improving the drug carrier strategy itself rather than to use a free solution of the drug (Huxley et al., 2010; Ruiz et al., 2012). By conjugating to the biomolecules that target a specific organ or receptor, the carriers would direct the drug towards the specified target (Sanchez-Cano & Hannon, 2009a). On the other hand, in regard to the organic portion of the drug molecule, androgens (e.g. testosterone), i.e., sex hormones, can be exploited with this strategy owing to their ability to interact with the androgen receptor and also to form a stable receptor-ligand molecular complex (Szyczewski et al., 2004; Manosroi et al., 2010). For instance, enhanced antiproliferative effects of several steroidal complexes of ferrocene against hormone-independent prostate cancer cell line PC-3 are known (Top et al. 2011). This strategy may even improve the delivery of an anticancer agent to androgen receptor positive cells such as prostate, breast, or even colon cells, since the expression of these receptors on the membrane of human colon cell lines is known in the literature (Gu et al., 2009).

Metal complexes of thiosemicarbazones are of current interest owing to their demonstrated array of biological activities such as antibacterial, antitumour, antifungal, antileukemic, and cytotoxic activities (Khan et al., 2008; Prabhakaran et al., 2013; Pahontu et al., 2015; Malik et al., 2018). Schiff base thiosemicarbazones constitute a class of versatile organic ligands that can be readily synthesized through condensation of thiosemicarbazide and a carbonyl compound, the condensation resulting in the formation

of C=N bond in the molecule while a molecule of water is lost (Kovala-Demertzi et al., 2002). Interestingly, the diversity of certain biological properties, such as cytotoxicity and nucleolytic properties, is increased by a steroidal constituent (Khan et al., 2008). The ligand synthesized from testosterone acetate and thiosemicarbazide, in the form of the copper and platinum derivatives, exhibited cytotoxicity (against MCF7 human breast cancer cell line) that is comparable with cisplatin itself (Murugkar et al., 1999). The cellular delivery of a range of other platinum complexes is also enhanced when the metal is linked to androgen, and cytotoxicity is also improved compared with their non-steroidal analogues (Huxley et al., 2010). The property of these testosterone-based complexes to unwind and to bend the DNA double-helix is known to be similar to the ability of those induced by cisplatin on DNA structure (Sanchez-Cano et al., 2010).

The undesirable side effect of some chemotherapeutics and the potential of androgen Schiff base compounds have led to a search for a cytotoxic compound to be more selective towards androgen receptors positive cancerous cells when it is conjugated to a testosterone molecule. The present study was undertaken with the following objectives:

a) To synthesize the Schiff base compounds (and metal complexes) of the testosterone derivative of thiosemicarbazide;
b) To evaluate the growth inhibitory properties of the new compounds against selected human cancer cell lines;
c) To elucidate the possible mechanism of cell death induced by these compounds;
d) To determine the interaction of compounds with DNA;
e) To estimate the inhibitory strength of the compounds on the activity of topoisomerase I.

CHAPTER 2: LITERATURE REVIEW

2.1 Transition metal complexes as chemotherapeutic agents

The use of metal salts for medical purposes can be traced back to antiquity; during the pharaonic era, copper was used by the Egyptians to sterilise water, and gold was used in China during the Shang dynasty (Fricker, 2007). Such activity is generally attributed to the positive nature of the ion and the stereoelectronic properties that alter the function and structure of biological targets (Tardito et al., 2011). The wide range of coordination geometries and coordination numbers, along with the kinetic properties of metal complexes enable delivery mechanisms that cannot otherwise be achieved by organic agents (Ott & Gust, 2007). In some clinical trials, metal ions have demonstrated therapeutic abilities, and they can be used in diagnostic medical imaging (Singh & Sharma, 2018). Research is intense on the application of transition metals as antitumour drugs, although platinum has remained as the mainstay of research in metal-based drugs, this arising from the documented success of cisplatin in the treatment of cancer.

2.1.1 Platinum complexes chemotherapeutic agents

The importance of platinum in anticancer therapy originated from the discovery of cisplatin (cis-diamine-dichloro-platinum^{II}) against *Escherichia coli* (Rosenberg et al., 1969; Jakupec et al., 2008). In 1978, the drug was regarded as a wonder drug as some patients were cured from several types of cancer that were otherwise not treatable (Hannon, 2007; Chabner, 2010). When the FDA granted approval, cisplatin replaced other drugs in the treatment of germ cell cancers (Dasari & Tchounwou, 2014).

In order to bind to primary cancerous cells, cisplatin must be activated through a series of chemical reactions which involve sequential replacement of the chlorine atoms with water molecules while the metal centre retains its square planar geometry (Kelland, 2000). The aquo compound then binds to DNA through the formation of intra- and inter-strand crosslinks (covalent Pt-DNA), which in turn causes kinks in the DNA. Transcription is then inhibited by stalling DNA polymerase, thereby resulting in controlled cell death (Suntharalingam et al., 2013). The steps involved in the biochemical activity of cisplatin are illustrated in Figure 2.1 (Ceron-Carrasco et al., 2012), and the structure of DNA with a kink that results from binding by cisplatin bound is depicted in Figure 2.2 (Takahara et al., 1995).

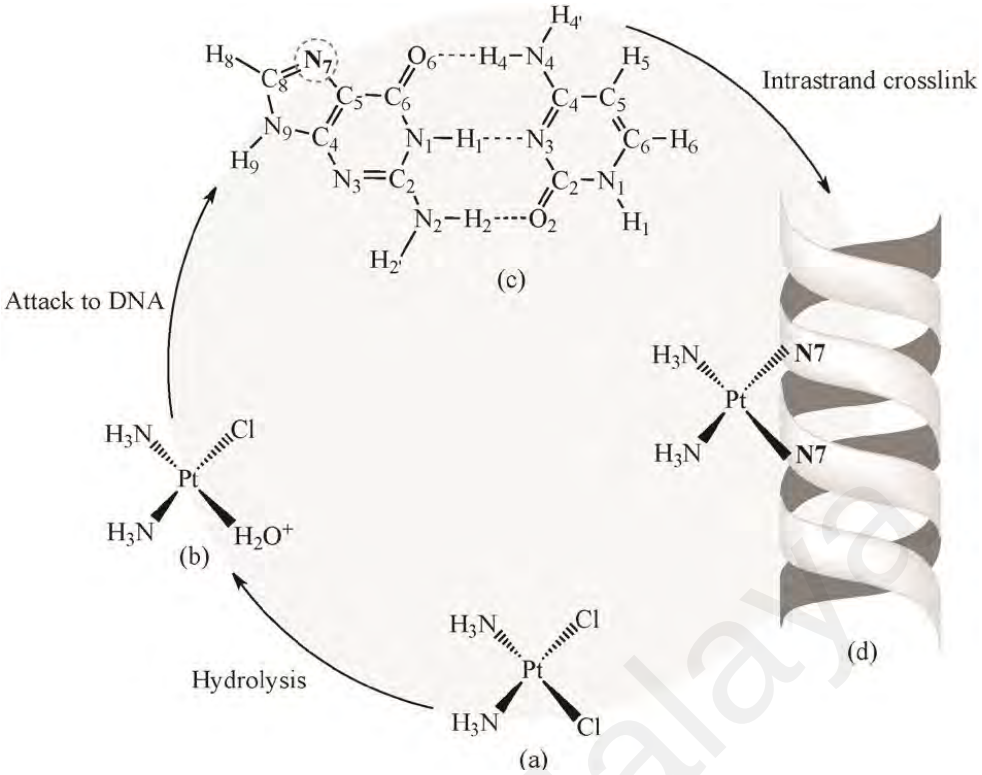

Figure 2.1: Main events in the biochemical activity of cisplatin. A water molecule is incorporated into cisplatin (a) with displacement of one chlorine atom once it has entered the cell. The resulting activated aqua platinum species (b) attacks DNA at the N7 positions of two adjacent GC base pairs (c), forming the Pt-DNA intrastrand cross-link adduct (d). (Ceron-Carrasco et al., 2012).

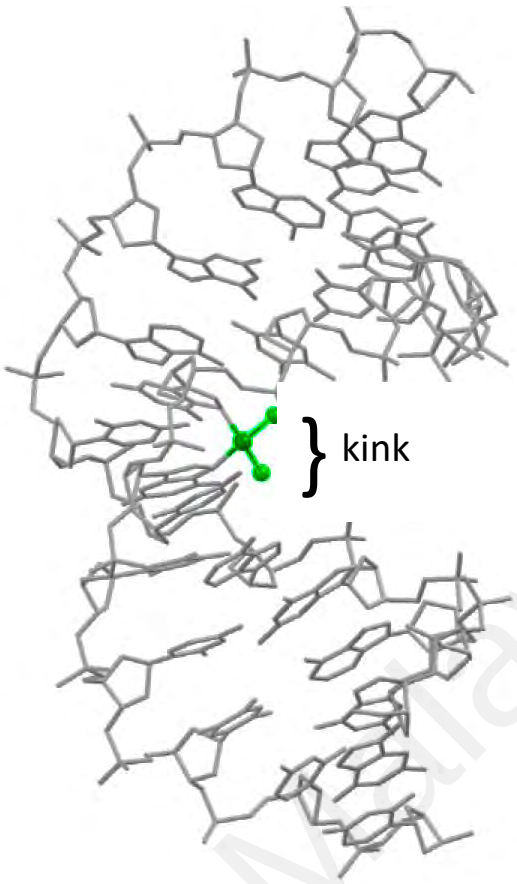

Figure 2.2: Structure of DNA with cisplatin (highlighted in green) bound. The platinum center is located in the major groove, and the DNA is bent (kink) by approximately 45° toward the site of platination (PDB ref. 1AIO). (Takahara et al., 1995).

Numerous analogues have been synthesized by researchers with the intention of enhance the therapeutic index of cisplatin. Some 13 underwent clinical trials (Dasari & Tchounwou, 2014), and to date, two (carboplatin and oxaliplatin) have been approved for clinical use worldwide while three (nedaplatin, heptaplatin and lobaplatin) are used in Asia (Japan, South Korea and China, respectively) (Kenny & Marmion, 2019).

Despite the use in the treatment of cancer worldwide, the administration of these drugs has some severe drawbacks, mainly resistance development in tumours, as well as severe side effects such as hepatotoxicity, nephrotoxicity, and neurotoxicity (Chang et al., 2002;

Chuang et al., 2002; Fuertes et al., 2003; Bruijnincx & Sadler, 2008). Furthermore, a lack of specificity at the active metal core sometimes leads to undesirable biological activity and interactions with other biomolecules (Spencer & Walden, 2018). Such side effects have reduced the effectiveness of these drugs in dealing with these life threatening diseases. Research of medicinal applications of other classes of metal-based anticancer drugs are expected to fill the gap in tumour chemotherapy, in the hope of overcoming this problem of resistance so that the range of activity can be broadened.

2.1.2 Nickel complexes as chemotherapeutic agents

Nickel, a group 10 element in the Periodic Table of elements, is an essential element required for the functions of enzymes such as urease, hydrogenase, and carbon monoxide dehydrogenase (Rau & van Eldik, 1996). Together with palladium and platinum, the group 10 elements are categorised as nickel triad, which often behaves as a set of elements that possess similarities in the reactions (Stromberg et al., 1997). Different geometries are possible, and these elements are also capable of forming organometallic compounds (Drennan, 2010). There is, however, limited literature on the biochemical aspects of nickel in the context of antitumour therapy.

In animal models, chronic exposure to particulate (insoluble) nickel compounds is known to give rise to alveolar/bronchiolar adenomas and carcinomas in rats, so that as antitumour agents in clinical tests, the physiological importance of nickel should be taken into account (Holmes et al., 2013). Several nickel complexes show promising anti-proliferative activities. These include (but not limited to) *N*-heterocyclic carbene complexes, nickel pyrithione, nickel thiosemicarbazones, Schiff-base nickel chelates, and other nickel complexes (Englinger et al., 2019). For instance, the cytotoxicity of the nickel complexes of naphtoquinone-based thiosemicarbazone ligands (NQTS) against MCF7

human breast cancer cell line is comparable with that of the commercial drug etoposide; furthermore, the nickel complexes also display enhanced antitumour activity at low IC_{50} values accompanied by topoisomerase II inhibitory activity (Chen et al., 2004).

2.1.3 Zinc complexes as chemotherapeutic agent

Zinc is the second most abundant metal in the human body, which plays a pivotal role in cell growth and division. Many researchers have reported a direct relationship between cancer cell progressions with the abundance of zinc in body. For example, breast cancer patients showed decreased and elevated zinc level in serum and malignant tissues (Frezza et al., 2010). Moreover, increased level of zinc is often associated with the decreased proliferation of prostate cancer cells, which might be due to the action of zinc on the mitochondria that resulted to the release of cytochrome c and ultimately leads to apoptotic cascading events (Costello et al., 2004).

The functional conformation of tumour suppressor p53 is correlated to the concentration of zinc, with increasing concentration of zinc may mediate the renaturation of wild type p53 (Méplan et al., 2000). It was also reported that Zn(II) complexes with bio-benzimidazole derived ligands displayed excellent cytotoxic activity and induced p53-dependent apoptosis in MCF7 human breast cancer carcinoma (Liu et al., 2013). Phospho-Akt is a pro-survival protein whereas $p21^{waf}$ often act as a cyclin inhibitor that involved in the regulation of cell survival. Zn(II) complexes of N,N-chelating ligand and diketonates were proven to downregulate the level of phosphor-Akt and increased the level of $p21^{waf}$, and these compounds showed potent cytotoxic activity towards human prostate cancer cell lines DU145, LNCaP, and PC3 (Liguori et al., 2010). Besides, ability of zinc with derivative of thiosemicarbazone in causing lysosomal permeabilization due to reactive oxygen production was reported (Palma et al., 2019).

2.1.4 Other transition metal complexes as chemotherapeutic agents

Other than the clinically approved drugs mentioned, several ruthenium, titanium, gallium and gold compounds have entered the clinical evaluation trials. The search for other transition metal-based anticancer drugs must be attributed to the success story of cisplatin; interestingly, many metal complexes with potential for antitumour activity have also been designed to behave differently from the platinum drug (Fricker, 2007). Although the ruthenium complexes NAMI-A and KP1019 are unsuccessful in phase 1 and combined phase 1/2 clinical trial, these are nonetheless promising alternatives to the platinum drug owing to a different resistance mechanism and a different interaction with protein targets as a predominant mode of action (Englinger et al., 2019).

Gold complexes currently represent alternative candidates for metal-based anticancer therapeutics. They have showed anticancer activity arises through a mechanism different from cisplatin in mitochondria instead of DNA are targeted (Au et al., 2008). Metallocenes have also been investigated, with ferrocene being the first studied. Ferrocene is reported to target the cell membrane, DNA, and topoisomerase II (Gasser et al., 2011). The metallocene complexes of titanium, such as titanocene dichloride are active against breast and gastrointestinal carcinomas. Although the efficacy of this compound in phase II clinical trials for patients with some cancer types is low (Gao et al., 2010), the fact that this chemical possesses significantly lower side effects has encouraged researchers to extend their search in other non-platinum compounds.

2.2 Safety issues associated with metal complexes

Metals can usually be divided into essential ones which are important for some cellular activities, and nonessential ones, which are not required by the organism. For instance, trace amounts of metals such as zinc, gallium, cobalt, silver, manganese and copper are

required to trigger catalytic processes while others such as cadmium, arsenic, chromium and nickel might be less beneficial to the body due to their carcinogenesis nature (Tchounwou et al., 2012; Ndagi et al., 2017).

The non-essential metals are sometimes being regarded as more toxic. Nevertheless, it has been a clear establishment that excessive essential metals can be as dangerous as nonessential ones. For example, nickel is essential in small dosage but it can cause various types of cancer on different sites within the bodies of animals when the maximum tolerable amounts are exceeded. Fortunately, nickel is not known to accumulate in plants or animals and therefore it has not been found to biomagnify up the food chain and therefore their therapeutic properties can be exploited (Wuana & Okieimen, 2011).

Unlike most of the metals, oral uptake of small amount of zinc is required for survival and zinc is found in muscle and bone, prostate, liver, gastrointestinal tract, kidney, skin, lung, brain, heart, and pancreas. Although zinc has a rather low toxicity and severe impact on human health by intoxication with zinc is relatively rare, excessive uptake of this metal will be lethal too. As reviewed by Plum et al. (2010), a woman was reported dead after oral intake of 28 g zinc sulphate, vomiting and hyperglycemia were observed and she died five days later due to hemorrhagic pancreatitis and renal failure. Besides, symptoms associated to excessive uptake of zinc such as nausea, epigastric pain, abdominal cramps, diarrhea, and zinc-induced copper deficiency were reported as well (Plum et al., 2010).

In short, a balance between the cellular need and its bioavailability is important for the normal physiological state. Meanwhile, the cytotoxicity properties of these metals complexes can be exploited and these toxins can be turned into medicines especially for therapeutic purposes.

2.3 Thiosemicarbazone and Schiff base compounds

Thiosemicarbazones are a class of organic compounds that possess several donor atoms that may coordinate to a metal centres. The organic compounds themselves are inhibitors of the enzyme ribonucleotide reductase and are also capable of interrupting the synthesis and repair mechanism of DNA (Kovala-Demertzi et al., 2002). Thiosemicarbazones and their derivatives such as triapine (3-aminopyridine-2-carbaxyaldehyde thiosemicarbazone) have been studied extensively for their use in anticancer therapy (Whitnall et al., 2006; Palanimuthu et al., 2013). Nevertheless, thiosemicarbazones belong to a huge group of thiourea derivatives that exhibit numerous biological activities, including antiviral, antibacterial, and anticancer (Khan & Yusuf, 2009; He et al., 2012). Their biological activities are a function of the parent aldehyde or ketone moiety, and the inhibitory action is mainly due to their chelating properties (Dilovic et al., 2008). The general formula of thiosemicarbazones is depicted in Figure 2.3.

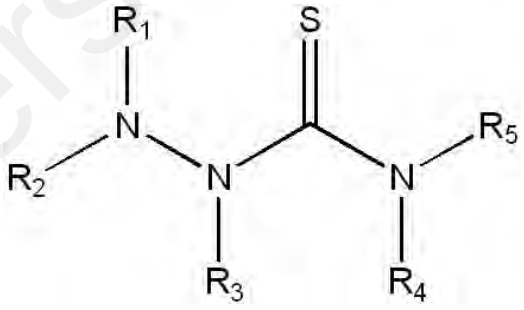

Figure 2.3: The general formula of thiosemicarbazones, where R_1, R_2, R_3, R_4, R_5 = H or any organic substituent.

Schiff base (imine) is an important class of ligands in coordination chemistry which are able to inhibit the growth of several types of animal tumours (Reddy et al., 2011). It can be synthesized from the condensation of carbonyl compounds and primary amine (i.e.

thiosemicarbazide), resulting in azomethine (C=N) bond at the expense of a water molecule (Schiff, 1864). The excellent chelating ability and flexibility in modifying the chemical environment about the C=N group has led to extensive study of this group of compound in coordination chemistry as well as medicinal chemistry (Ganguly et al., 2014). Interestingly, the biological activity of Schiff base can be further improved by complexation with transition metal ions (Gupta & Sutar, 2008). Numerous metal complexes of Schiff bases with different biological properties were reported, including applications as topoisomerase inhibitor (Arjmand & Muddassir, 2010; Lee et al., 2014), DNA cleaving agent (Reddy et al., 2004; Raman et al., 2007; Shahabadi et al., 2010), antibacterial agent (Jeewoth et al., 1999; Chohan et al., 2010), and potential anticancer agent (Adsule et al., 2006; Zhong et al., 2006; Creaven et al., 2010).

2.4 Metal complexes with testosterone derivatives

As described above, the application of the platinum chemotherapeutics (for instance, cisplatin) is accompanied by some unwanted and severe side effects. This is mainly attributed to the lack of selectivity (and specificity), in which virtually any types of cells in our body (both healthy and cancerous cells) will be targeted by these platinum chemotherapeutic agents, with DNA being their primary target (Jain et al., 2013). As a result, new strategies have been developed in order to minimize these side effects or to increase the activity spectrum through more effective delivery of the drug to the desired targets. The rationale behind this is, when the chemotherapeutics are delivered in a targeted fashion, they may have little side effects with an enhanced therapeutic efficacy as their availability at the target site is maximized besides only affecting the malignant cells (Bhattacharyya et al., 2011; Falciani et al., 2011). Target-based chemotherapeutics are one of the focuses on drug development nowadays. One of the strategies in designing

target-based drugs is by conjugating biomolecules which target a specific organ or receptor to cytotoxic compounds (Jakupec et al., 2008; Sava et al., 2012). The biomolecules will then function as carriers to direct the cytotoxic drugs toward the specified organ/receptor (Sanchez-Cano & Hannon, 2009b).

Different biomolecules have been explored with varying degrees of success and among all, sex hormones such as androgens are of particular interest due to their critical importance in the reproductive system cancers (Zamora et al., 2013). For example, androgens appear to play a critical role in prostate carcinogenesis as the high level of free testosterone was associated with increased incidents of prostate cancer (Debes & Tindall, 2002; Hyde et al., 2012). Besides their roles in the development of prostate cancer, testosterone (Figure 2.4), which is able to cross the cellular membrane by passive diffusion due to high lipophilicity, is undoubtedly an attractive carrier for target-based strategy because of its ability to bind to the androgen receptor in the cytoplasm and then be transferred into the nucleus (Foradori et al., 2008). Recognition and eventually binding to the androgen receptor by this hormone is highly valued in target-based strategy due to the fact that prostate cancer cells still expressing the androgen receptors despite androgen deprivation therapy was administered (Wang et al., 2007).

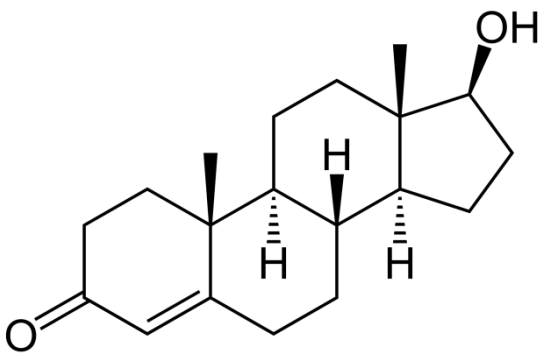

Figure 2.4: Structure of testosterone.

The idea of preparing steroid-bearing transition-metal complexes for biological applications has begun in the 1960s, where a number of metal ions were involved, including ruthenium, platinum, osmium, titanium, gold, nickel, and others. An extensive review on the strategies in preparing metal steroid compounds, metal-steroid designated for cancer therapy, and potential interest of certain steroid metal complexes for other biological developments, was prepared by Le Bideau and Dagorne (Le Bideau & Dagorne, 2013). Examples of metal-based drugs conjugated to testosterone were given and most, if not all of these compounds, were designed to target androgen receptor positive cells (e.g. prostate, and breast cancer).

Several reports on testosterone conjugated to platinum-based drugs were published recently by the group of Hannon et al. (2009-2010), where enhanced delivery was reported (Sanchez-Cano & Hannon, 2009a; Huxley et al., 2010; Sanchez-Cano et al., 2010). Some of these steroidal compounds showed better selectivity and uptake by androgen positive cells, while some displayed greater cytotoxicity. Meanwhile, Gao et al. (2010) reported higher antiproliferative activity alongside increased selectivity and sensitivity while titanocenyls were conjugated to androgens, including testosterone.

2.5 Testosterone thiosemicarbazone compound

A Schiff base containing testosterone and thiosemicarbazide was prepared by Al-Bayati et al. (2010). This ligand was then reacted to form metal complexes of chromium(III), cobalt(II), nickel(II), and copper(II). Although no crystal structure was reported, the structure of the ligand was proposed with evidence from FTIR and CHN-elemental analysis (Figure 2.5). These compounds displayed considerable antimicrobial properties with a number of microorganisms tested (Al-Bayati et al., 2010).

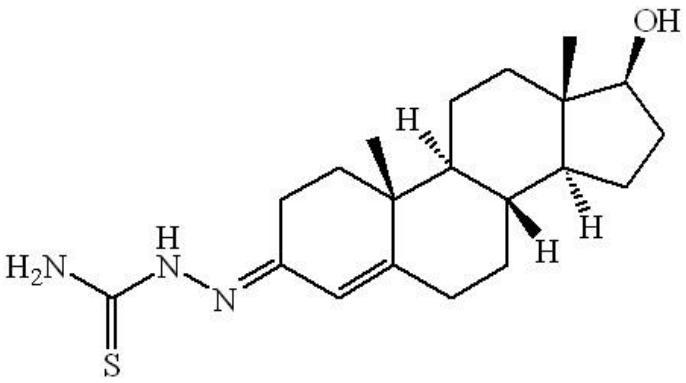

Figure 2.5: Proposed structure of testosterone thiosemicarbazone Schiff base (Al-Bayati et al., 2010)

Similar compound was prepared by Murugkar et al. (1999), with testosterone acetate was used for synthesis instead of testosterone. The structure of this compound was revealed by X-ray crystallography (Figure 2.6) and the formation of azomethine C=N linkage was confirmed. Platinum and copper complexes of this ligand were then prepared and these compounds, along with the free ligand, exhibit antitumour activity against the MCF7 breast cancer cell line (Murugkar et al., 1999).

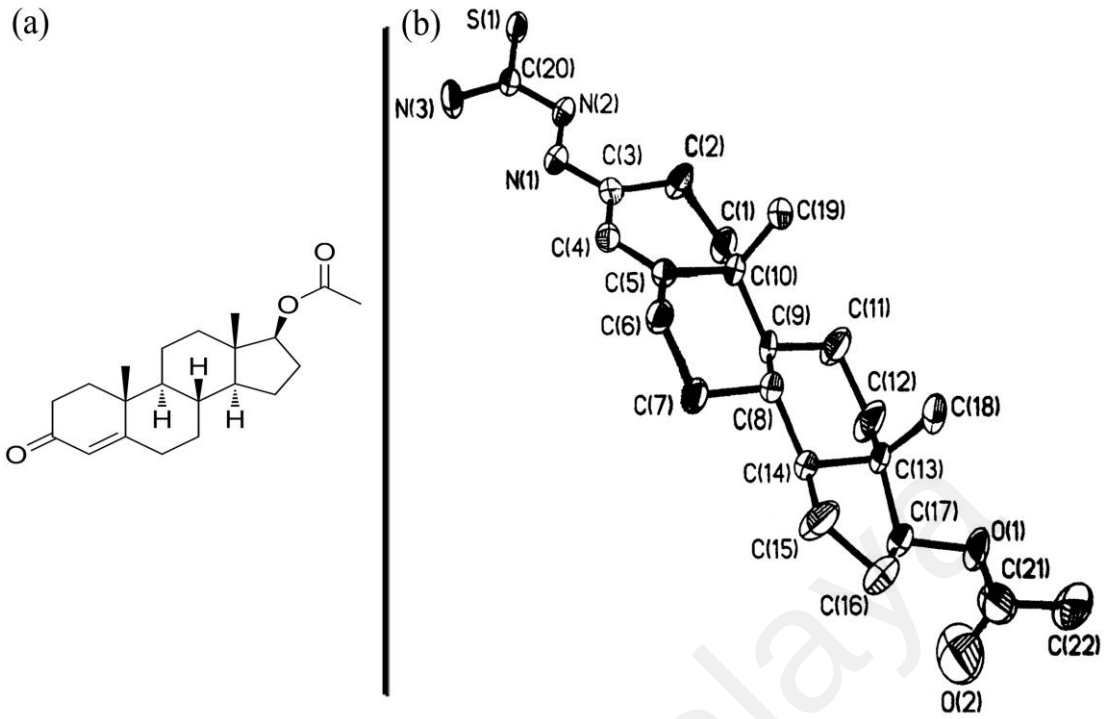

Figure 2.6: Structure of (a) testosterone acetate, and (b) ORTEP plot of testosterone acetate thiosemicarbazone (hydrogen atoms are not shown) (Murugkar et al., 1999).

Previously, a Schiff base ligand made of testosterone and thiosemicarbazide and its nickel(II) complex were synthesized. Despite failure in inhibiting topoisomerase I, both of the test compounds were selectively active in inhibiting the growth of human prostate cancer cell lines (PC-3 and LNCaP) and a human colorectal carcinoma cell line HCT 116. Although the primary targets of these compounds were not known, these DNA-minor groove binders displayed switch of preferences towards different cancer cell types upon complexation with nickel ion (Heng et al., 2015). The potential of other derivatives of thiosemicarbazide, as well as other transition metals, are therefore being explored in this project.

2.6 Antitumour targets of metal complexes

Conventional anticancer drug discovery and development are always focused on the cytotoxic agents. The discovery of these anticancer agents was mainly by serendipity and the exact mechanisms of actions were usually a subject of retrospective investigation (Chabner, 2010). Although this strategy has brought significant success especially in the case of cisplatin, recent development in drug design and better understanding of cancer biology have shifted the focus of researches to produce target-based drugs (Jakupec et al., 2008; Sava et al., 2012). Since the cytotoxic action of the drugs requires a combination of processes including cell entry, drug activation, DNA binding, and cellular responses, this new focus is indeed useful in identifying the potential targets in drug design, which is of importance as the fate of the drugs in the human body has to be taken into consideration (Ang et al., 2010). In fact, interactions of Schiff base complexes of nickel and zinc with DNA duplex and subsequently G-quadruplex were reported by other researchers (Bonsignore et al., 2018).

2.6.1 DNA as target

The interaction of metal complexes with DNA is always a major interest in the development of antitumour metal complexes. Reversible or irreversible modifications of DNA may lead to disruption of the transcription and/or replication process, which in turn block the cell division and ultimately results in cancer cell death (de Hoog et al., 2008; Liu et al., 2013). The design of effective DNA binding agents is therefore important for the development of new DNA-targeted antitumour agents.

The three most common platinating agents, namely cisplatin, carboplatin, and oxaliplatin, are indeed the best examples of DNA-targeted antitumour agents. It is widely accepted that DNA is the primary cytotoxic target for those platinum compounds. These

compounds form a covalent DNA crosslinks with adjacent guanine or adenine-guanine residues (Jain et al., 2013). Four different types of lesions can be formed on purine bases of DNA, namely monoadducts, intrastrand crosslinks, interstrand crosslinks, and DNA-protein crosslinks. All crosslinks would lead to contortion of the DNA and researchers believe that the crosslinks are cytotoxic due to the level of distortion in the DNA (Rabik & Dolan, 2007). Examples of different types of DNA lesions caused by platinating agents are illustrated in Figure 2.7.

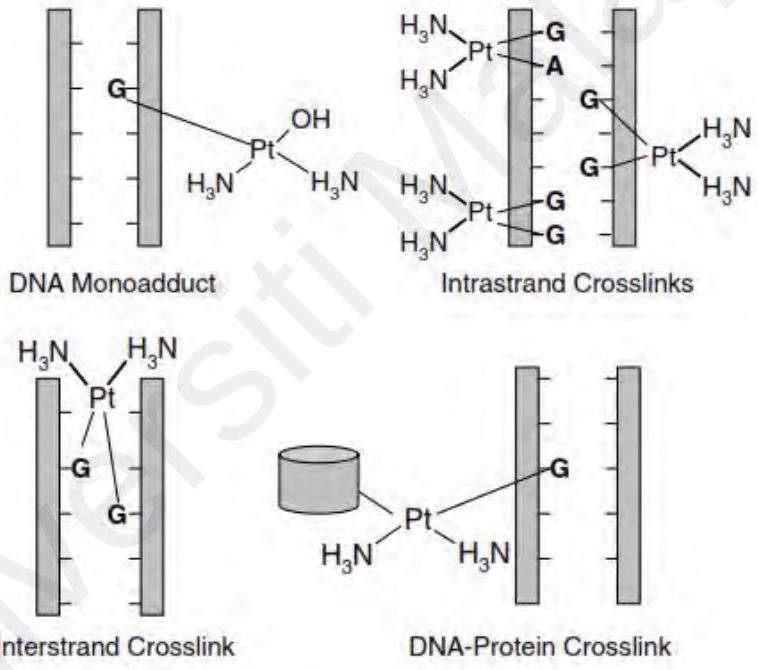

Figure 2.7: Platinating agent adducts on DNA. Platinating agents are capable of binding to DNA and form monoadducts, intrastrand crosslinks, interstrand crosslinks, and DNA-protein crosslinks. (Rabik & Dolan, 2007).

The DNA binding abilities are the reasons of success for the platinum drugs mentioned above. However, this ability also contributed to the limited clinical usefulness of these

drugs. As the target of these platinum agents is ubiquitously present in all the living cells, these complexes may damage the DNA of healthy cells apart from targeting cancerous cells, thereby resulting in adverse side effects such as hepatotoxicity, nephrotoxicity, and neurotoxicity on patients (Sava et al., 2012; Kilpin & Dyson, 2013). Intriguingly, evidences have proven that DNA-targeted anticancer agents are still the most effective agents in clinical use, which increased the survival rates of cancer patients, despite the aforementioned side effects were reported in some cases (Fricker, 2007). Consequently, the idea of targeting DNA in antitumour therapy is still alive and researchers are actively exploiting potential anticancer drugs that may interact specifically or selectively towards cancerous DNA.

The importance of DNA as the target of anticancer therapy has leads to the exploration of metal complexes that are capable of binding to DNA, preferably *via* different methods besides covalent binding (as seen in cisplatin). In fact, potential of metal complexes to bind to DNA through a multitude of interactions have been investigated and reported (Figure 2.8) (Zeglis & Barton, 2007; Sangeetha Gowda et al., 2014). For instance, DNA intercalators bind to DNA *via* non-covalent interactions, an interaction which is characterized by insertion of planar molecules between the DNA base pairs. This interaction is regarded as non-covalent as the stability of intercalation complexes is governed by van der Waals, hydrophobic, and electrostatic forces.

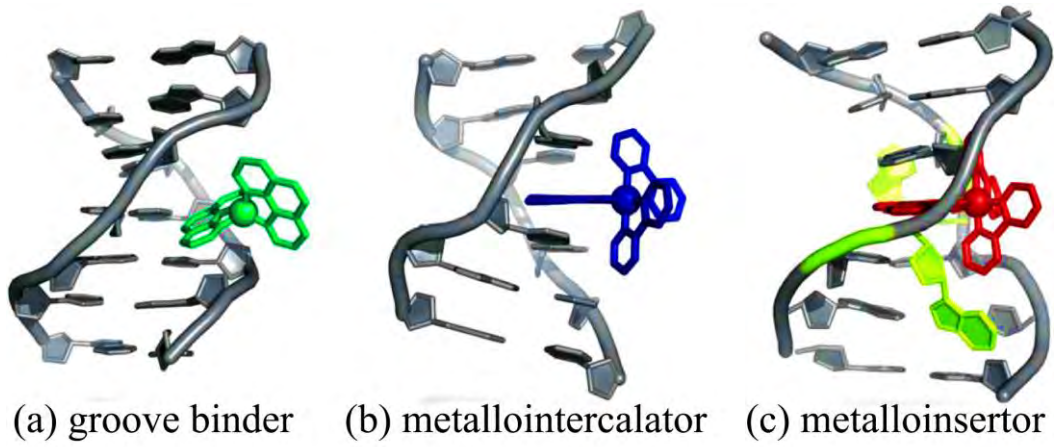

Figure 2.8: Three non-covalent binding modes of metal complexes with DNA: (a) groove binding, (b) intercalation, and (c) insertion. (Zeglis et al., 2007).

Unlike covalent binding, intercalation is commonly independent of base-pair sequence (Paul & Bhattacharya, 2012). Metallo-intercalators are metal complexes that bear at least one intercalating ligand. Generally, metallo-intercalators enter the double helix with no bases are ejected or displaced from the DNA duplex. However, intercalation often results in widening of the major groove (preferred binding site of intercalators) and this interaction distorts the structure of DNA (Zeglis et al., 2007). The functions of DNA-associated proteins such as DNA repair proteins, polymerases, topoisomerases, and transcription factors are therefore interrupted (Barone et al., 2013). Figure 2.9 shows the chemical structure of rhodium and ruthenium complexes bearing two common intercalators phi(9,10-phenanthrenequinone diamine) and dppz (dipyrido[3,2-a:2',3'-c]phenazine).

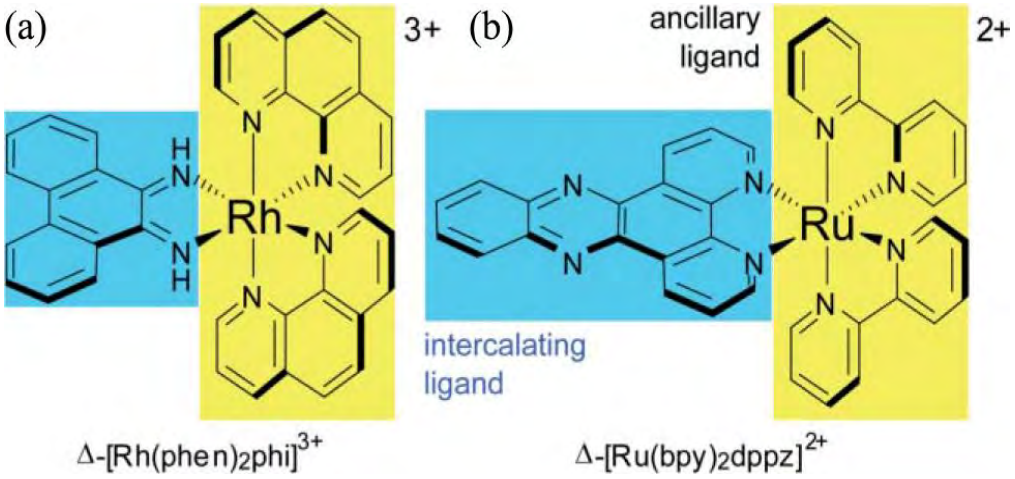

Figure 2.9: Chemical structure of two metallo-intercalators: (a) Δ-$[Rh(phen)_2(phi)]^{3+}$ and Δ-$[Ru(bpy)_2(dppz)]^{2+}$. The intercalating ligands are highlighted in blue, while the ancillary ligands in yellow. (Zeglis et al., 2007).

Groove binders are another major class of small molecules that bind to the DNA helix and their role in drug development are crucial. In principal, molecules are allowed to bind to both major and minor grooves of double-stranded DNA. However, the strategies for targeting them may be vastly different and different shaped molecules are required due to the differences in dimensions and size of the two grooves (Paul & Bhattacharya, 2012).

As the name implies, the major groove is wider compared to that of minor groove where the groove width values for averaged-sequence B-form double-stranded DNA are 11.6 and 6.0 Å, respectively (Neidle, 2001). The difference provides a tight fit to the groove binders that bind to minor and/or major groove (Raman & Selvan, 2012). The dimensional difference also rendered the major grooves the site for binding of many bulky DNA-interacting proteins, although limited amounts of non-protein molecules that bind to it are reported (Paul & Bhattacharya, 2012). In most of the cases, groove binders do not induce large conformational changes in DNA. Interestingly, the minor groove of DNA is usually the preferred binding site for crescent-shaped molecules (Palchaudhuri &

Hergenrother, 2007). Besides the potential to bind to DNA *via* electrostatic, H-bonding and van der Waals interactions, flexible structures have been claimed to be one of the main criteria of groove binders (Biver et al., 2005; Chaires, 2006). The minor groove binders are of interest due to their high specificity and they are prone to modulate the gene expression (Ruiz et al., 2010). Most of the antibiotics and antitumour drugs target the minor groove of DNA, including distamycin and netropsin (Figure 2.10) (Kopka et al., 1985; Hiraku et al., 2002; Jeon et al., 2019). The metal complexes of Cu(II), Ni(II), Co(II) and Zn(II) with tyramine and 4-aminoantipyrine derived Schiff base were demonstrated to bind to the minor groove of DNA efficiently (Raman et al., 2011; Raman & Sobha, 2012).

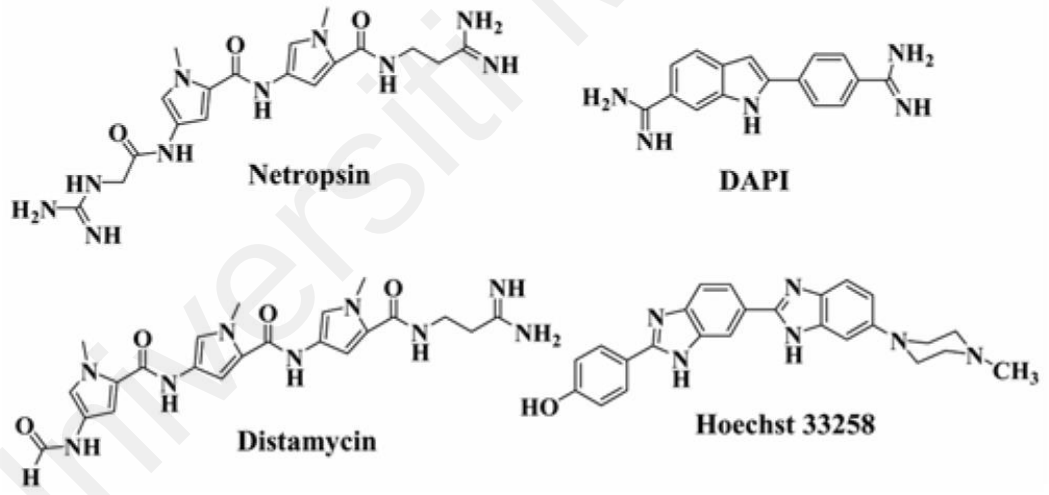

Figure 2.10: Chemical structure of some DNA minor-groove binding agents (Paul & Bhattacharya, 2012).

The vast majority of non-covalent DNA-binding metal complexes are indeed either groove-binders or intercalators. However, the possibility of molecules to bind to DNA by other means cannot be excluded. For example, insertion was proposed by Lerman (1961),

as he suggested a molecule may bind 'a DNA helix with separation and displacement of a base-pair' (Lerman, 1961). A more refined explanation for metal complexes that bind to DNA *via* insertion, namely metallo-insertors, was given by Zeglis et al. (2007). Like metallo-intercalators, these metal complexes contain a planar aromatic ligand that extends into the base-stack upon DNA binding. A clear difference between these modes of binding is, while metallo-intercalators insert their planar ligand between two intact base-pairs by unwinding the DNA, metallo-insertors eject the bases of a single base-pair, with their planar ligand served as a π-stacking replacement in the DNA base stack (Zeglis et al., 2007). Although only scarce amount of metallo-insertors reported, this group of DNA binders is potentially an answer to targeted chemotherapy as rhodium metallo-insertors with sterically expansive ligands were proven to specifically bind to nucleic acid base mismatches in DNA (Weidmann et al., 2014).

2.6.2 Topoisomerase I as target

DNA topoisomerase I (topo I) is nuclear enzyme that removes the torsional stress in DNA, which can be found in all free-living organisms. They are named so as they catalyze the interconversions between topological isomers of DNA rings and this enzyme is essential in solving topological problems associated with numerous pivotal processes such as DNA replication and transcription (Wang, 1996; Jain et al., 2009).

The functions of topo are of utmost importance for survival because separation of the two strands of helix (either temporarily as in transcription or recombination, or permanently as in replication) is required in many cellular processes in order to access the information stored in the DNA (Champoux, 2001). It is widely accepted that most free-living organisms have multiple topo from at least two major families (such as type I and type II topo) and apart from the mechanisms involved, these two major classes of

topo are usually distinguished by the number of DNA strands they cleave (Benarroch et al., 2006). Figure 2.11 shows the reactions catalyzed by these enzymes.

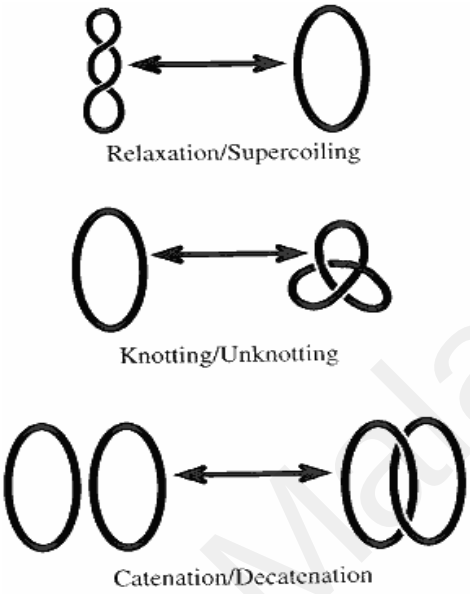

Figure 2.11: Reactions catalyzed by topoisomerase (Holden, 2001)

DNA topo are particularly vulnerable during their cleavage intermediate step or as a cleavage complex. Considering the importance of topo in virtually every major DNA process, these enzymes are targets for some of the most important anticancer drugs which are currently being utilized in the treatment of human malignancies (McClendon & Osheroff, 2006). In fact, elevated topo I levels in tumours, mostly due to the needs of replication and thereby cell divisions, are reported long ago (Teicher, 2008). DNA topo targeting drugs can be classified into two classes based on their mechanism of action, namely, topo poison and topo inhibitor. The first class, topo poison, acts after the cleavage of DNA by the enzyme and functions by stabilizing the intermediates during the catalytic cycle (topo-DNA complexes), re-ligation of the DNA is therefore inhibited. Unlike topo

poison, the topo inhibitor refers to the compound that suppresses the functions of the enzyme but does not freeze the intermediate DNA-topo complex. In brief, topo inhibitor interacts with the free enzyme or DNA, thus preventing all subsequent steps in the catalytic cycle (Nitiss & Wang, 1996; Bailly, 2000).

Camptothecin, a practically water-insoluble natural alkaloid, demonstrated promising antitumour activity in clinical trials, for example in gastric cancer. The mechanism of antitumour activity of camptothecin was identified as inhibition of topo in the early 1980s and researchers then began to modify comptothecin to create a host of analogues. Although several thousands of camptothecin derivatives have been synthesized, only two analogues (irinotecan and topotecan) were approved for cancer treatment (Li et al., 2017). In particular, irinotecan have enjoyed success in the treatment of metastatic colorectal cancer, ovarian cancer, small cell lung cancer, breast cancer, pancreatic cancer, esophageal cancer, gastric cancer, and locally advanced primary brain tumours (Conti et al., 1996; Kudoh et al., 1998; Friedman et al., 1999; Ilson et al., 1999; Bodurka et al., 2003; Perez et al., 2004; Shah et al., 2006; Vassal et al., 2007; Alemany, 2014). On the other hand, topotecan is often used in the treatment of ovarian and small cell lung cancer. However, major toxicities associated with these drugs such as neutropenia and diarrhoea should not be neglected (Rothenberg et al., 2001). Two key factors that hampered the development of this drug were poor water solubility and severe toxicity (Dexheimer & Pommier, 2008; Pommier, 2009; Wu et al., 2018). Examples of campothecin analogues are illustrated in Figure 2.12.

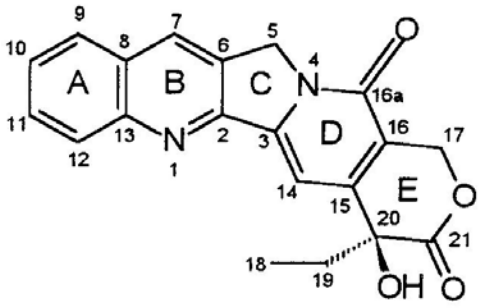

Substituent Group

Compound	C-11	C-10	C-9	C-7
Camptothecin	H	H	H	H
Irinotecan	H	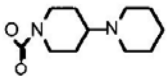	H	CH_2CH_3
SN-38	H	OH	H	CH_2CH_3
Topotecan	H	OH	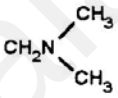	H
Lurtotecan	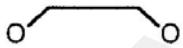		H	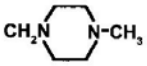
9-aminocamtothecin	H	H	NH_2	H
9-nitrocamptothecin	H	H	NO_2	H
DX-8951	F	CH_3	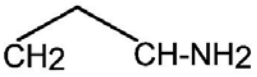	

Figure 2.12: Structure of camptothecin analogues (Herben et al., 1998)

As mentioned above, the therapeutic windows of camptothecins are restricted due to some unwanted side effects although they are the only topo I inhibitors approved for clinical use. Several non-camptothecin topo I inhibitors were developed and under clinical development now, which includes indolocarbazoles (a DNA intercalator), indenoisoquinolines (a topo I poison), and dibenzonaphthyridinones (Delgado et al., 2018).

Interestingly, most of the topo I inhibitors, in particular, the family of camptothecin, are planar molecules. Detailed mechanisms have shown that comptothecin mediates cytotoxic effect through binding to the DNA cleavage site of the topo-DNA complexes *via* π-π interactions. Therefore, Che et al. (2010) proposed that metal complexes with planar structures, such as platinum(II)-terpyridine complexes which are capable of inhibiting topo I, is likely to exert its action by forming π-π interaction with the DNA cleavage site (Che & Siu, 2010). For that reason, the potential of linear or square planar metal compounds as topo I inhibitors should not be overlooked.

2.7 Molecular docking simulations

Over the last three decades, computational methods have evolved into sophisticated tools that are routinely used in industry and academia to facilitate the drug discovery and development process, which is regarded as an intense, length, and an interdisciplinary venture (Drews, 2000; Drews, 2003). New methodologies were introduced in previous 30 years and drug discovery has then become a more rational concept based on our understanding of the fundamental principles of protein-ligand interactions (Gohlke & Klebe, 2002; Klebe, 2006). Rational drug design, which initiated with the predefined knowledge about a specific compound or drug and then studies its behaviour towards the disease, has emerged as the central paradigm in pharmaceutical research (Rognan, 2007). The development of new technologies, including high throughput screening and recombinant target expression may have evolved the drug design to more dependent of specific target instead of serendipity, which was a key of discovery of many drugs historically (Hung & Chen, 2014).

The experimental efforts to perform the biological screening of billions of compounds, which are usually labour extensive and expensive, are still considerably high. As a result,

computer-aided drug design approaches have developed into attractive alternatives (Reddy et al., 2007). Nowadays, virtual screening is extensively used to predict the binding of a huge database of ligands to a particular target, with the aim of identifying the most promising compounds from the database tested (Rester, 2008; Kolb et al., 2009; Kolb & Irwin, 2009).

2.7.1 Concept of virtual screening

There are generally two common types of virtual screening methods, which are structure-based and ligand-based virtual screenings. The former involves automated and fast docking of a large number of chemical compounds against a protein-binding or active site, thereby directing a way to utilize the rapidly increasing number of protein 3D-structures (Bissantz et al., 2000; Bender & Glen, 2005). On the other hand, ligand-based virtual screening tends to find the results that are closely linked to known active products, where databases of chemical structures are explored to discover compounds that are similar to known activities (similarity searching) or possess a pharmacophore of substructure in common with known activities (pharmacophore substructure searching) (Vidal et al., 2006). This method is based on the principle of similarity, where similar compounds are assume to produce similar effects (Lengauer et al., 2004). Structure-based virtual screening is more suitable for this research because all the synthesized compounds are not reported before.

Docking simulation refers to the process of bringing and binding two molecular structures together. This process can be subdivided into two steps. The first step, searching, is to explore the conformational space of ligands that bind to target molecules. Next, the scoring of this set will be performed, i.e. rank it according to the estimated binding affinity (Koehler & Villar, 2000; Kellenberger et al., 2004; Verdonk et al., 2004).

Conformation of the ligand-receptor complex will then be generated, and compared to the earlier conformations with the aid of scoring function. The current conformation generated is then accepted or rejected on the basis of the score for that respective conformation. A new conformation will then be generated, and the search process repeats until an endpoint is reached (Shoichet et al., 2002).

2.7.2 Searching methods

As mentioned above, searching and scoring are tightly coupled in docking simulations and it is important to possess better scoring function so that the highest rank ordered conformation would have higher experimental binding affinity (that correlates well) with the receptor. The docking algorithms of structure-based virtual screening can be classified into three groups based on the searching methodology that involved: a) Searching the conformational space during docking; b) Searching the conformational space before docking; c) Incremental docking (Reddy et al., 2007).

a) The first type of searching method focuses on optimization of the small molecule conformation and its orientation in the binding pocket of the receptor. However, it is difficult to utilize this method for larger databases due to the complexity of the combined optimization problem. Therefore, stochastic algorithms like genetic algorithm, and Monte Carlo method are usually implemented (Taylor et al., 2002). Genetic algorithm is especially popular with a range of programs employed for docking simulations, including Autodock, DARWIN, and GOLD (Ördög & Grolmusz, 2008; Morris et al., 2009). In fact, stochastic algorithms allow very precise docking solutions even for very large and flexible ligands, but this class of algorithms falls behind the other two due to the lack of speed, mostly because of

its confident structure prediction which requires the docking runs to be repeated every several times (Halperin et al., 2002).

b) The second type of algorithms work by separating the conformational search of the small molecule from their placement in the binding site. At first, conformational analysis is performed, and all the relevant low-energy conformations are then rigidly placed in the binding domain, with only the remaining six rotational and translational degree of freedom of the rigid conformers have to be considered. This type of docking algorithms is employed by programs such as SLIDE and Fred (Reddy et al., 2007).

c) The third type of algorithms is regarded as incremental construction algorithms. The rotating bonds of the ligand are broken and fragments are created. These fragments are then docked rightly at various favorable positions in the binding domain starting with a base fragment. A set of possible orientations for this fragment is recorded, and other fragments are added in various orientations and scored. The process is repeated until the whole ligand is assembled. Incremental construction algorithms are commonly implemented in programs such as Flex, HOOK, and a component of DOCK 4.0 (Reddy et al., 2007).

2.7.3 Scoring functions

Scoring functions play two significant roles in docking simulations. First, they act as an objective function to differentiate between diverse poses of a single ligand and receptor-binding site. Besides, processes such as estimation of binding affinities of different receptor-binding complexes and rank order the compounds are done after docking of a compound database. One must be aware that the binding affinity is estimated rather than calculated (Perez & Ortiz, 2001; Halperin et al., 2002).

Various assumptions and simplifications are made in docking programs for the evaluation of modeled complexes. Some of the physical phenomena that determine the molecular recognition are not fully accounted. A promising and consistent scoring scheme is therefore important to evaluate the protein-ligand complex, which in turn essential in order to select the best binding conformations. The scoring functions are commonly categorized as: a) force-field based; b) empirical-based; c) knowledge-based; and d) consensus scoring (Stahl & Rarey, 2001; Perola et al., 2004). Different strategies are eventually combinations of ensemble-averaged terms and they constitute a compromise between exactness and computational effort (Reddy et al., 2007).

2.7.4 AutoDock for virtual screening

Numerous methods for docking and virtual screening were developed, including AutoDock (Goodsell et al., 1996; Morris et al., 1996; Morris et al., 2009), DOCK (Lang et al., 2009), Flex (Claussen et al., 2001), Glide (Friesner et al., 2004), GOLD (Verdonk et al., 2003), SLIDE (Zavodszky et al., 2009), QXP (McMartin & Bohacek, 1997), RosettaDock (Davis & Baker, 2009), and Surflex (Jain, 2003). As suggested by Cole et al. (2005), it is difficult to compare these programs and it is easy to produce results that are not generally applicable. Therefore, one should always select the most suitable technique from a number of docking tools available today to answer the specific research needs (Cole et al., 2005).

From the docking suites listed above, AutoDock is acknowledged to be one of the most reliable and widely used public domain packages for docking simulations (Sousa et al., 2006). Like other computational programs, AutoDock introduces various approximations to simplify problems in docking. For example, rigid body docking model, which allows one to speed-up computations compared to flexible docking by pre-computing the forces

experienced by the ligand on a grid (Morris & Lim-Wilby, 2008). Besides, it offers well-benchmarked force field, efficient (grid-based) implementation of rigid body checking, a flexible (receptor) docking protocol with an active space consisting of residues which are allowed to undergo conformational changes, and efficient implementations of the Lamarckian genetic algorithm (GA) to search for the ligand pose with the highest binding affinity, while sampling and 'mixing' sub-optimal solutions to solve the underlying global optimization problem (Biesiada et al., 2011). Despite being useful in the prediction of ligand-receptor complex three-dimensional conformation, the time required for each molecular docking experiment *via* AutoDock remain as a major difficulty. High performance computing systems and tools are required if the compounds databases have up to hundreds of thousands of small molecules (Abreu et al., 2010).

2.7.5 Limitations of docking simulations

There have been numerous successful applications of molecular docking studies in rational drug design. However, there are limited applications in the study of metal complexes, mostly owing to the lack of appropriate force fields to take care of the metal atoms and their relativity properties (Hu & Shelver, 2003; Casini et al., 2008). There is limited number of docking studies done where metal is part of the ligands as docking suites such as Glide, GOLD, and some others can possibly take care of the metal atom only if it is part of the receptor and remain unbound (Casini et al., 2008). Moreover, parameters for the metal of interest must be incorporated into the parameter file of package in order for AutoDock to function (Adeniyi & Ajibade, 2013).

Another major challenge in the applications of this method is the high computational demands. For example, a one-microsecond simulation of a relatively small system with

approximately 25,000 atoms running on 24 processors will require several months to complete (Durrant & McCammon, 2011).

In silico docking simulations were often performed to generate the energetically most favorable conformation based on scoring of the resulting geometries with respect to binding energy. It is estimated using a single conformation. However, the ligand binding is usually not restricted to one active binding site (or even the proposed targeted site) in reality (Kitchen et al., 2004; Bikadi & Hazai, 2009; Dhanik et al., 2013). Moreover, the solvent-related terms and protein flexibility is often neglected in docking simulations (Okimoto et al., 2009).

2.8 Cell lines tested

Cancer is one of the leading causes of the mortality worldwide (Asadi et al., 2019) and therefore cytotoxicity of the compounds was tested against four human cancer cell lines (prostate adenocarcinomas PC-3 and LNCaP, breast adenocarcinomas MCF7, and colorectal carcinomas HCT 116), and their general toxicities against two normal cell lines (prostate epithelial RWPE-1, and colon fibroblast CCD-18Co) were further evaluated. These cell lines were selected based on the potential selectivity of the compounds synthesized against these cell lines.

2.8.1 Prostate cancer

Despite being the sixth leading cause of cancer death among men worldwide, prostate cancer is the second most commonly diagnosed cancer, with approximately 1.276 million new cases along with 359000 deaths in 2018. Furthermore, the worldwide prostate cancer incidence is estimated to be doubled by 2040, rising to around 2.3 million new cases with

740000 deaths (Culp et al., 2020). Although the overall 5-year relative survival rate for men diagnosed between ages 40 to 80 years was around 95 to 100% in United States, it was 80% for those aged 25 to 24 years, 50% for those aged 20 to 29 years, and only 30% for those aged 15 to 24 years (Bleyer et al., 2020).

PC-3 is one of the most common human prostate cancer cell line used in the prostate cancer research and drug formulation against it. It is derived from a bone metastasis of a grade IV prostatic adenocarcinoma of a 62 years old Caucasian. This cell line is androgen-independent as it does not respond to androgen receptor, prostate specific antigen, glucocorticoids, and fibroblast growth factors. Moreover, its dependency on serum for growth is greatly reduced when compared to normal prostatic epithelial cells. In general, the morphological and functional characteristics of PC-3 suggested it is a poorly-differentiated adenocarcinoma and it has been used as aggressive form of prostate cancer and it is often used to represent castration-resistant tumours in cancer research (Kaighn et al., 1979; Tai et al., 2011; Johnston et al., 2015).

Unlike PC-3, LNCaP is commonly used to represent the indolent and androgen-dependent form of prostate cancer due to its expression of androgen receptor and prostate specific antigen. This cell line is derived from the left supraclavicular lymph node metastasis from a 50 years old Caucasian male (Horoszewicz et al., 1983). It is androgen-dependent, as androgen withdrawal inhibits its growth, with indolent biological behaviour that are relatively similar to the vast majority of the prostate cancers encountered clinically (Tai et al., 2011).

The normal human prostate cell line RWPE-1 was obtained as non-neoplastic human prostatic epithelial cells from a 54 years old Caucasian male donor. It was then immortalized with human papillomavirus 18, thereby resulted in the androgen responsive RWPE-1 cell line (Bello et al., 1997).

2.8.2 Breast cancer

Breast cancer is the second most common cancer overall (with lung cancer accounted for the most number of cases) and it is the most frequently diagnosed cancer (in 154 of 185 countries) that disrupt the lives of millions of women, with approximately 2.1 million new cases of breast cancer are expected to be diagnosed in 2018. Moreover, about 626679 of these patients are estimated to die (Bray et al., 2018). In 2018, majority of cases (62%) are expected to have 5-year survival rate of 99% as these patients are diagnosed when they have not metastasized yet. In contrast, those with invasive breast cancer are estimated to have 5-year and 10-year survival rate of 90% and 83%, respectively (Ahmad, 2019).

Although breast cancer is typically classified based on the expression of progesterone receptor, estrogen receptor, and human epidermal growth factor receptor 2, numerous studies have demonstrated the genomic landscape of breast cancer have extended beyond these 3 receptors (Lehmann et al., 2011). In fact, recent studies have indicated the expression of androgen receptor and other luminal genes termed the luminal-androgen receptor subtype in breast cancer (Vidula et al., 2019). Since androgen receptor is expressed in approximately 60-70% of breast cancers (Iacopetta et al., 2012), a breast cancer cell line is chosen to evaluate the cytotoxicity of the compounds synthesized against this cancer.

The breast adenocarcinoma MCF-7 is the acronym of Michigan Cancer Foundation-7, which is isolated from the pleural effusion of a 69 years old Caucasian woman with metastatic disease (Soule et al., 1973). This cell line is commonly regarded as a model that is suitable for breast cancer investigations worldwide despite being recognized as a poorly-aggressive and non-invasive cell line (Comşa et al., 2015). This is mainly due to the expression of estrogen receptors in the cell cytoplasm of this cell line to process estrogen, thereby rendering it an ideal model for the study of hormonal response in cancer

studies (Levenson & Jordan, 1997). As the result, MCF-7 is ubiquitously utilized in research for estrogen receptor-positive breast cancer cell such as anti-hormone therapy resistance studies and targeted-therapy (Comşa et al., 2015; Giovannelli et al., 2018). Nonetheless, androgen receptor has been demonstrated to be expressed in MCF-7 (Iacopetta et al., 2012), thereby rendering this cell line suitable for current study.

2.8.3 Colorectal cancer

Colorectal cancer is regarded as the third most common malignancy worldwide and it is the second leading cause of cancer death in 2018 (Bray et al., 2018). The greatest increment of colorectal cancer incidence and mortality occurs in countries with high human development index and it imposes a substantial global burden due to its mortality, medical costs, utilization of healthcare services, complications and side effects of treatment (Wong et al., 2012; Arnold et al., 2017). In 2019, Kasi et al. reported the Kaplan-Meier Estimates of 5-year survival rate for patients with different stages of colorectal cancer, which is: 91.83% for stage 1; 85.12% for stage 2; 70.52% for stage 3; and 37.30% for stage 4 (Kasi et al., 2019).

Even though the presence of androgen receptor is commonly characterized in prostate and breast cancer cell lines, colon tissues are known to express this receptor (D'Errico & Moschetta, 2008). Moreover, various functional hormone receptors including androgen receptor and estrogen receptor have been associated with colon cancer (Slattery et al., 2005). Apart from that, studies have demonstrated that males tend to develop colonic lesions at an earlier age compared to that of females and its incidence patterns showed that colorectal cancer tends to occur in males (Xia et al., 2019). However, different isoform of androgen receptors was found on different of colonic cells. For instance, both androgen receptor A (87 kDa) and androgen receptor B (110 kDa) are found in the healthy

colonic mucosa whilst only androgen receptor A is found on neoplastic colonic mucosa (Catalano et al., 2000). Apart from these isoforms, membrane androgen receptor and intracellular androgen receptors are discovered too (Krasanakis et al., 2019). Interestingly, luciferase staining assay performed by Dart et al. (2013) illustrated that moderate staining for androgen receptor in the small intestine and colonic surfaces of female and male mice, indicating the expression of androgen receptor on both the female and male colonic cells (Dart et al., 2013).

Due to the importance of androgen receptor and androgen on progression (and regression) of colorectal cancer, a colon cell line is included in current study. HCT 116 is a human colorectal carcinoma cell line that is widely utilized in the studies of cancer biology. Although the source of this cell line is not well described in the webpage of American Type Culture Collection (ATCC), it is commonly referred to one of the three variant cells lines that was isolated from a primary cell culture of a single human colonic carcinoma from an adult male (Brattain et al., 1981). Nonetheless, this cell line is growth factor-independent and it is highly motile and invasive in *in vitro* studies (Rajput et al., 2008). In addition, expression of membrane androgen receptor in both *in vivo* and *in vitro* studies was reported by other researchers (Gu et al., 2009), therefore this cell line is chosen to be studied along with other cell lines bearing androgen receptor.

The non-malignant human colon fibroblast CCD-18Co was used to determine the toxicity of the compounds against a normal colon cell line. This cell line is originally obtained from a colonic mucosal biopsy of a 2-month old female infant (Valentich et al., 1997). As mentioned earlier, few isoforms of androgen receptor (including androgen receptor A and B) should be present in this cell type due to the non-malignant nature of these cells (Catalano et al., 2000).

CHAPTER 3: EXPERIMENTAL

3.1 Materials

The chemicals for syntheses (testosterone, 4-methyl-3-thiosemicarbazide, 4-(4-ethylphenyl)-3-thiosemicarbazide, 4-(4-fluorophenyl)-3-thiosemicarbazide, nickel acetate, and zinc acetate) were purchased from Sigma-Aldrich Co. (USA). Solvents were purchased from Merck (USA). The plasmid DNA pBR322, GeneRuler^{TM} 1kb DNA ladder, and 6X loading buffer were purchased from BioSynTech (Fermentas). Agarose was procured from Promega. *Escherichia coli* (*E. coli*) topoisomerase I was purchased from New England Biolabs (USA). Calf-thymus DNA, sodium chloride, and ethidium bromide were obtained from Sigma-Aldrich Co. (USA). Aqueous solutions for the DNA experiments were prepared with ultra-pure water from an Elga PURELAB ULTRA Bioscience water purification system equipped with a UV light accessory. Tris-NaCl (TN) buffer was prepared by combining tris base and sodium chloride. The pH of the TN buffer was adjusted to pH 7.4 with dilute hydrochloric acid. Test compounds were freshly prepared for the experiments.

3.2 Physical measurements

Infrared spectra were recorded as KBr pellets on a Perkin-Elmer Spectrum RX-1 spectrometer. ^{1}H-NMR and ^{13}C-NMR spectra were recorded in deuterated DMSO on a JEOL JNM-LA400 or an ECA 400 MHz instrument. Elemental analyses of carbon, hydrogen, and nitrogen were determined by using a Thermo Finnagan Eager 300 CHNS elemental analyser. UV-Vis spectroscopic measurements were recorded on a Shimadzu UV-1600 series spectrophotometer.

3.3 Syntheses

Three Schiff base ligands were synthesized from the condensation of testosterone with derivatives of thiosemicarbazide: the thiosemicarbazides were 4-methyl-3-thiosemicarbazide, 4-(4-ethylphenyl)-3-thiosemicarbazide and 4-(4-fluorophenyl)-3-thiosemicarbazide. The corresponding nickel and zinc complexes were then prepared according to the reaction scheme presented in Scheme 3.1.

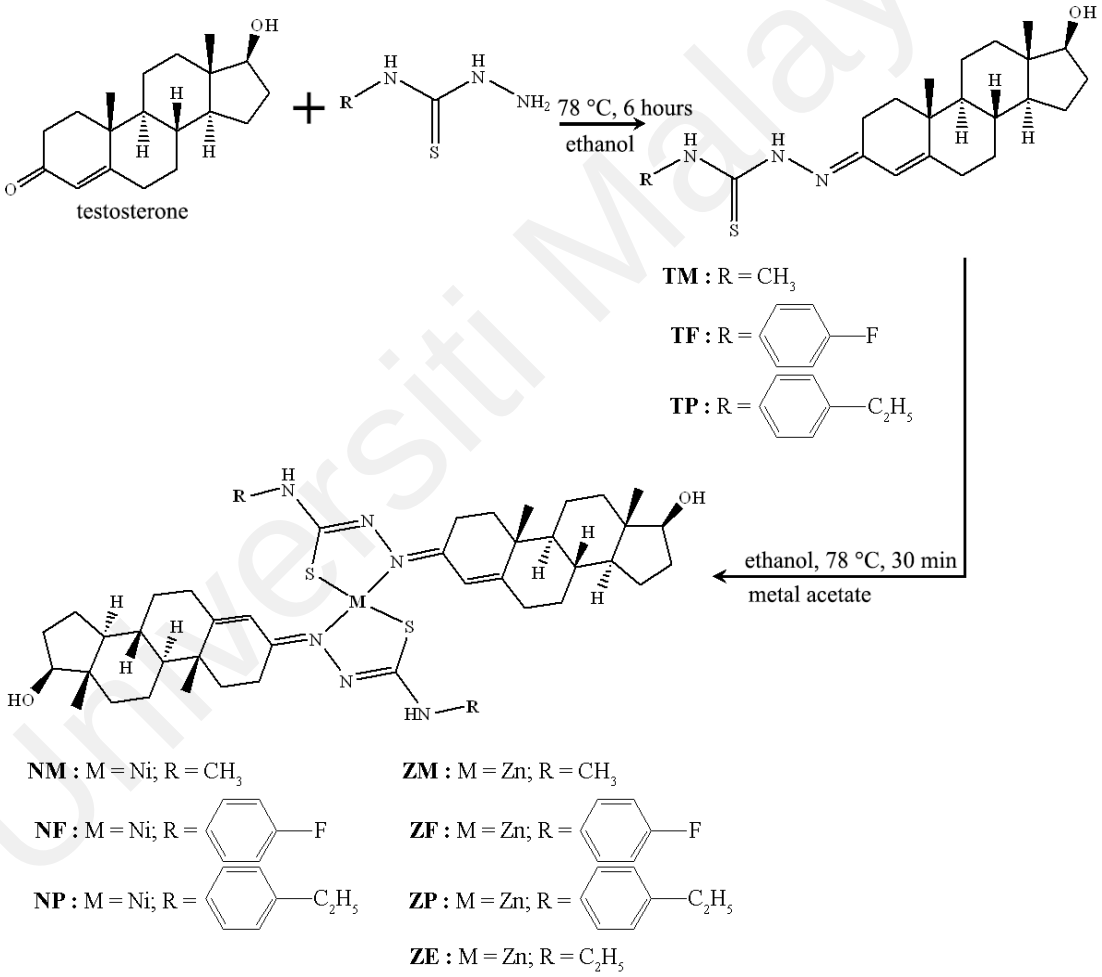

Figure 3.1: Schematic representation of synthesis of Schiff base ligands (**TM**, **TF**, **TP**) and their nickel complexes (**NM**, **NF**, **NP)** and their zinc complexes (**ZM**, **ZF**, and **ZP**) along with zinc complex **ZE**.

3.3.1 Synthesis of Schiff base testosterone-N^4-methylthiosemicarbazone

A Schiff base ligand (**TM**) of testosterone and 4-methyl-3-thiosemicarbazide was prepared. The nickel (**NM**) and zinc (**ZM**) complexes of this Schiff base ligands were then prepared. Crystals of **TM** and **NM** were collected.

3.3.1.1 Synthesis of testosterone-N^4-methylthiosemicarbazone, TM

Testosterone (288 mg; 1 mmol) was dissolved in ethanol (10 ml) and the solution was mixed with an ethanol (10 ml) solution of 4-methyl-3-thiosemicarbazide (105 mg; 1 mmol). The resulting solution was heated under reflux 6 hours. After cooling, the solution was filtered and the solvent was allowed to evaporate. Pale yellow crystals separated from the mixture after several days. The compound is insoluble in water but soluble in methanol, ethanol, chloroform and DMF.

Yield: 82 %; Anal. Calc. for $C_{21}H_{33}N_3OS{\cdot}C_2H_5OH$: C, 65.52; H, 9.32; N, 9.97. Found: 65.62; H, 9.42; N, 9.78.; IR (KBr) cm^{-1}: 3332br (OH), 2928s (CH_3), 2871m (CH_2), 1617m (C=N), 1062s (C=S) (br, broad; w, weak; m, medium; s, strong).

Characteristic ^{1}H-NMR signals (400 MHz, DMSO-d_6), δ (ppm): 10.04 (1H, s, N-H of 4-methyl-3-thiosemicarbazide), 8.39 (1H, m, N-H of 4-methyl-3-thiosemicarbazide), 5.76 (1H, s, C-H of testosterone), 4.48 (1H, d, O-H of testosterone), 2.96 (3H, m, CH_3 of 4-methyl-3-thiosemicarbazide), 3.43-0.67 (26H, m, 4 CH, 8 CH_2, and 2 CH_3 of testosterone)

Characteristic ^{13}C-NMR signals (400 MHz, DMSO-d_6), δ (ppm): 178.63 (C=S); 150.66 (C=N); 156.77, 121.13 (C=C); 80.40 (C-OH); 17.44 (N-CH_3).

3.3.1.2 Synthesis of nickel bis(testosterone-N^4-methylthiosemicarbazonate), NM

Nickel acetate (124 mg; 0.5 mmol) dissolved in ethanol (10 ml) was added to a solution of **TM** (421 mg; 1 mmol) in ethanol; the mixture was refluxed for 30 minutes. A green solid material was formed when the cooled solution was filtered. The compound was collected and washed with ethanol. The compound was purified by recrystallization from a DMF/methanol (3:8) mixture. The compound is soluble in DMF and DMSO.

Yield: 58 %; Anal. Calc. for $C_{42}H_{64}N_6NiO_2S_2\cdot(H_2O)_2$: C, 59.78; H, 8.12; N, 9.96. Found: 59.70; H, 8.40; N, 9.59.; IR (KBr) cm^{-1}: 3322br (OH), 2933s (CH_3), 2891m (CH_2), 1612m (C=N), 783m (C-S), 445m (Ni-N) (br, broad; w, weak; m, medium; s, strong).

3.3.1.3 Synthesis of zinc bis(testosterone-N^4-methylthiosemicarbazonate), ZM

Zinc acetate dihydrate (110 mg; 0.5 mmol) was dissolved in ethanol (10 ml); this was added to **TM** (421 mg; 1 mmol) in ethanol (10 ml). The mixture was heated for 30 minutes. The pale yellow product that separated out was collected and washed was washed with ethanol to remove the unchanged reactants. The compound is soluble in DMSO.

Yield: 64 %; Anal. Calc. for $C_{42}H_{64}N_6O_2S_2Zn\cdot1/2(C_2H_5OH)$: C, 61.66; H, 8.06; N, 10.03. Found: 61.47; H, 8.09; N, 10.15.; IR (KBr) cm^{-1}: 3329br (OH), 2924s (CH_3), 2856m (CH_2), 1613s (C=N), 780s (C-S), 442s (Zn-N) (br, broad; w, weak; m, medium; s, strong).

3.3.2 Synthesis of Schiff base compounds of testosterone-N^4-ethylphenylthiosemicarbazone

A Schiff base ligand (**TP**) was prepared from condensation of testosterone and 4-ethylphenyl-3-thiosemicarbazide. Its nickel (**NP**) and zinc (**ZP**) complexes were then prepared and crystal of **TP** was collected.

3.3.2.1 Synthesis of ligand testosterone-N^4-ethylphenylthiosemicarbazone, TP

Schiff base ligand **TP** was prepared with method similar to that of **TM**, with the choice of thiosemicarbazide being the main difference in between the two ligands. Ethanolic solution of testosterone (288 mg; 1 mmol; 10 ml) and 10 ml ethanolic solution of 4-(4-ethylphenyl)-3-thiosemicarbazone (195 mg; 1 mmol) were mixed together and the mixture was refluxed for 6 hours with continuous stirring. The solution was then filtered and allowed to evaporate at room temperature. The powder formed was then dissolved in methanol and pale yellow crystal suitable for X-ray crystal structure analysis was formed from slow evaporation of the solvent. Similar to **TM**, **TP** is soluble in organic solvent such as methanol, ethanol, chloroform, DMF, and DMSO.

Yield: 85 %; Anal. Calc. for $C_{28}H_{39}N_3OS \cdot 3/2(H_2O)$: C, 68.21; H, 8.68; N, 8.62. Found: 68.25; H, 8.59; N, 8.53.; IR (KBr) cm^{-1}: 3261br (OH), 2928s (CH_3), 2871m (CH_2), 1626m (C=N), 1064s (C=S) (br, broad; w, weak; m, medium; s, strong).

Characteristic ^{1}H-NMR signals (400 MHz, DMSO-d_6), δ (ppm): 10.04 (1H, s, N-H of 4(4-ethylphenyl)-3-thiosemicarbazide), 9.75 (1H, m, N-H of 4(4-ethylphenyl)-3-thiosemicarbazide), 7.50-7.49 (2H, s, s, aromatic CH of 4-(4-ethylphenyl)-3-thiosemicarbazide), 7.16-7.14 (2H, s, s, aromatic CH of 4-(4-ethylphenyl)-3-thiosemicarbazide), 5.88 (1H, s, C-H of testosterone), 4.48 (1H, d, O-H of testosterone), 2.61 (2H, m, CH_2 of 4-(4-ethylphenyl)-3-thiosemicarbazide), 1.21 (3H, m, CH_3 of 4-(4-ethylphenyl)-3-thiosemicarbazide), 3.44-0.67 (26H, m, 4 CH, 8 CH_2, and 2 CH_3 of testosterone)

Characteristic ^{13}C-NMR signals (400 MHz, DMSO-d_6), δ (ppm): 176.36 (C=S); 151.58 (C=N); 161.93, 148.94, 140.94, 140.90, 127.85, 125.27 (6 aromatic carbon); 157.72, 121.16 (C=C of testosterone); 80.46 (C-OH); 16.19 (CH_3 of 4-(4-ethylphenyl)-3-thiosemicarbazide).

3.3.2.2 Synthesis of complex nickel bis(testosterone-N^4-ethylphenylthiosemicarbazone), NP

Nickel acetate (124 mg; 0.5 mmol; 10 ml) was dissolved and added into a solution of **TP** (492 mg; 1 mmol) in ethanol and the mixture was refluxed for 30 minutes. Brownish green solid was formed and the mixture was filtered. Excess hot methanol was used to wash the green solid collected. The nickel complex **NP** is water insoluble and can only be dissolved in organic solvents such as DMF and DMSO. The attempts to harvest crystal of **NP** that are suitable for X-ray crystallography were unsuccessful.

Yield: 48 %; Anal. Calc. for $C_{56}H_{74}N_6NiO_2S_2\cdot(CH_3OH)_2$: C, 66.21; H, 8.05; N, 7.99. Found: 66.03; H, 7.94; N, 7.59.; IR (KBr) cm^{-1}: 3381br (OH), 2963s (CH_3), 2912m (CH_2), 1611m (C=N), 786m (C-S), 439m (Ni-N) (br, broad; w, weak; m, medium; s, strong).

3.3.2.3 Synthesis of complex zinc bis(testosterone-N^4-ethylphenylthiosemicarbazone), ZP

Zinc acetate dihydrate (110mg; 0.5 mmol) was dissolved in 10 ml of ethanol before added to 10 ml of **TP** (492 mg; 1 mmol) and the mixture was further refluxed for 30 minutes. Pale yellow solid was precipitated and filtered. The powder obtained was washed with excess amount of hot ethanol and methanol in order to remove impurities. The resulting zinc complex **ZP** can only be dissolved in organic solvents (such as DMF and DMSO) and attempts to isolate crystals of **ZP** were unsuccessful.

Yield: 54 %; Anal. Calc. for $C_{56}H_{76}N_6O_2S_2Zn\cdot(CH_3OH)_2$: C, 65.79; H, 8.00; N, 7.94. Found: 65.76; H, 7.97; N, 7.65.; IR (KBr) cm^{-1}: 3300br (OH), 2970s (CH_3), 2912m (CH_2), 1613s (C=N), 771s (C-S), 439m (Zn-N) (br, broad; w, weak; m, medium; s, strong).

3.3.3 Synthesis of Schiff base compounds of testosterone-N^4-fluorophenylthiosemicarbazone

Schiff base ligand **TF** was prepared from conjugation of testosterone and 4-fluorophenyl-3-thiosemicarbazide. Its nickel (**NF**) and zinc (**ZF**) complexes were then prepared. Crystals of **TF** and **NF** were harvested.

3.3.3.1 Synthesis of ligand testosterone-N^4-fluorophenylthiosemicarbazone, TF

Testosterone (288 mg; 1 mmol) was dissolved in 10 ml ethanol and mixed with 10 ml ethanolic solution of 4-(4-fluorophenyl)-3-thiosemicarbazone (185 mg; 1 mmol). The mixture was refluxed for 6 hours with continuous stirring before it was filtered and allowed to evaporate at room temperature. The yellow powder formed was then re-dissolved in ethanol and yellow crystal suitable for X-ray crystal structure analysis was formed from slow evaporation of the solvent. The resulting Schiff base **TF** is soluble in organic solvents such as methanol, ethanol, chloroform, DMF, and DMSO.

Yield: 92 %; Anal. Calc. for $C_{26}H_{34}FN_3OS \cdot 3/2(C2H_5OH)$: C, 66.38; H, 8.26; N, 8.01. Found: 66.39; H, 8.00; N, 7.82.; IR (KBr) cm^{-1}: 3259br (OH), 2933s (CH_3), 2912m (CH_2), 1621m (C=N), 1067s (C=S) (br, broad; w, weak; m, medium; s, strong).

Characteristic ^{1}H-NMR signals (400 MHz, DMSO-d_6), δ (ppm): 10.50 (1H, s, N-H of 4(4-fluorophenyl)-3-thiosemicarbazide), 9.87 (1H, m, N-H of 4(4-fluorophenyl)-3-thiosemicarbazide), 7.58-7.57 (2H, s, s, aromatic CH of 4-(4-fluorophenyl)-3-thiosemicarbazide), 7.17-7.15 (2H, s, s, aromatic CH of 4-(4-fluorophenyl)-3-thiosemicarbazide), 5.88 (1H, s, C-H of testosterone), 4.48 (1H, d, O-H of testosterone), 3.44-0.67 (26H, m, 4 CH, 8 CH_2, and 2 CH_3 of testosterone)

Characteristic ^{13}C-NMR signals (400 MHz, DMSO-d_6), δ (ppm): 176.76 (C=S); 151.84 (C=N); 162.02, 149.20, 135.95, 135.92, 127.59, 125.52 (6 aromatic carbon); 157.84, 121.13 (C=C of testosterone); 80.46 (C-OH).

3.3.3.2 Synthesis of complex nickel bis(testosterone-*N*^{4}-fluorophenylthiosemicarbazone), NF

Ethanol solution of nickel acetate (124 mg; 0.5 mmol; 10 ml) was added into a solution of **TF** (524 mg; 1 mmol; 10 ml) in ethanol and the mixture was refluxed for 30 minutes. Brownish green powder was formed and the mixture was filtered. Excess hot methanol was used to wash the green solid collected. Crystal of **NF** suitable for X-ray crystal structure analysis was crystallized from mixture of DMSO and methanol (ratio 3:8).

Yield: 53 %; Anal. Calc. for $C_{52}H_{68}F_2N_6NiO_2S_2{\cdot}2(C_2H_6OS)$: C, 59.72; H, 7.16; N, 7.46. Found: 60.05; H, 7.16; N, 7.74.; IR (KBr) cm^{-1}: 3302br (OH), 2932s (CH_3), 2872m (CH_2), 1603m (C=N), 768m (C-S), 433m (Ni-N) (br, broad; w, weak; m, medium; s, strong).

3.3.3.3 Synthesis of complex zinc bis(testosterone-*N*^{4}-fluorophenylthiosemicarbazone), ZF

Zinc acetate dihydrate (110 mg; 0.5 mmol) was dissolved in 10 ml of ethanol and refluxed with 10 ml of **TF** (524 mg; 1 mmol) for 30 minutes. Yellow solid was precipitated and filtered. Excess zinc acetate and ligand **TF** was then washed off with excess amount of hot ethanol and methanol. No crystal of **ZF** was collected and it can only be dissolved in solvents such as DMF and DMSO.

Yield: 47 %; Anal. Calc. for $C_{52}H_{66}F_2N_6O_2S_2Zn{\cdot}CH_3OH{\cdot}C_2H_5OH$: C, 62.75; H, 7.28; N, 7.98. Found: 62.97; H, 7.22; N, 7.74.; IR (KBr) cm^{-1}: 3264br (OH), 2936s (CH_3),

2853m (CH_2), 1610s (C=N), 766s (C-S), 435m (Zn-N) (br, broad; w, weak; m, medium; s, strong).

3.3.4 Synthesis of complex zinc bis(testosterone-*N*^{4}-ethylthiosemicarbazone), ZE

Testosterone (288 mg; 1 mmol) was dissolved in 10 ml ethanol and mixed with 10 ml ethanolic solution of 4-ethyl-3-thiosemicarbazone (119 mg; 1 mmol). The mixture was refluxed for 6 hours with continuous stirring, followed by addition of zinc acetate dehydrate (110 mg; 0.5 mmol; 10 ml ethanol) and further refluxed for 30 minutes. Pale yellow was formed and the solution was filtered. Excess hot ethanol was used to wash the solid collected. Crystal of **ZE** was crystallized from mixture of DMSO and methanol (ratio 3:8).

Yield: 56 %; Anal. Calc. for $C_{44}H_{72}N_6O_2S_2Zn{\cdot}C_2H_5OH$: C, 62.1; H, 8.39; N, 9.46. Found: 62.23; H, 8.69; N, 9.63.; IR (KBr) cm^{-1}: 3400br (OH), 2928s (CH_3), 2871m (CH_2), 1614m (C=N), 764m (C-S), 446m (Zn-N) (br, broad; w, weak; m, medium; s, strong).

3.4 X-ray crystallography

The solvent for crystallization of the compounds are: **TM** from ethanol; **NM** from DMF/methanol (3:8) mixture; **TP** from methanol; **TF** from ethanol; **NF** from DMSO/methanol (3:8) mixture; **ZE** from DMSO/methanol (3:8) mixture. The intensity data and unit cell parameters of the crystals obtained (**TM**, **NM**, **TP**, **TF**, **NF**, and **ZE**) were collected on a Bruker SMART APEX CCD diffractometer equipped with an APEX2 software was used for the data acquisition and the SAINT software for the cell refinement and data reduction. Absorption corrections on the data were made using SADABS. The structures were solved and refined using SHELXL97 (Sheldrick, 2008). Molecular graphics were drawn by using XSEED (Barbour, 2001). Material for publication was

prepared using PUBLCIF (Westrip, 2010). The structures were solved using direct-methods and refined by full-matrix least-squares procedures on F^2 with anisotropic displacement parameters for non-hydrogen atoms.

3.5 Cell culture

The human derived prostate adenocarcinomas PC-3 and LNCaP, human breast adenocarcinomas MCF7, human colorectal carcinomas HCT 116, human normal prostate RWPE-1, and normal colon fibroblasts CCD-18Co were purchased from American Type Cell Collection (ATCC, USA). The PC-3 and LNCaP were cultured in RPMI 1640 medium while MCF7 and CCD-18Co were cultured in EMEM. On the other hand, RWPE-1 was maintained in keratinocyte serum free medium supplied with bovine pituitary extract and human recombinant epidermal growth factor. Meanwhile, HCT 116 was cultured in McCoy's 5A medium. All media (except keratinocyte serum free medium) were supplemented with 10% fetal bovine serum, 2% penicillin/streptomycin (10×), and 1% amphotericin B. The cells were cultured at 37°C in CO_2 incubator and they were sub-cultured before reaching 80% confluency. Besides, the cells were maintained at low-passage number with their morphology observed from time to time.

3.6 MTT cytotoxicity assay

The MTT cytotoxicity assay was performed as described by Mosmann with modifications (Mosmann, 1983). All compounds were dissolved in DMSO to form stock solutions of 6 mM before the test. Briefly, cells were seeded into 96-well plate for 24 hours before treatment with compounds of various concentrations (range 0.1-30 μM). The final concentration of DMSO in each well was 0.5%. Untreated cells were used as negative controls. After 72 hours of incubation, 20 μL of MTT (5 mg/mL) was added into each well and further incubated for another three hours. The medium was then removed

and replaced with DMSO. Absorbance at 570 nm was measured using a microplate reader (Thermo Scientific Multiskan GO) with 650 nm as background. All the compounds were assayed in triplicate. Cisplatin was used as positive reference standard. IC_{50} value is the concentration of compounds or positive reference standard that inhibits 50% of the cells growth.

3.7 Calculation of selectivity index (SI)

Selectivity index (SI) was calculated by obtaining ratio of IC_{50} of normal cells over IC_{50} of cancer cells. In particular, $SI = \frac{IC_{50} \text{ of normal cells}}{IC_{50} \text{ of cancer cells}}$ (Peno-Moran et al., 2016).

3.8 Morphological assessment of apoptotic cells

Briefly, the cancer cells were seeded in 35 mm culture dish and supplemented with culture media (refer to Section **3.5** for choice of culture media). Cells in the absence or presence of test compounds (at their IC_{50}) were incubated at two different durations (24 and 48 hours) at 37°C. The culture dish was then removed from the incubator and cells were observed under Leica DMI 300B phase-contrast inverted microscope (Leica Microsystems, Germany) at 200× magnification and photographed.

3.9 Annexin V-FITC/PI double staining

The ability of the selected compounds to induce cell death on cancer cell line was evaluated by annexin V-FITC fluorescein isothiocyanate apoptosis detection kit (BD Biosciences, Pharmingen San Diego, CA, USA). Cells were seeded in 6-well plates (2.0×10^5 cells/well) and allowed to adhere overnight before treated with selected compounds (with their IC_{50} values) for 48 hours. The cells were then detached, washed with cold phosphate buffered saline (PBS) and stained with Annexin V-FITC conjugates with Propidium Iodide (PI). The cells were incubated for 15 minutes in dark before

analyzed using a BD FACS CantoII flow cytometer. A minimum of 10,000 events were recorded and evaluated (Navanesan et al., 2015).

3.10 Determination of mitochondrial membrane potential

Ability of the selected compounds to disrupt the mitochondrial membrane potential was assessed using the lipophilic cationic probe JC-1, according to the manufacturer's instruction (JC-1 MitoScreen Kit; BD Biosciences, Pharmingen San Diego, CA, USA). In brief, the cells were seeded into 6-well plates with the density of 2.0×10^5 cells/well. The cells were incubated for 24 hours prior to treatment with selected compounds (with their IC_{50}). The cells were harvested after 48 hours of treatment and incubated with JC-1 working solution for 15 minutes. The cells were then washed and resuspended in 1× assay buffer. The intracellular fluorescence signal intensity was measured using BD FACS CantoII flow cytometer (Wang et al., 2017).

3.11 Cell cycle analysis

The ability of selected compounds to cause cell cycle disruption was examined using BD Cycletest Plus DNA Reagent Kit (BD Biosciences, Pharmingen San Diego, CA, USA). Briefly, the cells were seeded into 6-well plates (2.0×10^5 cells/well) and cultured overnight before starvation in serum-free medium for 24 hours to be synchronized. Cells were then treated with the selected compounds (with their IC_{50}) for 48 hours harvested using kit. The PI stained nuclei were analyzed using the BD FACS CantoII flow cytometer. A minimum of 10,000 events were collected and the cell cycle data was analyzed using the ModFit software (Verify Software House, Topsham, ME, USA) (Navanesan et al., 2015; Gornowicz et al., 2017).

3.12 Statistical analysis

The IC_{50} values for cytotoxic activity were obtained from non-linear regression using GraphPad Prism statistical software. The data were expressed as mean ± standard deviation of triplicate experiments.

3.13 Interaction of the compounds with DNA

All experiments involving the compounds with DNA were done in 5 mM Tris-HCl/50 mM NaCl buffer (TN buffer, pH 7.5). A solution of CT-DNA in the buffer solution gave the ratio of UV absorbance at 260 and 280 nm (A_{260}/A_{280}) of about 1.75-1.90, indicating the DNA was sufficiently free from protein contamination (Loganathan et al., 2012). The concentration of DNA was determined spectrophotometrically by employing a molar absorption coefficient through monitoring the UV absorbance at 260 nm using ε_{260} = 6600 $mol^{-1}cm^{-2}$. The stock solution was stored at 4°C and used within four days. Spectrophotometric titration experiment was performed by keeping the compound concentration constant while varying the DNA concentration in the interaction medium. The absorption due to free CT-DNA was eliminated by adding equimolar CT-DNA to pure buffer solution in the reference compartment and the observed spectra were considered to be resulted from the compounds and DNA-complex aggregates. Titration curves were constructed from the fractional change in the absorption intensity as a function of DNA concentration. The intrinsic binding constant (K_b) was obtained by plotting [DNA]/(ε_a-ε_f) VS [DNA] according to the Wolfe-Shimmer equation as below:

$$\frac{[DNA]}{(\varepsilon_a - \varepsilon_f)} = \frac{[DNA]}{(\varepsilon_b - \varepsilon_f)} + \frac{1}{K_b(\varepsilon_b - \varepsilon_f)}$$

where [DNA] is the concentration of DNA in base pairs. The ε_a, ε_f, and ε_b are the apparent, free, and fully bound complex absorption coefficient (no absorption change despite further addition of DNA), respectively. In particular, ε_f was obtained from the calibration curve of the isolated ligand or metal complex according to the Beer's law. The ε_a was

determined as the ratio between measured absorbance and the ligand or complex concentration (A_{obs}/[complex]). The data obtained were fitted to the Wolfe-Shimmer equation above with a slope equal to $1/(\varepsilon_b-\varepsilon_f)$ and y-intercept equal to $1/[K_b(\varepsilon_b-\varepsilon_f)]$ and K_b was determined from the ratio of the slope to the intercept (Abdel-Rahman et al., 2014; Shahabadi & Maghsudi, 2014).

3.14 Molecular docking simulations

Molecular docking calculations of compounds with crystal structure (**TM**, **NM**, **TP**, **TF**, **NF**, and **ZE**) with DNA structure taken from Protein Data Bank (PDB) with PDB entry 1BNA and 1XRW (Suntharalingam et al., 2013; al-Rashida & Ahsen, 2015) were performed using AutoDock 4.2 software package (Huey et al., 2007; Morris et al., 2009). The graphical user interface Autodocktools 4.5.6 (ADT) was used to prepare the system. Gasteiger partial charges were assigned to both the receptor and ligands (Gasteiger & Marsili, 1980) and water molecules in 1BNA were removed. Hydrogen atoms were added. Autogrid 4.2 was used to calculate docking area of a grid box of 70 × 100 × 110 with grid spacing of 0.4 Å, which is sufficiently big to cover the whole DNA molecule as to make sure there is enough space to fit the receptor and also for free rotation of ligands (Xu et al., 2013). The ligands are therefore allowed to explore the whole conformation space. Docking experiment consisting of 100 simulations was performed for each compound, which were ranked in the order of increasing docking energy values and grouped in clusters of similar confirmation. Each docking run in this simulation consisted of 10 million energy evaluations using the Lamarckian genetic algorithm local search method. Otherwise default docking parameters were applied (Di Leva et al., 2014). The AutoDock scoring was performed based upon the estimated free energy of binding and includes the summation of the final intermolecular energy of docking, total internal energy, and the torsional free energy of the ligand, minus the system unbound energy

(Siddique et al., 2011). The 3D images of the DNA with docked ligands were rendered by UCSF Chimera Package (Pettersen et al., 2004).

3.15 *Escherichia coli* topoisomerase I inhibition assay

The *E. coli* topoisomerase I (topo I) inhibitory activity was examined by observing the degree of relaxation of supercoiled plasmid DNA, pBR322. The reaction mixtures for this assay consisted of 1× NE-buffer 4, 1× bovine serum albumin (BSA), 0.25 µg of plasmid pBR322, 0.25 units of *E. coli* topoisomerase I, and compounds of various concentrations (final concentration of 5, 10, 20, 40, 80, 160, 250, and 500 µM). All reactions were conducted at a final volume of 20 µL and were prepared on ice. The reaction mixtures were incubated at 37°C for 30 minutes upon addition of the enzyme. The reactions were halted by adding 2 µL of 10% sodium dodecyl sulfate (SDS), which prevents further functional enzymatic activity, followed by addition of 3 µL of 6× loading dye comprising of 0.03% bromophenol blue and 60% glycerol. The reaction mixtures were then loaded into 1.25% agarose gel and electrophoresed for three hours at 50 V with Tris-acetate-EDTA (TAE, pH 8.1) as running buffer. The gel was stained with ethidium bromide solution of 0.5 µg/ml, de-stained, and photographed under UV light using an Alphaimager red gel documentation system and the digital image was viewed using Pronto software.

CHAPTER 4: RESULTS AND DISCUSSION

4.1 Syntheses of ligands and their metal complexes

The Schiff base ligands were synthesized as products from condensation of testosterone with derivatives of thiosemicarbazide. Their nickel (II) and zinc (II) complexes were then prepared, as described in the experimental section.

The general formula of thiosemicarbazones is depicted in Figure 4.1. Thiosemicarbazide represents the simplest hydrazine derivative of thiocarbamic acid, where all the R groups are hydrogen atoms. When R_5 is replaced by a methyl group, the structure is known as 4-methyl-3-thiosemicarbazide. Similarly, 4-(4-fluorophenyl)-3-thiosemicarbazide and 4-(4-ethylphenyl)-3-thiosemicarbazide are formed by replacing R_5 with a fluorophenyl and an ethylphenyl group, respectively. Although the structures of these derivatives are similar (except R_5), the inductive effect of these substituents may dictate the chemical properties of these thiosemicarbazides and eventually the thiosemicarbazones formed. With thiosemicarbazide (R_5 = H) as the relatively neutral species, the presence of methyl group, which is an electron-donating substituent, leads to increase in electron density on the azomethine group which hinders the deprotonation and increases the basicity of the ligands formed. When an ethyl group is attached to the phenyl group (in the case of 4-(4-ethylphenyl)-3-thiosemicarbzide), this electron donating group would increase the electron density of the conjugated π-system, making it more susceptible to electrophilic attack and therefore more basic. In contrast, an electron withdrawing fluoro group in 4-(4-fluorophenyl)-3-thiosemicarbazide will removes electron density from the π-system, deactivate it from electrophilic attack and rendered it more acidic (Bader & Chang, 1989; Al-Hazmi et al., 2005; Liu, 2014).

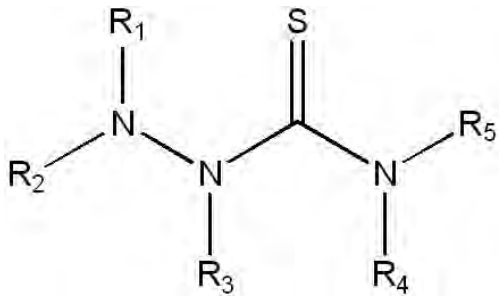

Figure 4.1: General formula of thiosemicarbazones, where R_1, R_2, R_3, R_4, R_5 = H or any organic substituent.

Thiosemicarbazides are readily interconverted constitutional isomers with a labile hydrogen atom and a double bond that can be rearranged in a tautomerization process. The thione tautomer has been observed regularly in their solid state structures but thiol tautomer is generally regarded as the one with extended conjugation and thermodynamic stability. The tautomers of thiosemicarbazones are depicted in Figure 4.2 (Pan et al., 2014; Hussain et al., 2017).

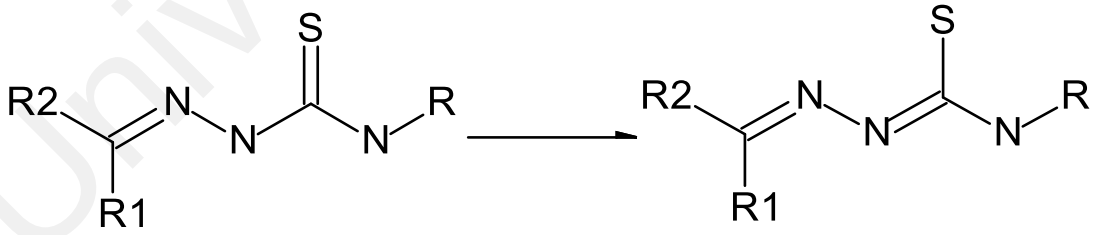

thione tautomer thiol tautomer

Figure 4.2: General structure showing thione and thiol tautomers of thiosemicarbazone.

4.1.1 TM and its metal complexes NM and ZM

Schiff base ligand **TM** was synthesized and isolated as pale yellow crystal from slow evaporation of ethanolic solution of **TM**. It is water insoluble, but soluble in organic solvents such as methanol, ethanol, chloroform, and DMF. The nickel (II) complex **NM** was collected as green powder after refluxing nickel acetate with **TM** in boiling ethanol. On the other hand, zinc (II) complex **ZM** was precipitated as pale yellow powder upon addition of zinc acetate into boiling ethanolic solution of **TM**. Attempt to isolate the crystals of **ZM** are futile. Unlike their parent ligand, nickel (II) complex **NM** is only soluble in DMF and DMSO, while the zinc (II) complex **ZM** can only be dissolved in DMSO.

Both **NM** and **ZM** can be prepared from one pot synthesis as well. Mixture of testosterone and thiosemicarbazide was refluxed in boiling ethanol for 6 hours before the addition of ethanolic solution of nickel acetate or zinc acetate. **NM** and **ZM** were collected from precipitation of green and pale yellow powder, respectively.

4.1.2 TP and its metal complexes NP and ZP

Schiff base ligand **TP** was prepared with method similar to that of **TM**, with the choice of thiosemicarbazide being the main difference in between the two ligands. **TP** was synthesized by refluxing testosterone and 4-(4-ethylphenyl)-3-thiosemicarbazide for 6 hours. Solid collected from evaporation of ethanol was collected and re-dissolved in methanol. Pale yellow crystal was collected from evaporation of methanol at room temperature. Similar to **TM**, **TP** is soluble is various organic solvent such as methanol, ethanol, chloroform, DMF, and DMSO.

The nickel (II) complex **NP** was collected as brownish green solid, precipitated immediately with the addition of nickel acetate with **TP** in ethanol. Meanwhile, the zinc (II) complex **ZP** was collected as pale yellow solid precipitated from refluxing zinc

acetate with **TP**. Both **NP** and **ZP** are insoluble in water and can be dissolved in organic solvents such as DMF and DMSO. The attempts to harvest crystals of **NP** and **ZP** that are suitable for X-ray crystallography were unsuccessful.

4.1.3 TF and its metal complexes NF and ZF

Schiff base ligand **TF** was prepared from condensation of testosterone with 4-(4-fluorophenyl)-3-thiosemicarbazide and the yellow solid collected was washed and re-dissolved in ethanol. Yellow crystal was collected from evaporation of ethanol. **TF** is soluble in organic solvents such as methanol, ethanol, chloroform, DMF, and DMSO.

Nickel (II) complex **NF** was collected as brownish green powder from addition of ethanolic solution of nickel acetate into **TF** in boiling ethanol. It was then re-dissolved in mixture of DMSO and methanol, and crystal was collected from slow evaporation of the solvent. The zinc (II) complex **ZF** was prepared in similar fashion but it was collected as yellow solid after refluxing **TF** with zinc acetate (instead of nickel acetate) for 30 minutes. No crystal of **ZF** was collected. Both complexes are soluble in DMF and DMSO.

4.1.4 Zinc complex ZE

The zinc complex **ZE** was included for comparison, due to the absence of crystal structures of other zinc complexes (**ZM**, **ZP**, and **ZF)** and it was prepared through one-pot synthesis. At first, testosterone was refluxed with 4-ethyl-3-thiosemicarbazide to form a Schiff base ligand testosterone-N^4-ethylthiosemicaarbazone (**TE**). Ethanolic solution of zinc acetate dehydrate was then added into the yellow solution. Yellow crystal was formed and collected. It was then re-dissolved in mixture of DMSO and methanol, and crystal was collected from slow evaporation of the solvent. **ZE** is soluble in DMF and DMSO.

4.2 Infrared spectra

The main FTIR vibrational bands of all the Schiff base ligands and their metal complexes were found in their expected regions. Their characteristic IR bands were listed in the experimental section and in Table 4.1.

Table 4.1: Characteristic FTIR vibrational bands of all the Schiff base ligands and their metal complexes.

Compound	FTIR vibrational band (cm^{-1})			
	C=N	C-S	C=S	Metal-N
TM	1617	-	1062	-
NM	1612	783	-	445
ZM	1613	780	-	442
TP	1626	-	1064	-
NP	1611	786	-	439
ZP	1613	771	-	439
TF	1621	-	1067	-
NF	1603	768	-	433
ZF	1610	766	-	435
ZE	1614	764	-	446

Condensation of testosterone was proven by the disappearance of parent band at 1657 cm^{-1}, which is originally attributed to the stretching vibrations of aldehyde ν(C=O) of testosterone (El-Bahy, 2005). The emergence of a strong band ascribed to azomethine linkage ν(C=N) at 1617, 1626, and 1621 cm^{-1}, respectively, further confirmed the formation of Schiff base ligands **TM**, **TP**, and **TF** (Teoh et al., 1999; Fatondji et al., 2013).

In the spectra of metal complexes, the band due to azomethine linkage ν(C=N) was shifted to lower frequency, which is due to the shift of lone pair density towards the metal ion center (Yeginer et al., 2017). Besides, the presence of a weak new band at the region of 433-445 cm^{-1} in the spectra of all the metal complexes might be due to the formation of metal-N linkage (Afrasiabi et al., 2005). Apart from that, another band appeared at the region of 766-786 cm^{-1} suggested the emergence of C-S stretching, and the coordination

through the thiolate sulfur of the ligand (Prabhakaran et al., 2011). The observations cumulatively supported the successful synthesis of metal complexes.

4.3 ^{1}H-NMR and ^{13}C-NMR

The ^{1}H and ^{13}C-NMR spectra can be used to deduce the structural information of the Schiff base ligands. The characteristic ^{1}H and ^{13}C-NMR chemical shift data are tabulated in Table 4.2 and 4.3, respectively. The previously reported Schiff base ligand testosterone-N^4-thiosemicarbazone (**TT**) was included for comparison (Heng et al., 2015).

Table 4.2: Characteristic ^{1}H-NMR data (ppm) of ligands in DMSO-d_6.

Name	NMR signal (ppm)				
	N-H	O-H	terminal CH_3 of thiosemicarbazide	Aromatic CH	4 CH, 8 CH_2, and 2 CH_3 of testosterone
TM	10.04 8.39	4.48	2.96	-	3.43-0.67
TP	10.04 9.75	4.48	1.21	7.50, 7.49 7.16, 7.14	3.44-0.67
TF	10.50 9.87	4.48	-	7.58, 7.57 7.17, 7.15	3.44-0.67
TT	10.05 8.04	4.46	-	-	3.44-0.67

Table 4.3: Characteristic ^{13}C-NMR data (ppm) of ligands in DMSO-d_6.

Name	NMR signal (ppm)					
	C=S	C=N	C-OH	Terminal CH_3	Aromatic CH	C=C
TM	178.63	150.66	80.40	17.44	-	156.77, 121.13
TP	176.36	151.58	80.46	16.19	161.93, 148.94, 140.94, 140.90, 127.85, 125.27	157.72, 121.16
TF	176.76	151.84	80.46	-	162.02, 149.20, 135.95, 135.92 127.59, 125.52	157.84, 121.13
TT	178.7	151.0	80.4	-	-	157.1, 121.1

The hydroxyl group of testosterone, which is susceptible to chemical reaction, was preserved as signal at 4.48 ppm was observed in the spectra of all ligands (Havaldar & Patil, 2008). Chemical shifts corresponding to the aromatic protons of **TP** and **TF** were found at their expected region, thereby confirming the formation of the proposed Schiff base. Besides, the proton of -NH group next to the terminal CH_3 of thiosemicarbazide in **TM** was observed at 8.39 ppm, while the one next to the phenyl group of **TP** and **TF** were found at 9.75 and 9.87 ppm, respectively (Gasser et al., 2011).

The chemical shift at the region of 150.66-151.84 ppm in the ^{13}C-NMR was assigned to the azomethine C=N linkage of the ligands synthesized, which indicates the formation of Schiff base (Choi et al., 1999). Furthermore, the involvement of C-O and C=C groups in the formation of new compounds was ruled out due to the presence of chemical shifts ascribed to the three carbons of C-O and C=C were observed in the spectra (Reich et al., 1969; Biersack et al., 2011). Apart from that, the chemical shifts due to the aromatic carbon atoms of **TP** and **TF** were recorded at their expected region, further confirming the formation of the proposed compounds.

4.4 Elemental analysis

The elemental contents such as carbon, hydrogen, and nitrogen are undoubtedly one of the most important fundamental information regarding the compounds synthesized. Generally, the errors of less than or equal to 0.4% reflect high accuracy and/or high purity of the analytes (Itoh et al., 2013). The relative percentage (experimental and theoretical) of these three elements in all the compounds synthesized are summarized in Table 4.4.

Table 4.4: Elemental analysis of all the compounds synthesized

Name	Found (%)			Calculated (%)			Solvent molecule
	Carbon	Hydrogen	Nitrogen	Carbon	Hydrogen	Nitrogen	
TM	65.62	9.42	9.78	65.52 (-0.10)	9.32 (-0.10)	9.97 (0.19)	ethanol
NM	59.70	8.40	9.59	59.78 (0.08)	8.12 (-0.28)	9.96 (0.37)	2 water
ZM	61.47	8.09	10.15	61.41 (-0.06)	8.20 (0.11)	9.77 (0.38)	ethanol
TP	68.21	8.68	8.62	68.25 (0.04)	8.59 (0.09)	8.53 (0.09)	1.5 water
NP	66.03	7.94	7.59	66.21 (0.18)	8.05 (0.11)	7.99 (0.40)	2 methanol
ZP	65.76	7.97	7.65	65.79 (0.03)	8.00 (0.03)	7.94 (0.29)	2 methanol
TF	66.39	8.00	7.82	66.38 (-0.01)	8.26 (0.26)	8.01 (0.19)	1.5 ethanol
NF	60.05	7.16	7.74	59.72 (-0.33)	7.16 (0.00)	7.46 (-0.28)	2 DMSO
ZF	62.97	7.22	7.74	62.75 (-0.22)	7.28 (0.06)	7.98 (0.24)	methanol, ethanol
ZE	62.23	8.69	9.63	62.17 (0.06)	8.39 (0.30)	9.46 (0.17)	ethanol

Results in Table 4.4 showed differences of less than 0.4% in between the experimental and calculated relative percentage of carbon, hydrogen, and nitrogen. This indicates the compounds synthesized and isolated are of high purity.

4.5 Crystal structure of ligands and complexes

Crystals of Schiff bases **TM**, **TP**, **TF**, and the nickel complexes **NM**, and **NF** were collected and the details of crystallographic data and structure refinement parameters are summarized in Table 4.5 and 4.6. The attempts to isolate crystals of **NP** and all the zinc complexes (**ZM**, **ZP**, and **ZF**) were unsuccessful. Crystal structure of **ZE** was collected and included in Table 4.6 for comparison.

Table 4.5: Crystal data and structure refinement parameters for **TM**, **TP**, and **TF**.

Compound	**TM**	**TP**	**TF**
Empirical formula	$C_{23}H_{33}N_3OS \cdot C_2H_5OH$	$C_{28}H_{39}N_3OS \cdot 2.5(CH_3OH)$	$C_{26}H_{34}FN_3OS \cdot H_2O$
Formula weight	421.63	545.78	473.64
Crystal system	Monoclinic	Monoclinic	Orthorhombic
Space group	$P2_1$	$P2_1$	$P2_12_12_1$
Unit cell dimensions			
a (Å)	8.3094(6)	12.3361(3)	7.5066(3)
b (Å)	15.2118(9)	35.9867(12)	13.8181(11)
c (Å)	19.0762(11)	13.8567(17)	48.3281(18)
α (º)	90.00	90.00	90.00
β (º)	100.972 (6)	90.055(3)	90.00
γ (º)	90.00	90.00	90.00
V (Å^3)	2367.2(3)	6151.5(3)	5012.9(5)
Z	4	8	8
F(000)	920	2376	2032
D_x (Mg m^{-3})	1.183	1.179	1.255
T (K)	100	100	100
Absorption coefficient, μ (mm^{-1})	0.16	0.14	1.43
θ ranges (º)	2.86-27.56	3.37-27.40	3.7-74.68
Reflections collected	15893	66290	14562
Independent reflections	8713	28050	9040
Data/Restraints/Parameters	8713/37/533	28050/1356/199	9040/12/598
Range of *h, k, l*	-10/10, -18/19, -24/24	-16/15, -46/46, -18/18	-9/6,-16/17,-27/59
Goodness-of-fit on F^2	1.089	1.022	1.048
$R[F^2 > 2\sigma(F^2)]$	0.081	0.072	0.075
wR(F^2)	0.190	0.176	0.227

Table 4.6: Crystal data and structure refinement parameters for **NM**, **NF**, and **ZE**.

Compound	**NM**	**NF**	**ZE**
Empirical formula	$C_{42}H_{64}N_6NiO_2S_2 \cdot CH_3OH \cdot H_2O$	$C_{52}H_{68}F_2N_6NiO_2S_2 \cdot 2(C_2H_6OS)$	$Zn(C_{22}H_{34}N_3OS)_2$
Formula weight	857.88	1126.21	842.53
Crystal system	Orthorhombic	Monoclinic	Triclinic
Space group	$P2_12_12_1$	$P2_1$	P1
Unit cell dimensions			
a (Å)	7.9838(2)	8.5375(7)	8.8798(11)
b (Å)	14.5069(4)	31.403(3)	10.6513(13)
c (Å)	37.0524(12)	10.8302(9)	14.2422(18)
α (º)	90.00	90.00	97.97(10)
β (º)	90.00	97.00(9)	106.13(11)
γ (º)	90.00	90.00	114.62(12)
V (Å^3)	4291.4(2)	2881.94	1125.4(2)
Z	4	2	1
F(000)	1848	1200	452
D_x (Mg m^{-3})	1.328	1.298	1.243
T (K)	100	100	100
Absorption coefficient, μ (mm^{-1})	1.95	2.29	0.68
θ ranges (º)	3.9-74.34	4.1-76.9	3.0-27.6
Reflections collected	11271	14229	9515
Independent reflections	7324	8384	6751
Data/Restraints/Parameters	7324/8/528	8384/337/661	6751/3/499
Range of *h, k, l*	-9/5, -17/16, -31/46	-9/10,-25/39,-13/13	-11/11,-13/13,-18/18
Goodness-of-fit on F^2	1.065	1.114	1.393
$R[F^2 > 2\sigma(F^2)]$	0.043	0.099	0.100
wR(F^2)	0.118	0.206	0.249

4.5.1 Crystal structure of ligand testosterone-N^4-methylthiosemicarbazone, TM

The Schiff base ligand **TM** was crystallized in monoclinic system with $P2_1$ space group and the perspective view of this compound is shown in Figure 4.3.

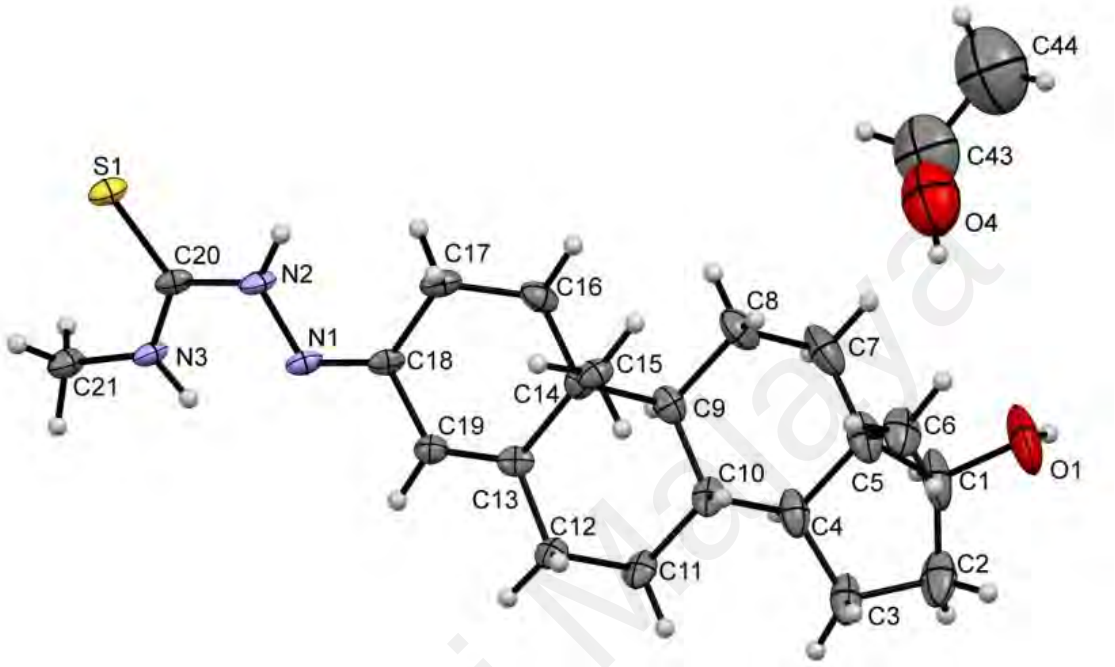

Figure 4.3: Ortep plot of **TM** drawn at 50% probability level. Hydrogen atoms are drawn at arbitrary radii.

From the perspective view of **TM** (Figure 4.3), it is obvious that a testosterone molecule was joined to the molecule of 4-methyl-3-thiosemicarbazide through the formation of a new imine bond (C18-N1), and the resulting compound adopted an *E* configuration. Its bond lengths and angles are within normal ranges. Selected bond lengths and angles of **TM** are shown in Table 4.7, while the details of hydrogen bonds are tabulated in Table 4.8.

Table 4.7: Selected bond lengths and bond angles of **TM**.

Bond lengths (Å)		Bond angles (°)	
N1-C18	1.288 (5)	C18-N1-N2	117.9 (4)
N1-N2	1.390 (5)	N1-N2-C20	117.2 (4)
N2-C20	1.362 (6)	N2-C20-N3	116.6 (4)
C20-S1	1.691 (5)	N2-C20-S1	119.6 (3)
C20-N3	1.326 (6)	N3-C20-S1	123.8 (4)
C21-N3	1.449 (6)		
C18-C19	1.466 (6)		

Table 4.8: Hydrogen bonds of **TM**.

D─H···*A*	D─H (Å)	H···*A* (Å)	D···*A* (Å)	D─H···*A* (°)
O1─H1O···O3	0.84	2.04	2.652 (9)	129
O2─H2O···O1	0.84	1.95	2.736 (8)	156
O3─H3O···O1	0.84	1.89	2.652 (9)	150
O4─H4O···O3	0.84	2.02	2.613 (11)	127
Symmetry operation (i): x, y, z				
Symmetry operation (ii): -x, 1/2+y, -z				

By referring to information in Table 4.7, the azomethine linkage (C=N double bond) can be confirmed by the shorter bond length in between carbon and nitrogen atom (1.288 Å for C18-N1; 1.449 Å for C21-N3). The hydroxyl group of molecule **TM** serves as a hydrogen-bond donor to ethanol molecule. As shown in Figure 4.4, hydrogen bonds of the type O─H···O linked molecules of **TM** and ethanol into a linear chain in which all molecules having the same orientation (Imramovský et al., 2012).

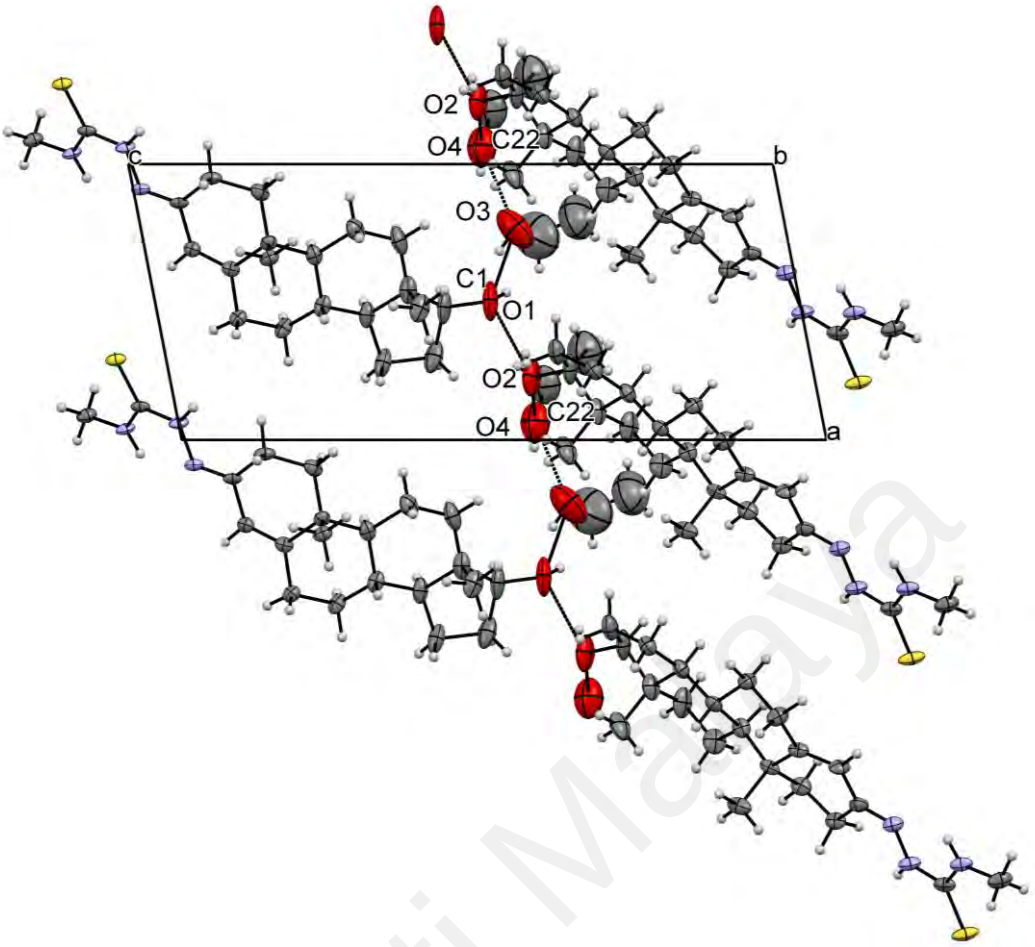

Figure 4.4: Linear chain formed from hydrogen bonds of the type O─H···O link **TM** and ethanol molecules.

4.5.2 Crystal structure of complex nickel bis(testosterone-N^4-methylthiosemicarbazone), NM

The nickel complex **NM** was synthesized by joining two ligands **TM** to a nickel metal center ion and it was crystallized in an orthorhombic crystal system, with the space group of $P2_12_12_1$. The perspective view of this complex is illustrated in Figure 4.5.

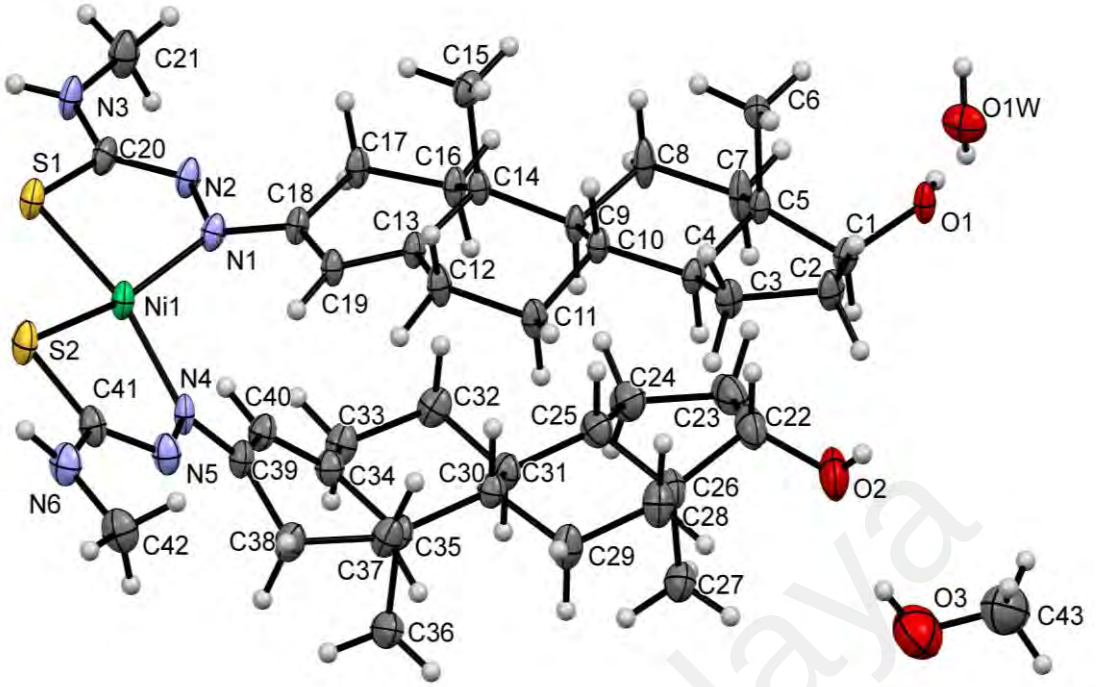

Figure 4.5: Ortep plot of **NM** drawn at 50% probability level. Hydrogen atoms are drawn at arbitrary radii.

It is clearly shown that the mononuclear nickel complex is coordinated to two Schiff base ligands **TM** *via* two imine nitrogens and two tautomeric thiosulfurs. Selected bond lengths and angles of **NM** are listed in Table 4.9, while hydrogen bonds are included in Table 4.10.

Table 4.9: Selected bond lengths and bond angles of **NM**.

Bond lengths (Å)		Bond angles (°)	
Ni1-S1	2.154 (12)	S1-Ni1-N1	86.22 (11)
Ni1-S2	2.162 (12)	S2-Ni1-N4	86.69 (10)
Ni1-N1	1.933 (4)	S1-Ni1-S2	89.38 (5)
Ni1-N4	1.943 (4)	N1-Ni1-N4	101.51 (14)
S1-C20	1.754 (5)	Ni1-N1-C18	128.3 (3)
S2-C41	1.757 (5)	Ni1-N4-C39	128.8 (3)
N1-C18	1.312 (5)		
N4-C39	1.292 (5)		
N1-N2	1.403 (5)		
N4-N5	1.398 (5)		
N2-C20	1.307 (6)		
N5-C41	1.297 (6)		
N3-C21	1.444 (6)		
N6-C42	1.456 (6)		

Table 4.10: Hydrogen bonds of **NM**.

D─H···*A*	D─H (Å)	H···*A* (Å)	D···*A* (Å)	D─H···*A* (°)
O1─H1···O1*W*	0.84 (1)	1.84 (1)	2.674 (4)	175 (6)
O2─H2···S2^{i}	0.84 (1)	2.45 (2)	3.277 (4)	168 (7)
O3─H3···O2	0.86 (1)	1.92 (3)	2.748 (7)	162 (10)
O1*W*─H11···S1^{i}	0.83 (1)	2.51 (2)	3.343 (4)	175 (5)
O1*W*─H12···O1^{ii}	0.83 (1)	1.96 (2)	2.789 (5)	172 (6)
N3─H3*N*···O1^{iii}	0.88 (1)	2.11 (3)	2.929 (4)	156 (5)
Symmetry operation (i): x, y-1, z				
Symmetry operation (ii): x+1/2, -y+1/2, -z+2				
Symmetry operation (iii): x+1, y+1, z				

Information in Table 4.9 shows that the bite angle for S1-Ni1-N1 and S2-Ni1-N4 are 86.22 (11) and 86.69 (10)°, respectively. These angles are deviated from the ideal 90.00° and thereby reflecting the distorted square planar geometry with cis configuration (Meghdadi et al., 2015). The observed Ni-N bonds are shorter (Ni1-N1, 1.933 (4) Å; Ni1-N4, 1.943 (4) Å) compared with Ni-S bonds (Ni1-S1, 2.154 (12) Å; Ni1-S2, 2.162 (12) Å), which is due to the strong π-interaction between nickel and imine nitrogen (Prabhakaran et al., 2011). Apart from that, Figure 4.5 shows the imine nitrogens and tautomeric thiosulfurs (S1 with N1, and S2 with N4 in **NM**) were rotated to cis-

confirmation during the formation of the nickel complex **NM** (S1 was cis to N1 in **TM**, Figure 4.3).

The bond distances for S1-C20 and S2-C41 are 1.754 (5) and 1.757 (5) Å respectively. These are longer compared with the C20-S1 bond of its parent ligand **TM** (1.691 (5) Å). This indicates the ligands are bound to the nickel atom in the thiolate form (C-S-Ni). Besides, new C=N bonds were formed upon tautomerization, which can be deduced based on the changes in bond length. For instance, the bond distances for C20-N2 and C41-N5 are 1.307 (6) and 1.297 (6) Å respectively, which are shorter compared to the one in its parent ligand (N2-C20 = 1.362 (6) Å, Table 4.7), thereby reflecting the formation of C=N bonds (Md Yusof et al., 2015; Schmidt et al., 2016). A parallel sheet is formed *via* hydrogen bonds of the type O1─H1···O1*W*, O2─H2···S2, O3─H3···O2, O1*W*─H11···S1, O1*W*─H12···O1, and N3─H3*N*···O1 that link molecules of **NM**, water, and methanol, as shown in Figure 4.6.

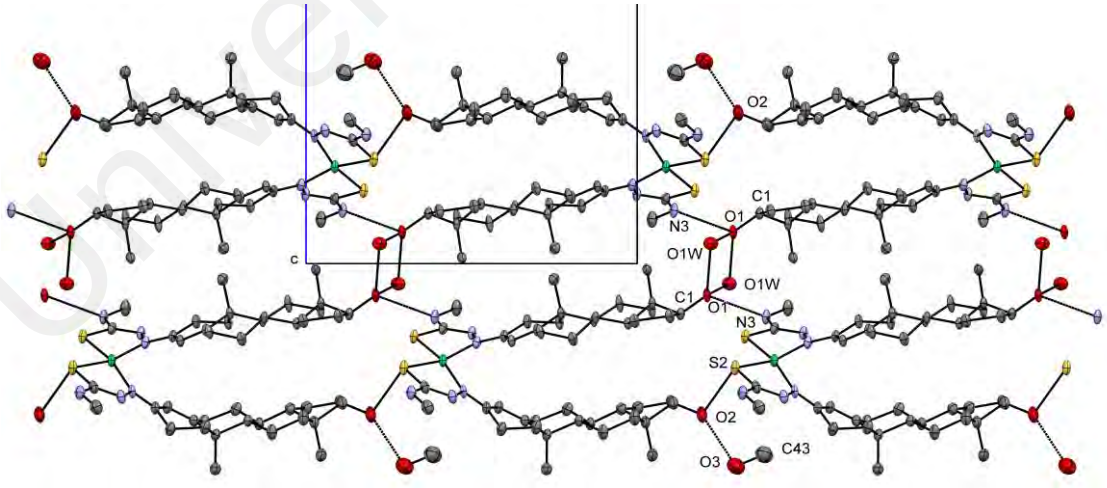

Figure 4.6: Parallel sheet formed from hydrogen bonds the type O1─H1···O1*W*, O2─H2···S2, O3─H3···O2, O1*W*─H11···S1, O1*W*─H12···O1, and N3─H3*N*···O1 of complex **NM**, water, and methanol (hydrogen atoms are omitted for clarity).

4.5.3 Crystal structure of ligand testosterone-N^4-ethylphenylthiosemicarbazone, TP

Schiff base ligand **TP** was synthesized by conjugating testosterone to 4-(4-ethylphenyl)-3-thiosemicarbazide. It was crystallized in a monoclinic system with the space group of $P2_1$, and the Ortep plot of this ligand with atom numbering scheme is given in Figure 4.7.

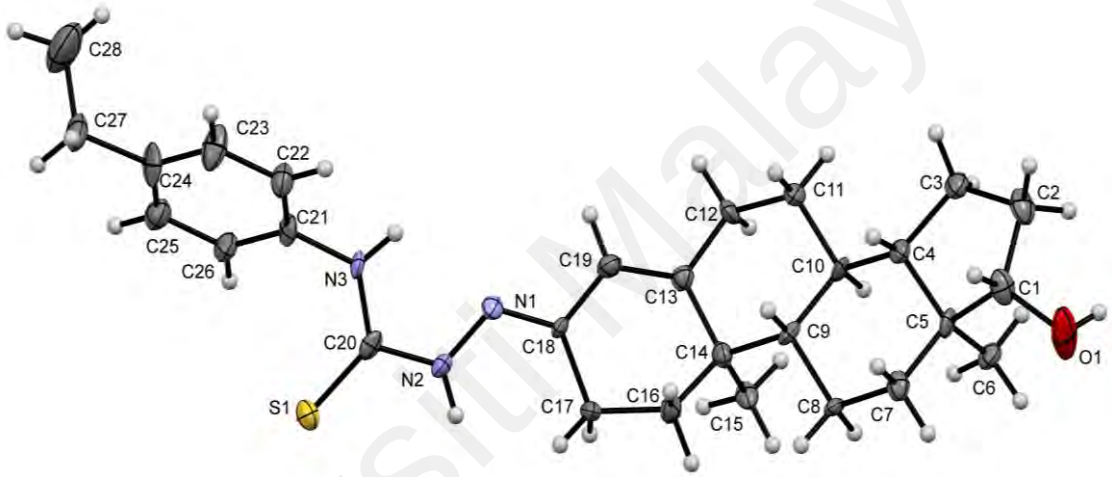

Figure 4.7: Ortep plot of **TP** drawn at 50% probability level. Hydrogen atoms are drawn at arbitrary radii.

Figure 4.7 shows that a molecule of testosterone was successfully joined to a molecule of 4-(4-ethylphenyl)-3-thiosemicarbazide through the formation of a new azomethine linkage (C18-N1) and it adopted an *E* conformation. Characteristic bond lengths and angles are summarized in Table 4.11.

Table 4.11: Selected bond lengths and bond angles of **TP**.

Bond lengths (Å)		Bond angles (°)	
N1-C18	1.293 (9)	N1-N2-C20	119.5 (6)
N1-N2	1.386 (9)	C18-N1-N2	119.5 (6)
N2-C20	1.353 (10)	N2-C20-N3	114.9 (7)
N3-C20	1.383 (10)	N2-C20-S1	119.9 (6)
S1-C20	1662 (9)	N3-C20-S1	125.2 (6)
N3-C21	1.420 (6)		
C18-C19	1.430 (10)		
C17-C18	1.525 (10)		

Information in Table 4.8 shows the lengths and angles of the characteristic bonds of **TP** are within normal ranges. The formation of imine linkage is confirmed with the shorter bond length of N1-C18 (1.293 (9) Å) compared to that of N2-C20 (1.353 (10) Å) or N3-C21 (1.420 (6) Å). Besides, the details of hydrogen bonds are presented in Table 4.12.

Table 4.12: Hydrogen bonds of **TP**.

D─H···*A*	D─H (Å)	H···*A* (Å)	D···*A* (Å)	D─H···*A* (°)
O1─H1o···O5	0.84 (2)	2.01 (8)	2.76 (1)	148 (14)
O5─H5o···O6	0.84	2.09	2.73 (1)	133
O6─H6o···O2	0.84	2.19	2.73 (1)	121
O2─H2o···O7	0.84 (1)	1.90 (4)	2.71 (1)	121
O7─H7o···O8	0.84	1.90	2.67 (1)	151
O8─H8o···O9	0.84	1.98	2.62 (2)	132
O9─H9o···O1	0.84	2.05	2.50 (1)	113
O3─H3o···O10	0.84 (2)	1.92 (5)	2.72 (1)	158 (12)
O10─H10o···O11	0.84	2.01	2.73 (1)	143
O211─H11o···O4	0.84	2.03	2.68 (1)	135
O4─H4o···O12	0.84 (2)	1.86 (4)	2.67 (1)	162 (10)
O12─H12o···O13	0.84	1.84	2.62 (1)	153
O13─H13o···O14	0.84	1.99	2.43 (2)	111
O14─H14o···O3	0.84	1.84	2.58	147
Symmetry operation (i): x, y, z				
Symmetry operation (ii): -x, y+1/2, -z				

Ligand **TP** was solvated by molecules of methanol. Methanol clusters were formed from hydrogen bonds listed in Table 4.12 linked molecules of **TP** and methanol. Oxygen atoms from five methanol molecules were connected to two oxygen from two molecules of **TP**, forming a heptagon that linked these molecules. Structure of the methanol clusters are depicted in Figure 4.8.

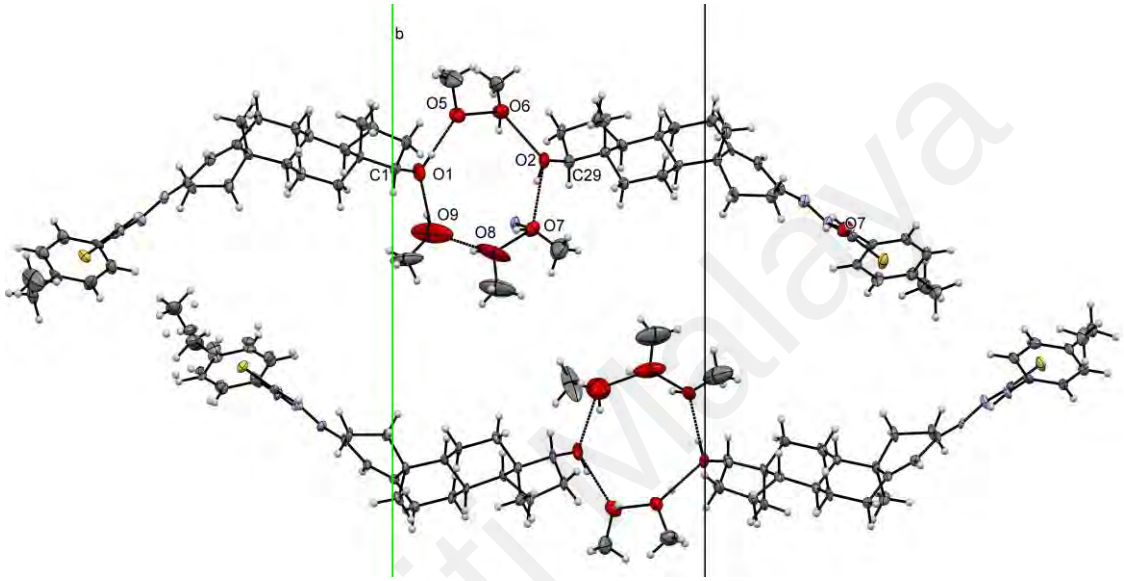

Figure 4.8: Methanol clusters formed from hydrogen bonds that linked molecules of complex **TP** and methanol.

4.5.4 Crystal structure of ligand testosterone-N^4-fluorophenylthiosemicarbazone, TF

The Schiff base ligand **TF** was crystallized in monoclinic system with $P2_12_12_1$ space group and it was solvated by a water molecule. Ortep plot of this compound is displayed in Figure 4.9.

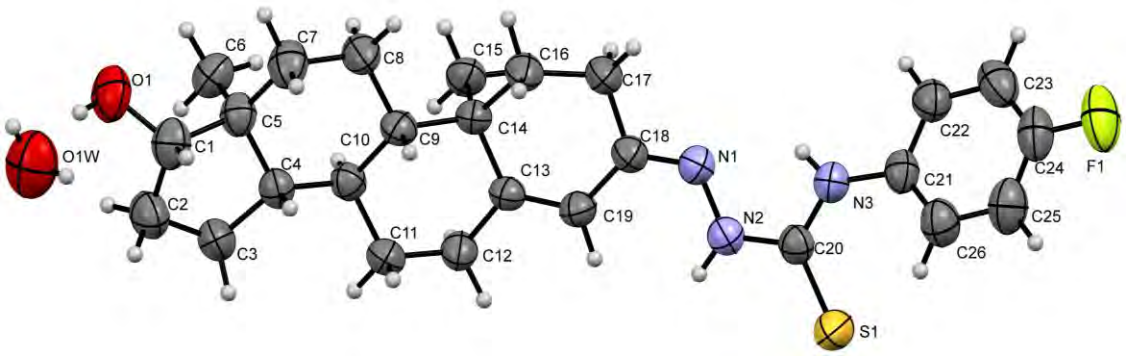

Figure 4.9: Ortep plot of **TF** drawn at 50% probability level. Hydrogen atoms are drawn at arbitrary radii.

Figure 4.9 shows that a molecule of testosterone was successfully joined to a molecule of 4-(4-ethylphenyl)-3-thiosemicarbazide through the formation of a new azomethine linkage (C18-N1). Unlike other Schiff base ligands mentioned before, **TF** adopted a *Z* configuration. Characteristic bond lengths and angles are summarized in Table 4.13 and information of selected hydrogen bonds are tabulated in Table 4.14.

Table 4.13: Selected bond lengths and bond angles of **TF**.

Bond lengths (Å)		Bond angles (°)	
N1-C18	1.289 (6)	N1-N2-C20	117.5 (5)
N1-N2	1.379 (6)	C18-N1-N2	119.5 (5)
N2-C20	1.349 (6)	N2-C20-N3	115.7 (5)
N3-C20	1.341 (8)	N2-C20-S1	118.9 (4)
S1-C20	1.680 (6)	N3-C20-S1	125.4 (4)
N3-C21	1.396 (7)		
C18-C19	1.450 (8)		
C17-C18	1.490 (8)		

Table 4.14: Hydrogen bonds of **TF**.

D—H···*A*	D—H (Å)	H···*A* (Å)	D···*A* (Å)	D—H···*A* (°)
O1—H1O···O1*W*	0.84	2.08	2.889 (9)	162
O2—H2O···O1*W*^{i}	0.84	2.04	2.836 (10)	157
O1*W*—H11···O2*W*^{ii}	0.84	2.03	2.812 (10)	156
O2*W*—H21···O2	0.84	1.98	2.814 (10)	172
O2*W*—H22···O1^{iii}	0.84	2.21	2.933 (10)	144
Symmetry operation (i): -x+3/2, -y+1, z-1/2				
Symmetry operation (ii): -x+1, y+1/2, -z+3/2				
Symmetry operation (iii): -x+1/2, -y+1, z-1/2				

TF was solvated by water molecule and these solvent molecules linked molecules of **TF** to form a linear chain with hydrogen bonds of O2-H20···O1, O2*W*-H21···O2, and O2-H20···O1*W*. The structure was depicted in Figure 4.10.

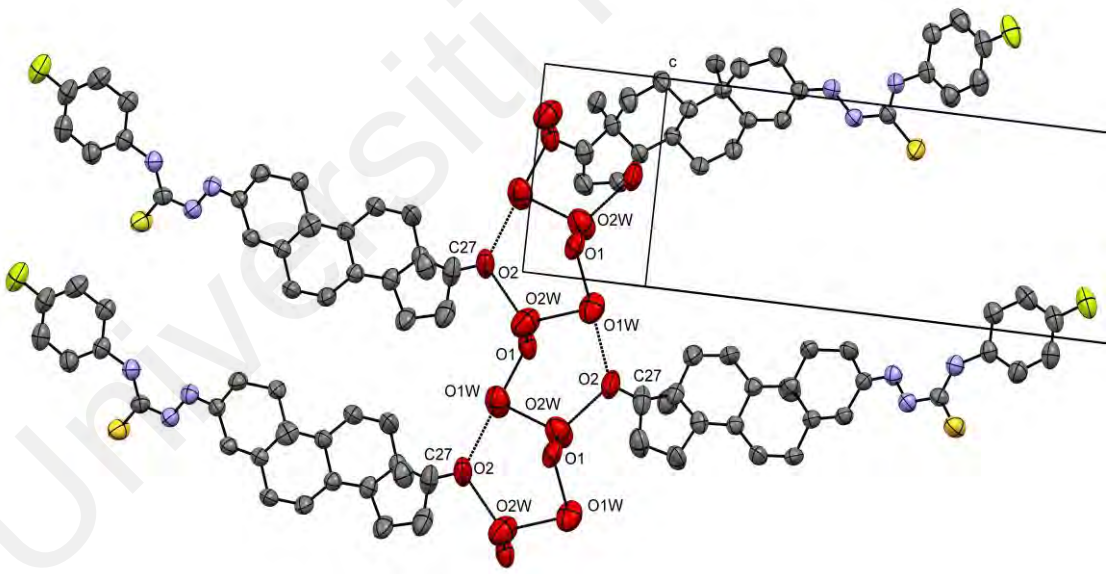

Figure 4.10: Helical chain formed from hydrogen bonds link **TF** and water molecules (hydrogen atoms are omitted for clarity).

4.5.5 Crystal structure of complex nickel bis(testosterone-N^4-fluorophenylthiosemicarbazone), NF

The Schiff base ligand **NF** was crystallized in monoclinic system, with the space group of $P2_1$, and the perspective view of this compound is shown in Figure 4.11.

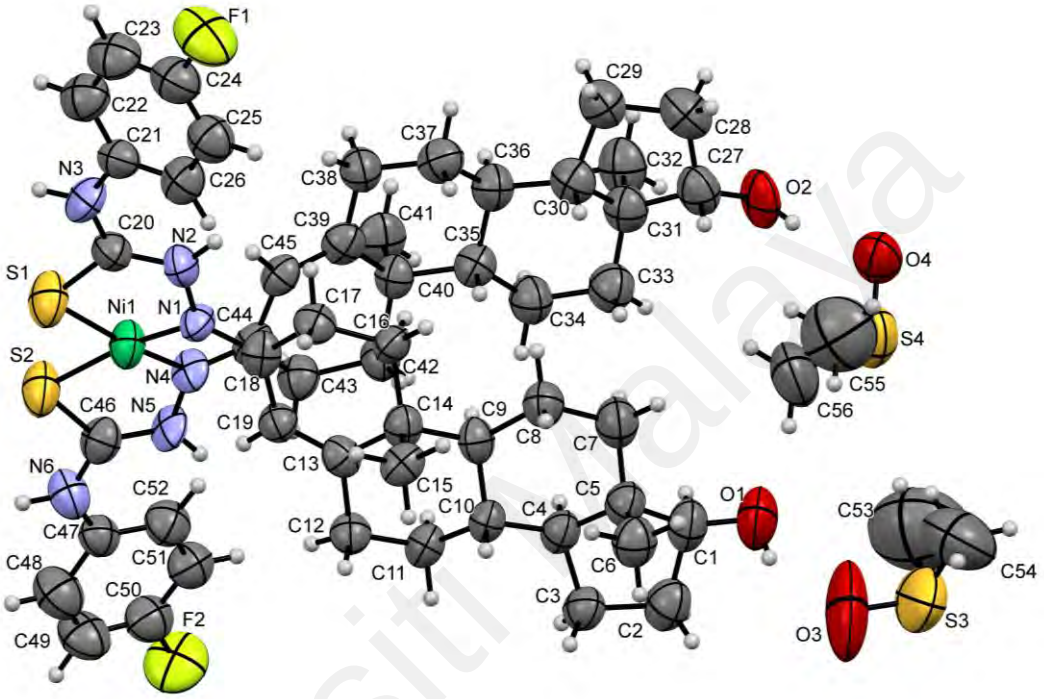

Figure 4.11: Ortep plot of **NF** drawn at 50% probability level. Hydrogen atoms are drawn at arbitrary radii.

The mononuclear nickel complex in Figure 4.11 is formed by two Schiff base ligands **TF** coordinated to a nickel ion *via* two imine nitrogens and two tautomeric thiosulfurs. Selected bond lengths and angles of **NF** are listed in Table 4.15, while hydrogen bonds are included in Table 4.16.

Table 4.15: Selected bond lengths and bond angles of **NF**.

Bond lengths (Å)		Bond angles (°)	
Ni1-S1	2.145 (4)	S1-Ni1-N1	86.1 (3)
Ni1-S2	2.149 (4)	S2-Ni1-N4	85.9 (3)
Ni1-N1	1.910 (9)	S1-Ni1-S2	90.15 (17)
Ni1-N4	1.903 (9)	N1-Ni1-N4	100.1 (4)
S1-C20	1.742 (13)	Ni1-N1-C18	128.7 (8)
S2-C46	1.749 (14)	Ni1-N4-C44	130.4 (9)
N1-C18	1.322 (14)		
N4-C44	1.306 (16)		
N1-N2	1.392 (12)		
N4-N5	1.373 (13)		
N2-C20	1.306 (16)		
N5-C46	1.277 (16)		

Table 4.16: Hydrogen bonds of **NF**.

D─H···*A*	D─H (Å)	H···*A* (Å)	D···*A* (Å)	D─H···*A* (°)
O1─H1···O3	0.84	2.26	2.60 (3)	104
O2─H2···O4	0.84	1.94	2.764 (15)	167
N3─H3···O2	0.88	2.08	2.957 (16)	171
Symmetry operation (i): x, y, z				
Symmetry operation (ii): -x, y+1/2, -z				

Similar to the case of **NM**, a distorted square planar geometry with cis configuration was observed in the case of **NF** as the bite angle for S1-Ni1-N1 and S2-Ni1-N4 are 86.1 (3) and 85.9 (3)°, respectively (Meghdadi et al., 2015). Moreover, shorter Ni-N bonds (Ni1-N1, 1.910 (9) Å; Ni1-N4, 1.903 (9) Å) are observed when compared with Ni-S bonds (Ni1-S1, 2.145 (4) Å; Ni1-S2, 2.149 (4) Å), which is due to the strong π-interaction between nickel and imine nitrogen (Prabhakaran et al., 2011).

Longer bond distances for S1-C20 and S2-C41, which are 1.754 (5) and 1.757 (5) Å respectively, were observed upon formation of nickel complex **NF** (1.680 (6) Å for C20-S1 in **TF**), which is corresponding to the thiolate form (C-S-Ni). Apart from that, when compared to its parent ligand **TF** (N2-C20 =1.349 (6) Å, Table 4.13), shorter bond distances for C20-N2 and C46-N5 (1.306 (16) and 1.277 (16) Å respectively) were

observed, which indicates the formation of C=N bonds upon tautomerization. On the other hand, hydrogen bonds of the type N3─H3···O2*W* linked molecules of **NF** to form a linear chain, which is shown in Figure 4.12.

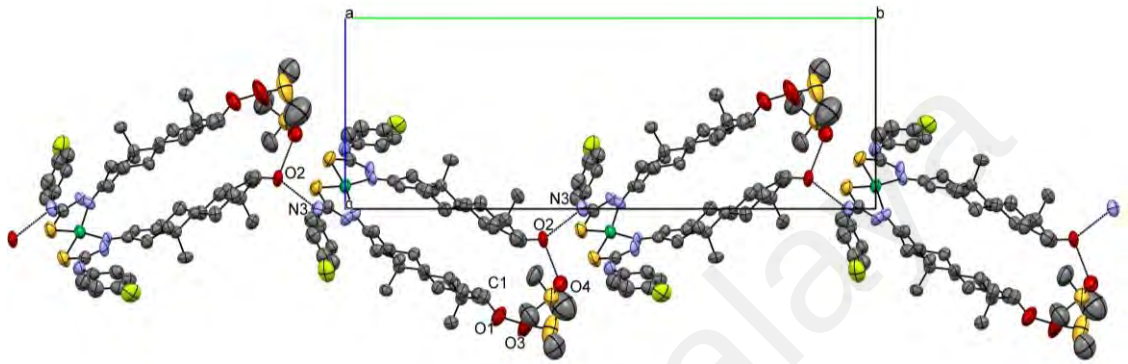

Figure 4.12: Linear chain formed from hydrogen bonds link **NF** and DMSO molecules (hydrogen atoms are omitted for clarity).

4.5.6 Crystal structure of complex zinc bis(testosterone-*N*^{4}-ethylthiosemicarbazone), ZE

The zinc complex **ZE** was crystallized in triclinic system with the space group of P1, and the perspective view of this compound is shown in Figure 4.13.

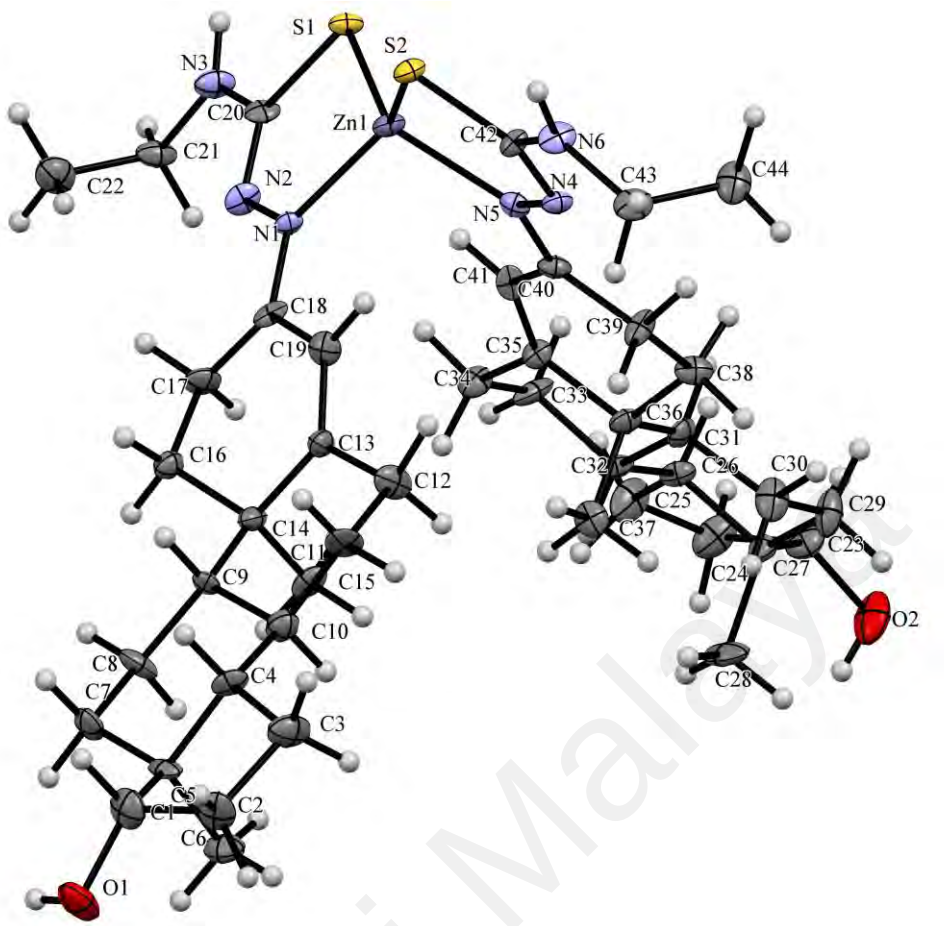

Figure 4.13: Ortep plot of **ZE** drawn at 50% probability level. Hydrogen atoms are drawn at arbitrary radii.

The mononuclear Zinc complex in Figure 4.13 is formed by two Schiff base ligands **TE** coordinated to a nickel ion *via* two imine nitrogens and two tautomeric thiosulfurs. Selected bond lengths and angles of **ZE** are listed in Table 4.17, while hydrogen bonds are included in Table 4.18.

Table 4.17: Selected bond lengths and bond angles of **ZE**.

Bond lengths (Å)		Bond angles (°)	
Zn1-N1	2.044 (8)	S1-Zn1-N1	86.9 (2)
Zn1-N4	2.053 (8)	S2-Zn1-N4	87.1 (2)
Zn1-S1	2.289 (2)	S1-Zn1-S2	128.7 (2)
Zn1-S2	2.291 (2)	N1-Zn1-N4	105.5 (3)
S1-C20	1.773 (10)	Zn1-N1-C18	128.0 (6)
S2-C42	1.751 (10)	Zn1-N4-C40	128.2 (6)
N1-C18	1.331 (12)		
N4-C40	1.299 (13)		
N1-N2	1.389 (10)		
N4-N5	1.397 (10)		
N2-C20	1.299 (13)		
N5-C42	1.315 (12)		

Table 4.18: Hydrogen bonds of **ZE**.

D─H···*A*	D─H (Å)	H···*A* (Å)	D···*A* (Å)	D─H···*A* (°)
C16─H16A···O2	0.99	2.49	3.287 (13)	137
C22─H22C···N2	0.98	2.60	3.128 (15)	114
C44─H44C···N5	0.98	2.58	3.111 (15)	114
C15─H15···S1	0.98	2.93	3.864	160
N3─H3···S2	0.88	2.95	3.58	124
Symmetry operation: x, y, z				

A distorted tetrahedral geometry with cis configuration was observed in the case of **ZE** as the bite angle for S1-Zn1-N1 and S2-Zn1-N4 are 86.9 (2) and 87.1 (2)°, respectively. Besides, shorter Zn-N bonds (Zn1-N1, 2.044 (8) Å; Zn1-N5, 2.053 (8) Å) are observed when compared with Zn-S bonds (Zn1-S1, 2.289 (2) Å; Ni1-S2, 2.291 (2) Å), which is due to the strong π-interaction between zinc and imine nitrogen (Tan et al., 2009; Cruz Santana et al., 2015).

The bond distances for S1-C20 (1.773 (10) Å) and S2-C42 (1.751 (10) Å) are similar to the one observed in the nickel complexes **NM** and **NF**, which is corresponding to the thiolate form (C-S-Zn). On the other hand, hydrogen bonds of the type C15─H15···S1,

C16─H16A···O2, and N3─H3···S2 linked molecules of **ZE** to form a zig-zag chain, which is shown in Figure 4.14.

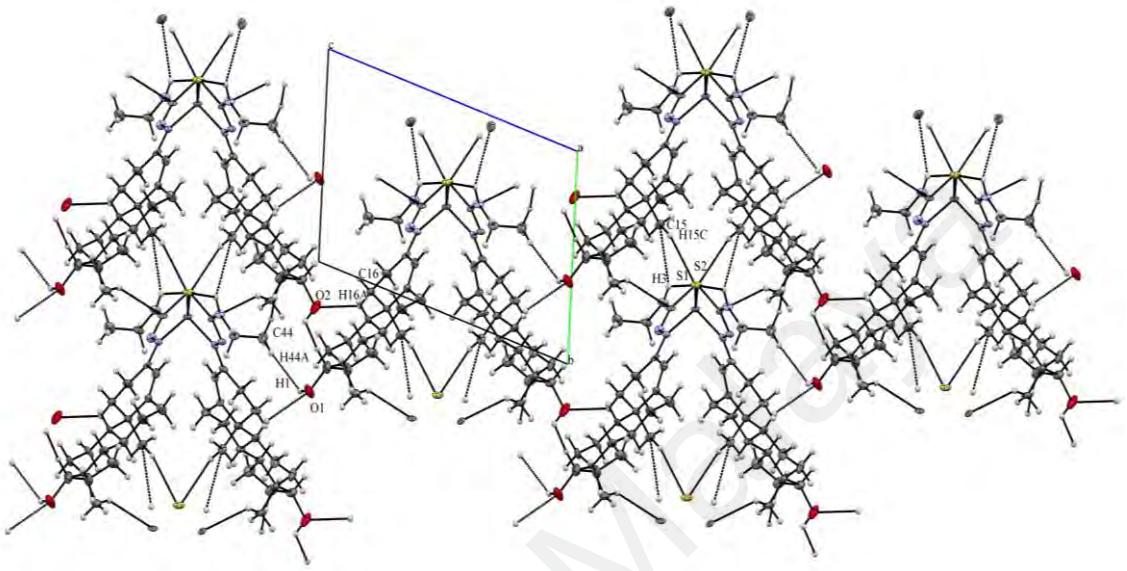

Figure 4.14: Zig-zag chain formed from hydrogen bonds link molecules of **ZE** along b-axis.

4.6 Cytotoxicity test

Testosterone was chosen as the main building element in the skeleton of all the Schiff base compounds synthesized, primarily due to its pivotal importance in cancers of the reproductive systems (Hyde et al., 2012; Michaud et al., 2015). The rationale of the design is, by joining a cytotoxic component such as thiosemicarbazide to a molecule with specific preferences towards certain cells, this molecule may act as a vector/vehicle that provide improved selectivity and/or selectivity to the compound synthesized (Zamora et al., 2013; Levine et al., 2014). However, the androgen receptor binding affinity of the testosterone moiety in the Schiff base compounds synthesized may also vanished. This is due to the disappearance of 3-keto group of testosterone, which is considered to be

essential for the recognition by androgen receptor, in the formation of azomethine linkage (Gao et al., 2005; Top et al., 2009).

Besides the potential setback described above, there might be a chance for the hormone molecule to behave as a two-edge sword. Ideally, testosterone will play a role as vector/vehicle, carrying the cytotoxic moiety to the cancerous cells with androgen receptor. However, the cell death-inducing ability of the Schiff base compounds against hormone-dependent prostate cancer cells may be dampened if the function of testosterone in Schiff base is well preserved, because androgen is generally acknowledged to aid in the promotion and growth of prostate cancer (Kimura et al., 2001).

In order to verify the usefulness of the compounds synthesized, the cytotoxicity of all the compounds against four human cancer cell lines (human derived prostate adenocarcinomas PC-3 and LNCaP, human breast adenocarcinomas MCF7, and human colorectal carcinomas HCT 116) and two normal cell line (human normal prostate RWPE-1 and normal colon fibroblasts CCD-18Co) were examined. The chemotherapy drug cisplatin was utilized as a positive reference standard in this assay and the results are summarized in Table 4.19.

Table 4.19: *In vitro* cytotoxicity (IC_{50} ± standard deviation) of compounds synthesized against six human cell lines.

	IC_{50} µM ± standard deviation (SI*)					
Compound	Prostate cancer PC-3	Prostate cancer LNCaP	Normal prostate RWPE-1	Colon cancer HCT 116	Normal colon CCD-18Co	Breast cancer MCF7
TM	>30	>30	3.88±0.86	14.27±0.64 (>2.10)	>30	25.51±1.32
NM	>30	26.26±2.03 (0.13)	3.37±0.20	16.52±1.05 (>1.82)	>30	20.00±1.27
ZM	>30	>30	20.32±0.92	>30	>30	>30
TP	22.40±1.49 (0.14)	16.29±0.71 (0.20)	3.24±0.08	12.71±1.01 (>2.36)	>30	19.45±0.16
NP	17.89±1.20 (0.20)	>30	3.56±0.08	11.72±0.17 (1.47)	17.24±0.29	>30
ZP	11.84±0.26 (0.38)	>30	4.47±0.06	9.31±0.34 (>3.22)	>30	17.55±0.49
TF	16.34±2.00 (0.97)	15.51±0.41 (1.02)	15.78±1.93	12.03±0.46 (2.46)	29.37±0.78	22.22±1.34
NF	>30	>30	3.81±0.012	18.08±1.82 (>1.66)	>30	>30
ZF	>30	>30	5.08±0.28	14.71±0.53 (>2.04)	>30	>30
ZE	>30	NT**	NT**	>30	>30	>30
Cisplatin	20.97±1.32 (0.78)	>30	16.28±1.66	23.88±1.73 (0.75)	17.87±0.47	20.16±1.00

* Selectivity index (SI) = (IC_{50} of normal cells/IC_{50} of cancer cells)

**NT = not tested

Ability of the synthesized compounds to inhibit the growth of prostate cancer LNCaP and PC-3 cells was tested. The LNCaP cell line is commonly regarded as a cell line that expresses androgen receptor and their growth is inhibited by androgen withdrawal. Meanwhile, PC-3 cells are relatively insensitive to androgen and their proliferation is independent of androgens (Tai et al., 2011). Based on the results in Table 4.19, some of the synthesized compounds are cytotoxic towards the prostate cancer cells tested (although at different magnitudes). Interestingly, the compounds are less cytotoxic towards the hormone-sensitive LNCaP cells compared to that of hormone-insensitive PC-3 cells, with only three compounds capable of inhibiting growth of LNCaP (at concentration up to 30 μM), namely **NM**, **TP**, and **TF**. This observation suggested that biomolecules/receptors other than the androgen receptors were involved in the cytotoxic mechanisms of these compounds.

The relatively low IC_{50} values obtained when the normal human prostate cell line was treated with the compounds indicated high general toxicity and low selectivity of these compounds towards cancerous prostate cells. Although cisplatin is also toxic against the normal prostate cell line tested, only **TF** has selectivity index (SI = 0.97) that is slightly better than this chemotherapy agent (SI = 0.78). This further suggests the unsuitability of these compounds synthesized in targeting human prostate cells.

Despite its importance in the development of prostate, the membrane androgen receptors are not solely expressed by prostate cells. Gu et al. (2009) have proved the expression of these receptors on the membrane of human colon cells. Moreover, a G-protein coupled receptor that is only found in colonic cancer cells (such as CaCo2 and HCT 116 cell lines) but not on normal colon cells, which is typically regarded as the third type of membrane androgen receptor, could be the potential target of the cytotoxic compounds albeit detailed mechanisms are not tested in this study (Gu et al., 2009; Gu et al., 2011; Nikolaou et al., 2019). Although colorectal carcinoma is not a hormone-

dependent cancer in the classical sense, increased evidence has demonstrated that testosterone and androgen receptor are relevant to the development of colorectal carcinoma despite studies thus far are still unable to reach a consensus regarding the direct connection between androgens and the risk of developing colorectal carcinoma (Lin & Giovannucci, 2010; Amos-Landgraf et al., 2014; Roshan et al., 2016). Nonetheless, the potential cytotoxicity of the compounds against human colorectal carcinoma cell line HCT 116 was tested due to potential importance of androgen receptor by treatment with the same compounds and current results showed that only **ZM** (up to 30 μM) was unable to halt the growth of this cell. Apart from that, some of the compounds (most remarkably **ZP**, with IC_{50} = 9.31 μM) displayed IC_{50} values that are lower compared to that of cisplatin (IC_{50} = 23.88 μM), which indicates better inhibitory properties. Moreover, only two (**NP** and **TF**) out of the eight HCT 116 inhibitory compounds are toxic against the human normal colon cell line CCD-18Co, namely **NP** and **TF**, with IC_{50} values of 17.24 and 29.37 μM, respectively.

Selectivity index (SI) of the synthesized compounds against human colorectal carcinoma cell line HCT 116 was calculated and included in Table 4.19 (in bracket). SI value of more than 1.0 was obtained in all the eight cytotoxic compounds, which showed excellent preferences towards the colorectal carcinoma cell line tested. Although it is generally accepted that SI value of more than or equal to 2.0 is considered to be less toxic (or possess anticancer property), all the cytotoxic compounds displayed SI value that is greater than cisplatin (Oliveira et al., 2015; Wiji Prasetyaningrum et al., 2018). Moreover, SI value of more than 3.0 was obtained in the case of **ZP**, which represents relatively low toxicity of this compound against the human colon cell line tested. These results cumulatively suggested high preferences of the compounds towards the colorectal carcinoma cell line tested (compared to cisplatin with lowest selectivity index of 0.75).

Apart from the cell lines mentioned above, the potential function of the testosterone moiety to facilitate in targeting the androgen receptor was further examined by treating the human breast cancer cell line MCF7 with the same compounds, since the presence and importance of androgen receptors on breast cancer cells were reported (Macedo et al., 2006; Cochrane et al., 2014). According to results in Table 4.19, only five out of the nine compounds tested were capable of inhibiting the growth of this cell line despite eight of them were proven cytotoxic (against human colorectal carcinoma HCT 116). Therefore, the function of testosterone in these compounds may have little to no effect on the recognition of androgen receptor because almost half of these compounds were unable to target the androgen receptor responsive MCF7 and LNCaP cells. Moreover, their IC_{50} values are generally higher compared to the IC_{50} values obtained from other cell lines, which indicates weaker cytotoxicity of these compounds against this cell line. No breast normal cell line was tested because of the relatively weaker cytotoxicity (and hence higher IC_{50} values) of the synthesized compounds against the breast cancer cell line tested compared to other cell lines (such as colorectal cancer HCT 116).

A zinc complex (**ZE**) of testosterone-N^4-ethylthiosemicarbazone was added into comparison and according to results in Table 4.18, this complex is non-cytotoxic towards the cell lines tested. The potency of **ZE** in inhibiting the growth of prostate cancer LNCaP and prostate normal RWPE-1 was not tested due to the weak cytotoxicity of this complex against other cell lines tested. According to the results, cytotoxicity of zinc thiosemicarbazone complexes might be subdued by the presence of alkane substituent, as both **ZM** and **ZE** are not cytotoxic towards almost all the cell lines tested (**ZM** is only toxic towards human normal prostate RWPE-1). In contrast, introduction of phenyl substituent might had improved the potency of the zinc complexes, as both **ZP** and **ZF** possessed growth inhibitory effects on at least one cancerous cell line (both are active against colorectal cancer HCT 116, while **ZP** is also cytotoxic towards prostate cancer

PC-3 and breast cancer MCF7). However, such effect is not applicable to the nickel complexes, as **NM** is cytotoxic against three cancer cell lines (prostate cancer LNCaP, colorectal cancer HCT 116, and breast cancer MCF7) while **NF** is only active against the colorectal cancer HCT 116.

Complexation with metal ion is commonly performed to enhance the cytotoxicity of their parent ligands. However, complexation with nickel and zinc ions has brought about different alterations to the cytotoxicity in this project. Briefly, complexation with nickel has improved the cytotoxicity of **TM** (in the case of **NM** against LNCaP) and **TP** (**NP** in the case of PC-3), but worsened the overall cytotoxicity of **TF**. Besides, formation of zinc complex has only improved the cytotoxicity of **TP**. The decreased in cytotoxicity might be due to the relatively bulkier size and change in geometries upon complexation. Also, it could be due to the loss of chelating ability of the ligand (Richardson et al., 2006), as reduced cytotoxicity upon complexation of triapine, the ribonucleotide reductase (an enzyme involved in rate-limiting step of DNA synthesis) inhibiting thiosemicarbazone, with iron was reported (Rejmund et al., 2018).

4.7 Post treatment morphological changes

The first description for the term "apoptosis" was based on the morphological changes of cell death including chromatin condensation, fragmentation, membrane blebbing, and cell shrinkage (Kerr et al., 1972; Doonan & Cotter, 2008). The morphological changes on HCT 116, PC-3 and MC7 cell lines were observed under phase contrast inverted microscope after 24 and 48 hours of exposure to the cytotoxic compounds (at their respective IC_{50}). Results were illustrated in Figure 4.15-4.17, untreated (control) cells were photographed to verify the morphology of the cells in the absence of any cytotoxic compounds.

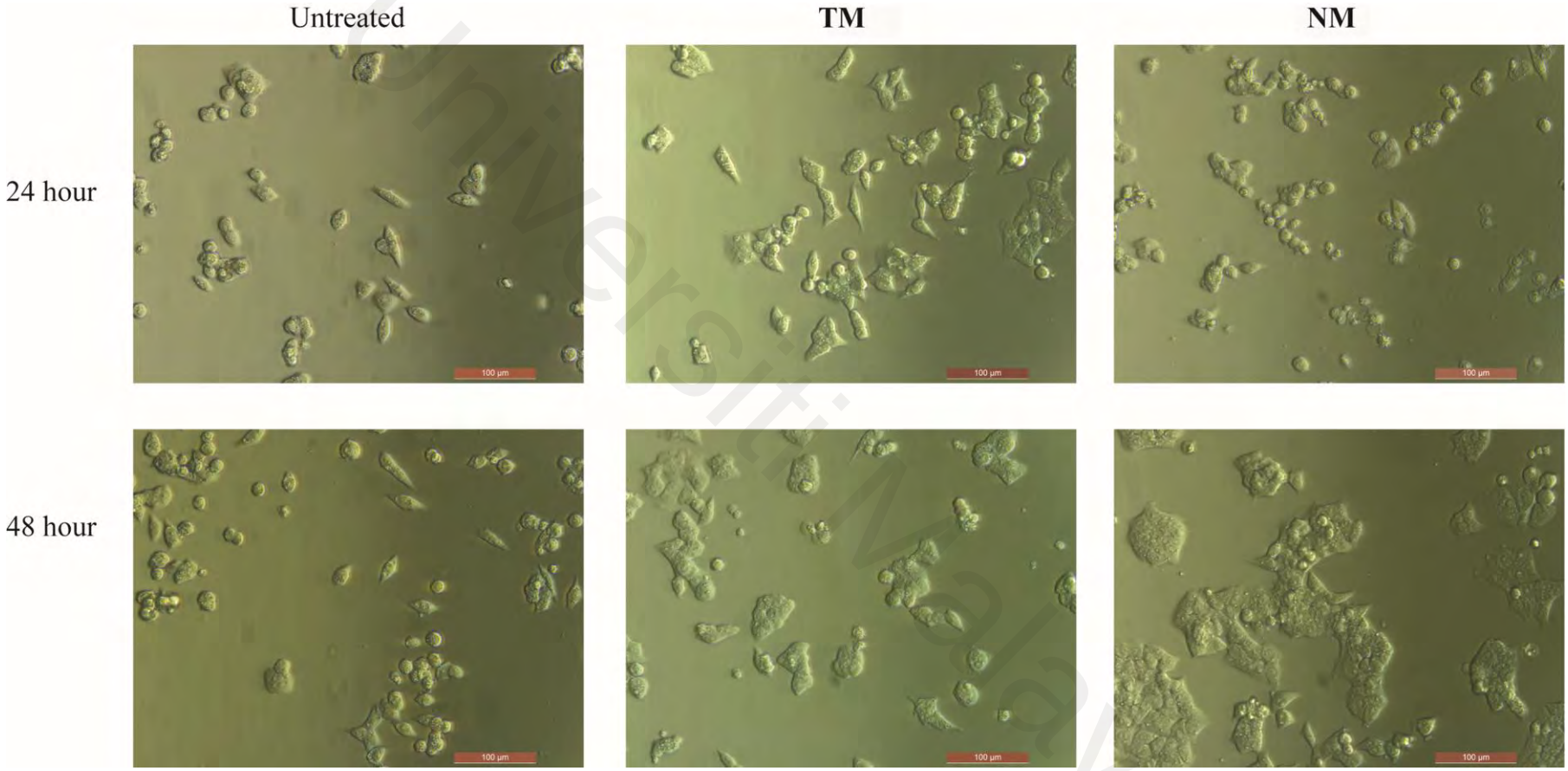

Figure 4.15: Morphological changes on HCT 116 cells in the absence and presence of the cytotoxic compounds (200× magnification).

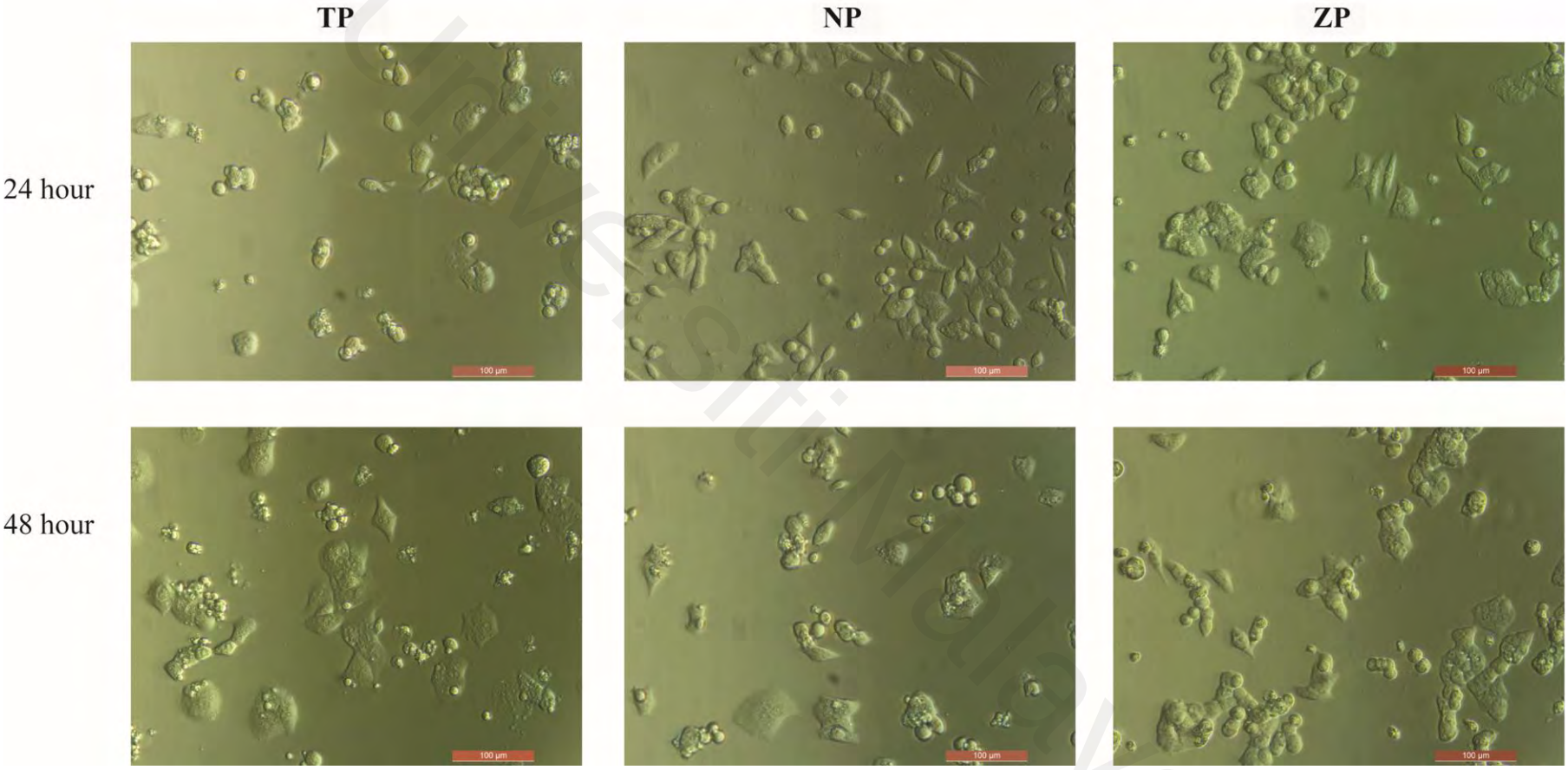

Figure 4.15, continued

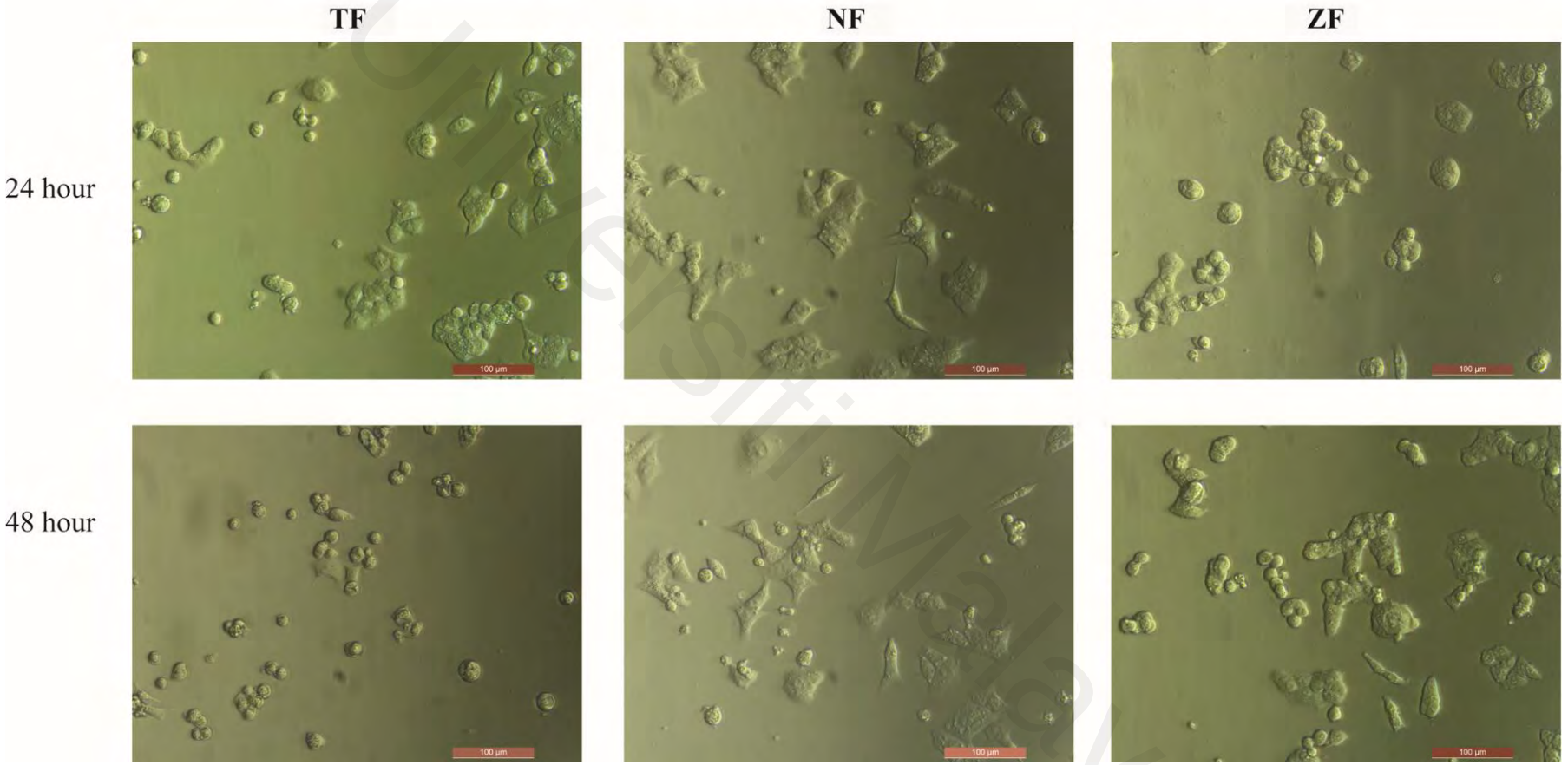

Figure 4.15, continued

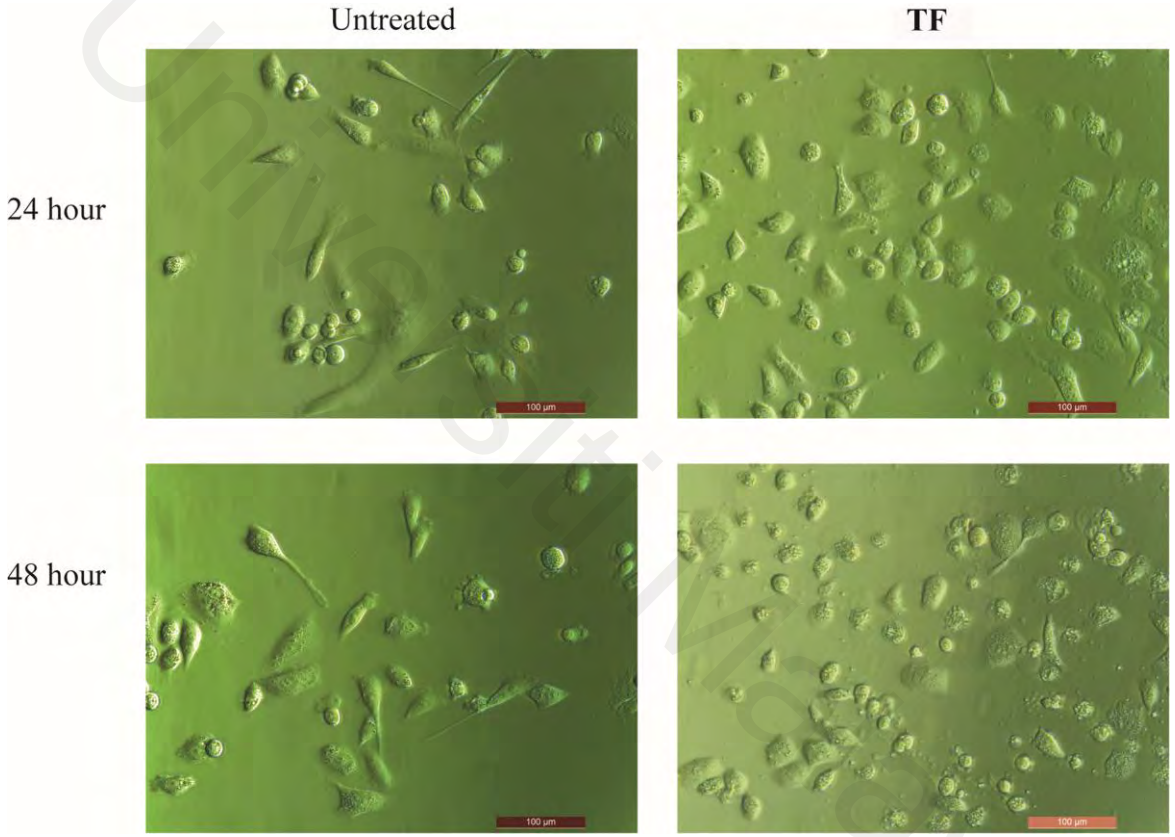

Figure 4.16: Morphological changes on PC-3 cells in the absence and presence of the cytotoxic compounds (200× magnification).

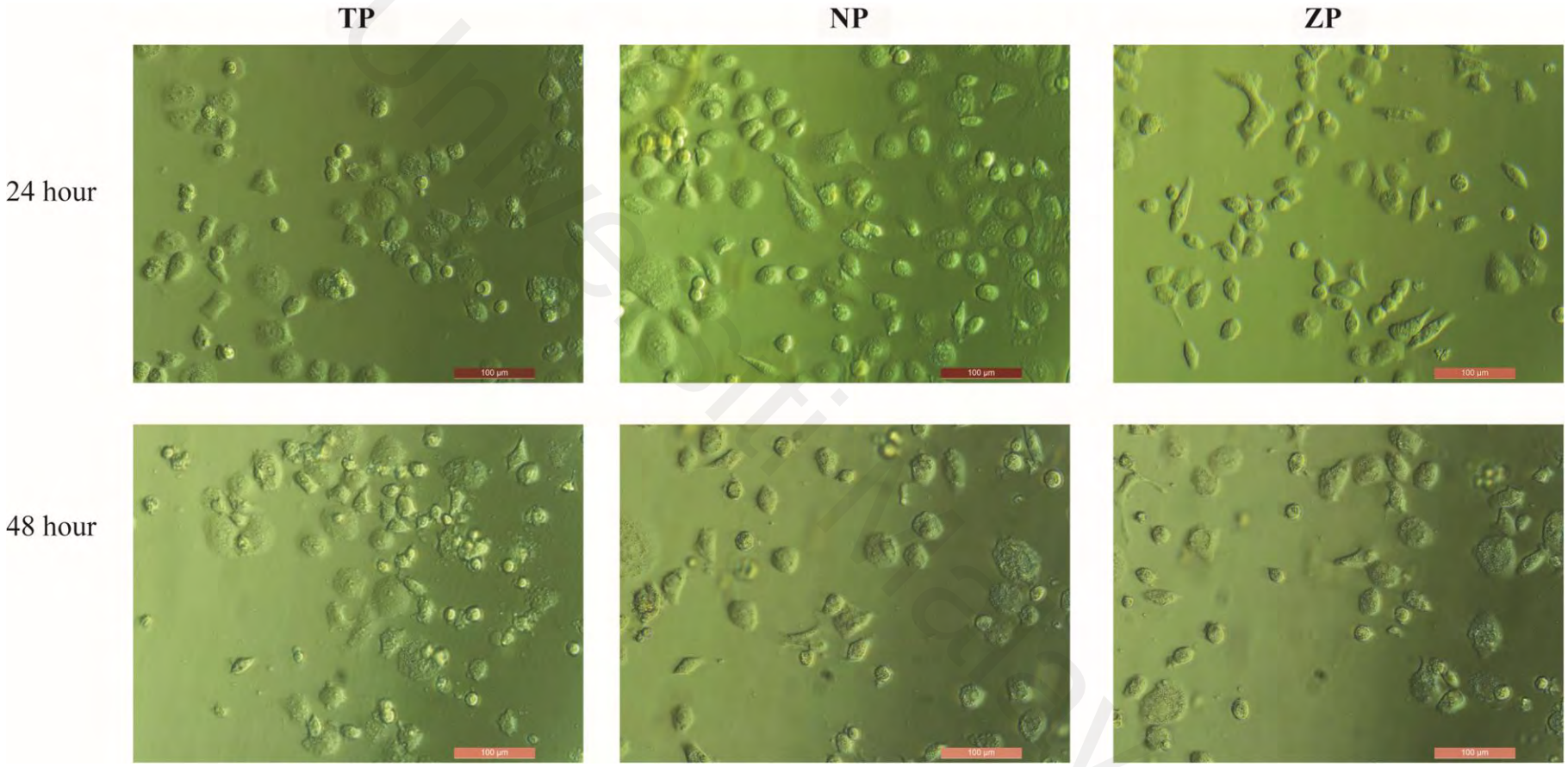

Figure 4.16, continued

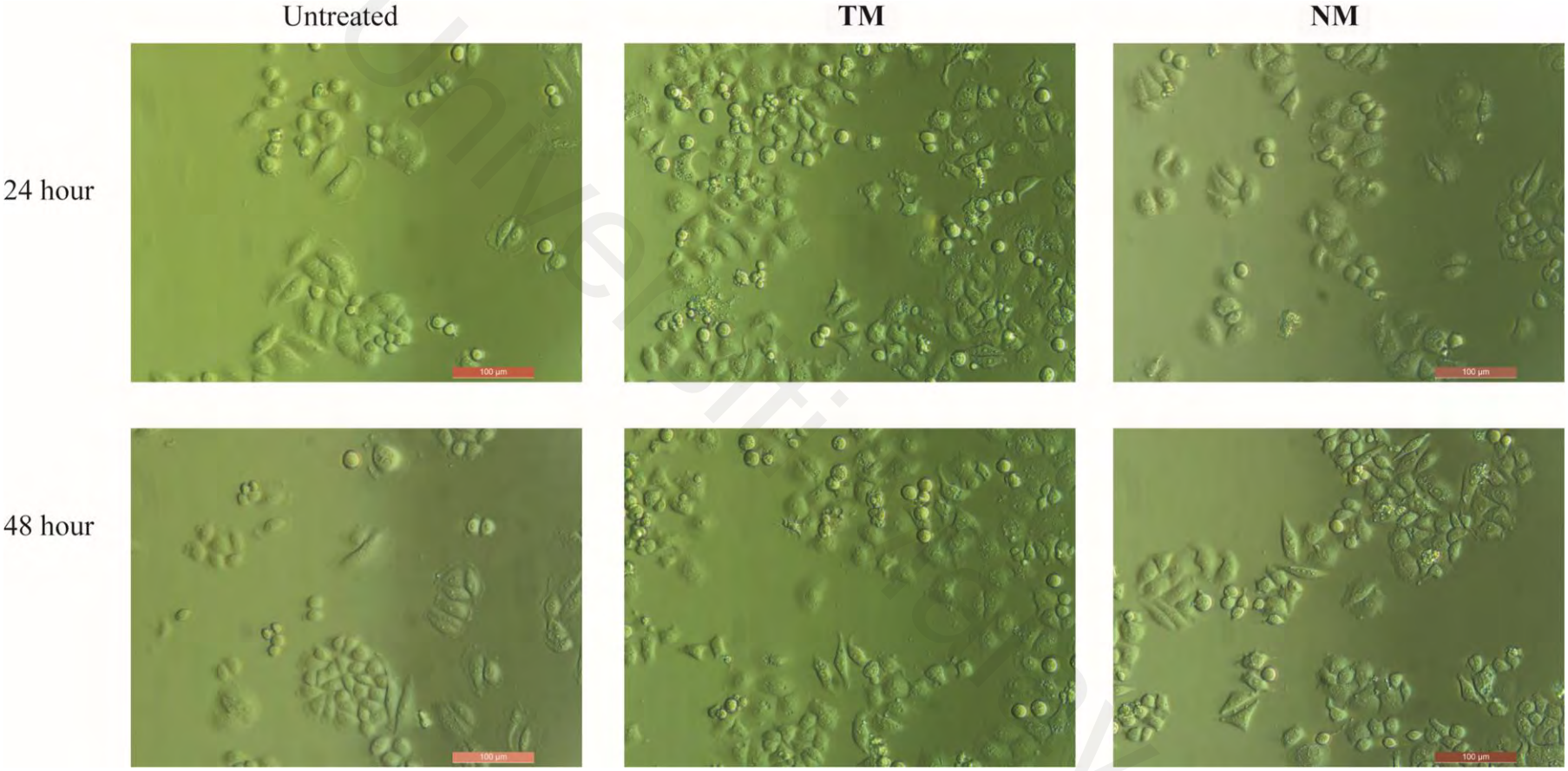

Figure 4.17: Morphological changes on MCF7 cells in the absence and presence of the cytotoxic compounds (200× magnification).

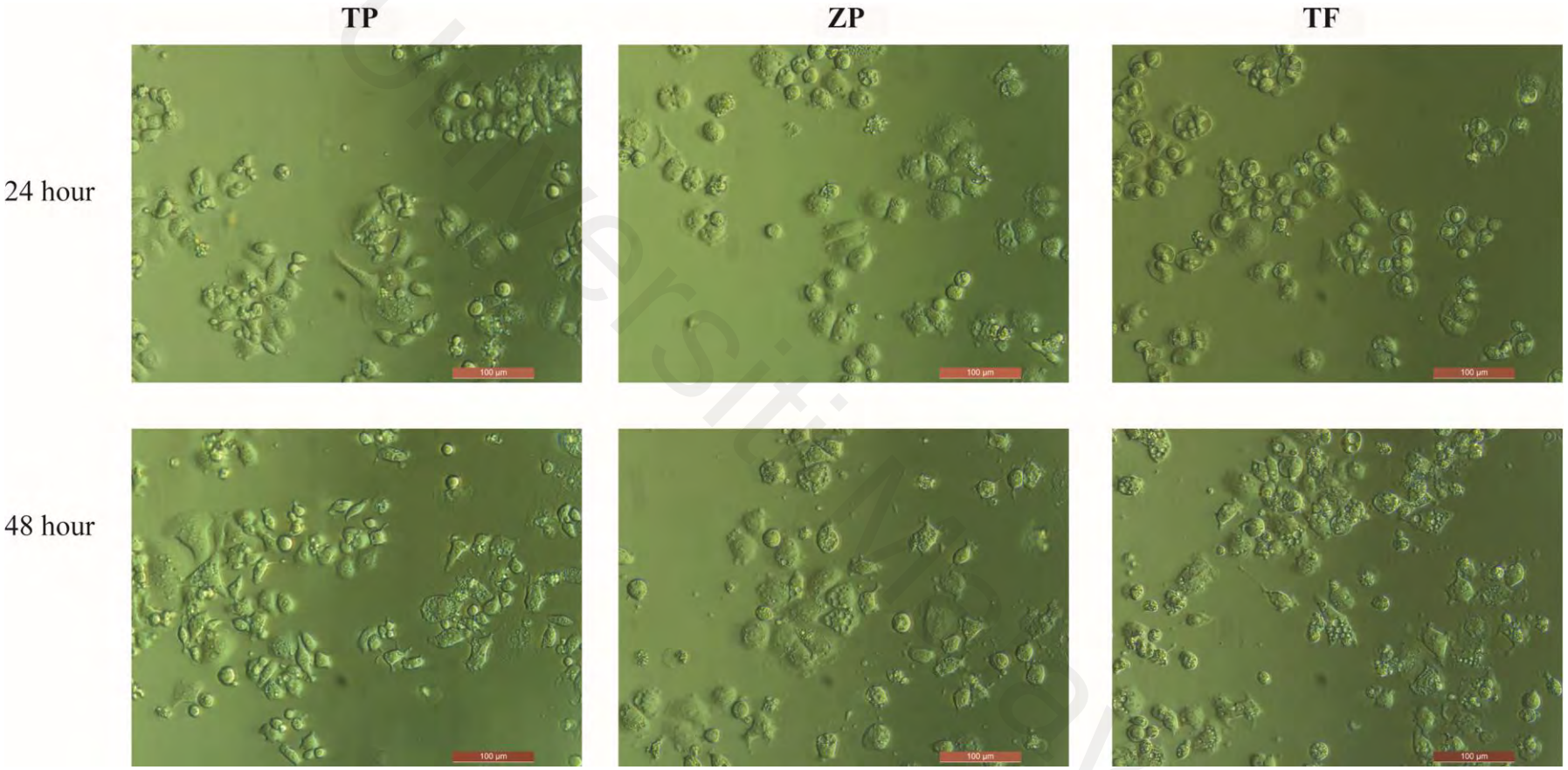

Figure 4.17, continued

Figure 4.15 showed the morphology of HCT 116 cells in the absence and presence of different cytotoxic compounds. The cells adopted a spindle or angular shape prior treatment with the compounds (Tan et al., 2019). Membrane blebbing was observed after 24 hours of treatment with almost all the treatment. The cells lost their integrity and appeared clustered together, especially **TM**, **NM**, and **NF**. Morphological changes such as rounding up and cell shrinkage were observed. For instance, most of the cells treated with **TF** for 48 hours have shrunken. This observation might be due to the extreme alteration in intracellular water content. Although necrotic cells might absorb water resulting in enlargement in the size before finally bursting, apoptotic cells would eventually lose water and therefore reduce the size of the cells. Subsequently, the cell will lose its contact with adjacent cells and lead to detachment from the extracellular matrix resulting in more rounded morphology (Farghadani et al., 2017; Wu et al., 2018).

Similar observations were recorded when the prostate cancer PC-3 and breast cancer MCF7 were subjected to similar treatments. Cell shrinkage, detachment and rounding up as well as membrane blebbing were observed. These observations suggested that the cells were undergoing apoptosis/necrosis upon treatment of the test compounds. Abilities of these compounds to induce cell death through apoptosis or necrosis were then investigated.

4.8 Assessment of apoptotic cells

Apoptosis and necrosis are two major cell death mechanisms. Usually, the cells are subjected to external injury would undergo necrosis, whereas cells would be requiring some internal or external stimuli to commit programmed suicide (apoptosis). Externalization of phosphatidylserine on the outer surface of plasma membrane is regarded as the hallmark of early apoptosis (Shi et al., 2019). Annexin V is a Ca^{2+}-dependent phospholipid-binding protein with high affinity for the exposed apoptotic cell surface phosphatidylserine. Moreover, annexin V can be conjugated to fluorochromes such as FITC while retaining its excellent affinity for phosphatidylserine and hence serves as a sensitive probe for flow cytometric detection of cells undergoing apoptosis. However, the vital dye propidium iodide (PI) is usually used in conjunction with annexin V for identification of early and late apoptotic cells because translocation of phosphatidylserine is observed in both apoptotic or necrotic processes. In brief, viable cells with intact membranes exclude PI, whereas dead and damaged cells are permeable to this dye. Therefore, viable cells are both annexin V and PI negative, while early apoptotic cells are annexin V positive and PI negative, whereas late apoptotic or dead cells are both annexin V and PI positive. However, this assay is unable to distinguish between cells that have died from necrosis versus cells that have undergone apoptotic cell death as they will be stained with both annexin V and PI (Hingorani et al., 2011).

In this assay, the cells were stained with annexin V-FITC and PI after treatment with selected compounds. The incidence of apoptosis was then detected by flow cytometry and results are summarized in Figure 4.18-4.23.

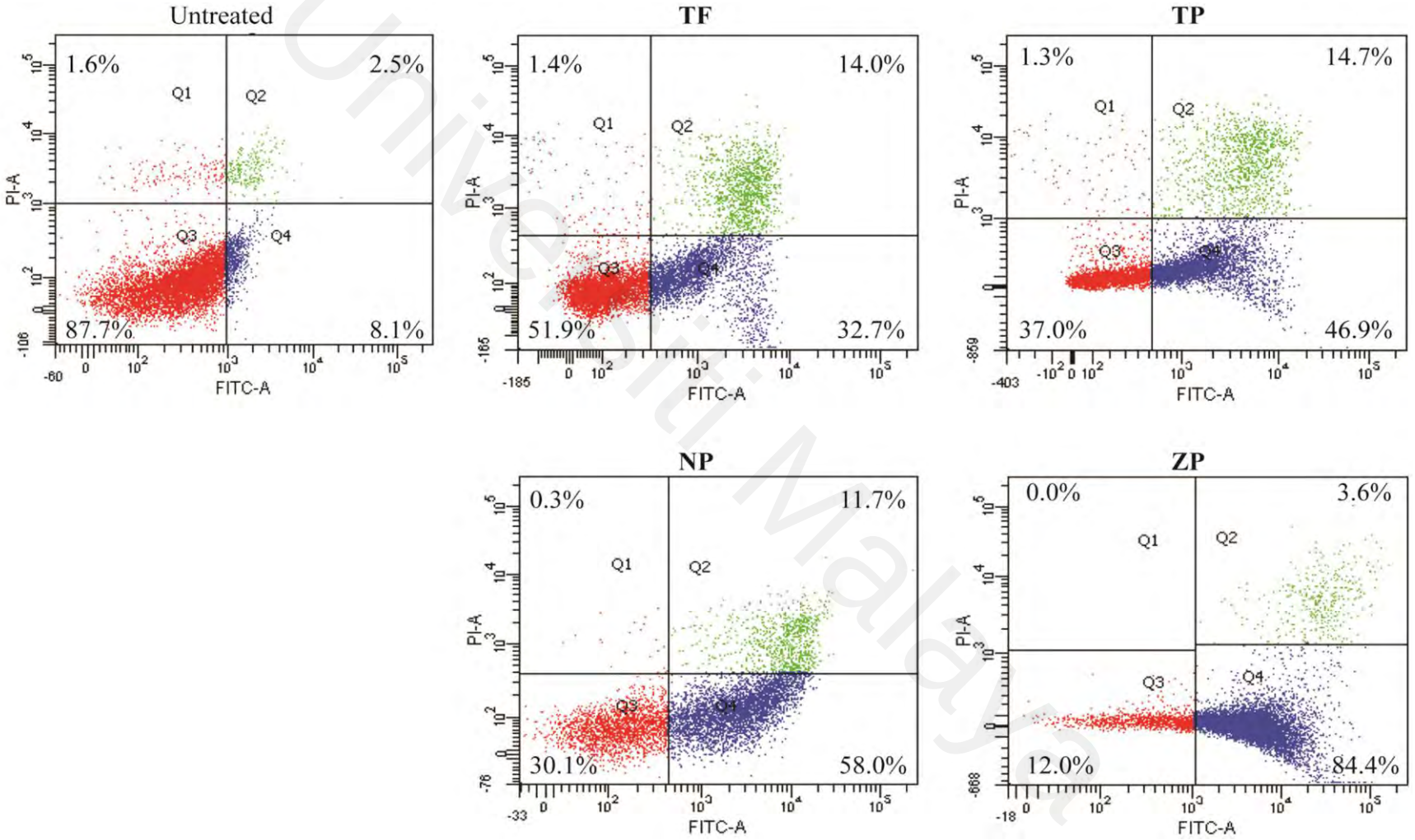

Figure 4.18: Effects of exposure to selected compounds on the externalization of phosphatidylserine in human prostate cancer PC-3 cells for 48 hours.

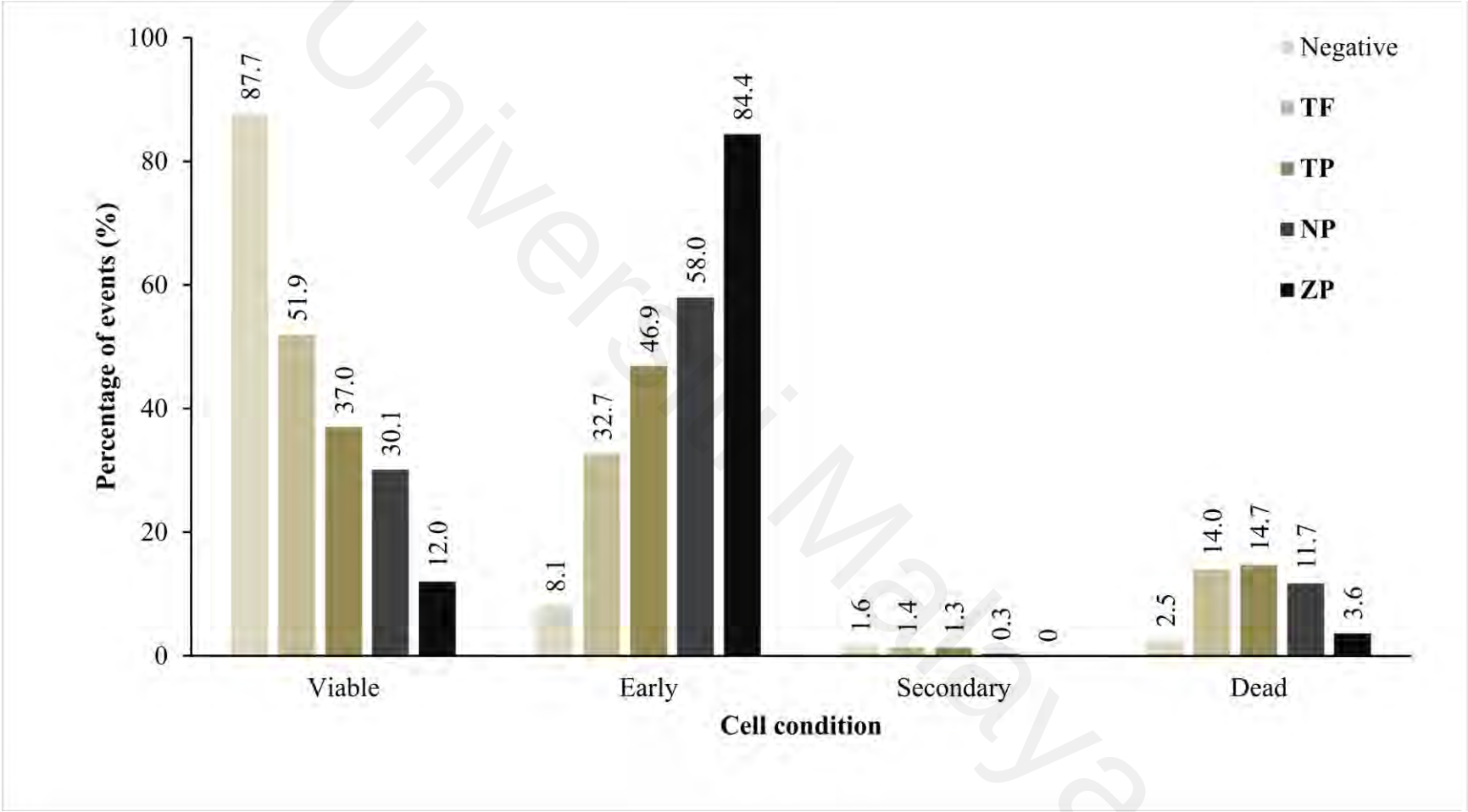

Figure 4.19: Histogram summarizing the effects of exposure to selected compounds on the externalization of phosphatidylserine in human prostate cancer PC-3 cells for 48 hours.

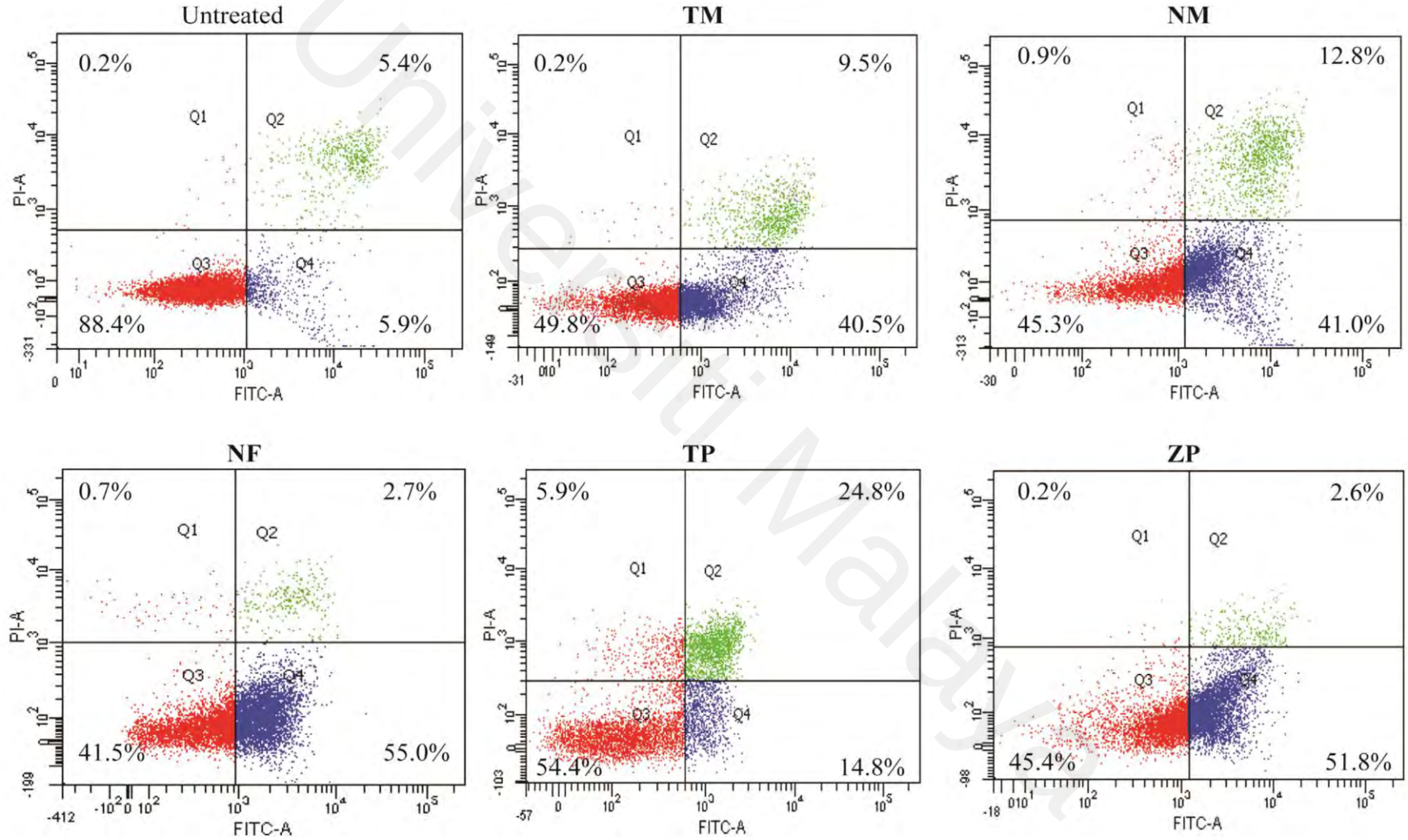

Figure 4.20: Effects of exposure to selected compounds on the externalization of phosphatidylserine in human breast cancer MCF7 cells for 48 hours.

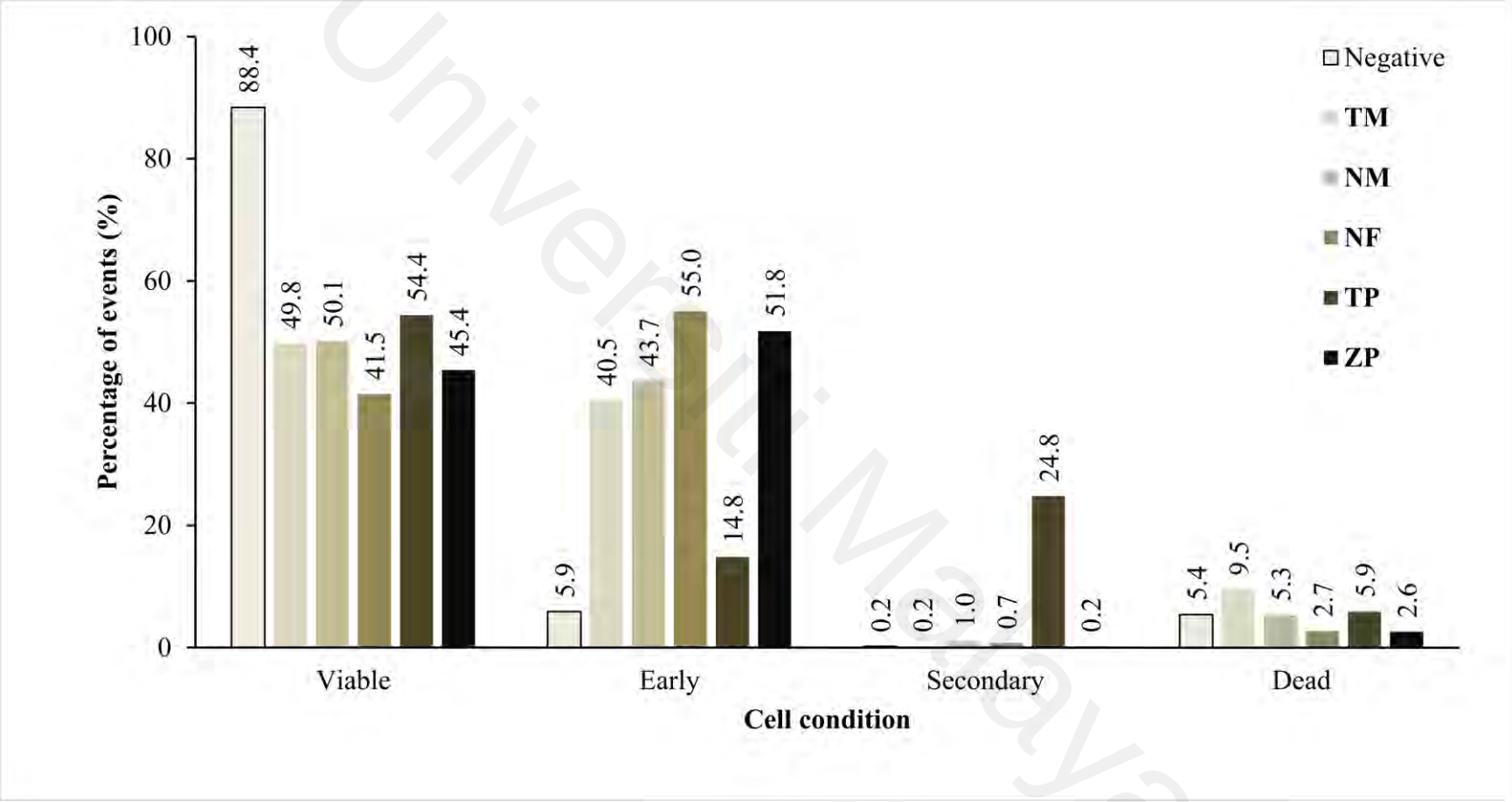

Figure 4.21: Histogram summarizing the effects of exposure to selected compounds on the externalization of phosphatidylserine in human breast cancer MCF7 cells for 48 hours.

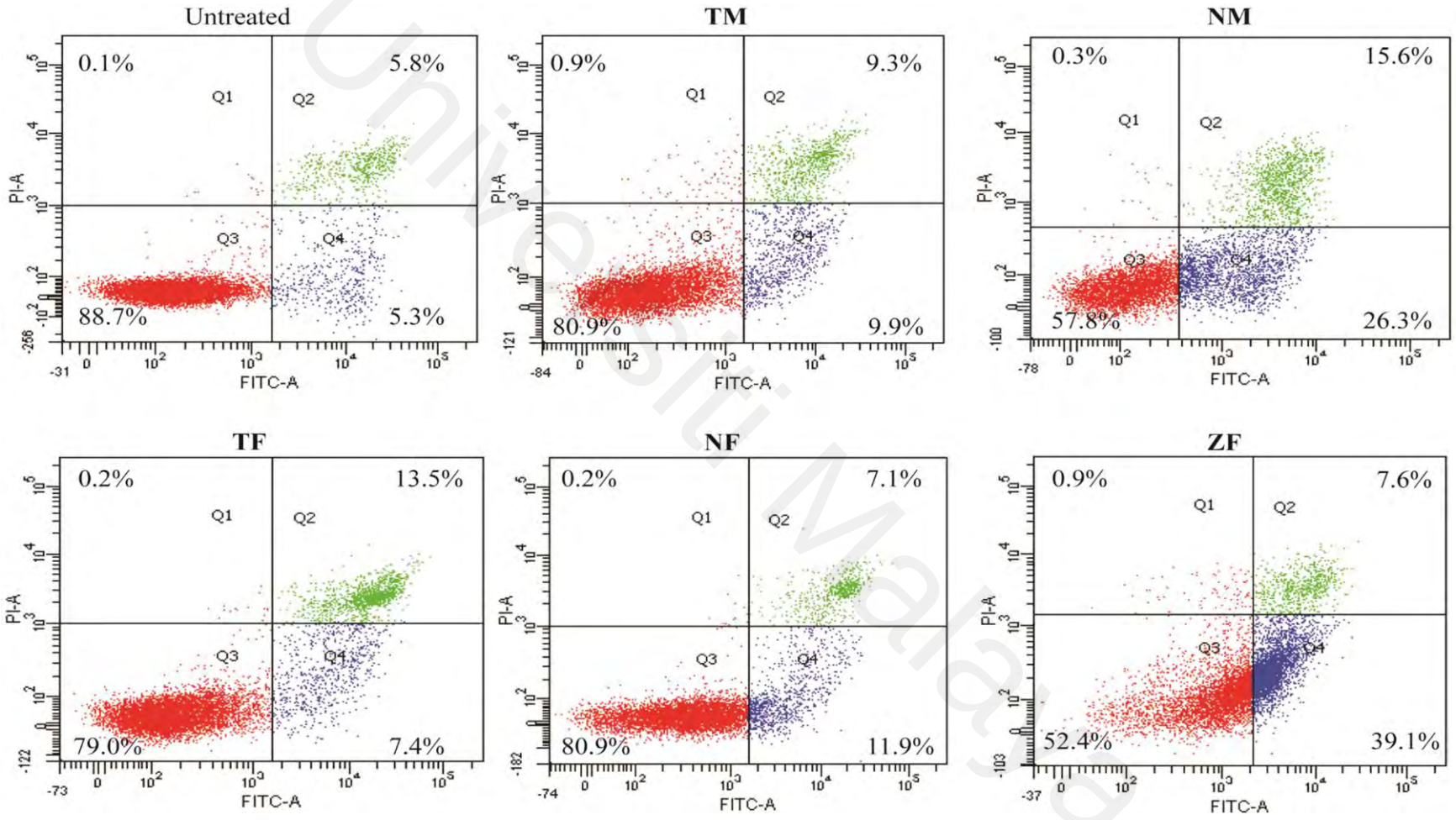

Figure 4.22: Effects of exposure to selected compounds on the externalization of phosphatidylserine in human colon cancer HCT 116 cells for 48 hours.

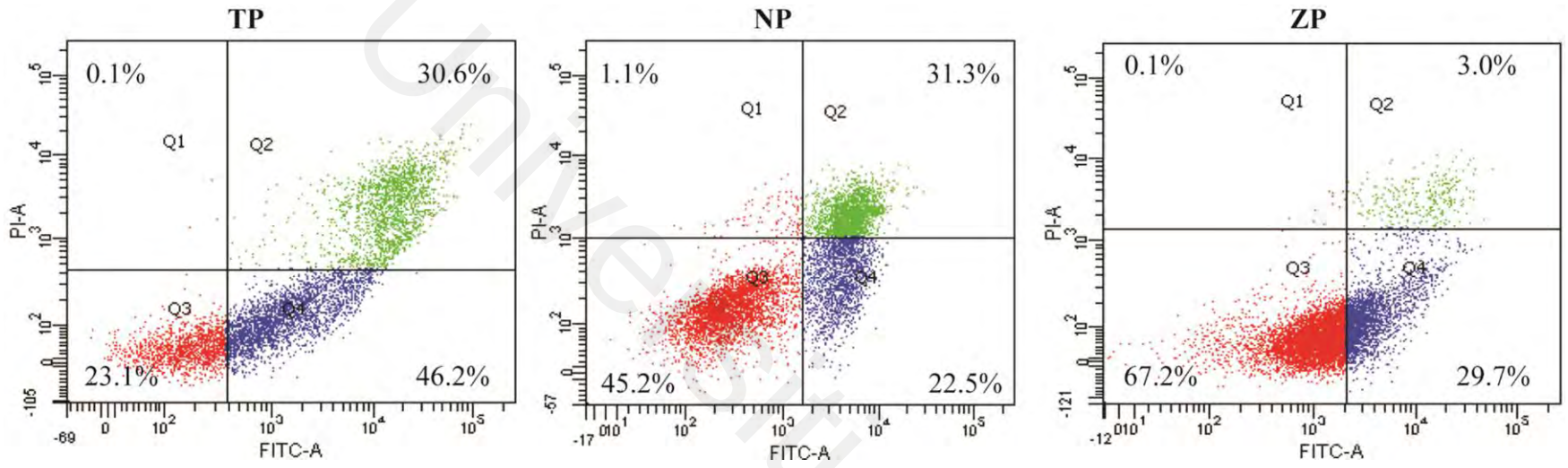

Figure 4.22, continued.

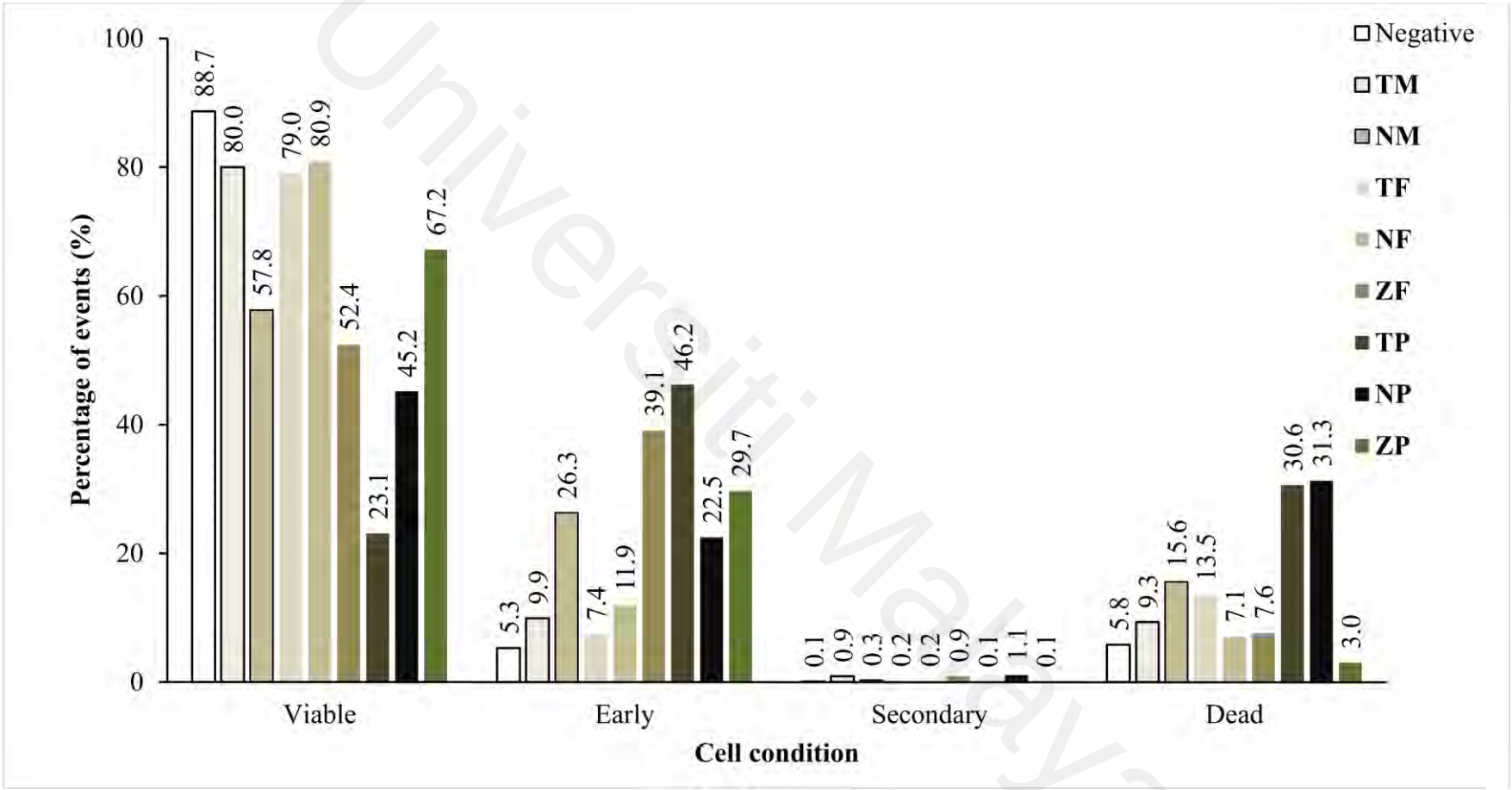

Figure 4.23: Histogram summarizing the effects of exposure to selected compounds on the externalization of phosphatidylserine in human colon cancer HCT 116 cells for 48 hours.

The phosphatidylserine of more than 85% of the negative control cells are still intact (Figure 4.18-4.23), indicating the cells were viable and healthy. However, the number of viable cells decreased to different extend after treatment with different compounds.

Figure 4.18 and 4.19 shows the effects of the test compounds on the prostate cancer PC-3 cells. This cell line was chosen (instead of LNCaP) because more compounds are cytotoxic towards this cell line and their IC_{50} values are lower compared to that of LNCaP. Exposure to the test compounds for 48 hours has increased the early apoptotic and dead populations. Most apoptotic incidences were recorded in the case of **ZP** (84.4% early apoptotic cells), which is in great agreement with its lowest IC_{50} among all. However, this might reflect the ability of this cell type to recover once the test compound is worn out, since IC_{50} values (72 hours) of the test compounds were used as references in this assay (50% of healthy population is remained after 72 hours of treatment with the test compounds in cell cytotoxicity assay).

In order to compare the growth inhibitory efficacy of the test compounds, the human breast cancer cell line MCF7 was also included in this study (Figure 4.20-4.21). Apoptotic cells were present after treatment with the test compounds, with early apoptotic cells ranging from 14.8 to 55.0% (compared to 5.9% in untreated cells), thereby reflecting apoptosis-inducing properties of the test compounds. A steep decrease in the healthy population was observed after the cells were treated with the test compounds for 48 hours (Figure 4.20-4.21), with almost all the compounds were capable of reducing approximately half of the cell population. After treatment with **TP**, about 24.8% of the population was recorded in the annexin V-FITC negative/PI positive region, which attributed to the necrotic or late apoptotic cells (Zamai et al., 2001).

The ability of the cytotoxic compounds to induce apoptosis on human colorectal carcinoma cell line HCT 116 was then tested (Figure 4.22-4.23). Similarly, the test

compounds have decreased the incidences of viable cells. All the test compounds were capable of inducing apoptosis in this cell line, although four of the eight compounds tested (**TM**, **TF**, **NF**, and **ZP**) were unable to reduce half of the healthy populations (viable cells ranging from 67.2% to 80.9%, compared to that of 88.7% in untreated cells) despite the administration of these compounds with their respective IC_{50} as reference. This may indicate slow and stable rate of growth inhibition of these compounds, as IC_{50} of these compounds were calculated as the concentration required to reduce the population by half after 72 hours of treatment.

In a nutshell, almost all the test compounds in this assay are capable of inducing apoptosis in the cell lines tested, with the notable exception of **TP** that caused necrosis in MCF7 cells. Besides, complexation with nickel and zinc has no clear effect on the apoptotic/necrotic inducing effect of the compounds. For instance, complexation of **TP** with nickel and zinc has reduced the rate of apoptosis in HCT 116 cells despite slight improvement in their IC_{50} in cytotoxicity test. Moreover, choice of thiosemicarbazide has no significant effect on the apoptosis-inducing abilities of the compounds tested. For example, two compounds from **TP** family (**TP** and **ZP**) induced lesser early apoptotic cells in MCF7 cells (14.8% and 51.8%, respectively) compared to that of **NF** (55.0%), but they were able to induce 46.2% and 29.7% of early apoptotic population in HCT 116 cells (11.9% early apoptotic cells in the case of **NF**).

The human colorectal carcinoma cell line HCT 116 was then chosen for all the cell-based experiments performed in following sections due to the relative low IC_{50} values of the compounds and their excellent selectivity against this cancer cell type.

4.9 Evaluation of mitochondrial membrane potential

To further investigate the cellular mechanism underlying test compound-induced apoptosis in human colorectal carcinoma cell line HCT 116, the changes in mitochondrial transmembrane potential (ΔΨm) were assessed by using lipophilic fluorochrome JC-1 and flow cytometry analysis. In healthy cells, JC-1 dye will penetrate the plasma membrane as monomers and it will be taken up into the mitochondria due to the polarized state of the ΔΨm. The uptake of this dye will lead to the aggregation of fluorochromes in the mitochondria and the transition of these monomers to aggregates can be visualized using a flow cytometer monitoring the red spectral shift. Accumulation of these aggregates in the mitochondria will be detected at a higher intensity of red fluorescence (emission maximum at 590 nm) compared to that of monomers. Any loss of ΔΨm will results in increased monomers (or lesser aggregates) and therefore the intensity of red fluorescence will be lower (Czarnomysy et al., 2018) and as a result, green fluorescent monomers (emission maximum at approximately 529 nm) reflecting loss of mitochondrial membrane potential will be observed (Elefantova et al., 2018). Results were summarized and displayed in Figure 4.24-4.25.

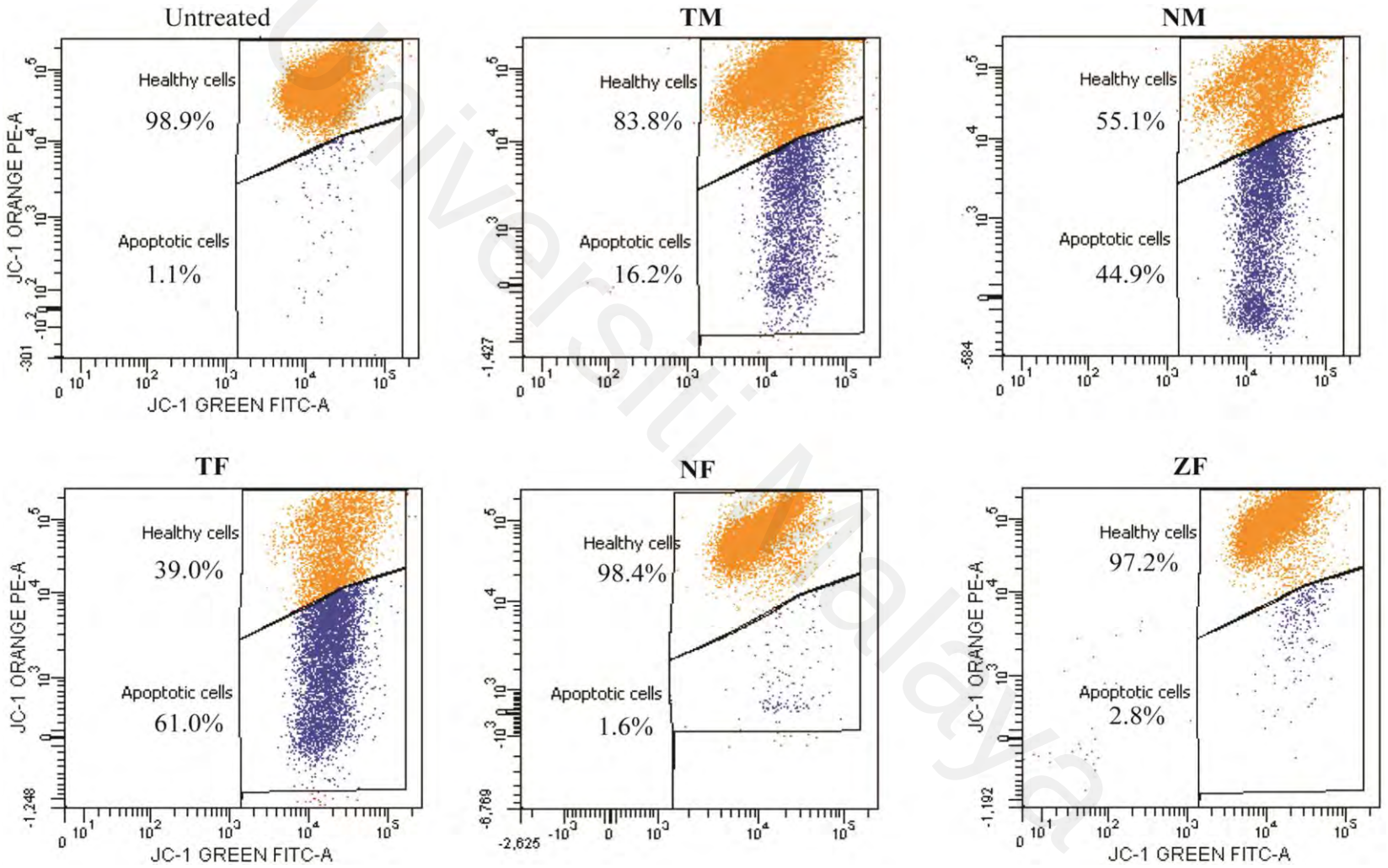

Table 4.24: Effects of exposure to selected compounds on the mitochondria membrane potential in human colon cancer HCT 116 cells for 48 hours.

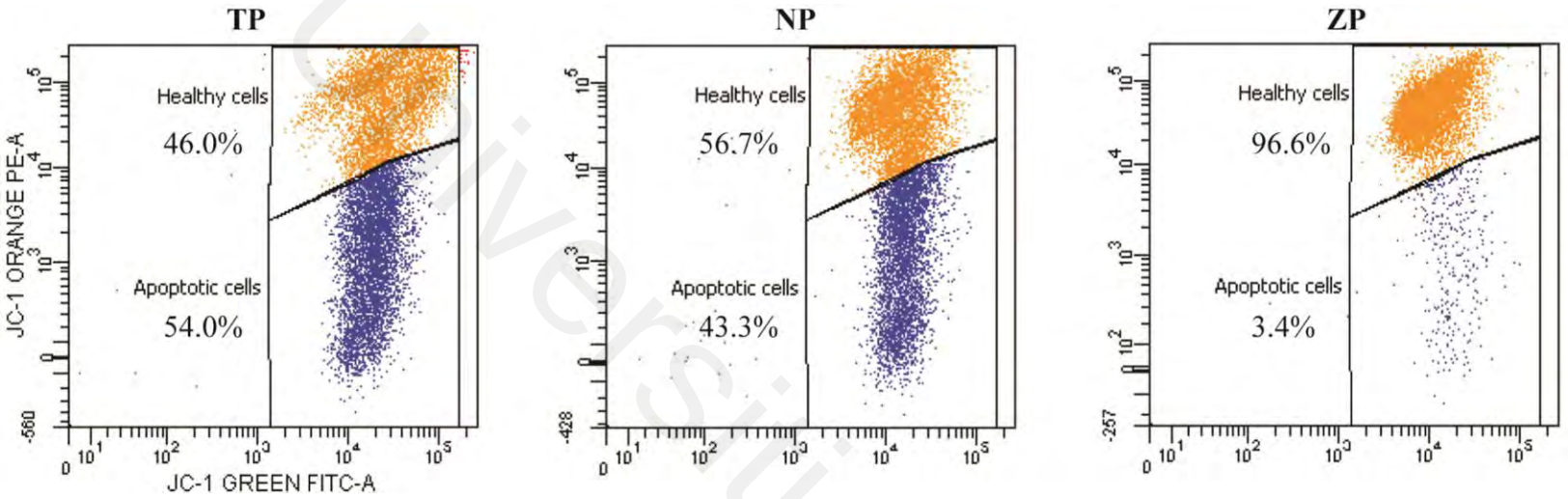

Figure 4.24, continued

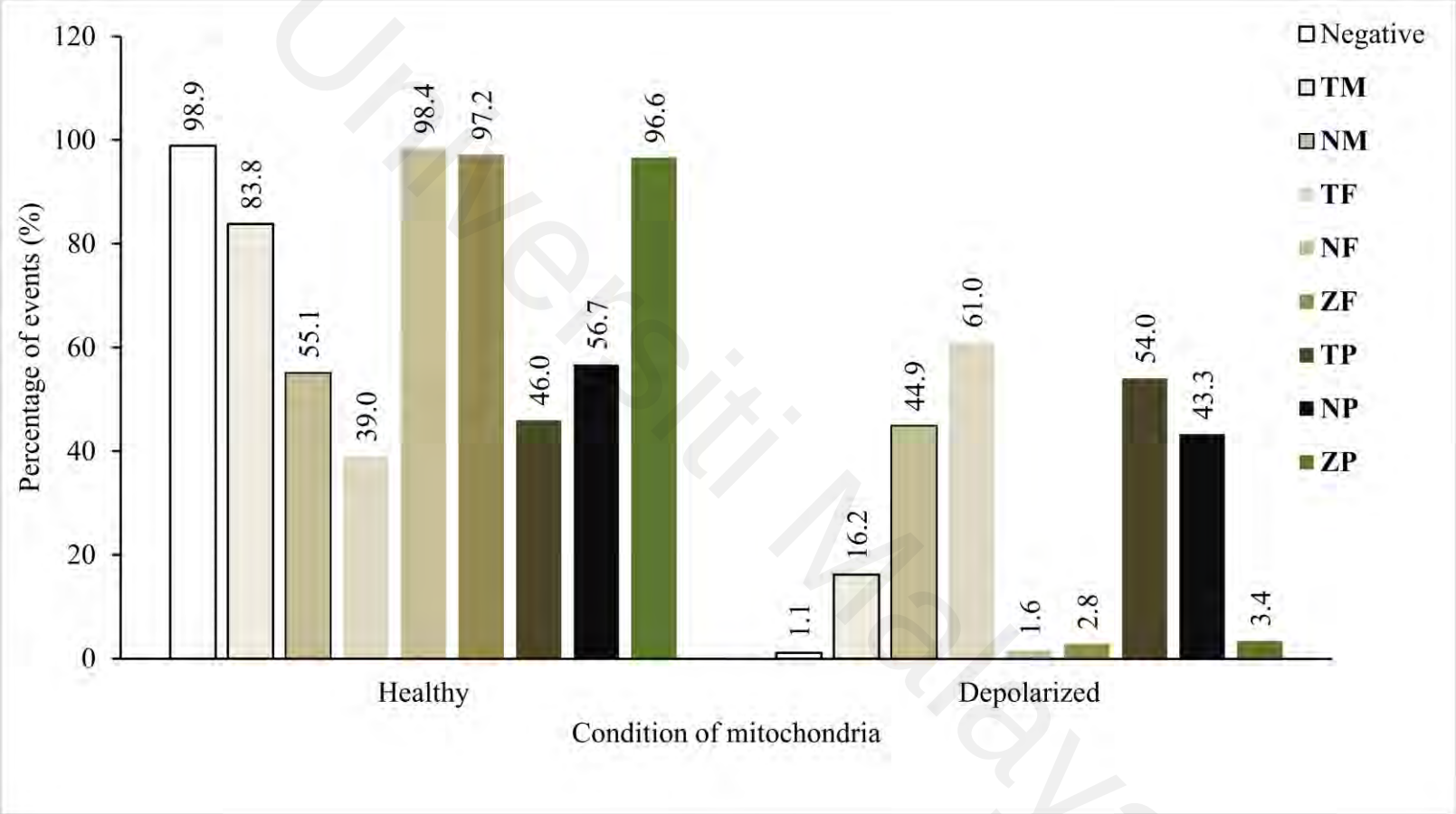

Figure 4.25: Histogram summarizing the effects of exposure to selected compounds on the mitochondria membrane potential in human colorectal carcinoma HCT 116 cells for 48 hours.

Results in Figure 4.24-4.25 showed five out of the eight compounds tested (**TM**, **NM**, **NF**, **TP**, and **NP**) were able to induce depolarization of the ΔΨm. Such decreased in ΔΨm is typically regarded as a sign of the occurrence of mitochondrial swelling, which indicates the alterations in the internal mitochondrial membrane that gradually loses it crista ridges. This will then cause volume expansion and loss of the capacity to generate energy. This mitochondrial edema is required for the release of cytochrome c in the intrinsic pathway of apoptosis (Ly et al., 2003; Marcondes et al., 2019). Therefore, these five compounds, were considered to be able to induce apoptosis *via* intrinsic or the mitochondrial pathway (Heffeter et al., 2019).

Unlike the aforementioned compounds, **NF**, **ZF**, and **ZP** were unable to cause significant disruption to the mitochondrial membrane potential. However, previous experiment has proven that these compounds were apoptotic-inducing, especially when the early apoptotic populations were increased after treatment with these compounds (Figure 4.22-4.23). These results cumulatively suggested these compounds caused cell death *via* the extrinsic pathway, which is induced by death receptors and utilizes protein interaction modules that are known as death domains and death effector domains to induce apoptosis (Natoni et al., 2005). Their cell death mechanisms are therefore mitochondria-independent.

Although similar treatment was subjected to the same cell line, approximately 61.0% of depolarized mitochondria was recorded after treatment with **TF** for 48 hours despite only 7.4% early apoptotic and 13.5% late apoptotic or dead events were recorded in the previous assay (Figure 4.22-4.23). This might be due to the involvement of other pathways in the cytotoxic mechanisms of this Schiff base, for example, the engagement of the extrinsic pathway beyond the intrinsic pathway (Winter et al., 2014).

Once again, the choice of transition metal and thiosemicarbazide in the syntheses of these compounds showed no significant effects on their activities. For instance, complexation with nickel was able to cause higher percentage of depolarized mitochondrial membrane potential in the case of **NM**, while opposite effect was observed in the other two nickel complexes (**NP** and **NF**). Similarly, complexation with zinc has different effects on their parent ligands too. On the other hand, the choice of thiosemicarbazide was unable to tune the cytotoxic properties of one Schiff base ligand family to a similar behavior too. For example, not all the compounds with fluorophenyl derivative (**TF**, **NF**, and **ZF**) were capable of depolarizing the mitochondrial membrane potential.

In short, the eight compounds tested exert their apoptotic-inducing effects through different mechanisms. It is noteworthy that the three compounds from the family of **TP**, which displayed excellent cytotoxicity against HCT 116 (Table 4.19), stimulated programmed-cell death through different mechanisms with the zinc complex **ZP** caused mitochondrial-independent apoptosis.

4.10 Cell cycle analysis

The propidium iodide (PI) flow cytometric assay has been widely performed for the evaluation of apoptosis in different experimental models, mainly based on the principle that apoptotic cells, among other typical features, are characterized by DNA fragmentation and loss of nuclear DNA content (Riccardi & Nicoletti, 2006). This PI dye, which is capable of binding and labelling DNA rapidly, is commonly used in the flow cytometry analysis of DNA content in different stages of cell cycle. In brief, the cell nuclei contain different amounts of DNA at different stages of the cell cycle, varying from two complete sets of chromosome (2N, diploid), to tetraploid state (4N). The DNA content at different stages can be measured when this DNA intercalator is bound to DNA and the fluorescence signal generated correlates with the amount of DNA within the given cell (Zhang et al., 2019). In order to determine whether the cytotoxic effects of the compounds involved alterations in cell cycle progression, the cell cycle distribution analysis *via* flow cytometry using PI as probe was performed and the results were summarized in Figure 4.26-4.27.

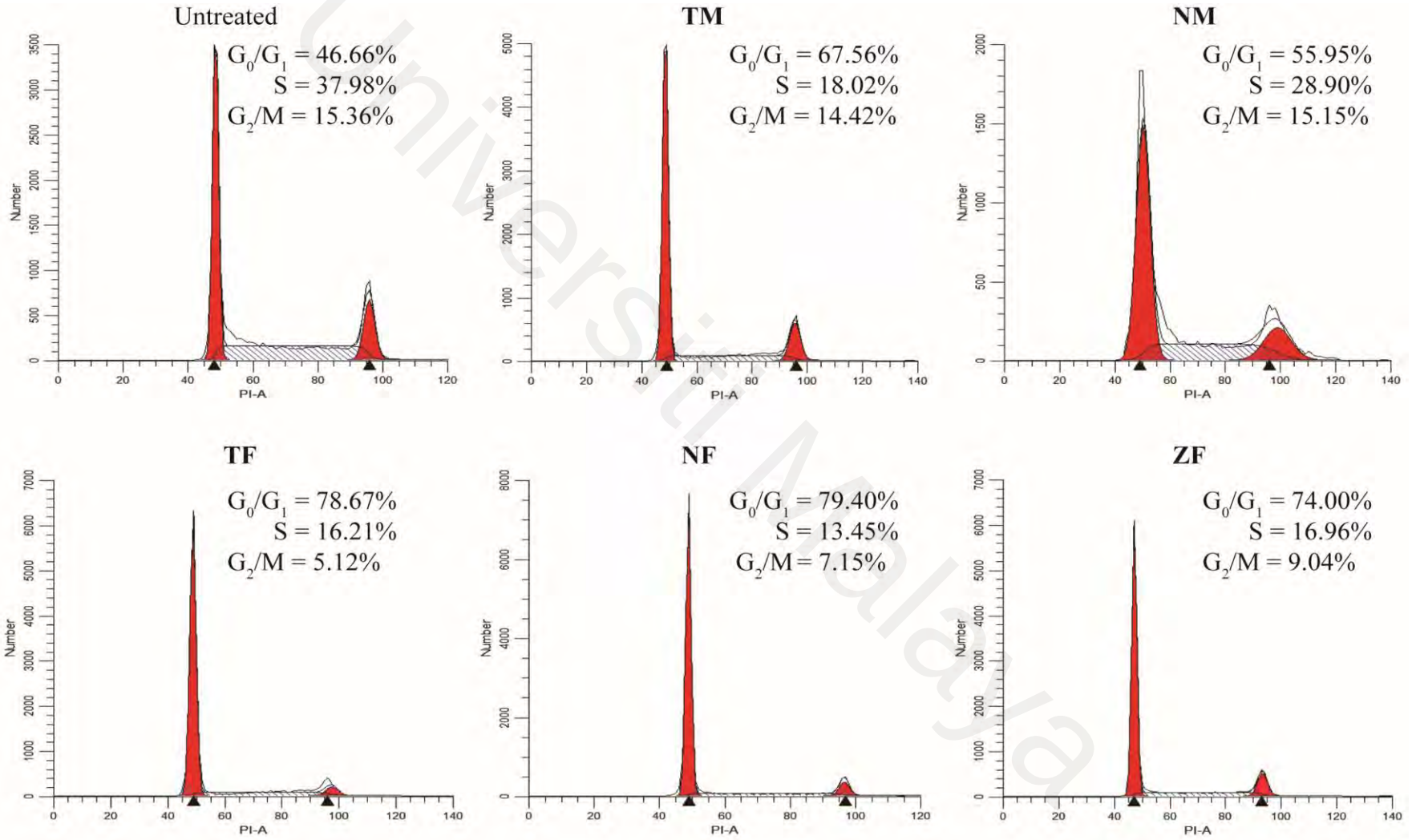

Figure 4.26: Effects of exposure to selected compounds on the cell cycle distribution in human colorectal carcinoma HCT 116 cells for 48 hours.

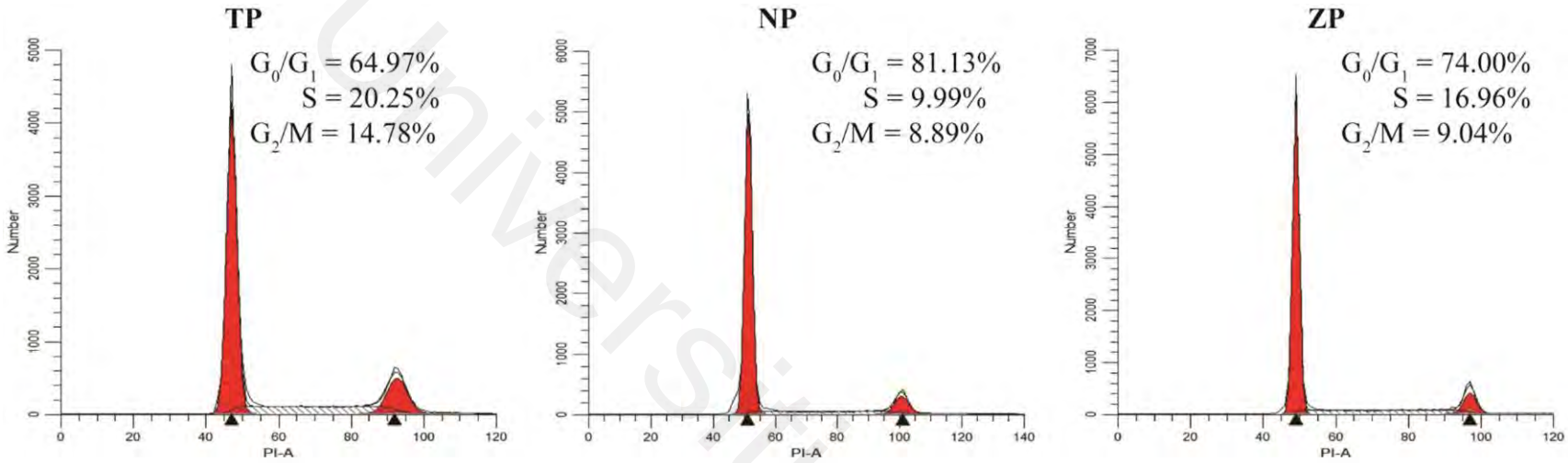

Figure 4.26, continued

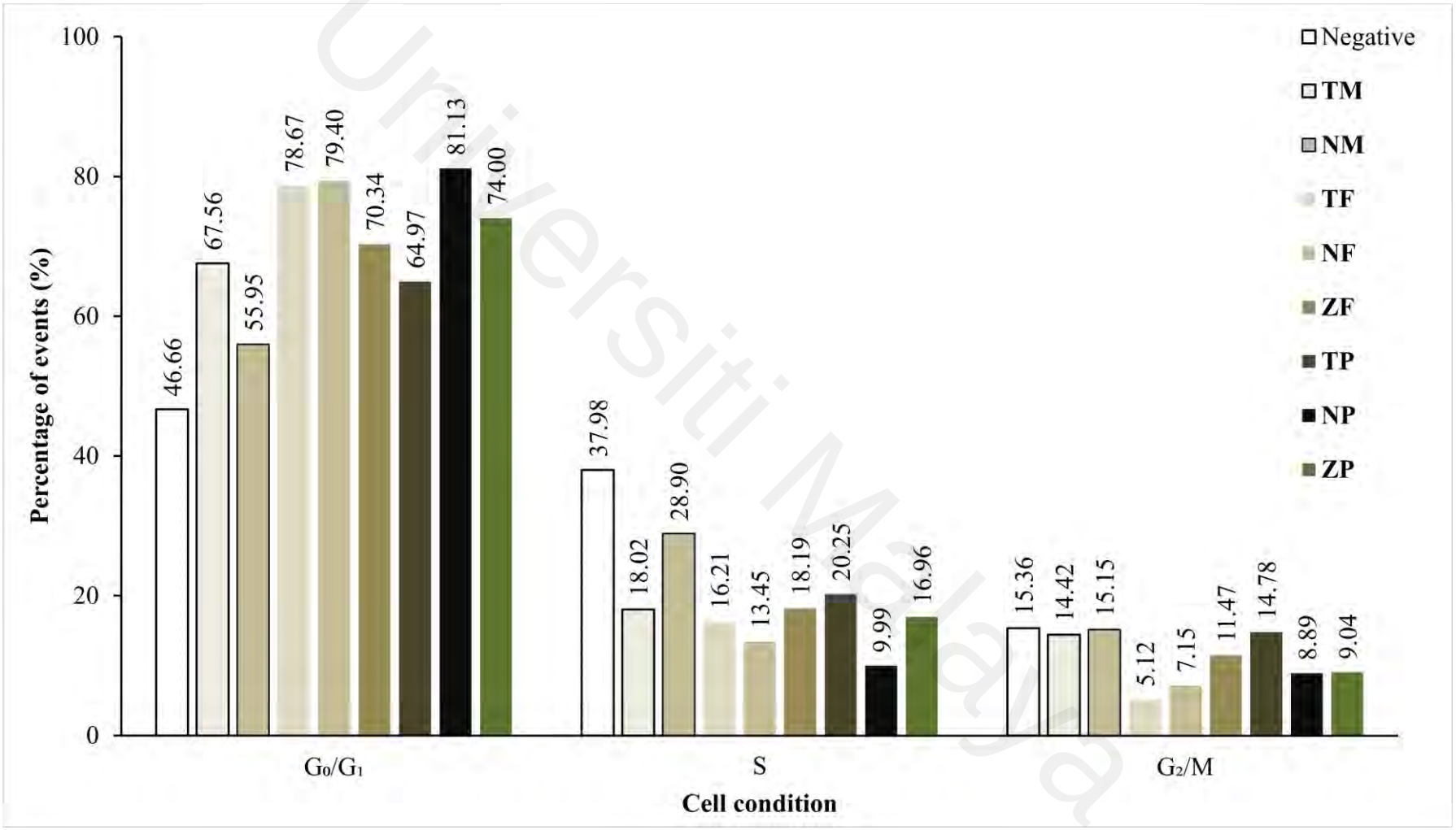

Figure 4.27: Histogram summarizing the effects of exposure to selected compounds on the cell cycle distribution in human colorectal carcinoma HCT 116 cells for 48 hours

There are three main phases in the cell cycle, including the quiescent (G_0) and gap1 (G_1), synthesis (S), and gap2 (G_2)/mitosis (M). In healthy noncancerous cells, there is a mechanism to ensure stoppages in the cell cycle to allow the repair of damaged or mutated DNA and these stoppages usually occur before the commencement of the next cell cycle. This mechanism is especially crucial in preventing the errors of transcription (i.e. caused by mutations of the DNA) to be passed on to the daughter cells in each mitosis. This cell cycle arrest usually occur in the G_1 phase (before the S phase) as to make sure the damaged DNA will not be replicated (Gnewuch & Sosnovsky, 2002). However, cancer cells are unable to block the inheritance of these mutated DNA due to the fact that loss of cell cycle checkpoints is regarded as a hallmark of human cancers. The impaired checkpoint arrest control in these cells allowed the initiation of S phase or mitosis occurs through cellular damage and subsequently the genetic instability may lead to the eventual emergence of a malignant clone, or even worse (Shapiro & Harper, 1999). Also, overgrowth of cancer cells is mainly due to the dysfunction in the regulation of the cell cycle (Balachandran et al., 2018).

Based on the results shown in Figure 4.26-4.27, elevated populations of G_0/G_1 after treatment with the test compounds was observed. For instance, seven out of the eight compounds (**TM**, **TF**, **NF**, **ZF**, **TP**, **NP**, and **ZP**) increased this population to at least 64.97% (46.66% for negative control). Apart from that, treatment with these compounds has decreased populations in S and G_2/M phase. These results indicated that all the test compounds were capable of disrupting the cell cycle at G_0/G_1 stage. As mentioned above, the blockage of cell cycle at G_0/G_1 phase is preferred, mainly due to the prevention of cancerous cells that carry mutated genetic content to multiply without correction. The ability of the tested compounds to induce cell cycle arrest at G_0/G_1 phase is therefore favourable as it may help to limit the inheritance of the mutated genetic materials.

Besides the accumulation of cells in G_0/G_1 phase, the decrease in S and G_2/M populations after treatment with the compounds were also observed. This may explain the excellent cytotoxicity of these compounds (low IC_{50}) against this cell line (Table 4.19) as the proliferation of the cells were blocked and disrupted. Lesser cells were allowed to enter the synthesis phase and subsequently the mitotic phase, thereby resulting in lower growth rate and ultimately decreased cell counts.

Previous assays (Section **4.8**) have demonstrated the apoptosis-inducing ability of these compound on HCT 116 cell line (Figure 4.22-4.23). It is commonly accepted that the efforts to restore the G_1 checkpoint may slow cancer cell growth and induce cell death, while defective G_1 arrest check point may cause a cancer cell to enhanced proliferation (DiPaola, 2002). Therefore, the apoptosis-inducing ability of these compounds might be resulted from their capabilities in arresting the cell cycle at G_0/G_1 phase.

In this assay, the formation of nickel complex has improved the efficacy of **NP** in arresting the cell cycle at G_0/G_1 phase (from 64.97% in **TP** to 81.13%). However, such complexation process has different effects on the other Schiff base ligands. **TF** and its nickel complex **NF** has similar effects in cell cycle arrest, with not much differences in the percentage of G_0/G_1 phase (78.67% and 79.40%), S phase (16.21% and 13.45%), and G_2/M phase (5.12% and 7.15%). In contrast, nickel complex **NM** was unable to match the efficacy of its parent ligand **TM** in reducing the population is S phase (18.02% for **TM** and 28.90% for **NM**) and accumulate cells in G_0/G_1 (67.56% in **TM** and 55.95% in **NM**) phase.

Similarly, formation of zinc complex has different effects too. Zinc complex **ZF** accumulated lesser cells in G_0/G_1 phase (78.67% is **TF** and 70.34% in **ZF**) but the efficacy of **ZP** was improved (G_0/G_1 phase = 64.97% in **TP** and 74.00% in **ZP**). Besides

that, choice of thiosemicarbazide has no specific/fixed effects on the cell cycle arrest efficacy too.

Together with results from previous assays, these observations cumulatively suggested involvement of different pathway/biomolecules in the cytotoxicity of these compounds. For example, zinc complex **ZP** was able to induce apoptosis independent of mitochondria and least amount of this complex was required to reduce 50% of the growth rate of colorectal carcinoma cell line HCT 116 (lowest IC_{50}) despite not being the most effective in reducing the populations entering S phase. In contrast, relatively higher IC_{50} value for **NF** was obtained (18.08±1.82 nmol/mL compared to 9.31±0.34 nmol/ml for **ZP**) despite being more effective in arresting cell cycle at G_0/G_1 phase (79.40% in **NF** and 74.00% in **ZP**) and reducing populations in S phase (13.45% in **NF** and 16.96% in **ZP**).

4.11 DNA binding studies

The interaction of metal complexes (or other potential chemotherapeutics) with DNA is always a major interest in the development of antitumour compounds. UV spectrophotometry is one of the most commonly utilized techniques in the investigation of such interaction. It is widely accepted that a molecule will be positioned in an environment that is different from the uncomplexed molecule in the solution upon binding to DNA. These different features will lead to distortion in electron distribution upon π-stacking with the bases, and ultimately lead to the significantly different absorption properties in the complexed and uncomplexed forms (Ihmels & Otto, 2005).

The absorption spectra of all the compounds in the presence and absence of CT-DNA were recorded. CT-DNA was added until the compound is fully bound to DNA (where further addition of DNA results in no absorption change). Results are shown is Figure 4.28-4.37 and the details were summarized in Table 4.20.

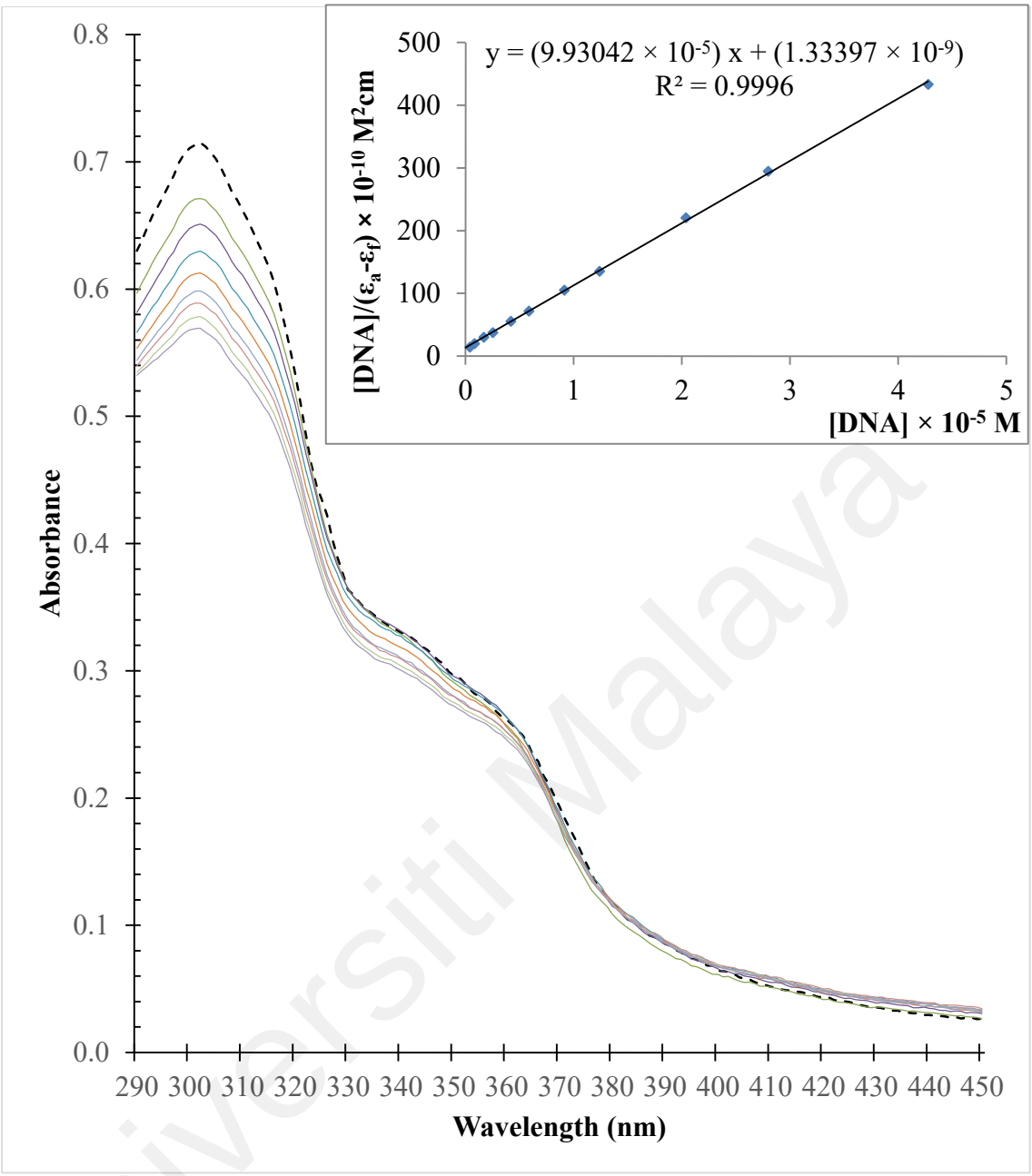

Figure 4.28: Spectrophotometer titration of **TM** (150 µM) dissolved in 10% DMSO-TN buffer (pH 7.5) with CT-DNA from 0 µM (top, dotted line ---) to 42.75 µM (bottom). Inset: Plot for calculation of binding constant K_b.

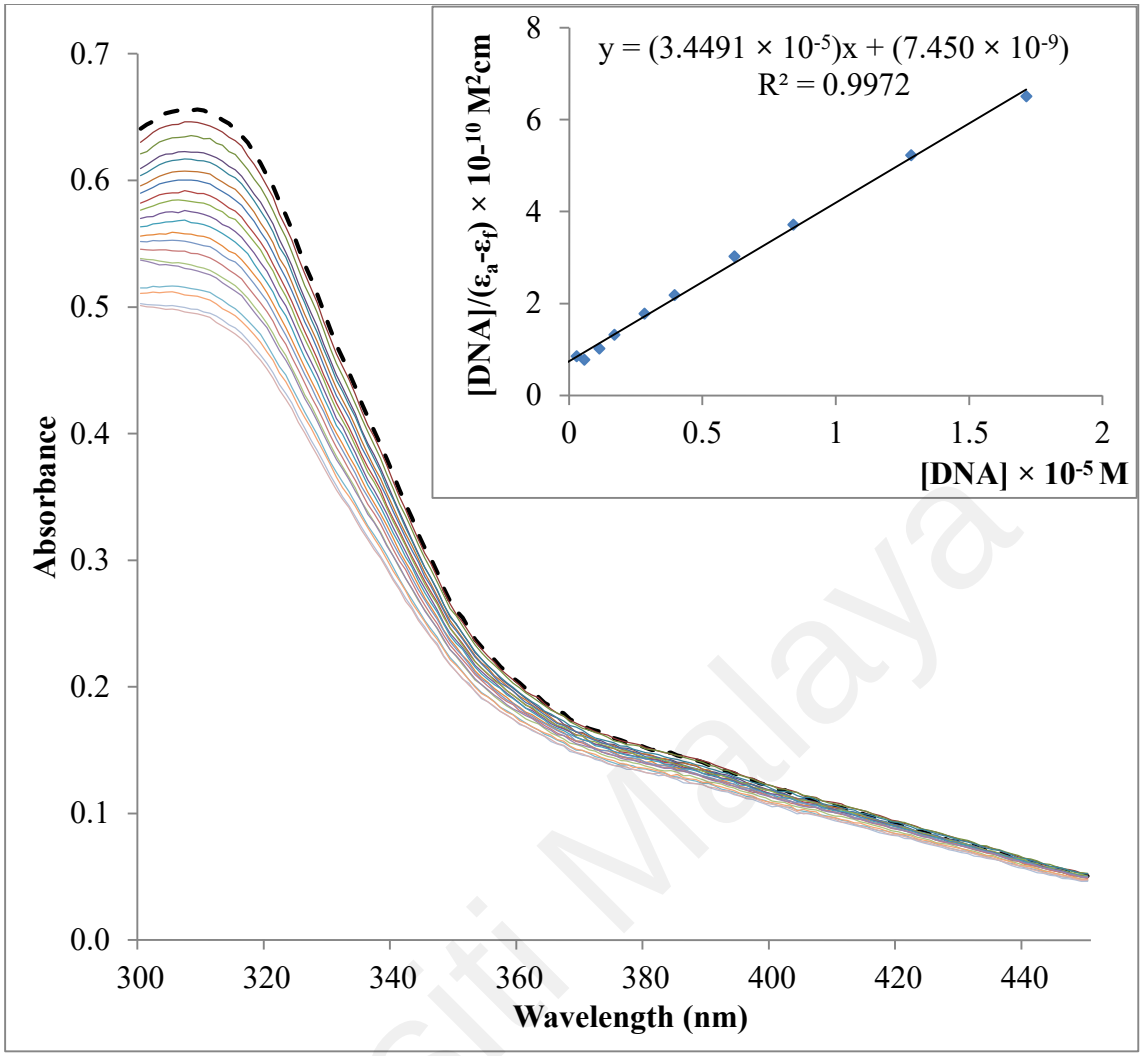

Figure 4.29: Spectrophotometer titration of **NM** (150 µM) dissolved in 10% DMSO-TN buffer (pH 7.5) with CT-DNA from 0 µM (top, dotted line ---) to 17.14 µM (bottom). Inset: Plot for calculation of binding constant K_b.

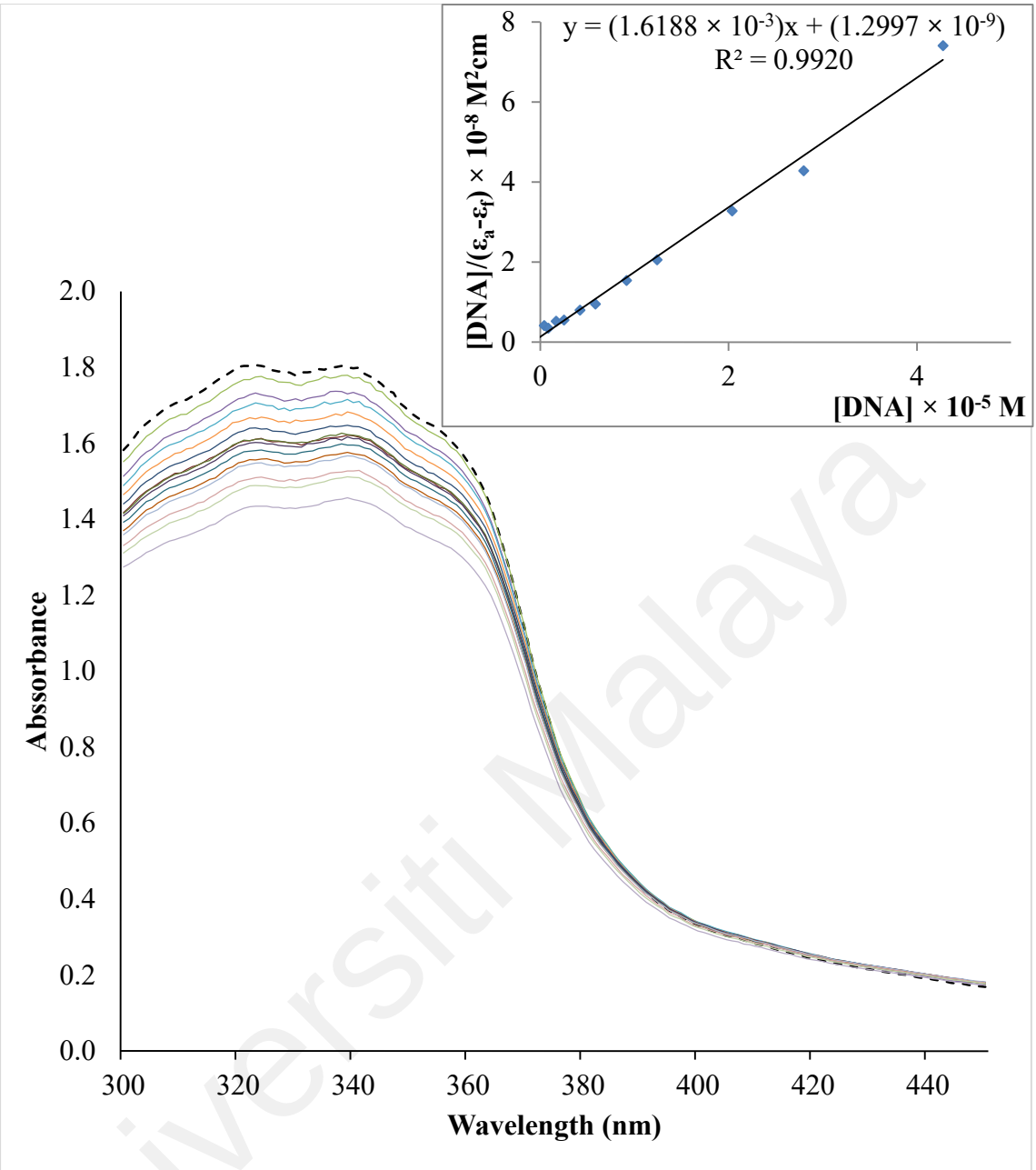

Figure 4.30: Spectrophotometer titration of **ZM** (300 µM) dissolved in 10% DMSO-TN buffer (pH 7.5) with CT-DNA from 0 µM (top, dotted line ---) to 43.75 µM (bottom). Inset: Plot for calculation of binding constant K_b.

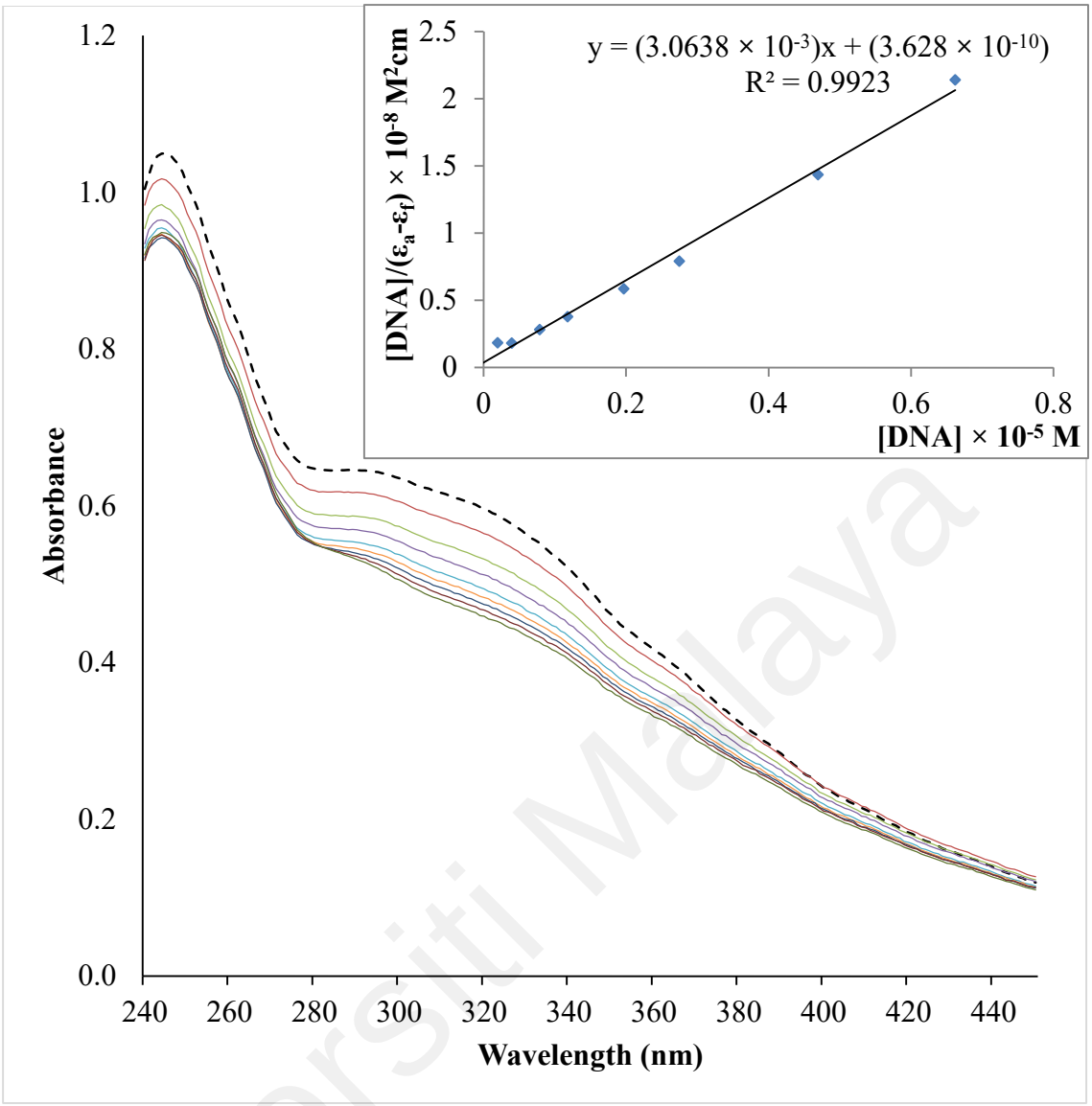

Figure 4.31: Spectrophotometer titration of **TP** (300 µM) dissolved in 10% DMSO-TN buffer (pH 7.5) with CT-DNA from 0 µM (top, dotted line ---) to 4.69 µM (bottom). Inset: Plot for calculation of binding constant K_b.

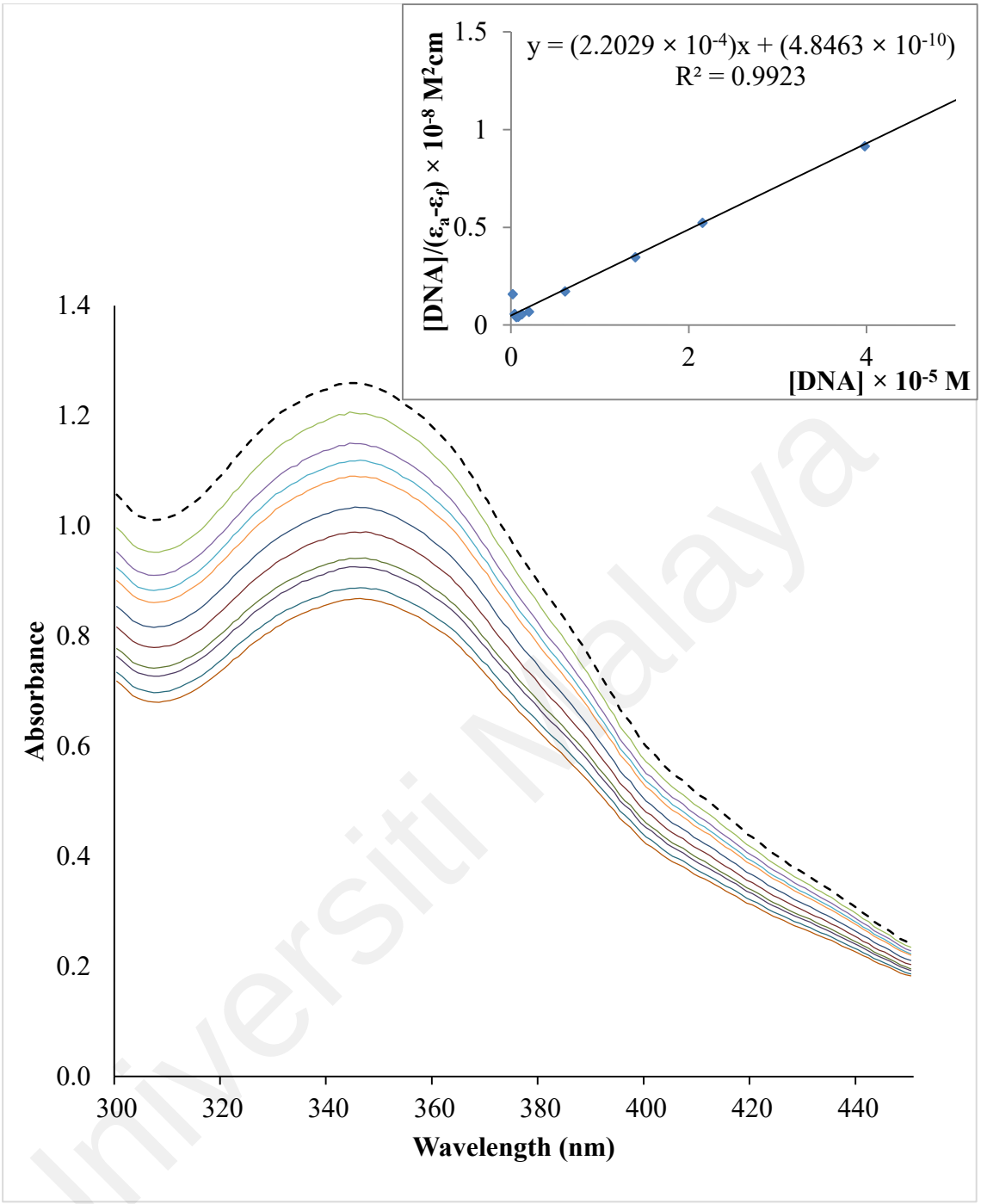

Figure 4.32: Spectrophotometer titration of **NP** (75 µM) dissolved in 10% DMSO-TN buffer (pH 7.5) with CT-DNA from 0 µM (top, dotted line ---) to 56.18 µM (bottom). Inset: Plot for calculation of binding constant K_b.

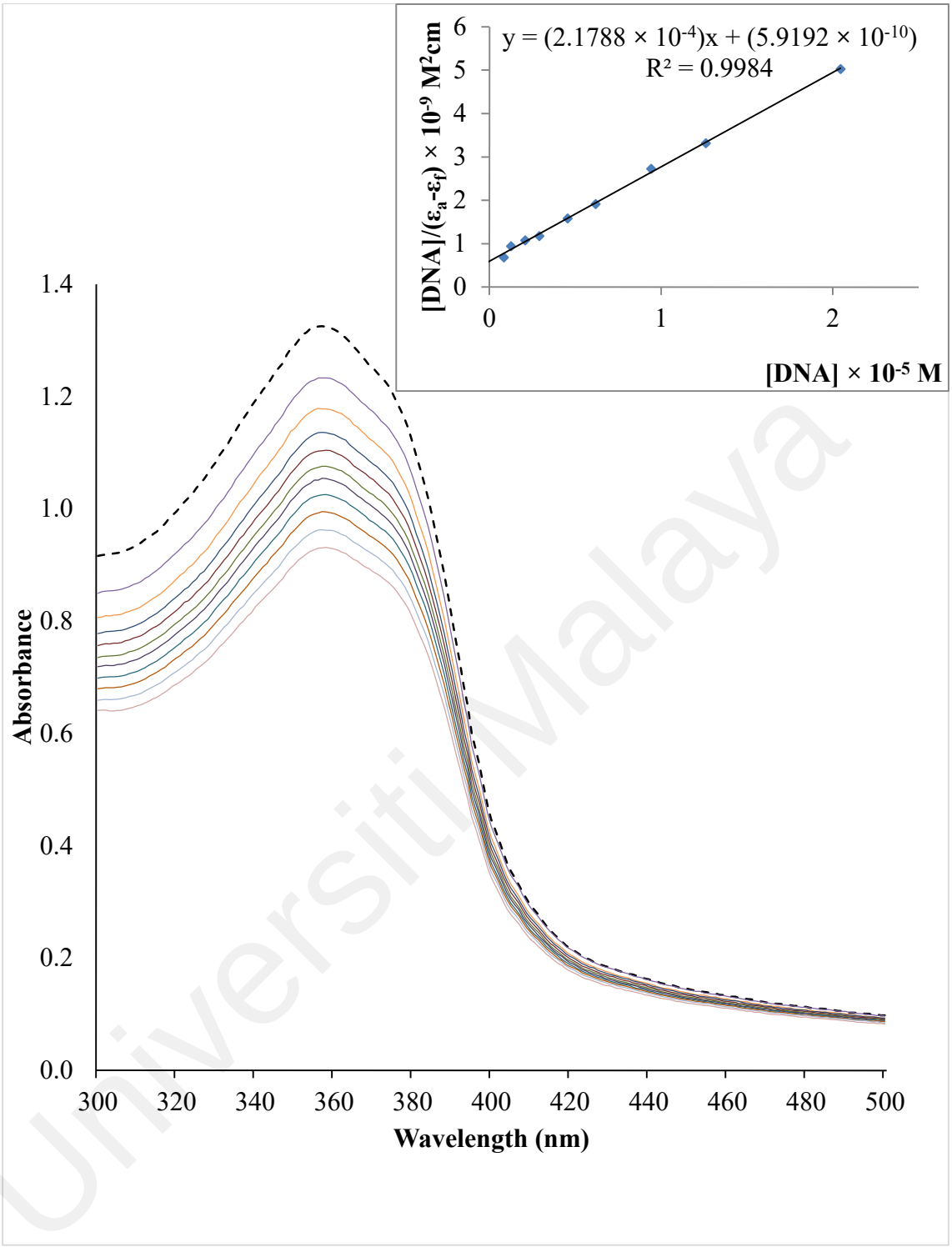

Figure 4.33: Spectrophotometer titration of **ZP** (75 µM) dissolved in 10% DMSO-TN buffer (pH 7.5) with CT-DNA from 0 µM (top, dotted line ---) to 20.44 µM (bottom). Inset: Plot for calculation of binding constant K_b.

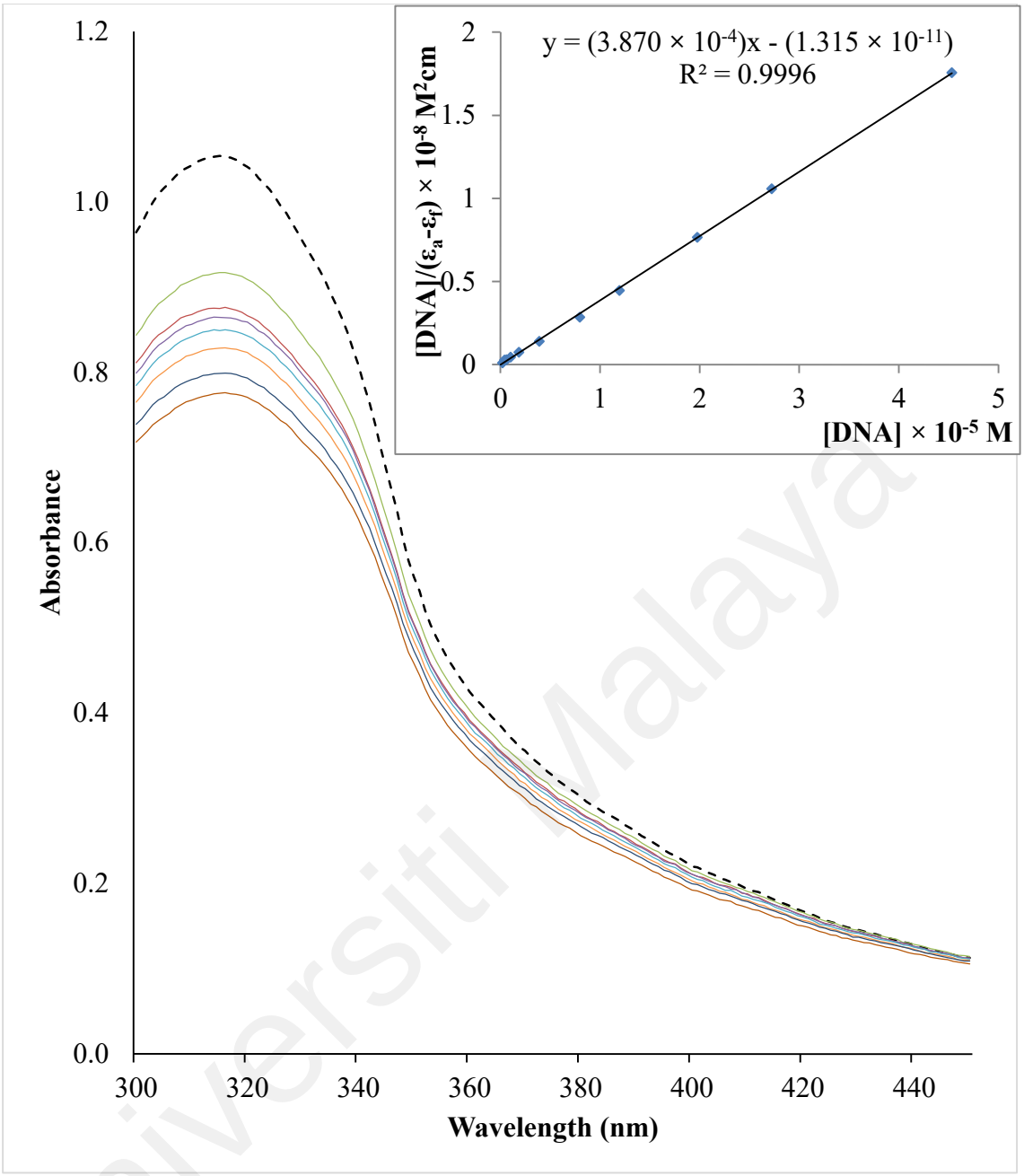

Figure 4.34: Spectrophotometer titration of **TF** (90 µM) dissolved in 10% DMSO-TN buffer (pH 7.5) with CT-DNA from 0 µM (top, dotted line ---) to 45.34 µM (bottom). Inset: Plot for calculation of binding constant K_b.

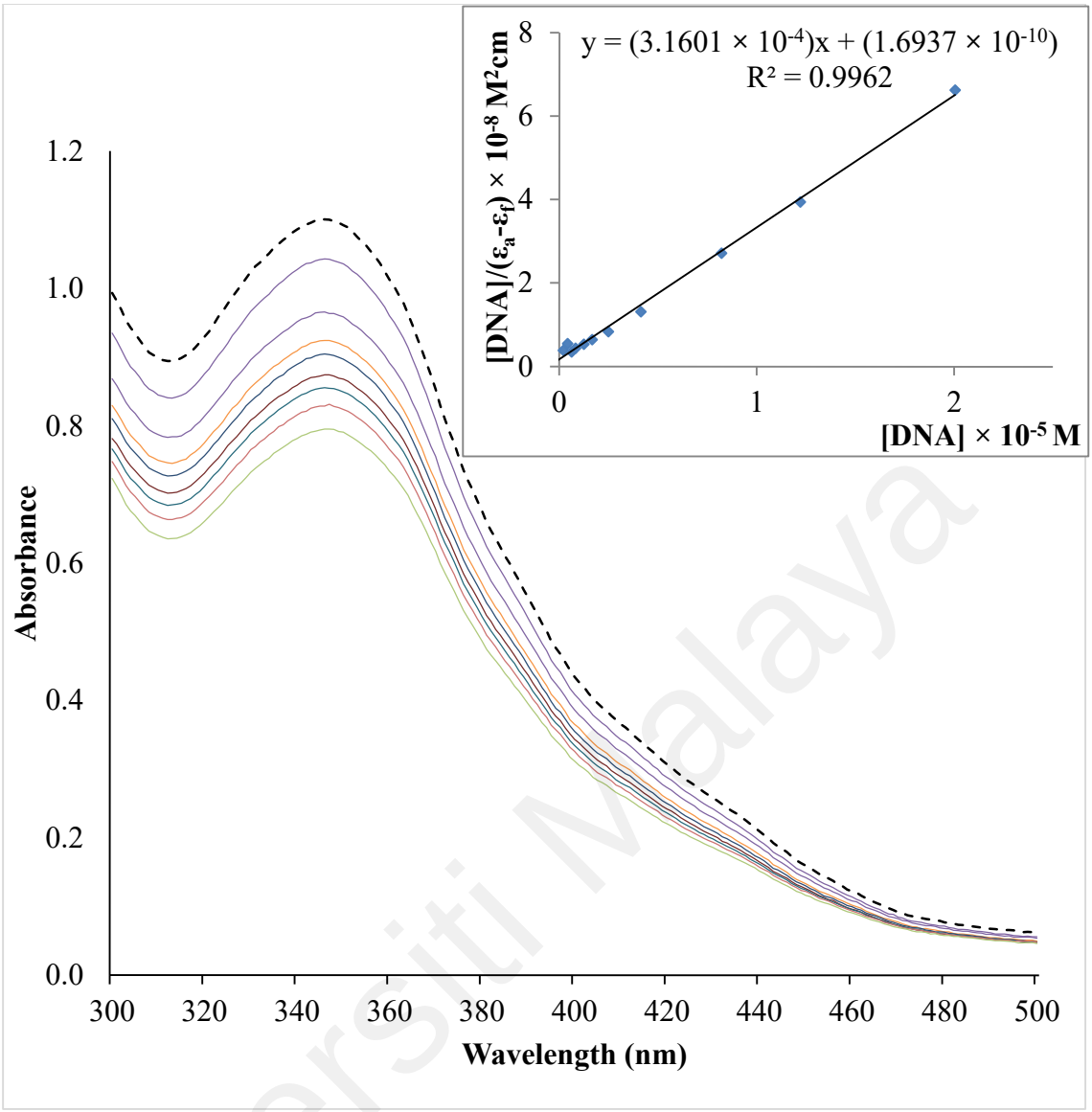

Figure 4.35: Spectrophotometer titration of **NF** (75 µM) dissolved in 10% DMSO-TN buffer (pH 7.5) with CT-DNA from 0 µM (top, dotted line ---) to 20.05 µM (bottom). Inset: Plot for calculation of binding constant K_b.

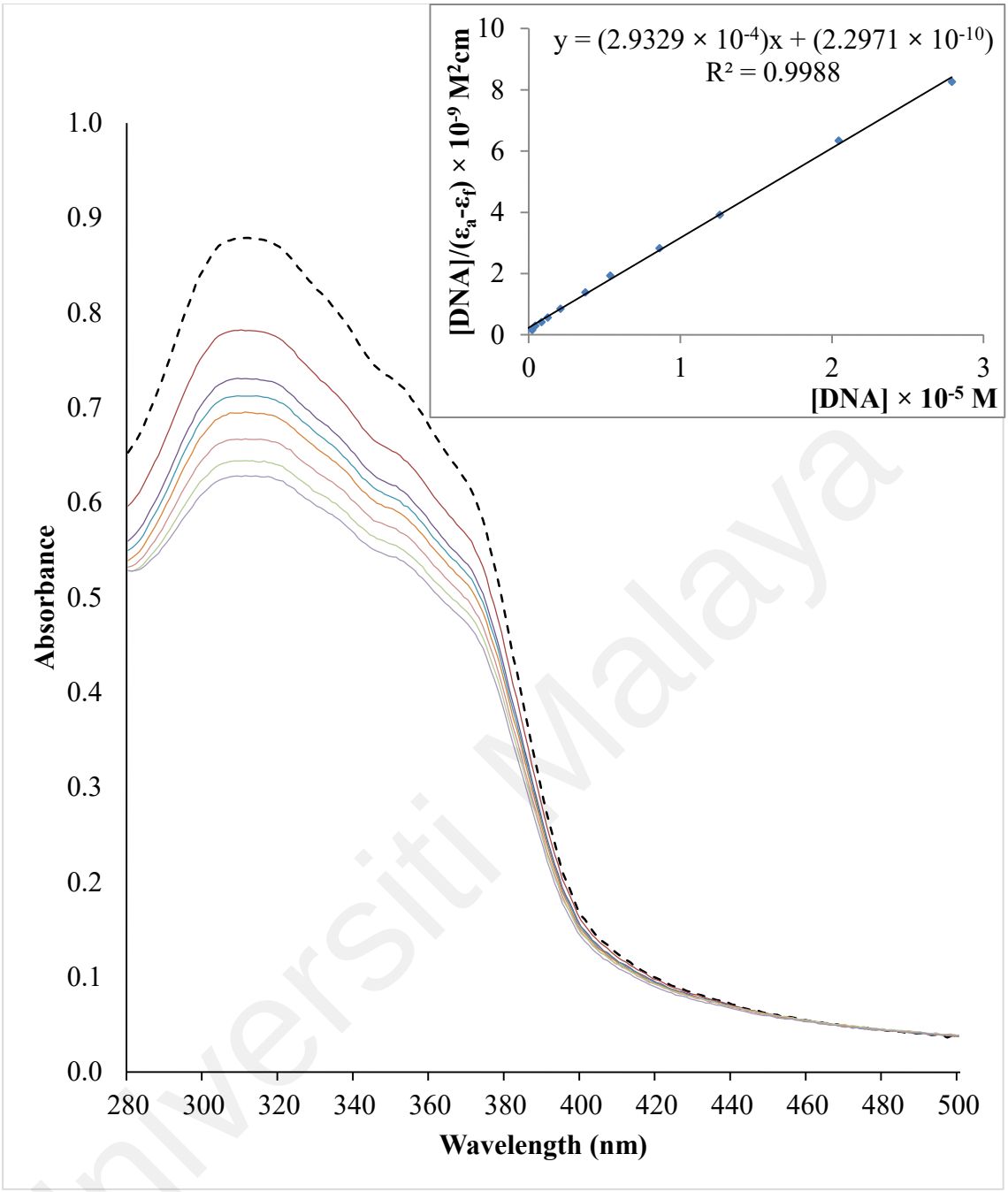

Figure 4.36: Spectrophotometer titration of **ZF** (75 µM) dissolved in 10% DMSO-TN buffer (pH 7.5) with CT-DNA from 0 µM (top, dotted line ---) to 27.90 µM (bottom). Inset: Plot for calculation of binding constant K_b.

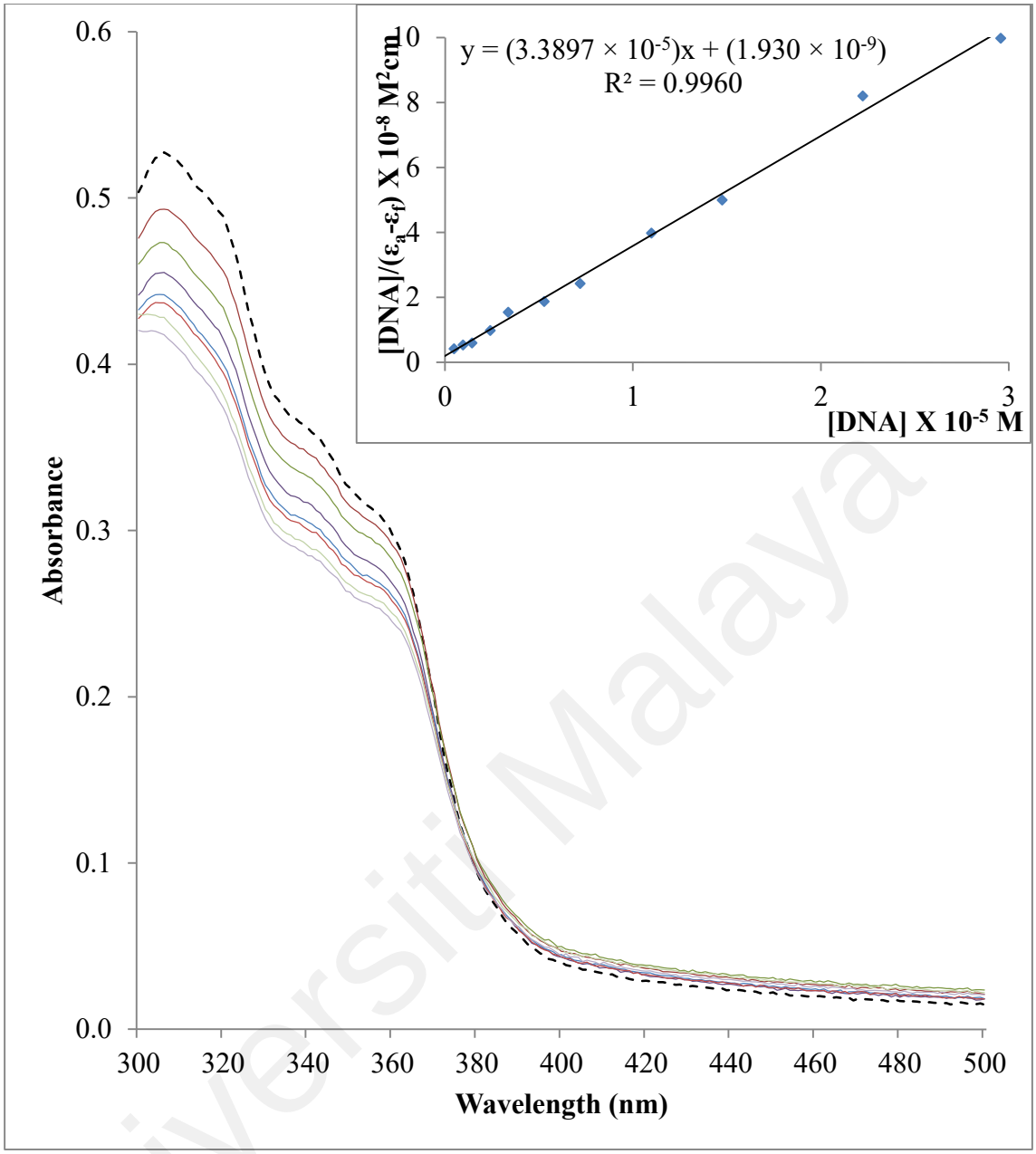

Figure 4.37: Spectrophotometer titration of **ZE** (300 µM) dissolved in 10% DMSO-TN buffer (pH 7.5) with CT-DNA from 0 µM (top, dotted line ---) to 29.56 µM (bottom). Inset: Plot for calculation of binding constant K_b.

Table 4.20: The binding constant (K_b) values of the compounds with CT-DNA.

Compound	λ_{max} (nm)	Blue shift (nm)	[Compound] (μM)	[DNA] added (μM)	Hypochromism (%)[a]	Binding constant K_b (M^{-1})
TM	302	0	150	42.75	24.84	7.4×10^5
NM	312	0	150	17.14	13.38	4.6×10^3
ZM	323	0	300	43.75	14.30	1.2×10^6
TP	244	0	300	4.69	9.88	8.4×10^6
NP	345	0	75	56.18	31.11	4.5×10^5
ZP	357	0	90	20.44	24.93	3.7×10^5
TF	315	1	90	45.34	26.44	2.9×10^7
NF	346	0	75	20.05	22.55	1.9×10^6
ZF	311	0	75	27.90	31.23	1.3×10^6
ZE	306	0	300	29.56	18.15	1.8×10^4

[a]Hypochromism (%) = $(A_{free} - A_{bound})/A_{free}$

Hypochromism (decrease absorbance) was observed in the intra-ligand bands of the compounds upon addition of CT-DNA. As suggested by literatures, the hypochromism observed might be resulted from the contraction of DNA structure upon intercalative binding of the compounds (Reddy et al., 2011; Lafayette et al., 2013). However, these compounds are unlikely to bind to DNA through intercalation, due to the fact that no bathochromic and/or isosbestic point were observed (Afrati et al., 2010). Therefore, the binding of these compounds to DNA are most probably due to multiple modes such as DNA surface binding, or non-classical intercalation that is different compared to that of ethidium bromide (Ishida & Asao, 2002). Covalent binding mode can be excluded because the well-recognized covalent DNA binder cisplatin was reported to generate hyperchromism along with red shift when it is bound to DNA (Arjmand et al., 2011).

Decreased in absorbance of nickel complexes with increasing DNA concentration was reported by some other researchers including Zhu et al. (2015) and Wu et al. (2012). However, these two groups concluded their experiment by intercalation (or partial intercalation) binding mode because red shift was observed in both cases (Wu et al., 2012; Zhu et al., 2015). Therefore, this binding mode can be excluded safely, since no red shift

was observed in current results. As a result, the compounds are most likely surface binders (such as groove binders).

The binding affinity of the compounds synthesized was further investigated *via* calculations of their intrinsic binding constant K_b (Table 4.20). The increasing order of binding energy is: **TF**>**TP**>**NF**>**ZF**>**ZM**>**TM**>**NP**>**ZP**>**ZE**>**NM**.

The results showed that the Schiff base ligand **TF** has the K_b value of highest magnitude, which is indicative of strongest binding affinity towards the CT-DNA compared to others. This outstanding affinity towards DNA might be the reason why **TF** was able to inhibit the growth of all the cell lines tested, including the noncancerous one, as DNA is ubiquitously present in all cell types.

This assay has proved that complexation does not always help in improving the binding affinity towards DNA, as stronger binding strength was recorded in almost all the case of organic Schiff base ligand. For instance, only the zinc complex **ZM** has better binding strength towards DNA while all the other metal complexes bind weaker compared to their respective parent ligand. In this case, the binding strength of the compounds were dictated by the molecular size rather than the type of metal ion center, as the small size ligands displayed higher K_b values compared to their metal complexes.

All the compounds from the family of **TF** exhibit stronger binding strength towards DNA. This might be due to the electron withdrawing nature of fluoro group in these molecules. As mentioned earlier, the fluoro group in 4-(4-fluorophenyl)-3-thiosemicarbazide will drain electron density from the π-system, deactivate it from electrophilic attack and rendered it more acidic (Bader & Chang, 1989; Al-Hazmi et al., 2005; Liu, 2014). These compounds will have higher tendency towards the DNA backbone, which is negatively charged in nature and therefore resulting in stronger binding strength. Together with the relatively acidic property of the compound, it is not

surprised to realize strongest binding strength was recorded in the case of **TF**, which has the smallest molecular size among the three compounds from this family.

The presence of electron donating groups (methyl, ethyl, and ethylphenyl) in the families of **TM** and **TP**, as well as **ZE**, might have rendered these compounds more basic and their interactions with DNA might be weaker (compared to **TF**). However, the binding of compounds from the family of **TP** has resulted in higher K_b values compared to that of **TM**. This is probably due to the effective stacking interaction due to the extended rings in testosterone moiety and extra planar ring of the phenyl group. In fact, increased in planarity may enhanced the DNA binding strength and therefore resulting in higher K_b values (Lauria et al., 2014).

4.12 Docking simulations

The spectroscopic results explained above were further corroborated by computational docking simulations that provide theoretical insight into the interaction between the Schiff base compounds with DNA double helix. The crystal structures of **TM**, **NM**, **TP**, **TF**, **NF**, and **ZE** were docked with a DNA duplex of sequence d(CGCGAATTCGCG)$_2$ dodecamer (PDB entry: 1BNA) using Autodock 4.2 to check their DNA surface binding ability (Morris et al., 1998; Morris et al., 2009). Besides, the ability of these compounds to bind to DNA through intercalation was tested by replacing 1BNA with 1XRW (al-Rashida & Ahsen, 2015). Results are illustrated in Figure 4.38 and 4.39.

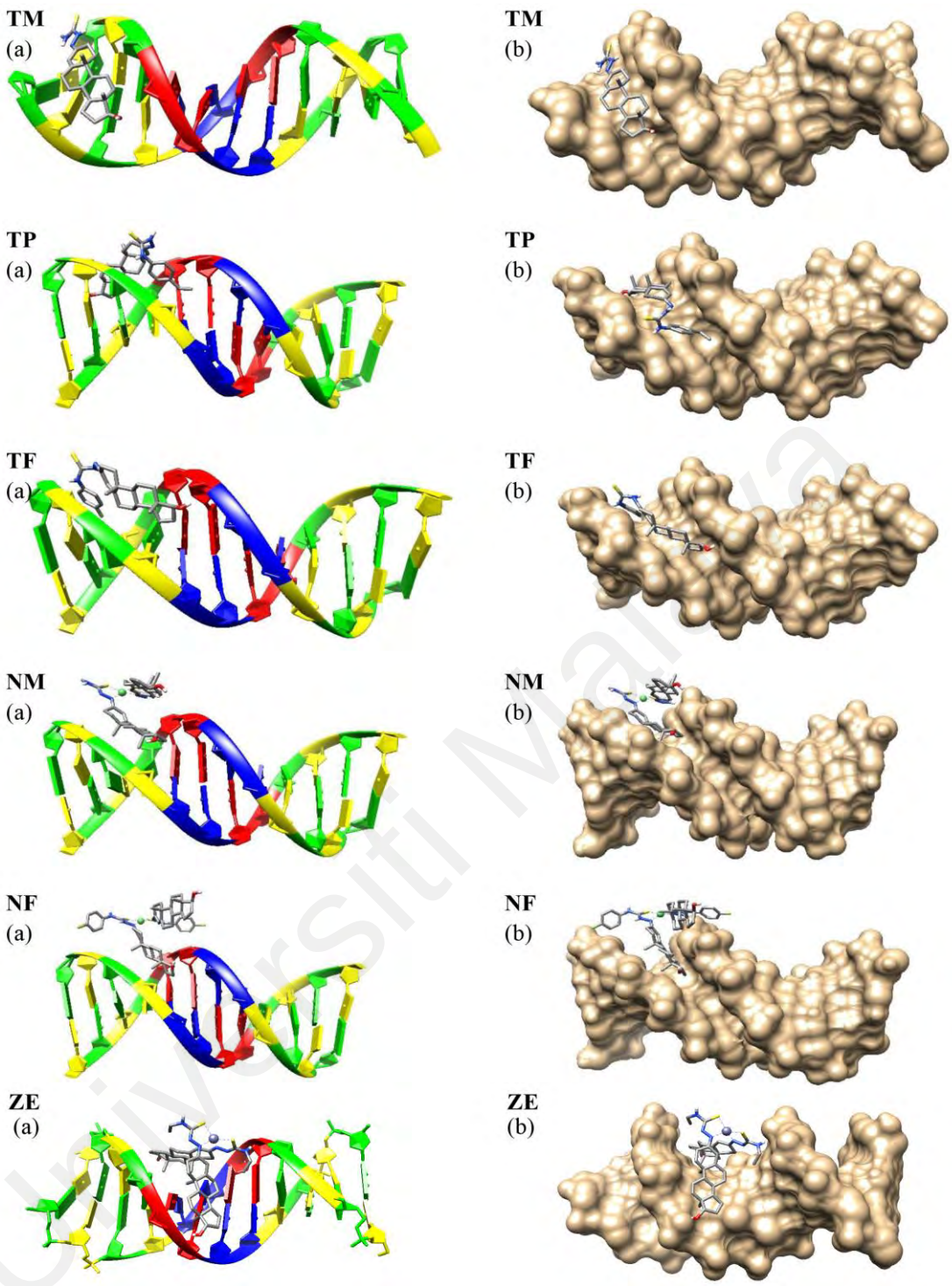

Figure 4.38: (A) Computational docking model illustrating the interaction between compounds synthesized and B-DNA (red = adenine; blue = thymine; yellow = cytosine; green = guanine). (b) Interaction between compounds synthesized and B-DNA (hydrophobic surface).

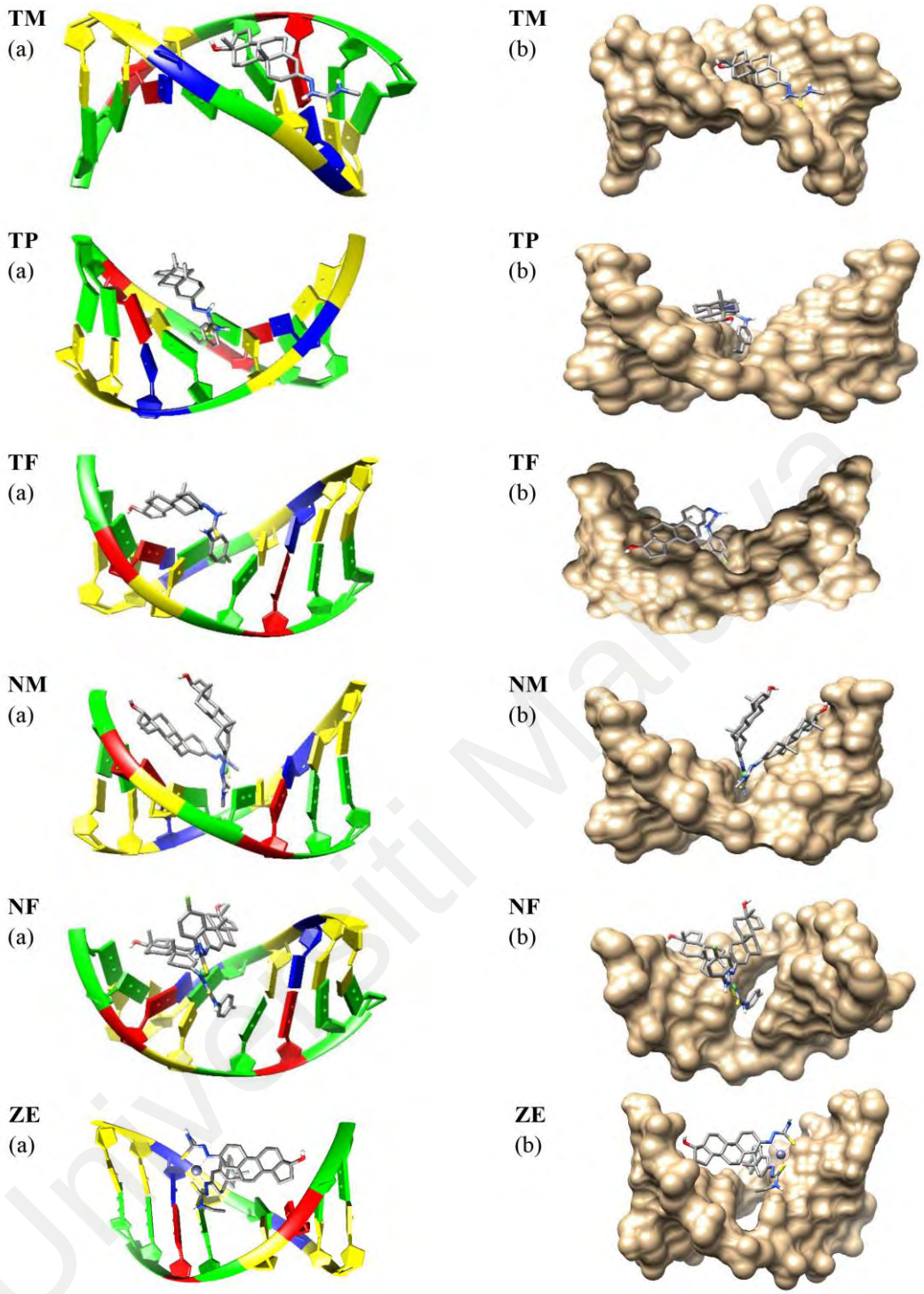

Figure 4.39: (A) Computational docking model illustrating the interaction between compounds synthesized and 1XRW (red = adenine; blue = thymine; yellow = cytosine; green = guanine). (b) Interaction between compounds synthesized and 1XRW (hydrophobic surface).

Results in Figure 4.38 showed that all the test compounds preferred to fit into the minor groove of DNA in a parallel manner with respect to the DNA backbone, with the exception of **ZE**. In particular, all the Schiff base ligands tested were sandwiched in between double helix of DNA. This might be due to the extended rings in testosterone moiety that allowed the compounds to stack in between the DNA backbone effectively. Apart from that, the crescent-shape of these molecules allowed better binding to the minor groove of DNA (Sangeetha Gowda et al., 2014). Unlike the Schiff base ligands, only part of the nickel complexes **NM** and **NF** were inserted into the minor groove, which is undoubtedly due to the increased molecular size. The preferences of zinc complex **ZE** towards the major groove of DNA might be due to the relatively larger molecular size.

The same compounds were then docked to 1XRW to check their ability to bind to DNA as intercalator (Figure 4.39). Although these compounds bound to the DNA model at the region nearby the intercalation pocket, none of these compounds enter the gap in between the DNA backbone. However, the preferences of these compounds to bind this region may suggest their potential to bind to DNA *via* partial intercalation.

Based on results displayed in Figure 4.38 and 4.39, all the compounds tested preferred to bind to the GC-rich region of the DNA (except **ZE**), regardless of the DNA model. This might be due to the presence of extra hydrogen bond donors and acceptors at the GC region, as guanine and cytosine were bound by three hydrogen bonds while adenine and thymine were paired by two hydrogen atoms. The compounds tested may bind to the DNA as stacked dimers with hydrogen-bond accepting or donating groups, due to the presence of donors (such as oxygen and fluorine atoms) and acceptors in the molecules (Fonseca Guerra et al., 2000; Nanjunda & Wilson, 2012).

Besides the possible binding site, binding strength of the compounds can be deduced from docking simulations as well. Results in Table 4.21 showed stronger estimated

binding energy for the docked surface binders (1BNA) compared to that of intercalators (1XRW), which indicates the compounds' preferences to bind to DNA as surface binders. Apart from that, both the estimated binding energy for surface binders and the binding constant K_b recorded *via* UV-Vis displayed similar order of binding affinity with the sequence of **TF**>**TP**>**NF**>**TM**>**ZE**>**NM**.

Table 4.21: The estimated free energy for binding of **TM**, **TP**, **TF**, **NM**, **NF**, and **ZE** to DNA.

Compound	Binding Energy (kcal mol^{-1})	
	1BNA	1XRW
TM	-6.52	-4.95
TP	-6.61	-4.65
TF	-7.67	-4.49
NM	-6.08	-5.07
NF	-6.59	-6.38
ZE	-6.22	-5.21

Results from UV-Vis spectroscopy and *in silico* studies suggested all the synthesized compounds preferred to bind to DNA *via* surface binding, with **TF** being the strongest DNA binder.

4.13 Topoisomerase I inhibition

Increased expression of DNA topoisomerase I (topo I) is detected in numerous neoplastic tissues. Elevated expression level of this enzyme is thought to be important in the replication of DNA and ultimately the proliferation of cancer cells. For instance, increased topo I activity was observed in colorectal carcinomas, ranging from 43-86% in various studies (Tsavaris et al., 2009). Derivatives of the camptothecin family are the drugs that are mainly used in the treatment of colon cancer (Lafayette et al., 2013).

Despite effective in treating colon cancer, administration of these drugs is usually accompanied by notorious side effects such as high toxicity and development of resistance (Ping et al., 2006; Beretta et al., 2012). Hence, the development of non-camptothecin-based topo I inhibitors, or compounds that are capable of inhibiting the growth of colon cancer cells without primarily targeting topo I, are highly encouraged. Apart from that, the ability of the synthesized compounds to bind to DNA has aroused the curiosity of their potential as topo I inhibitor since topo inhibitors usually exert their effect by binding to DNA.

The topo I inhibitory properties of the synthesized compounds were examined and results were shown in Figure 4.40-4.42. The plasmid DNA pBR322 served as a good substrate for the study of topo I activity. In the absence of topo I, the native/compact supercoiled DNA (Form I) is capable of travelling faster in the gel during electrophoresis (Figure 4.40-4.42, lane 2). When it is relaxed by topo I, the relaxed closed circular DNA (Form II) will migrate slower compared to the Form I DNA. In this DNA relaxation experiment, 0.25 unit of *E. coli* topo I is proven to be able to convert all the supercoiled pBR322 DNA to fully relaxed topoisomers (Figure 4.40-4.42, lane 4) (Webb & Ebeler, 2004).

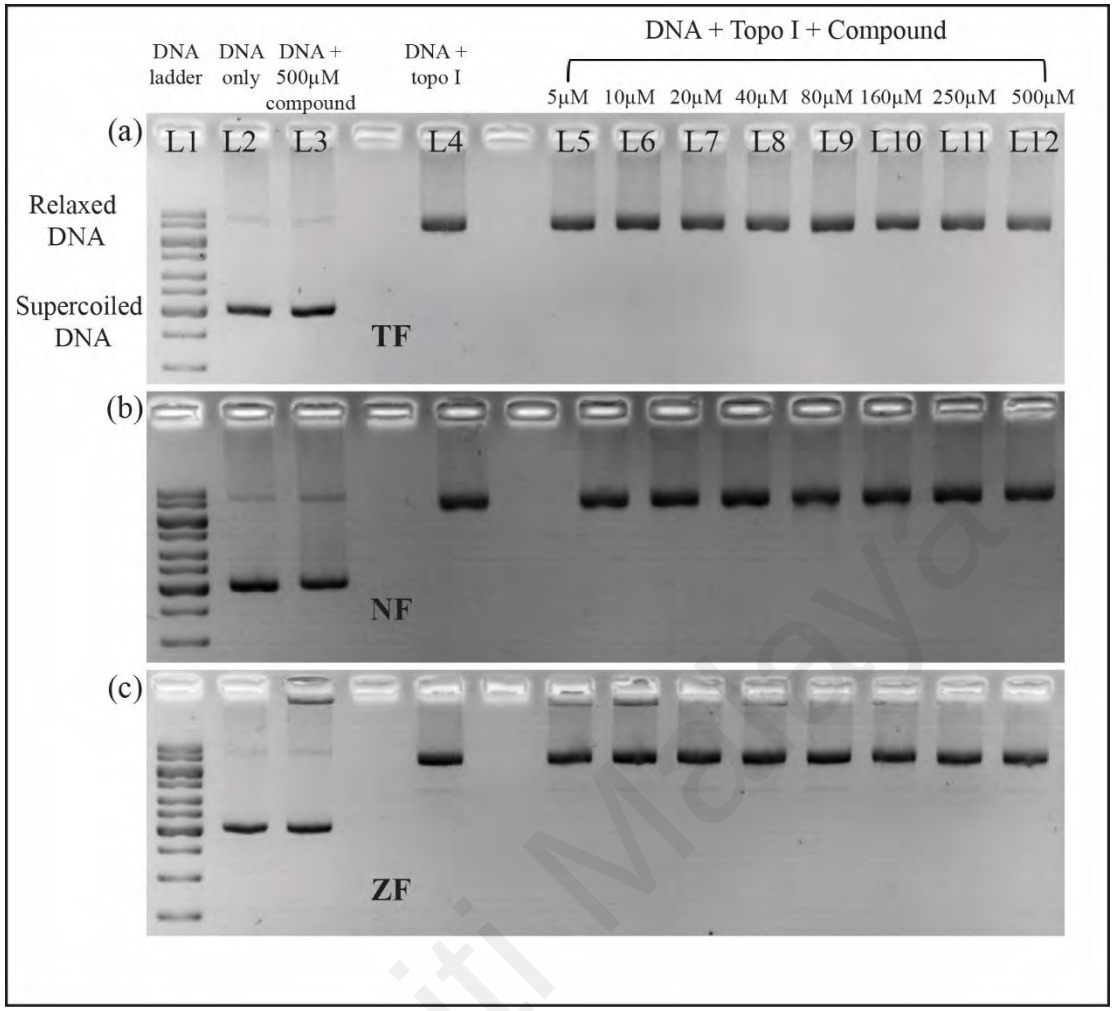

Figure 4.40: Electrophoresis result of incubating *E. coli* topo I (0.25 unit) with pBR322 in the absence and presence of various concentration of (a) **TF**, (b) **NF**, and (c) **ZF**.

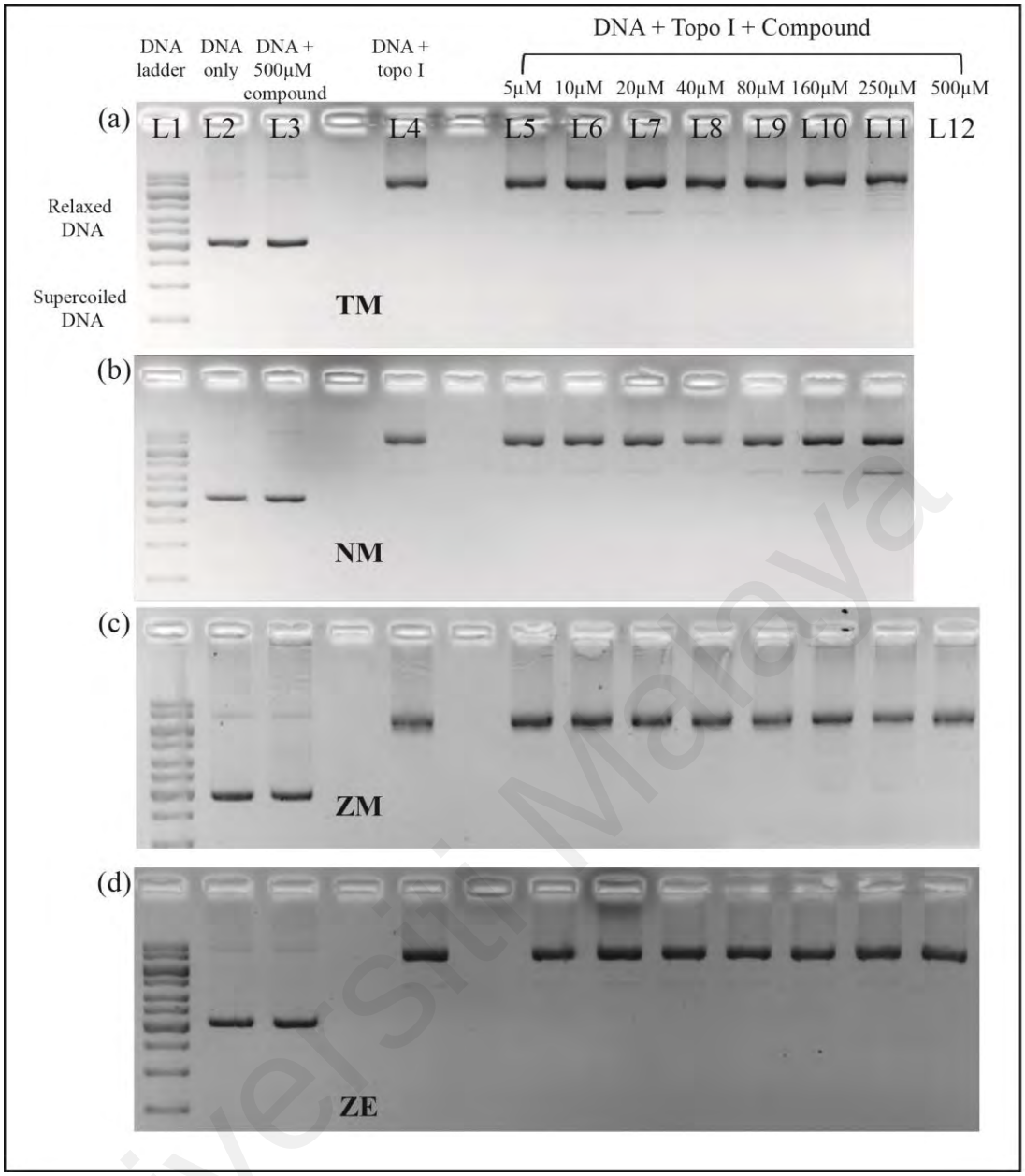

Figure 4.41: Electrophoresis result of incubating *E. coli* topo I (0.25 unit) with pBR322 in the absence and presence of various concentration of (a) **TM**, (b) **NM**, (c) **ZM**, and (d) **ZE**.

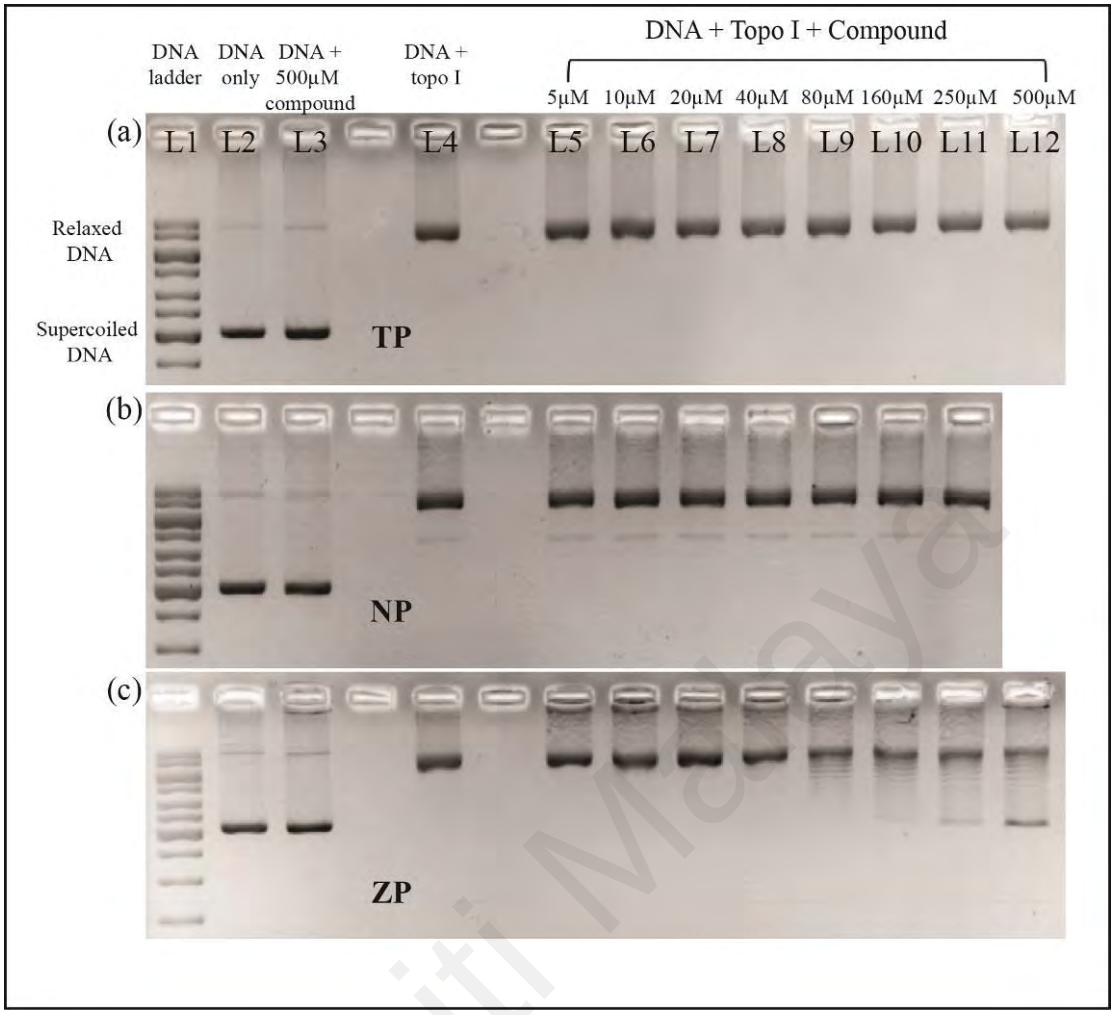

Figure 4.42: Electrophoresis result of incubating *E. coli* topo I (0.25 unit) with pBR322 in the absence and presence of various concentration of (a) **TP**, (b) **NP**, and (c) **ZP**.

Gel images in Figure 4.40-4.42 showed that despite highest concentration of the synthesized compounds were incubated with pBR322, the resulting bands (lane 3) were similar compared to the bands corresponding to the plasmid DNA alone (lane 2). This indicates that the compounds and the solvent in the reaction medium caused no observable changes to the plasmid DNA, for example, no cleavage or unwinding of the DNA.

When compounds of different concentration were included in the incubation of DNA with topo I, almost all the compounds (six out of nine) were unable to inhibit the action

of topo I as the resulting bands are of similar pattern like the DNA plus topo I. However, **TM**, **NM**, and **ZP** were able to inhibit the function of topo I.

The inhibition of topo enzymes can occur by two generally accepted molecular mechanisms. Topo inhibitors refer to compounds that suppress the enzyme without stabilizing the intermediate DNA-topo I covalent complex. This class of inhibitors usually bind to the topo active site that prevents the binding of the DNA substrate, thus preventing the subsequent steps in the catalytic cycle. In contrast, the topo poisons, such as camptothecin, act after the cleavage of DNA by the enzyme and inhibit the religation. This class of compounds may freeze the topo-DNA complex and lock the enzyme into a cleavage-complex, which in turn prevents the enzyme turnover (Bailly, 2000; Hevener et al., 2018).

Figure 4.41(a) showed the electrophoresis results of incubating topo I with pBR322 in the presence and absence of **TM**. A band in between the form I and II DNA corresponding to DNA aggregates or relaxed form of the DNA topoisomers was observed when 20 μM of **TM** was added. DNA laddering was then observed when 250 μM of **TM** was added, which indicates the function of this compound as topo I poison. On the other hand, approximately 80 μM of its nickel complex **NM** was able to inhibit the function of this enzyme, as shown in Figure 4.41(b). However, there was no DNA laddering, which reflects the function of **NM** as a topo I inhibitor. Meanwhile, gel image in Figure 4.42(c) showed the zinc complex **ZP** was able to induce DNA laddering in a concentration dependent manner, with 80 μM of this complex is able to inhibit the function of topo I and the degree of inhibition became stronger with increased concentration (Palanimuthu et al., 2013).

As mentioned earlier, elevated expression of topo I was reported in a few types of cancers, including colorectal carcinoma. Topotecan, a topo I inhibitor, is commonly used

to treat ovarian and certain types of lung cancers. This medicine was reported to inhibit tumour growth *via* inhibition of topo I and thereby inducing cell cycle arrest, most particularly through accumulation of cells at G_0/G_1 phase, and S phase in some cases (Zhang et al., 2013). The ability of the three compounds (**TM**, **NM**, and **ZP**) to suppress the enzymatic functions of topo I in a concentration dependent manner and subsequently inducing cell cycle arrest at G_0/G_1 phase (Section **4.10**) might be one of the important contributors to the cytotoxicity of these compounds towards the colorectal carcinoma HCT 116 cell line. On the other hand, this assay also showed that the cytotoxicity of other six compounds are independent of topo I inhibition.

CHAPTER 5: CONCLUSION AND RECOMMENDATIONS

Three Schiff base ligands (**TM**, **TF**, and **TP**) containing testosterone and derivatives of thiosemicarbazides, along with their nickel (**NM**, **NF**, and **NP**) and zinc (**ZM**, **ZF**, and **ZP**) complexes, and a zinc complex **ZE**, were synthesized. Derivatives of thiosemicarbazides were chosen as to incorporate different inductive effects on the ligands produced and thereby potentially confer different structural properties. For example, the methyl group in 4-methyl-3-thiosemicarbazide will increase the electron density of the azomethine group of compounds under the family of **TM**, thereby increase the basicity of these compounds. On the other hand, introduction of an electron withdrawing fluoro group in the 4-(4-fluorophenyl)-3-thiosemicarbazide will make compounds of **TF** more acidic.

The chemical structures of the compounds synthesized were evaluated through FTIR spectroscopy, H^1-NMR and C^{13}-NMR (Schiff base ligands), and CHN analysis. Besides, the structure and geometry of **TM**, **NM**, **TF**, **NF**, **TP**, and **ZE** were further confirmed by single-crystal x-ray diffraction studies. X-ray crystallography has confirmed that the structure of these two nickel complexes were similar, with two Schiff base ligands were coordinated to a single nickel(II) metal center and the resulting metal complexes adopted a distorted square planar geometry.

Cytotoxicity of all the compounds against four human cancer cell lines and two normal cell lines were investigated, with the conventional chemotherapeutic cisplatin as positive reference standard. Although some of the compounds displayed cytotoxicity that is comparable to cisplatin when they were tested against the prostate cancer cell lines, the high toxicity of these compounds against the normal prostate cell line RWPE-1 indicates

the low suitability of these compounds to be used in targeting prostate cancer cells. Moreover, the presence of testosterone moiety in the structures of these compounds did not facilitate much in the recognition of androgen receptor, especially when approximately half of these compounds were unable to inhibit the growth of androgen receptor responsive human prostate cancer LNCaP and human breast cancer MCF7 cell lines.

The ability of these compounds to inhibit the growth of colorectal carcinoma cell line HCT 116, which is androgen receptor responsive, were tested and eight out of the nine compounds (except **ZM**）, were cytotoxic towards this cell line, with compounds from family of **TP** displaying outstanding potency. In addition, only two out of these eight cytotoxic compounds (**NP** and **TF**) were toxic against the human normal colon cell line CCD18-Co, which reflects high selectivity index (SI≥1.47) of these compounds against the human colorectal carcinoma cell line tested.

The cell death mechanisms behind the cytotoxicity of these compounds were then evaluated. At first, the morphological changes induced by the cytotoxic compounds were observed and photographed. The ability of all the eight cytotoxic compounds (**ZM**, up to 30 μM, was unable to inhibit growth of all the cancer cell lines tested) to induce apoptosis in the cancer cell lines were then confirmed. Their ability to depolarize the mitochondrial membrane potential, which in turn induce apoptosis *via* intrinsic or extrinsic pathway, was then evaluated. Three out of the eight cytotoxic compounds (**NF**, **ZF**, and **NP**) were unable to depolarize the mitochondrial membrane potential of human colorectal carcinoma HCT 116 cell line and therefore these three compounds are most likely extrinsic apoptosis pathway inducer (or mitochondria-independent apoptosis).

All the eight cytotoxic compounds were then proven to disrupt the cell cycle of the human colorectal carcinoma HCT 116 and arrest it at G_0/G_1 phase. Cells were

accumulated at resting phase and decreased S phase population means lesser cells were allowed to enter the subsequent mitotic phase and therefore resulting in lower rate of cell growth. Moreover, cell cycle arrest at G_0/G_1 phase might be the reason of cells undergoing programmed cell death.

With the aid of UV-Vis spectroscopy, the function of the synthesized compounds as DNA binders were proven, with the results suggested their potential roles as DNA surface or groove binders. Apart from that, the increasing order of binding strength were calculated: **TF**>**TP**>**NF**>**ZF**>**ZM**>**TM**>**NP**>**ZP**>**ZE**>**NM**. Similar results were obtained from docking simulations, as the test compounds preferred to bind to the minor groove of DNA and they favoured the GC-rich region. **TF** was proven to be the strongest DNA binder among these nine compounds, which may explain the high general toxicity of this compound since DNA is ubiquitously present in all cell types, including normal cell. In contrast, the high selectivity index of **ZP** against the human colorectal carcinoma cell line might be due to its weak DNA binding affinity.

The DNA binding affinity and their cytotoxicity against the colorectal carcinoma cell lines have led to the evaluation of their potential as topo I inhibitor. Although most of the topo inhibitors are found to exert the cytotoxic effect through DNA binding, only three of these DNA binders are able to suppress the activity of this enzyme. **ZP**, which exhibited highest selectivity index against the human colorectal carcinoma cell line tested, might function as a topo I poison, suppressing the enzymatic reaction by limiting the turnover of topo I. Cells were accumulated in G_0/G_1 phase due to the lack of functional topo I and lesser cells were allowed to enter the synthesis (S) phase in cell cycle. The cells with the frozen cleavage complex might then be subjected to mitochondria-independent apoptosis.

The formulation of strategies to overcome the lack of selectivity and/or high general toxicity are thought to be the major challenge and solutions in anticancer therapy, as these are the main factors that haunted the development and limit the clinical usefulness of the chemotherapeutics. Nine Schiff base compounds, including three nickel and zinc complexes, were synthesized *via* conventional reflux method and they displayed different affinity towards the minor groove of DNA. Though the primary targets of some of the compounds are yet to be confirmed, these compounds tested in this study seems selective as the parent ligands and their respective metal complexes possess different affinities towards different cancer cell lines. The switch of preferences towards other cancer cells upon complexation was observed, although complexation is usually performed to enhance the cytotoxicities. The importance of nickel and zinc in anticancer therapy can be envisaged as these relatively cheaper metal may help in promoting selectivity (or even different activities) and thereby widen the therapeutic windows.

The potential of other transition metal ions such as copper, cobalt, ruthenium, rhenium, and others can be tested in future studies. Apart from that, cytotoxic behaviour of these compounds can be further monitored with the aid of real-time assay such as iCelligence. *In vivo* cytotoxicity and (acute and chronic) toxicity evaluation of these compounds (especially **ZP**, **TF** and **TP** due to their selectivity index of greater than 2.0) can also be determined by using zebrafish and/or human tumour xenograft-bearing mice as test animals. Moreover, the lethal dosages of these compounds can be evaluated to further understand their potential practical usefulness. The compounds with excellent selectivity index could potentially be employed in clinical trials in patients suffering from colorectal cancer after the detailed toxicity and chemotherapeutic effect on this cancer type is evaluated. In fact, these compounds can be envisaged as relatively cheaper chemotherapeutics (compared to platinum drugs) and thereby widen the therapeutic windows.

REFERENCES

Abdel-Rahman, L. H., El-Khatib, R. M., Nassr, L. A. E., Abu-Dief, A. M., Ismael, M., & Seleem, A. A. (2014). Metal based pharmacologically active agents: Synthesis, structural characterization, molecular modeling, CT-DNA binding studies and in vitro antimicrobial screening of iron(II) bromosalicylidene amino acid chelates. *Spectrochimica Acta Part A: Molecular and Biomolecular Spectroscopy, 117*(0), 366-378.

Abreu, R. M., Froufe, H. J., Queiroz, M. J., & Ferreira, I. C. (2010). MOLA: a bootable, self-configuring system for virtual screening using AutoDock4/Vina on computer clusters. *Journal of Cheminformatics, 2*(1), Article#10.

Adeniyi, A. A., & Ajibade, P. A. (2013). Comparing the suitability of autodock, gold and glide for the docking and predicting the possible targets of Ru(II)-based complexes as anticancer agents. *Molecules, 18*(4), 3760-3778.

Adsule, S., Barve, V., Chen, D., Ahmed, F., Dou, Q. P., Padhye, S., & Sarkar, F. H. (2006). Novel Schiff base copper complexes of quinoline-2 carboxaldehyde as proteasome inhibitors in human prostate cancer cells. *Journal of Medicinal Chemistry, 49*(24), 7242-7246.

Afrasiabi, Z., Sinn, E., Lin, W., Ma, Y., Campana, C., & Padhye, S. (2005). Nickel (II) complexes of naphthaquinone thiosemicarbazone and semicarbazone: Synthesis, structure, spectroscopy, and biological activity. *Journal of Inorganic Biochemistry, 99*(7), 1526-1531.

Afrati, T., Pantazaki, A. A., Dendrinou-Samara, C., Raptopoulou, C., Terzis, A., & Kessissoglou, D. P. (2010). Copper inverse-9-metallacrown-3 compounds interacting with DNA. *Dalton Transactions, 39*(3), 765-775.

Ahmad, A. (2019). Breast cancer statistics: Recent Trends. *Advances in Experimental Medicine and Biology, 1152*, 1-7.

Al-Bayati, R. I., Amier, A. A., Al-Amiery, A., & Al-Majedy, Y. K. (2010). Synthesis and antimicrobial studies of novel metal complexes of testoterone thiosemicarbazone and methandrostenolon thiosemicarbazone. *Journal of Biotechnology Research Center (special edition), 4*(1), 73-84.

Al-Hazmi, G. A. A., El-Shahawi, M. S., Gabr, I. M., & El-Asmy, A. A. (2005). Spectral, magnetic, thermal and electrochemical studies on new copper(II) thiosemicarbazone complexes. *Journal of Coordination Chemistry, 58*(8), 713-733.

al-Rashida, M., & Ahsen, S. (2015). In search of a docking protocol to distinguish between DNA intercalators and groove binders: genetic algorithm vs. shape-complementarity based docking methods. *RSC Advances, 5*(88), 72394-72404.

Alemany, C. (2014). Etirinotecan Pegol: Development of a novel conjugated topoisomerase I inhibitor. *Current Oncology Reports, 16*(2), Article#367.

Amos-Landgraf, J. M., Heijmans, J., Wielenga, M. C. B., Dunkin, E., Krentz, K. J., Clipson, L., Ederveen, A. G., Groothuis, P. G., Mosselman, S., Muncan, V., Hommes, D. W., Shedlovsky, A., Dove, W. F., & van den Brink, G. R. (2014). Sex disparity in colonic adenomagenesis involves promotion by male hormones, not protection by female hormones. *Proceedings of the National Academy of Sciences, 111*(46), 16514-16519.

Ang, W. H., Myint, M., & Lippard, S. J. (2010). Transcription inhibition by platinum-DNA cross-links in live mammalian cells. *Journal of American Chemistry Society, 132*(21), 7429-7435.

Arjmand, F., & Muddassir, M. (2010). Design and synthesis of heterobimetallic topoisomerase I and II inhibitor complexes: In vitro DNA binding, interaction with 5'-GMP and 5'-TMP and cleavage studies. *Journal of Photochemistry and Photobiology B: Biology, 101*(1), 37-46.

Arjmand, F., Sayeed, F., & Muddassir, M. (2011). Synthesis of new chiral heterocyclic Schiff base modulated Cu(II)/Zn(II) complexes: their comparative binding studies with CT-DNA, mononucleotides and cleavage activity. *Journal of Photochemistry and Photobiology B: Biology, 103*(2), 166-179.

Arnold, M., Sierra, M. S., Laversanne, M., Soerjomataram, I., Jemal, A., & Bray, F. (2017). Global patterns and trends in colorectal cancer incidence and mortality. *Gut, 66*(4), 683-691.

Asadi, Z., Mandegani, Z., Asadi, M., Pakiari, A. H., Salarhaji, M., Manassir, M., Karbalaei-Heidari, H. R., Rastegari, B., & Sedaghat, M. (2019). Substituted effect on some water-soluble Mn(II) salen complexes: DNA binding, cytotoxicity, molecular docking, DFT studies and theoretical IR & UV studies. *Spectrochimica Acta Part A: Molecular and Biomolecular Spectroscopy, 206*, 278-294.

Au, L., Zheng, D., Zhou, F., Li, Z. Y., Li, X., & Xia, Y. (2008). A quantitative study on the photothermal effect of immuno gold nanocages targeted to breast cancer cells. *ACS Nano, 2*(8), 1645-1652.

Bader, R. F. W., & Chang, C. (1989). Properties of atoms in molecules: energetics of electrophilic aromatic substitution. *The Journal of Physical Chemistry, 93*(13), 5095-5107.

Bailly, C. (2000). Topoisomerase I poisons and suppressors as anticancer drugs. *Current Medicinal Chemistry, 7*(1), 39-58.

Balachandran, C., Haribabu, J., Jeyalakshmi, K., Bhuvanesh, N. S. P., Karvembu, R., Emi, N., & Awale, S. (2018). Nickel(II) bis(isatin thiosemicarbazone) complexes induced apoptosis through mitochondrial signaling pathway and G0/G1 cell cycle arrest in IM-9 cells. *Journal of Inorganic Biochemistry, 182*, 208-221.

Barbour, L. J. (2001). X-Seed — a software tool for supramolecular crystallography. *Journal of Supramolecular Chemistry, 1*(4–6), 189-191.

Barone, G., Terenzi, A., Lauria, A., Almerico, A. M., Leal, J. M., Busto, N., & García, B. (2013). DNA-binding of nickel(II), copper(II) and zinc(II) complexes: Structure–affinity relationships. *Coordination Chemistry Reviews, 257*(19–20), 2848-2862.

Benarroch, D., Claverie, J. M., Raoult, D., & Shuman, S. (2006). Characterization of mimivirus DNA topoisomerase IB suggests horizontal gene transfer between eukaryal viruses and bacteria. *Journal of Virology, 80*(1), 314-321.

Bender, A., & Glen, R. C. (2005). A discussion of measures of enrichment in virtual screening: comparing the information content of descriptors with increasing levels of sophistication. *Journal of Chemican Information and Modeling, 45*(5), 1369-1375.

Beretta, G. L., Zuco, V., Perego, P., & Zaffaroni, N. (2012). Targeting DNA topoisomerase I with non-camptothecin poisons. *Current Medicinal Chemistry, 19*(8), 1238-1257.

Bhattacharyya, S., Gonzalez, M., Robertson, J. D., Bhattacharya, R., & Mukherjee, P. (2011). A simple synthesis of a targeted drug delivery system with enhanced cytotoxicity. *Chemical Communications (Camb), 47*(30), 8530-8532.

Biersack, B., Dietrich, A., Zoldakova, M., Kalinowski, B., Paschke, R., Schobert, R., & Mueller, T. (2011). Lipophilic Pt(II) complexes with selective efficacy against cisplatin-resistant testicular cancer cells. *Journal of Inorganic Biochemistry, 105*(12), 1630-1637.

Biesiada, J., Porollo, A., Velayutham, P., Kouril, M., & Meller, J. (2011). Survey of public domain software for docking simulations and virtual screening. *Human Genomics, 5*(5), 497-505.

Bikadi Z., & Hazai, E. (2009). Application of the PM6 semi-empirical method to modeling proteins enhances docking accuracy of AutoDock. *Journal of Cheminformatics, 1*, Article#15.

Bissantz, C., Folkers, G., & Rognan, D. (2000). Protein-based virtual screening of chemical databases. 1. Evaluation of different docking/scoring combinations. *Journal of Medicinal Chemistry, 43*(25), 4759-4767.

Biver, T., Secco, F., & Venturini, M. (2005). Relaxation kinetics of the interaction between RNA and metal-intercalators: the Poly(A).Poly(U)/platinum-proflavine system. *Archives of Biochemistry and Biophysics, 437*(2), 215-223.

Bleyer, A., Spreafico, F., & Barr, R. (2020). Prostate cancer in young men: An emerging young adult and older adolescent challenge. *Cancer, 126*(1), 46-57.

Bonsignore, R., Russo, F., Terenzi, A., Spinello, A., Lauria, A., Gennaro, G., Almerico, A. M., Keppler, B. K., & Barone, G. (2018). The interaction of Schiff base complexes of nickel(II) and zinc(II) with duplex and G-quadruplex DNA. *Journal of Inorganic Biochemistry, 178*, 106-114.

Bodurka, D. C., Levenback, C., Wolf, J. K., Gano, J., Wharton, J. T., Kavanagh, J. J., & Gershenson, D. M. (2003). Phase II trial of irinotecan in patients with metastatic epithelial ovarian cancer or peritoneal cancer. *Journal of Clinical Oncology, 21*(2), 291-297.

Bray, F., Ferlay, J., Soerjomataram, I., Siegel, R. L., Torre, L. A., & Jemal, A. (2018). Global cancer statistics 2018: GLOBOCAN estimates of incidence and mortality worldwide for 36 cancers in 185 countries. *CA: A Cancer Journal for Clinicians, 68*(6), 394-424.

Bruijnincx, P. C., & Sadler, P. J. (2008). New trends for metal complexes with anticancer activity. *Current Opinion in Chemical Biology, 12*(2), 197-206.

Casini, A., Hartinger, C., Gabbiani, C., Mini, E., Dyson, P. J., Keppler, B. K., & Messori, L. (2008). Gold(III) compounds as anticancer agents: relevance of gold-protein interactions for their mechanism of action. *Journal of Inorganic Biochemistry, 102*(3), 564-575.

Catalano, M. G., Pfeffer, U., Raineri, M., Ferro, P., Curto, A., Capuzzi, P., Corno, F., Berta, L., & Fortunati, N. (2000). Altered expression of androgen-receptor isoforms in human colon-cancer tissues. *International Journal of Cancer, 86*(3), 325-330.

Ceron-Carrasco, J. P., Jacquemin, D., & Cauet, E. (2012). Cisplatin cytotoxicity: a theoretical study of induced mutations. *Physical Chemistry Chemical Physics, 14*(36), 12457-12464.

Chabner, B. A. (2010). Barnett Rosenberg: In memoriam (1924–2009). *Cancer Research, 70*(1), 428-429.

Chaire,J. B. (2006). A thermodynamic signature for drug-DNA binding mode. *Archives of Biochemistry and Biophysics, 453*(1), 26-31.

Chamoux, J. J. (2001). DNA topoisomerase I-mediated nicking of circular duplex DNA. *Methods in Molecular Biology, 95*, 81-87.

Chang, B., Nishikawa, M., Sato, E., Utsumi, K., & Inoue, M. (2002). L-Carnitine inhibits cisplatin-induced injury of the kidney and small intestine. *Archives of Biochemistry and Biophysics, 405*(1), 55-64.

Che, C.-M., & Siu, F.-M. (2010). Metal complexes in medicine with a focus on enzyme inhibition. *Current Opinion in Chemical Biology, 14*(2), 255-261.

Chen, J., Huang, Y.-w., Liu, G., Afrasiabi, Z., Sinn, E., Padhye, S., & Ma, Y. (2004). The cytotoxicity and mechanisms of 1,2-naphthoquinone thiosemicarbazone and its metal derivatives against MCF-7 human breast cancer cells. *Toxicology and Applied Pharmacology, 197*(1), 40-48.

Chohan, Z. H., Sumrra, S. H., Youssoufi, M. H., & Hadda, T. B. (2010). Metal based biologically active compounds: Design, synthesis, and antibacterial/antifungal/cytotoxic properties of triazole-derived Schiff bases and their oxovanadium(IV) complexes. *European Journal of Medicinal Chemistry, 45*(7), 2739-2747.

Choi, Y.-K., Park, J.-K., & Jeon, S. (1999). Electrocatalytic reduction of dioxygen at carbon electrodes modified with Co(II)-Schiff base complexes in various pH solutions. *Electroanalysis, 11*(2), 134-138.

Chuang, S. E., Yeh, P. Y., Lu, Y. S., Lai, G. M., Liao, C. M., Gao, M., & Cheng, A. L. (2002). Basal levels and patterns of anticancer drug-induced activation of nuclear factor-kappaB (NF-kappaB), and its attenuation by tamoxifen, dexamethasone, and curcumin in carcinoma cells. *Biochemical Pharmacology, 63*(9), 1709-1716.

Claussn, H., Buning, C., Rarey, M., & Lengauer, T. (2001). FlexE: efficient molecular docking considering protein structure variations. *Journal of Molecular Biology, 308*(2), 377-395.

Cochrne, D. R., Bernales, S., Jacobsen, B. M., Cittelly, D. M., Howe, E. N., D'Amato, N. C., Spoelstra, N. S., Edgerton, S. M., Jean, A., Guerrero, J., Gomez, F., Medicherla, S., Alfaro, I. E., McCullagh, E., Jedlicka, P., Torkko, K. C., Thor, A. D., Elias, A. D., Protter, A. A., & Richer, J. K. (2014). Role of the androgen receptor in breast cancer and preclinical analysis of enzalutamide. *Breast Cancer Research, 16*(1), Article#R7.

Cole, JC., Murray, C. W., Nissink, J. W., Taylor, R. D., & Taylor, R. (2005). Comparing protein-ligand docking programs is difficult. *Proteins, 60*(3), 325-332.

Comşa, Ş., Cîmpean, A. M., & Raica, M. (2015). The Story of MCF-7 Breast cancer cell line: 40 years of experience in research. *Anticancer Research, 35*(6), 3147-3154.

Conti, J. A., Kemeny, N. E., Saltz, L. B., Huang, Y., Tong, W. P., Chou, T. C., Sun, M., Pulliam, S., & Gonzalez, C. (1996). Irinotecan is an active agent in untreated patients with metastatic colorectal cancer. *Journal of Clinical Oncology, 14*(3), 709-715.

Costelo, L. C., Feng, P., Milon, B., Tan, M., & Franklin, R. B. (2004). Role of zinc in the pathogenesis and treatment of prostate cancer: critical issues to resolve. *Prostate Cancer And Prostatic Diseases, 7*, 111-117.

Creavn, B. S., Duff, B., Egan, D. A., Kavanagh, K., Rosair, G., Thangella, V. R., & Walsh, M. (2010). Anticancer and antifungal activity of copper(II) complexes of quinolin-2(1H)-one-derived Schiff bases. *Inorganica Chimica Acta, 363*(14), 4048-4058.

Cruz Santana, G., Gimenez, I. d. F., Näther, C., Jess, I., & de Oliveira, A. B. (2015). Crystal structure of bis-[N-phenyl-2-(1,2,3,4-tetrahydronaphthalen-1-ylidene)hydrazinecarbothio-amidato-κ(2) N (2),S]zinc dimethyl sulfoxide monosolvate. *Acta crystallographica. Section E, Crystallographic communications, 71*(Pt 5), 440-442.

Culp, M. B., Soerjomataram, I., Efstathiou, J. A., Bray, F., & Jemal, A. (2020). Recent global patterns in prostate cancer incidence and mortality rates. *European Urology, 77*(1), 38-52.

Czarnomysy, R., Surażyński, A., Muszynska, A., Gornowicz, A., Bielawska, A., & Bielawski, K. (2018). A novel series of pyrazole-platinum(II) complexes as potential anti-cancer agents that induce cell cycle arrest and apoptosis in breast cancer cells. *Journal of Enzyme Inhibition and Medicinal Chemistry, 33*(1), 1006-1023.

D'Errico, I., & Moschetta, A. (2008). Nuclear receptors, intestinal architecture and colon cancer: an intriguing link. *Cellular and Molecular Life Sciences, 65*(10), 1523-1543.

Dart, D. A., Waxman, J., Aboagye, E. O., & Bevan, C. L. (2013). Visualising androgen receptor activity in male and female mice. *PLoS One, 8*(8), Article#e71694.

Dasari, S., & Tchounwou, P. B. (2014). Cisplatin in cancer therapy: molecular mechanisms of action. *European Journal of Pharmacology, 740*, 364-378.

Davis, I. W., & Baker, D. (2009). RosettaLigand docking with full ligand and receptor flexibility. *Journal of Molecular Biology, 385*(2), 381-392.

de Hoog, P., Pitie, M., Amadei, G., Gamez, P., Meunier, B., Kiss, R., & Reedijk, J. (2008). DNA cleavage and binding selectivity of a heterodinuclear Pt-Cu(3-Clip-Phen) complex. *Journal of Biological Inorganic Chemistry, 13*(4), 575-586.

Debes, J. D., & Tindall, D. J. (2002). The role of androgens and the androgen receptor in prostate cancer. *Cancer Letters, 187*(1-2), 1-7.

Delgado, J. L., Hsieh, C.-M., Chan, N.-L., & Hiasa, H. (2018). Topoisomerases as anticancer targets. *Biochemical Journal, 475*(2), 373-398.

Dexheimer, T. S., & Pommier, Y. (2008). DNA cleavage assay for the identification of topoisomerase I inhibitors. *Nature Protocols, 3*(11), 1736-1750.

Dhanik, A., McMurray, J. S., & Kavraki, L. E. (2013). DINC: a new AutoDock-based protocol for docking large ligands. *BMC Structural Biology, 13 Suppl 1*, Article#S11.

Di Leva, F. S., Novellino, E., Cavalli, A., Parrinello, M., & Limongelli, V. (2014). Mechanistic insight into ligand binding to G-quadruplex DNA. *Nucleic Acids Research, 42*(9), 5447-5455.

Dilovic, I., Rubcic, M., Vrdoljak, V., Kraljevic Pavelic, S., Kralj, M., Piantanida, I., & Cindric, M. (2008). Novel thiosemicarbazone derivatives as potential antitumor agents: Synthesis, physicochemical and structural properties, DNA interactions and antiproliferative activity. *Bioorganic and Medicinal Chemistry, 16*(9), 5189-5198.

DiPaola, R. S. (2002). To Arrest or Not To G_2-M Cell-Cycle Arrest. *Commentary re: A. K. Tyagi et al., Silibinin strongly synergizes human prostate carcinoma DU145 cells to doxorubicin-induced growth inhibition, G_2-M arrest, and apoptosis. Clinical Cancer Research, 3512–3519, 2002. 8*(11), 3311-3314.

Dixon, I. M., Lopez, F., Esteve, J. P., Tejera, A. M., Blasco, M. A., Pratviel, G., & Meunier, B. (2005). Porphyrin derivatives for telomere binding and telomerase inhibition. *Chembiochem, 6*(1), 123-132.

Doonan, F., & Cotter, T. G. (2008). Morphological assessment of apoptosis. *Methods, 44*(3), 200-204.

Drennan, C. L. (2010). In the nickel of time. *Nature Chemistry, 2*(10), Article#900.

Drews, J. (2000). Drug discovery: a historical perspective. *Science, 287*(5460), 1960-1964.

Drews, J. (2003). Stategic trends in the drug industry. *Drug Discovery Today, 8*(9), 411-420.

Durrant, J. D., & McCammon, J. A. (2011). Molecular dynamics simulations and drug discovery. *BMC Biology, 9*, Article#71.

El-Bahy, G. M. S. (2005). FTIR and Raman spectroscopic study of Fenugreek (Trigonella foenum graecum L.) seeds. *Journal of Applied Spectroscopy, 72*(1), 111-116.

Elefantova, K., Lakatos, B., Kubickova, J., Sulova, Z., & Breier, A. (2018). Detection of the mitochondrial membrane potential by the cationic dye JC-1 in L1210 cells with massive overexpression of the plasma membrane ABCB1 drug transporter. *International Journal of Molecular Sciences, 19*(7), Article#1985.

Englinger, B., Pirker, C., Heffeter, P., Terenzi, A., Kowol, C. R., Keppler, B. K., & Berger, W. (2019). Metal drugs and the anticancer immune response. *Chemical Reviews, 119*(2), 1519-1624.

Falciani, C., Accardo, A., Brunetti, J., Tesauro, D., Lelli, B., Pini, A., Bracci, L., & Morelli, G. (2011). Target-selective drug delivery through liposomes labeled with oligobranched neurotensin peptides. *ChemMedChem, 6*(4), 678-685.

Farghadani, R., Rajarajeswaran, J., Mohd Hashim, N. B., Abdulla, M. A., & Muniandy, S. (2017). A novel β-diiminato manganeseIII complex as the promising anticancer agent induces G0/G1 cell cycle arrest and triggers apoptosis via mitochondrial-dependent pathways in MCF-7 and MDA-MB-231 human breast cancer cells. *RSC Advances, 7*(39), 24387-24398.

Fatondji, H., Kpoviessi, S., Gbaguidi, F., Bero, J., Hannaert, V., Quetin-Leclercq, J., Poupaert, J., Moudachirou, M., & Accrombessi, G. (2013). Structure–activity relationship study of thiosemicarbazones on an African trypanosome: Trypanosoma brucei brucei. *Medicinal Chemistry Research, 22*(5), 2151-2162.

Fonseca Guerra, C., Bickelhaupt, F. M., Snijders, J. G., & Baerends, E. J. (2000). Hydrogen bonding in DNA base pairs: reconciliation of theory and experiment. *Journal of the American Chemical Society, 122*(17), 4117-4128.

Foradori, C. D., Weiser, M. J., & Handa, R. J. (2008). Non-genomic actions of androgens. *Frontiers in Neuroendocrinology, 29*(2), 169-181.

Frezza, M., Hindo, S., Chen, D., Davenport, A., Schmitt, S., Tomco, D., & Dou, Q. P. (2010). Novel metals and metal complexes as platforms for cancer therapy. *Current Pharmaceutical Design, 16*(16), 1813-1825.

Fricker, S. P. (2007). Metal based drugs: from serendipity to design. *Dalton Transactions,* (43), 4903-4917.

Friedman, H. S., Petros, W. P., Friedman, A. H., Schaaf, L. J., Kerby, T., Lawyer, J., Parry, M., Houghton, P. J., Lovell, S., Rasheed, K., Cloughsey, T., Stewart, E. S., Colvin, O. M., Provenzale, J. M., McLendon, R. E., Bigner, D. D., Cokgor, I., Haglund, M., Rich, J., Ashley, D., Malczyn, J., Elfring, G. L., & Miller, L. L. (1999). Irinotecan therapy in adults with recurrent or progressive malignant glioma. *Journal of Clinical Oncology, 17*(5), 1516-1516.

Friesner, R. A., Banks, J. L., Murphy, R. B., Halgren, T. A., Klicic, J. J., Mainz, D. T., Repasky, M. P., Knoll, E. H., Shelley, M., Perry, J. K., Shaw, D. E., Francis, P., & Shenkin, P. S. (2004). Glide: a new approach for rapid, accurate docking and scoring. 1. Method and assessment of docking accuracy. *Journal of Medicinal Chemistry, 47*(7), 1739-1749.

Fuertes, M. A., Castilla, J., Alonso, C., & Perez, J. M. (2003). Cisplatin biochemical mechanism of action: from cytotoxicity to induction of cell death through interconnections between apoptotic and necrotic pathways. *Current Medicinal Chemistry, 10*(3), 257-266.

Ganguly, A., Chakraborty, P., Banerjee, K., & Choudhuri, S. K. (2014). The role of a Schiff base scaffold, N-(2-hydroxy acetophenone) glycinate-in overcoming multidrug resistance in cancer. *European Journal of Pharmaceutical Sciences, 51*, 96-109.

Gao, L. M., Vera, J. L., Matta, J., & Melendez, E. (2010). Synthesis and cytotoxicity studies of steroid-functionalized titanocenes as potential anticancer drugs: sex steroids as potential vectors for titanocenes. *Journal of Biological Inorganic Chemistry, 15*(6), 851-859.

Gao, W., Bohl, C. E., & Dalton, J. T. (2005). Chemistry and structural biology of androgen receptor. *Chemical Reviews, 105*(9), 3352-3370.

Gasser, G., Ott, I., & Metzler-Nolte, N. (2011). Organometallic anticancer compounds. *Journal of Medicinal Chemistry, 54*(1), 3-25.

Gasteiger, J., & Marsili, M. (1980). Iterative partial equalization of orbital electronegativity—a rapid access to atomic charges. *Tetrahedron, 36*(22), 3219-3228.

Giovannelli, P., Di Donato, M., Galasso, G., Di Zazzo, E., Bilancio, A., & Migliaccio, A. (2018). The androgen receptor in breast cancer. *Frontiers in Endocrinology, 9*, 492-492.

Gnewuch, C. T., & Sosnovsky, G. (2002). Critical appraisals of approaches for predictive designs in anticancer drugs. *Cellular and Molecular Life Sciences CMLS, 59*(6), 959-1023.

Gohlke, H., & Klebe, G. (2002). Approaches to the description and prediction of the binding affinity of small-molecule ligands to macromolecular receptors. *Angewandte Chemie International Edition in English, 41*(15), 2644-2676.

Goodsell, D. S., Morris, G. M., & Olson, A. J. (1996). Automated docking of flexible ligands: applications of AutoDock. *Journal of Molecular Recognition, 9*(1), 1-5.

Gornowicz, A., Pawłowska, N., Czajkowska, A., Czarnomysy, R., Bielawska, A., Bielawski, K., Michalak, O., Staszewska-Krajewska, O., & Kałuża, Z. (2017). Biological evaluation of octahydropyrazin[2,1-a:5,4-a′]diisoquinoline derivatives as potent anticancer agents. *Tumor Biology, 39*(6), 1-13.

Gu, S., Papadopoulou, N., Gehring, E. M., Nasir, O., Dimas, K., Bhavsar, S. K., Foller, M., Alevizopoulos, K., Lang, F., & Stournaras, C. (2009). Functional membrane androgen receptors in colon tumors trigger pro-apoptotic responses in vitro and reduce drastically tumor incidence in vivo. *Molecular Cancer, 8*, Article#114.

Gu, S., Papadopoulou, N., Nasir, O., Föller, M., Alevizopoulos, K., Lang, F., & Stournaras, C. (2011). Activation of membrane androgen receptors in colon cancer inhibits the prosurvival signals Akt/bad in vitro and in vivo and blocks migration via vinculin/actin signaling. *Molecular Medicine (Cambridge, Mass.), 17*(1-2), 48-58.

Gupta, K. C., & Sutar, A. K. (2008). Catalytic activities of Schiff base transition metal complexes. *Coordination Chemistry Reviews, 252*(12–14), 1420-1450.

Halperin, I., Ma, B., Wolfson, H., & Nussinov, R. (2002). Principles of docking: An overview of search algorithms and a guide to scoring functions. *Proteins, 47*(4), 409-443.

Hannon, M. J. (2007). Metal-based anticancer drugs: From a past anchored in platinum chemistry to a post-genomic future of diverse chemistry and biology. *Pure and Applied Chemistry, 79*(12), 2243-2261.

Havaldar, F. H., & Patil, A. R. (2008). Syntheses of 1, 2, 4 Triazole derivatives and their biological activity. *E-Journal of Chemistry, 5*, 347-354.

He, J., Wang, X., Zhao, X., Liang, Y., He, H., & Fu, L. (2012). Synthesis and antitumor activity of novel quinazoline derivatives containing thiosemicarbazide moiety. *European Journal of Medicinal Chemistry, 54*(0), 925-930.

Heffeter, P., Pape, V. F. S., Enyedy, E. A., Keppler, B. K., Szakacs, G., & Kowol, C. R. (2019). Anticancer thiosemicarbazones: chemical properties, interaction with iron metabolism, and resistance development. *Antioxid Redox Signal, 30*(8), 1062-1082.

Heng, M. P., Sinniah, S. K., Teoh, W. Y., Sim, K. S., Ng, S. W., Cheah, Y. K., & Tan, K. W. (2015). Synthesis of a DNA-targeting nickel (II) complex with testosterone thiosemicarbazone which exhibits selective cytotoxicity towards human prostate cancer cells (LNCaP). *Spectrochimica Acta Part A: Molecular and Biomolecular Spectroscopy, 150*, 360-372.

Herbe, V. M., Beijnen, J., ten Bokkel Huinink, W., & Schellens, J. M. (1998). Clinical pharmacokinetics of camptothecin topoisomerase I inhibitors. *Pharmacy World and Science, 20*(4), 161-172.

Hevenr, K., Verstak, T. A., Lutat, K. E., Riggsbee, D. L., & Mooney, J. W. (2018). Recent developments in topoisomerase-targeted cancer chemotherapy. *Acta pharmaceutica Sinica. B, 8*(6), 844-861.

Hingorani, R., Deng, J., Elia, J., Mclntyre, C., & Mittar, D. (2011). Detection of apoptosis using the BD annexin V FITC assay on the BD FACSVerse^{TM} system. 1-12. Retrieved on Mar 10, 2019 from https://www.bdbiosciences.com/documents/BD_FACSVerse_Apoptosis_Detection_AppNote.pdf

Hiraku, Y., Oikawa, S., & Kawanishi, S. (2002). Distamycin A, a minor groove binder, changes enediyne-induced DNA cleavage sites and enhances apoptosis. *Nucleic Acids Research Supplement,* (2), 95-96.

Holden, J. A. (2001). DNA topoisomerases as anticancer drug targets: from the laboratory to the clinic. *Current Medicinal Chemistry - Anticancer Agents, 1*(1), 1-25.

Holmes, A., The, T., Thompson, K., Mason, M., Kandpal, S., Zheng, T., & Wise, J. (2013). Chronic exposure to particulate nickel induces neoplastic transformation in human lung epithelial cells. *Toxics, 1*(1), 46-59.

Horoszewicz, J. S., Leong, S. S., Kawinski, E., Karr, J. P., Rosenthal, H., Chu, T. M., Mirand, E. A., & Murphy, G. P. (1983). LNCaP model of human prostatic carcinoma. *Cancer Research, 43*(4), 1809-1818.

Hu, X., & Shelver, W. H. (2003). Docking studies of matrix metalloproteinase inhibitors: zinc parameter optimization to improve the binding free energy prediction. *Journal of Molecular Graphics and Modelling, 22*(2), 115-126.

Huey, R., Morris, G. M., Olson, A. J., & Goodsell, D. S. (2007). A semiempirical free energy force field with charge-based desolvation. *Journal of Computational Chemistry, 28*(6), 1145-1152.

Hung, C. L., & Chen, C. C. (2014). Computational approaches for drug discovery. *Drug Development Research, 75*(6), 412-418.

Hussain, M., Jawaria, R., Shafiq, Z., Abbas, G., & Naseer, M. M. (2017). Ferrocene-based thiosemicarbazones: Solvent effect on thiol-thione tautomerism and conformational polymorphism. *Journal of Organometallic Chemistry, 846*, 121-128.

Huxley, M., Sanchez-Cano, C., Browning, M. J., Navarro-Ranninger, C., Quiroga, A. G., Rodger, A., & Hannon, M. J. (2010). An androgenic steroid delivery vector that imparts activity to a non-conventional platinum(II) metallo-drug. *Dalton Transactions, 39*(47), 11353-11364.

Hyde, Z., Flicker, L., McCaul, K. A., Almeida, O. P., Hankey, G. J., Chubb, S. A., & Yeap, B. B. (2012). Associations between testosterone levels and incident prostate, lung, and colorectal cancer. A population-based study. *Cancer Epidemiology, Biomarkers and Prevention, 21*(8), 1319-1329.

Iacopetta, D., Rechoum, Y., & Fuqua, S. A. (2012). The role of androgen receptor in breast cancer. *Drug Discovery Today. Disease Mechanisms, 9*(1-2), e19-e27.

Ibrahim, M. E., Chang, C., Hu, Y., Hogan, S. L., Mercke, N., Gomez, M., O'Bryant, C. L., Bowles, D. W., George, B., Wen, X., Buckley, B., Aleksunes, L., & Joy, M. S. (2019). Pharmacokinetic determinants of cisplatin-induced subclinical kidney injury in oncology patients. *European Journal of Clinical Pharmacology, 75*(1), 51-57.

Ihmels, H., & Otto, D. (2005). Intercalation of Organic Dye Molecules into Double-Stranded DNA -- General principles and recent developments. In F. Würthner (Ed.), *Supermolecular Dye Chemistry* (Vol. 258, pp. 161-204): Springer Berlin Heidelberg.

Ilson, D. H., Saltz, L., Enzinger, P., Huang, Y., Kornblith, A., Gollub, M., O'Reilly, E., Schwartz, G., DeGroff, J., Gonzalez, G., & Kelsen, D. P. (1999). Phase II trial of weekly irinotecan plus cisplatin in advanced esophageal cancer. *Journal of Clinical Oncology, 17*(10), 3270-3275.

Imramovský, A., Pauk, K., Padělková, Z., & Hanusek, J. (2012). Crystal structure of the 5-chloro salicylamides: three different types of the H-bonding influenced linear chain formation in the solid state. *Crystals, 2*(2), 349-361.

Ishida, K., & Asao, T. (2002). Self-association and unique DNA binding properties of the anti-cancer agent TAS-103, a dual inhibitor of topoisomerases I and II. *Biochimica et Biophysica Acta (BBA) - Molecular Basis of Disease, 1587*(2–3), 155-163.

Itoh, N., Sato, A., Yamazaki, T., Numata, M., & Takatsu, A. (2013). Determination of the carbon, hydrogen and nitrogen contents of alanine and their uncertainties using the certified reference material L-alanine (NMIJ CRM 6011-a). *Analytical Sciences, 29*(12), 1209-1212.

Jain, A. N. (2003). Surflex: fully automatic flexible molecular docking using a molecular similarity-based search engine. *Journal of Medicinal Chemistry, 46*(4), 499-511.

Jain, S. S., Anderson, C. M., DiRienzo, F., Taylor, I. R., Jain, K., Guha, S., & Hoque, N. (2013). RNA binding and inhibition of primer extension by a Ru(III)/Pt(II) metal complex. *Chemical Communications (Camb), 49*(44), 5031-5033.

Jain, T., Roper, B. J., & Grove, A. (2009). A functional type I topoisomerase from Pseudomonas aeruginosa. *BMC Molecular Biology, 10*, Article#23.

Jakupec, M. A., Galanski, M., Arion, V. B., Hartinger, C. G., & Keppler, B. K. (2008). Antitumour metal compounds: more than theme and variations. *Dalton Transactions,* (2), 183-194.

Jeewoth, T., Bhowon, M., & Wah, H. (1999). Synthesis, characterization and antibacterial properties of Schiff bases and Schiff base metal complexes derived from 2,3-diamino-pyridine. *Transition Metal Chemistry, 24*(4), 445-448.

Jeon, H., Nam, H., & Lee, J. B. (2019). Sustained release of minor-groove-binding antibiotic netropsin from calcium-coated Groove-rich DNA particles. *Pharmaceutics, 11*(8), 387.

Johnston, S. T., Shah, E. T., Chopin, L. K., Sean McElwain, D. L., & Simpson, M. J. (2015). Estimating cell diffusivity and cell proliferation rate by interpreting IncuCyte ZOOM™ assay data using the Fisher-Kolmogorov model. *BMC Systems Biology, 9*(1), Article#38.

Kaighn, M. E., Narayan, K. S., Ohnuki, Y., Lechner, J. F., & Jones, L. W. (1979). Establishment and characterization of a human prostatic carcinoma cell line (PC-3). *Investigative Urology, 17*(1), 16-23.

Kasi, P. M., Shahjehan, F., Cochuyt, J. J., Li, Z., Colibaseanu, D. T., & Merchea, A. (2019). Rising proportion of young individuals with rectal and colon cancer. *Clinical Colorectal Cancer, 18*(1), e87-e95.

Kelland, L. R. (2000). Preclinical perspectives on platinum resistance. *Drugs, 59 Suppl 4*, 1-8; discussion 37-38.

Kellenberger, E., Rodrigo, J., Muller, P., & Rognan, D. (2004). Comparative evaluation of eight docking tools for docking and virtual screening accuracy. *Proteins, 57*(2), 225-242.

Kenny, R. G., & Marmion, C. J. (2019). Toward multi-targeted platinum and ruthenium drugs—a new paradigm in cancer drug treatment regimens? *Chemical Reviews, 119*(2), 1058-1137.

Kerr, J. F., Wyllie, A. H., & Currie, A. R. (1972). Apoptosis: a basic biological phenomenon with wide-ranging implications in tissue kinetics. *British journal of cancer, 26*(4), 239-257.

Khan, S. A., Kumar, P., Joshi, R., Iqbal, P. F., & Saleem, K. (2008). Synthesis and in vitro antibacterial activity of new steroidal thiosemicarbazone derivatives. *European Journal of Medicinal Chemistry, 43*(9), 2029-2034.

Khan, S. A., & Yusuf, M. (2009). Synthesis, spectral studies and in vitro antibacterial activity of steroidal thiosemicarbazone and their palladium (Pd (II)) complexes. *European Journal of Medicinal Chemistry, 44*(5), 2270-2274.

Kilpin, K. J., & Dyson, P. J. (2013). Enzyme inhibition by metal complexes: concepts, strategies and applications. *Chemical Science, 4*(4), 1410-1419.

Kimura, K., Markowski, M., Bowen, C., & Gelmann, E. P. (2001). Androgen blocks apoptosis of hormone-dependent prostate cancer cells. *Cancer Research, 61*(14), 5611-5618.

Kitchen, D. B., Decornez, H., Furr, J. R., & Bajorath, J. (2004). Docking and scoring in virtual screening for drug discovery: methods and applications. *Nature Reviews Drug Discovery, 3*(11), 935-949.

Klebe, G. (2006). Virtual ligand screening: strategies, perspectives and limitations. *Drug Discovery Today, 11*(13-14), 580-594.

Koehler, R. T., & Villar, H. O. (2000). Design of screening libraries biased for pharmaceutical discovery. *Journal of Computational Chemistry, 21*(13), 1145-1152.

Kolb, P., Ferreira, R. S., Irwin, J. J., & Shoichet, B. K. (2009). Docking and chemoinformatic screens for new ligands and targets. *Current Opinion in Biotechnology, 20*(4), 429-436.

Kolb, P., & Irwin, J. J. (2009). Docking screens: right for the right reasons? *Current Topics in Medicinal Chemistry, 9*(9), 755-770.

Kopka, M. L., Yoon, C., Goodsell, D., Pjura, P., & Dickerson, R. E. (1985). The molecular origin of DNA-drug specificity in netropsin and distamycin. *Proceedings of the National Academy of Sciences of the United States of America, 82*(5), 1376-1380.

Kovala-Demertzi, D., Demertzis, M. A., Miller, J. R., Frampton, C. S., Jasinski, J. P., & West, D. X. (2002). Structure of bis(2-acetylpyridine 3-hexamethyleneiminylthiosemicarbazonato) palladium II, a potential antitumor complex. *Journal of Inorganic Biochemistry, 92*(2), 137-140.

Krasanakis, T., Nikolouzakis, T. K., Sgantzos, M., Mariolis-Sapsakos, T., Souglakos, J., Spandidos, D. A., Tsitsimpikou, C., Tsatsakis, A., & Tsiaoussis, J. (2019). Role of anabolic agents in colorectal carcinogenesis: Myths and realities (Review). *Oncology Reports, 42*(6), 2228-2244.

Kudoh, S., Fujiwara, Y., Takada, Y., Yamamoto, H., Kinoshita, A., Ariyoshi, Y., Furuse, K., & Fukuoka, M. (1998). Phase II study of irinotecan combined with cisplatin in patients with previously untreated small-cell lung cancer. West Japan Lung Cancer Group. *Journal of Clinical Oncology, 16*(3), 1068-1074.

Lafayette, E., Vitalino de Almeida, S., da Rocha Pitta, M., Carneiro Beltrão, E., Gonçalves da Silva, T., Olímpio de Moura, R., da Rocha Pitta, I., de Carvalho, L., & do Carmo Alves de Lima, M. (2013). Synthesis, DNA binding and topoisomerase I inhibition activity of thiazacridine and imidazacridine derivatives. *Molecules, 18*(12), 15035-15050.

Lang, P. T., Brozell, S. R., Mukherjee, S., Pettersen, E. F., Meng, E. C., Thomas, V., Rizzo, R. C., Case, D. A., James, T. L., & Kuntz, I. D. (2009). DOCK 6: combining techniques to model RNA-small molecule complexes. *RNA, 15*(6), 1219-1230.

Lauria, A., Bonsignore, R., Terenzi, A., Spinello, A., Giannici, F., Longo, A., Almerico, A. M., & Barone, G. (2014). Nickel(ii), copper(ii) and zinc(ii) metallo-intercalators: structural details of the DNA-binding by a combined experimental and computational investigation. *Dalton Transactions*, 43(16), 6108-6119.

Le Bideau, F., & Dagorne, S. (2013). Synthesis of transition-metal steroid derivatives. *Chemical Reviews, 113*(10), 7793-7850.

Le, F., Sun, D., Liu, D., Zheng, C., Liu, Y., & Liu, J. (2013). Stabilization of G-quadruplex DNA and antitumor activity by different structures of nickel (II) complexes. *Inorganic Chemistry Communications, 38*(0), 20-27.

Lehmann, B. D., Bauer, J. A., Chen, X., Sanders, M. E., Chakravarthy, A. B., Shyr, Y., & Pietenpol, J. A. (2011). Identification of human triple-negative breast cancer subtypes and preclinical models for selection of targeted therapies. *The Journal of Clinical Investigation, 121*(7), 2750-2767.

Lee, S. K., Tan, K. W., Ng, S. W., Ooi, K. K., Ang, K. P., & Abdah, M. A. (2014). Zinc (II) complex with a cationic Schiff base ligand: Synthesis, characterization, and biological studies. *Spectrochimica Acta Part A: Molecular and Biomolecular Spectroscopy, 121*(0), 101-108.

Lengauer, T., Lemmen, C., Rarey, M., & Zimmermann, M. (2004). Novel technologies for virtual screening. *Drug Discovery Today, 9*(1), 27-34.

Lerman, L. S. (1961). Structural considerations in the interaction of DNA and acridines. *Journal of Molecular Biology, 3*, 18-30.

Levenson, A. S., & Jordan, V. C. (1997). MCF-7: The first hormone-responsive breast cancer cell line. *Cancer Research, 57*(15), 3071-3078.

Levine, P. M., Garabedian, M. J., & Kirshenbaum, K. (2014). Targeting the androgen receptor with steroid conjugates. *Journal of Medicinal Chemistry, 57*(20), 8224-8237.

Li, F., Jiang, T., Li, Q., & Ling, X. (2017). Camptothecin (CPT) and its derivatives are known to target topoisomerase I (Top1) as their mechanism of action: did we miss something in CPT analogue molecular targets for treating human disease such as cancer? *American Journal of Cancer Research, 7*(12), 2350-2394.

Liguori, P. F., Valentini, A., Palma, M., Bellusci, A., Bernardini, S., Ghedini, M., Panno, M. L., Pettinari, C., Marchetti, F., Crispini, A., & Pucci, D. (2010). Non-classical anticancer agents: synthesis and biological evaluation of zinc(ii) heteroleptic complexes. *Dalton Transactions, 39*(17), 4205-4212.

Lin, J. H., & Giovannucci, E. (2010). Sex hormones and colorectal cancer: what have we learned so far? *Journal of the National Cancer Institute, 102*(23), 1746-1747.

Liu, S. (2014). Where does the electron go? The nature of ortho/para and meta group directing in electrophilic aromatic substitution. *The Journal of Chemical Physics, 141*(19), 1941091-1941097.

Liu, S., Cao, W., Yu, L., Zheng, W., Li, L., Fan, C., & Chen, T. (2013). Zinc(II) complexes containing bis-benzimidazole derivatives as a new class of apoptosis inducers that trigger DNA damage-mediated p53 phosphorylation in cancer cells. *Dalton Transactions, 42*(16), 5932-5940.

Loganathan, R., Ramakrishnan, S., Suresh, E., Riyasdeen, A., Akbarsha, M. A., & Palaniandavar, M. (2012). Mixed ligand copper(II) complexes of N,N-bis(benzimidazol-2-ylmethyl)amine (BBA) with diimine co-ligands: efficient chemical nuclease and protease activities and cytotoxicity. *Inorganic Chemistry, 51*(10), 5512-5532.

Ly, J. D., Grubb, D. R., & Lawen, A. (2003). The mitochondrial membrane potential (deltapsi(m)) in apoptosis; an update. *Apoptosis, 8*(2), 115-128.

Macedo, L. F., Guo, Z., Tilghman, S. L., Sabnis, G. J., Qiu, Y., & Brodie, A. (2006). Role of androgens on MCF-7 breast cancer cell growth and on the inhibitory effect of letrozole. *Cancer Research, 66*(15), 7775-7782.

Malik, M., Dar, O., Gull, P., Wani, M., & Hashmi, A. A. (2018). Heterocyclic Schiff base transition metal complexes in antimicrobial and anticancer chemotherapy. *Medicinal Chemistry Communications, 9*, 409-436.

Manosroi, J., Rueanto, K., Boonpisuttinant, K., Manosroi, W., Biot, C., Akazawa, H., Akihisa, T., Issarangporn, W., & Manosroi, A. (2010). Novel ferrocenic steroidal drug derivatives and their bioactivities. *Journal of Medicinal Chemistry, 53*(10), 3937-3943.

Marcondes, N. A., Terra, S. R., Lasta, C. S., Hlavac, N. R. C., Dalmolin, M. L., Lacerda, L. A., Faulhaber, G. A. M., & Gonzalez, F. H. D. (2019). Comparison of JC-1 and MitoTracker probes for mitochondrial viability assessment in stored canine platelet concentrates: A flow cytometry study. *Cytometry Part A, 95*(2), 214-218.

Maxwell, T., & Bates, A. (2009). Topo2008: DNA topoisomerases in biology and medicine. *Nucleic Acids Research, 37*(3), 659-660.

McClendon, A. K., & Osheroff, N. (2006). The geometry of DNA supercoils modulates topoisomerase-mediated DNA cleavage and enzyme response to anticancer drugs. *Biochemistry, 45*(9), 3040-3050.

McMartin, C., & Bohacek, R. S. (1997). QXP: powerful, rapid computer algorithms for structure-based drug design. *Journal of Computer Aided Molecular Design, 11*(4), 333-344.

Md Yusof, E. N., S A Ravoof, T. B., Tiekink, E. R. T., Veerakumarasivam, A., Crouse, K. A., Mohamed Tahir, M. I., & Ahmad, H. (2015). Synthesis, characterization and biological evaluation of transition metal complexes derived from N, S bidentate ligands. *International Journal of Molecular Sciences, 16*(5), 11034-11054.

Meghdadi, S., Amirnasr, M., Mereiter, K., Motaharipour, S., Nasehi, M., Bagheri, M., & Abbasi, S. (2015). Ni(II) and Cu(II) complexes of new unsymmetrical N2O2 Schiff bases derived from 3-(2-aminobenzylimino)-1-phenylbutan-1-ol: synthesis, structure, antibacterial properties, and electrochemistry. *Journal of Coordination Chemistry, 68*(22), 4055-4069.

Méplan, C., Richard, M.-J., & Hainaut, P. (2000). Metalloregulation of the tumor suppressor protein p53: zinc mediates the renaturation of p53 after exposure to metal chelators in vitro and in intact cells. *Oncogene, 19*(46), 5227-5236.

Michaud, J. E., Billups, K. L., & Partin, A. W. (2015). Testosterone and prostate cancer: an evidence-based review of pathogenesis and oncologic risk. *Therapeutic Advances in Urology, 7*(6), 378-387.

Morris, G. M., Goodsell, D. S., Halliday, R. S., Huey, R., Hart, W. E., Belew, R. K., & Olson, A. J. (1998). Automated docking using a Lamarckian genetic algorithm and an empirical binding free energy function. *Journal of Computational Chemistry, 19*(14), 1639-1662.

Morris, G. M., Goodsell, D. S., Huey, R., & Olson, A. J. (1996). Distributed automated docking of flexible ligands to proteins: parallel applications of AutoDock 2.4. *Journal of Computer Aided Molecular Design, 10*(4), 293-304.

Morris, G. M., Huey, R., Lindstrom, W., Sanner, M. F., Belew, R. K., Goodsell, D. S., & Olson, A. J. (2009). AutoDock4 and AutoDockTools4: Automated docking with selective receptor flexibility. *Journal of Computational Chemistry, 30*(16), 2785-2791.

Morris, G. M., & Lim-Wilby, M. (2008). Molecular docking. *Methods in Molecular Biology, 443*, 365-382.

Mosmann, T. (1983). Rapid colorimetric assay for cellular growth and survival: Application to proliferation and cytotoxicity assays. *Journal of Immunological Methods, 65*(1–2), 55-63.

Murugkar, A., Unnikrishnan, B., Padhye, S., Bhonde, R., Teat, S., Triantafillou, E., & Sinn, E. (1999). Hormone anchored metal complexes. 1. Synthesis, structure, spectroscopy and in vitro antitumor activity of testosterone acetate thiosemicarbazone and its metal complexes. *Metal-Based Drugs, 6*(3), 177-182.

Nanjunda, R., & Wilson, W. D. (2012). Binding to the DNA minor groove by heterocyclic dications: from AT-specific monomers to GC recognition with dimers. *Current Protocols in Nucleic Acid Chemistry, Chapter 8*, Unit8.8-Unit8.8.

Natoni, F., Diolordi, L., Santoni, C., & Gilardini Montani, M. S. (2005). Sodium butyrate sensitises human pancreatic cancer cells to both the intrinsic and the extrinsic apoptotic pathways. *Biochimica et Biophysica Acta, 1745*(3), 318-329.

Navanesan, S., Abdul Wahab, N., Manickam, S., & Sim, K. S. (2015). *Leptospermum flavescens* constituent-LF1 causes cell death through the induction of cell cycle arrest and apoptosis in human lung carcinoma cells. *PLoS One, 10*(8), Article#e0135995.

Ndagi, U., Mhlongo, N., & Soliman, M. E. (2017). Metal complexes in cancer therapy - an update from drug design perspective. *Drug Design, Development and Therapy, 11*, 599-616.

Neidle, S. (2001). DNA minor-groove recognition by small molecules. *Nature Product Reports, 18*(3), 291-309.

Nikolaou, S., Qiu, S., Fiorentino, F., Rasheed, S., Tekkis, P., & Kontovounisios, C. (2019). The prognostic and therapeutic role of hormones in colorectal cancer: a review. *Molecular Biology Reports, 46*(1), 1477-1486.

Nitiss, J. L., & Wang, J. C. (1996). Mechanisms of cell killing by drugs that trap covalent complexes between DNA topoisomerases and DNA. *Molecular Pharmacology, 50*(5), 1095-1102.

Okimoto, N., Futatsugi, N., Fuji, H., Suenaga, A., Morimoto, G., Yanai, R., Ohno, Y., Narumi, T., & Taiji, M. (2009). High-performance drug discovery: computational screening by combining docking and molecular dynamics simulations. *PLoS Computational Biology, 5*(10), Article#e1000528.

Oliveira, P. F. d., Alves, J. M., Damasceno, J. L., Oliveira, R. A. M., Dias, H. J., Crotti, A. E. M., & Tavares, D. C. (2015). Cytotoxicity screening of essential oils in cancer cell lines. *Revista Brasileira de Farmacognosia, 25*(2), 183-188.

Ördög, R., & Grolmusz, V. (2008). Evaluating Genetic Algorithms in Protein-Ligand Docking. In I. Măndoiu, R. Sunderraman, & A. Zelikovsky (Eds.), *Bioinformatics Research and Applications* (Vol. 4983, pp. 402-413): Springer Berlin Heidelberg.

Ott, I., & Gust, R. (2007). Non platinum metal complexes as anti-cancer drugs. *Archiv de Pharmazie (Weinheim), 340*(3), 117-126.

Pahontu, E., Julea, F., Rosu, T., Purcarea, V., Chumakov, Y., Petrenco, P., & Gulea, A. (2015). Antibacterial, antifungal and in vitro antileukaemia activity of metal complexes with thiosemicarbazones. *Journal of Cellular and Molecular Medicine, 19*(4), 865-878.

Palanimuthu, D., Shinde, S. V., Somasundaram, K., & Samuelson, A. G. (2013). In vitro and in vivo anticancer activity of copper bis(thiosemicarbazone) complexes. *Journal of Medicinal Chemistry, 56*(3), 722-734.

Palchaudhuri, R., & Hergenrother, P. J. (2007). DNA as a target for anticancer compounds: methods to determine the mode of binding and the mechanism of action. *Current Opinion in Biotechnology, 18*(6), 497-503.

Palma, E., Botelho, H. M., Morais, G. R., Rodrigues, I., Santos, I. C., Campello, M. P. C., Raposinho, P., Belchior, A., Gomes, S. S., Araújo, M. F., Correia, I., Ribeiro, N., Gama, S., Mendes, F., & Paulo, A. (2019). Unravelling the antitumoral potential of novel bis(thiosemicarbazonato) Zn(II) complexes: structural and cellular studies. *JBIC Journal of Biological Inorganic Chemistry, 24*(1), 71-89.

Pan, Z.-H., Zhou, J.-W., & Luo, G.-G. (2014). Experimental and theoretical study of enol-keto prototropic tautomerism and photophysics of azomethine-BODIPY dyads. *Physical Chemistry Chemical Physics, 16*(30), 16290-16301.

Paul, A., & Bhattacharya, S. (2012). Chemistry and biology of DNA-binding small molecules. *Current Science, 102*(2), 212-231.

Pena-Moran, O. A., Villarreal, M. L., Alvarez-Berber, L., Meneses-Acosta, A., & Rodriguez-Lopez, V. (2016). Cytotoxicity, post-treatment recovery, and selectivity analysis of naturally occurring podophyllotoxins from bursera fagaroides var. fagaroides on breast cancer cell lines. *Molecules, 21*(8), Article#1013.

Perez, E. A., Hillman, D. W., Mailliard, J. A., Ingle, J. N., Ryan, J. M., Fitch, T. R., Rowland, K. M., Kardinal, C. G., Krook, J. E., Kugler, J. W., & Dakhil, S. R. (2004). Randomized phase II study of two irinotecan schedules for patients with metastatic breast cancer refractory to an anthracycline, a taxane, or both. *Journal of Clinical Oncology, 22*(14), 2849-2855.

Perez, C., & Ortiz, A. R. (2001). Evaluation of docking functions for protein-ligand docking. *Journal of Medicinal Chemistry, 44*(23), 3768-3785.

Perola, E., Walters, W. P., & Charifson, P. S. (2004). A detailed comparison of current docking and scoring methods on systems of pharmaceutical relevance. *Proteins, 56*(2), 235-249.

Pettersen, E. F., Goddard, T. D., Huang, C. C., Couch, G. S., Greenblatt, D. M., Meng, E. C., & Ferrin, T. E. (2004). UCSF Chimera--a visualization system for exploratory research and analysis. *Journal of Computational Chemistry, 25*(13), 1605-1612.

Ping, Y. H., Lee, H. C., Lee, J. Y., Wu, P. H., Ho, L. K., Chi, C. W., Lu, M. F., & Wang, J. J. (2006). Anticancer effects of low-dose 10-hydroxycamptothecin in human colon cancer. *Oncology Reports, 15*(5), 1273-1279.

Plum, L. M., Rink, L., & Haase, H. (2010). The essential toxin: impact of zinc on human health. *International Journal of Environment Research and Public Health, 7*(4), 1342-1365.

Pommier, Y. (2009). DNA topoisomerase I inhibitors: chemistry, biology, and interfacial inhibition. *Chemical Reviews, 109*(7), 2894-2902.

Prabhakaran, R., Kalaivani, P., Poornima, P., Dallemer, F., Huang, R., Vijaya Padma, V., & Natarajan, K. (2013). Synthesis, DNA/protein binding and in vitro cytotoxic studies of new palladium metallothiosemicarbazones. *Bioorganic Medicinal Chemistry, 21*(21), 6742-6752.

Prabhakaran, R., Sivasamy, R., Angayarkanni, J., Huang, R., Kalaivani, P., Karvembu, R., Dallemer, F., & Natarajan, K. (2011). Topoisomerase II inhibition activity of new square planar Ni(II) complexes containing N-substituted thiosemicarbazones: Synthesis, spectroscopy, X-ray crystallography and electrochemical characterization. *Inorganica Chimica Acta, 374*(1), 647-653.

Rabik, C. A., & Dolan, M. E. (2007). Molecular mechanisms of resistance and toxicity associated with platinating agents. *Cancer Treatment Reviews, 33*(1), 9-23.

Raman, N., Dhaveethu Raja, J., & Sakthivel, A. (2007). Synthesis, spectral characterization of Schiff base transition metal complexes: DNA cleavage and antimicrobial activity studies. *Journal of Chemical Sciences, 119*(4), 303-310.

Raman, N., & Selvan, A. (2012). Investigation of DNA binding mechanism, photoinduced cleavage activity, electrochemical properties and biological functions of mixed ligand copper(II) complexes with benzimidazole derivatives: synthesis and spectral characterization. *Journal of Enzyme Inhibition and Medicinal Chemistry, 27*(3), 380-389.

Raman, N., & Sobha, S. (2012). Exploring the DNA binding mode of transition metal based biologically active compounds. *Spectrochimica Acta Part A: Molecular and Biomolecular Spectroscopy, 85*(1), 223-234.

Raman, N., Sobha, S., & Thamaraichelvan, A. (2011). A novel bioactive tyramine derived Schiff base and its transition metal complexes as selective DNA binding agents. *Spectrochimica Acta Part A: Molecular and Biomolecular Spectroscopy, 78*(2), 888-898.

Rau, T., & van Eldik, R. (1996). Mechanistic insight from kinetic studies on the interaction of model palladium (II) complexes with nucleic acid components. *Metal Ions in Biological Systems, 32*, 339-378.

Reddy, A. S., Pati, S. P., Kumar, P. P., Pradeep, H. N., & Sastry, G. N. (2007). Virtual screening in drug discovery -- a computational perspective. *Current Protein and Peptide Science, 8*(4), 329-351.

Reddy, P. A. N., Santra, B. K., Nethaji, M., & Chakravarty, A. R. (2004). Metal-assisted light-induced DNA cleavage activity of 2-(methylthio)phenylsalicylaldimine Schiff base copper(II) complexes having planar heterocyclic bases. *Journal of Inorganic Biochemistry, 98*(2), 377-386.

Reddy, P. R., Shilpa, A., Raju, N., & Raghavaiah, P. (2011). Synthesis, structure, DNA binding and cleavage properties of ternary amino acid Schiff base-phen/bipy Cu(II) complexes. *Journal of Inorganic Biochemistry, 105*(12), 1603-1612.

Reich, H. J., Jautelat, M., Messe, M. T., Weigert, F. J., & Roberts, J. D. (1969). Nuclear magnetic resonance spectroscopy. Carbon-13 spectra of steroids. *Journal of the American Chemical Society, 91*(26), 7445-7454.

Rejmund, M., Mrozek-Wilczkiewicz, A., Malarz, K., Pyrkosz-Bulska, M., Gajcy, K., Sajewicz, M., Musiol, R., & Polanski, J. (2018). Piperazinyl fragment improves anticancer activity of Triapine. *PLoS One, 13*(4), Article#e0188767.

Rester, U. (2008). From virtuality to reality - Virtual screening in lead discovery and lead optimization: a medicinal chemistry perspective. *Current Opinion in Drug Discovery and Development, 11*(4), 559-568.

Riccardi, C., & Nicoletti, I. (2006). Analysis of apoptosis by propidium iodide staining and flow cytometry. *Nature Protocols, 1*(3), 1458-1461.

Richardson, D. R., Sharpe, P. C., Lovejoy, D. B., Senaratne, D., Kalinowski, D. S., Islam, M., & Bernhardt, P. V. (2006). Dipyridyl thiosemicarbazone chelators with potent and selective antitumor activity form iron complexes with redox activity. *Journal of Medicinal Chemistry, 49*(22), 6510-6521.

Rognan, D. (2007). Chemogenomic approaches to rational drug design. *British Journal of Pharmacology, 152*(1), 38-52.

Rosenberg, B., VanCamp, L., Trosko, J. E., & Mansour, V. H. (1969). Platinum compounds: a new class of potent antitumour agents. *Nature, 222*(5191), 385-386.

Roshan, M. H. K., Tambo, A., & Pace, N. P. (2016). The role of testosterone in colorectal carcinoma: pathomechanisms and open questions. *The EPMA journal, 7*(1), 22-22.

Rothenberg, M. L., Kuhn, J. G., Schaaf, L. J., Rodriguez, G. I., Eckhardt, S. G., Villalona-Calero, M. A., Rinaldi, D. A., Hammond, L. A., Hodges, S., Sharma, A., Elfring, G. L., Petit, R. G., Locker, P. K., Miller, L. L., & von Hoff, D. D. (2001). Phase I dose-finding and pharmacokinetic trial of irinotecan (CPT-11) administered every two weeks. *Annals of Oncology, 12*(11), 1631-1641.

Ruiz, J., Rodriguez, V., Cutillas, N., Espinosa, A., & Hannon, M. J. (2011). A potent ruthenium(II) antitumor complex bearing a lipophilic levonorgestrel group. *Inorganic Chemistry, 50*(18), 9164-9171.

Ruiz, J., Rodriguez, V., Cutillas, N., Samper, K. G., Capdevila, M., Palacios, O., & Espinosa, A. (2012). Novel C,N-chelate rhodium(III) and iridium(III) antitumor complexes incorporating a lipophilic steroidal conjugate and their interaction with DNA. *Dalton Transactions, 41*(41), 12847-12856.

Ruiz, R., García, B., Garcia-Tojal, J., Busto, N., Ibeas, S., Leal, J., Martins, C., Gaspar, J., Borrás, J., Gil-García, R., & González-Álvarez, M. (2010). Biological assays and noncovalent interactions of pyridine-2-carbaldehyde thiosemicarbazonecopper(II) drugs with [poly(dA–dT)]2, [poly(dG–dC)]2, and calf thymus DNA. *JBIC Journal of Biological Inorganic Chemistry, 15*(4), 515-532.

Sanchez-Cano, C., & Hannon, M. J. (2009a). Cytotoxicity, cellular localisation and biomolecular interaction of non-covalent metallo-intercalators with appended sex hormone steroid vectors. *Dalton Transactions,* (48), 10765-10773.

Sanchez-Cano, C., & Hannon, M. J. (2009b). Novel and emerging approaches for the delivery of metallo-drugs. *Dalton Transactions,* (48), 10702-10711.

Sanchez-Cano, C., Huxley, M., Ducani, C., Hamad, A. E., Browning, M. J., Navarro-Ranninger, C., Quiroga, A. G., Rodger, A., & Hannon, M. J. (2010). Conjugation of testosterone modifies the interaction of mono-functional cationic platinum(ii) complexes with DNA, causing significant alterations to the DNA helix. *Dalton Transactions, 39*(47), 11365-11374.

Sangeetha Gowda, K. R., Mathew, B. B., Sudhamani, C. N., & Naik, H. S. B. (2014). Mechanism of DNA binding and cleavage. *Biomedicine and Biotechnology, 2*(1), 1-9.

Sava, G., Jaouen, G., Hillard, E. A., & Bergamo, A. (2012). Targeted therapy vs. DNA-adduct formation-guided design: thoughts about the future of metal-based anticancer drugs. *Dalton Transactions, 41*(27), 8226-8234.

Schiff, H. (1864). Mittheilungen aus dem Universitätslaboratorium in Pisa: Eine neue Reihe organischer Basen. *European Journal of Organic Chemistry, 131*(1), 118-119.

Schmidt, M., Görls, H., & Plass, W. (2016). Facile high-yield synthesis of unsymmetric end-off compartmental double Schiff-base ligands: easy access to mononuclear precursor and unsymmetric dinuclear complexes. *RSC Advances, 6*(79), 75844-75854.

Shah, M. A., Ramanathan, R. K., Ilson, D. H., Levnor, A., D'Adamo, D., O'Reilly, E., Tse, A., Trocola, R., Schwartz, L., Capanu, M., Schwartz, G. K., & Kelsen, D. P. (2006). Multicenter phase II study of irinotecan, cisplatin, and bevacizumab in patients with metastatic gastric or gastroesophageal junction adenocarcinoma. *Journal of Clinical Oncology, 24*(33), 5201-5206.

Shahabadi, N., Kashanian, S., & Darabi, F. (2010). DNA binding and DNA cleavage studies of a water soluble cobalt(II) complex containing dinitrogen Schiff base ligand: the effect of metal on the mode of binding. *European Journal of Medicinal Chemistry, 45*(9), 4239-4245.

Shahbadi, N., & Maghsudi, M. (2014). Multi-spectroscopic and molecular modeling studies on the interaction of antihypertensive drug; methyldopa with calf thymus DNA. *Molecular BioSystems, 10*(2), 338-347.

Shapir, G. I., & Harper, J. W. (1999). Anticancer drug targets: cell cycle and checkpoint control. *Journal of Clinical Investigation, 104*(12), 1645-1653.

Sheldrick, G. M. (2008). A short history of SHELX. *Acta Crystallographica Section A, 64*(Pt 1), 112-122.

Shi, X., Fang, H., Guo, Y., Yuan, H., Guo, Z., & Wang, X. (2019). Anticancer copper complex with nucleus, mitochondrion and cyclooxygenase-2 as multiple targets. *Journal of Inorganic Biochemistry, 190*, 38-44.

Shoichet, B. K., McGovern, S. L., Wei, B., & Irwin, J. J. (2002). Lead discovery using molecular docking. *Current Opinion in Chemical Biology, 6*(4), 439-446.

Siddique, H. R., Mishra, S. K., Karnes, R. J., & Saleem, M. (2011). Lupeol, a novel androgen receptor inhibitor: implications in prostate cancer therapy. *Clinical Cancer Research, 17*(16), 5379-5391.

Singh, R., & Sharma, B. (2018). Metal-based therapy in traditional and modern medicine systems. In M. Rai, A. P. Ingle, & S. Medici (Eds.), *Biomedical Applications of Metals* (pp. 195-211). Cham: Springer International Publishing.

Slattery, M. L., Sweeney, C., Murtaugh, M., Ma, K. N., Wolff, R. K., Potter, J. D., Caan, B. J., & Samowitz, W. (2005). Associations between ERα, ERβ, and AR genotypes and colon and rectal cancer. *Cancer Epidemiology Biomarkers & Prevention, 14*(12), 2936-2942.

Soule, H. D., Vazguez, J., Long, A., Albert, S., & Brennan, M. (1973). A human cell line from a pleural effusion derived from a breast carcinoma. *Journal of the National Cancer Institute, 51*(5), 1409-1416.

Sousa, S. F., Fernandes, P. A., & Ramos, M. J. (2006). Protein-ligand docking: current status and future challenges. *Proteins, 65*(1), 15-26.

Spencer, J., & Walden, B. (2018). Special focus: metals in medicine. *Future Medicinal Chemistry, 10*(6), 607-609.

Stahl, M., & Rarey, M. (2001). Detailed analysis of scoring functions for virtual screening. *Journal of Medicinal Chemistry, 44*(7), 1035-1042.

Stromberg, S., Zetterberg, K., & E. M. Siegbahn, P. (1997). Trends within a triad: comparison between ς-alkyl complexes of nickel, palladium and platinum with respect to association of ethylene, migratory insertion and β-hydride elimination. A theoretical study. *Journal of the Chemical Society, Dalton Transactions,* (22), 4147-4152.

Suntharalingam, K., Mendoza, O., Duarte, A. A., Mann, D. J., & Vilar, R. (2013). A platinum complex that binds non-covalently to DNA and induces cell death via a different mechanism than cisplatin. *Metallomics, 5*(5), 514-523.

Szyczewski, A., Hołderna-Natkaniec, K., & Natkaniec, I. (2004). Progesterone and testosterone studies by neutron scattering and nuclear magnetic resonance methods and quantum chemistry calculations. *Journal of Molecular Structure, 693*(1–3), 49-71.

Tai, S., Sun, Y., Squires, J. M., Zhang, H., Oh, W. K., Liang, C. Z., & Huang, J. (2011). PC3 is a cell line characteristic of prostatic small cell carcinoma. *Prostate, 71*(15), 1668-1679.

Takahara, P. M., Rosenzweig, A. C., Frederick, C. A., & Lippard, S. J. (1995). Crystal structure of double-stranded DNA containing the major adduct of the anticancer drug cisplatin. *Nature, 377*(6550), 649-652.

Tan, K. W., Ng, C. H., Maah, M. J., & Ng, S. W. (2009). Bis(acetone 4-phenyl-thio-semicarbazonato-κN,S)zinc(II). *Acta crystallographica. Section E, Structure reports online, 65*(Pt 8), m969-m969.

Tan, L. T., Chan, C. K., Chan, K. G., Pusparajah, P., Khan, T. M., Ser, H. L., Lee, L. H., & Goh, B. H. (2019). Streptomyces sp. MUM256: a source for apoptosis inducing and cell cycle-arresting bioactive compounds against colon cancer cells. *Cancers (Basel), 11*, Article#1742.

Tardito, S., Bassanetti, I., Bignardi, C., Elviri, L., Tegoni, M., Mucchino, C., Bussolati, O., Franchi-Gazzola, R., & Marchio, L. (2011). Copper binding agents acting as copper ionophores lead to caspase inhibition and paraptotic cell death in human cancer cells. *Journal of American Chemistry Society, 133*(16), 6235-6242.

Taylor, R. D., Jewsbury, P. J., & Essex, J. W. (2002). A review of protein-small molecule docking methods. *Journal of Computer Aided Molecular Design, 16*(3), 151-166.

Tchounwou, P. B., Yedjou, C. G., Patlolla, A. K., & Sutton, D. J. (2012). Heavy metal toxicity and the environment. *Experientia Supplementum (2012), 101*, 133-164.

Teicher, B. A. (2008). Next generation topoisomerase I inhibitors: Rationale and biomarker strategies. *Biochemical Pharmacology, 75*(6), 1262-1271.

Teoh, S.-G., Ang, S.-H., Fun, H.-K., & Ong, C.-W. (1999). Synthesis, crystal structure and biological activity of thiophene-2-carboxaldehyde thiosemicarbazone and its tin complexes. *Journal of Organometallic Chemistry, 580*(1), 17-21.

Tiwari, A. D., Mishra, A. K., Mishra, S. B., Mamba, B. B., Maji, B., & Bhattacharya, S. (2011). Synthesis and DNA binding studies of Ni(II), Co(II), Cu(II) and Zn(II) metal complexes of N(1),N(5)-bis[pyridine-2-methylene]-thiocarbohydrazone Schiff-base ligand. *Spectrochimica Acta Part A: Molecular and Biomolecular Spectroscopy, 79*(5), 1050-1056.

Top, S., Thibaudeau, C., Vessières, A., Brulé, E., Le Bideau, F., Joerger, J. M., Plamont, M. A., Samreth, S., Edgar, A., Marrot, J., Herson, P., & Jaouen, G. (2009). Synthesis and structure activity relationship of organometallic steroidal androgen derivatives. *Organometallics, 28*(5), 1414-1424.

Tsavaris, N., Lazaris, A., Kosmas, C., Gouveris, P., Kavantzas, N., Kopterides, P., Papathomas, T., Agrogiannis, G., Zorzos, H., Kyriakou, V., & Patsouris, E. (2009). Topoisomerase I and IIalpha protein expression in primary colorectal cancer and recurrences following 5-fluorouracil-based adjuvant chemotherapy. *Cancer Chemother Pharmacol, 64*(2), 391-398.

Vassal, G., Couanet, D., Stockdale, E., Geoffray, A., Geoerger, B., Orbach, D., Pichon, F., Gentet, J. C., Picton, S., Bergeron, C., Cisar, L., Assadourian, S., & Morland, B. (2007). Phase II trial of irinotecan in children with relapsed or refractory rhabdomyosarcoma: a joint study of the French Society of Pediatric Oncology and the United Kingdom Children's Cancer Study Group. *Journal of Clinical Oncology, 25*(4), 356-361.

Verdonk, M. L., Berdini, V., Hartshorn, M. J., Mooij, W. T., Murray, C. W., Taylor, R. D., & Watson, P. (2004). Virtual screening using protein-ligand docking: avoiding artificial enrichment. *Journal of Chemical Information and Computer Sciences, 44*(3), 793-806.

Verdonk, M. L., Cole, J. C., Hartshorn, M. J., Murray, C. W., & Taylor, R. D. (2003). Improved protein-ligand docking using GOLD. *Proteins, 52*(4), 609-623.

Vidal, D., Thormann, M., & Pons, M. (2006). A novel search engine for virtual screening of very large databases. *Journal of Chemical Information and Modeling, 46*(2), 836-843.

Vidula, N., Yau, C., Wolf, D., & Rugo, H. S. (2019). Androgen receptor gene expression in primary breast cancer. *npj Breast Cancer, 5*(47), Article#47.

Wang, J. C. (1996). DNA topoisomerases. *Annual Review of Biochemistry, 65*, 635-692.

Wang, M., Lee, R. J., Bi, Y., Li, L., Yan, G., Lu, J., Meng, Q., Teng, L., & Xie, J. (2017). Transferrin-conjugated liposomes loaded with novel dihydroquinoline derivatives as potential anticancer agents. *PLoS One, 12*(10), Article#e0186821.

Wang, X., Yin, L., Rao, P., Stein, R., Harsch, K. M., Lee, Z., & Heston, W. D. (2007). Targeted treatment of prostate cancer. *Journal of Cellular Biochemistry, 102*(3), 571-579.

Webb, M. R., & Ebeler, S. E. (2004). Comparative analysis of topoisomerase IB inhibition and DNA intercalation by flavonoids and similar compounds: structural determinates of activity. *Biochemical Journal, 384*(3), 527-541.

Weidmann, A. G., Komor, A. C., & Barton, J. K. (2014). Targeted chemotherapy with metal complexes. *Comments on Inorganic Chemistry, 34*(3-4), 114-123.

Westrip, S. (2010). publCIF: software for editing, validating and formatting crystallographic information files. *Journal of Applied Crystallography, 43*(4), 920-925.

Whitnall, M., Howard, J., Ponka, P., & Richardson, D. R. (2006). A class of iron chelators with a wide spectrum of potent antitumor activity that overcomes resistance to chemotherapeutics. *Proceedings of the National Academy of Sciences, 103*(40), 14901-14906.

Wiji Prasetyaningrum, P., Bahtiar, A., & Hayun, H. (2018). Synthesis and cytotoxicity evaluation of novel asymmetrical mono-carbonyl analogs of curcumin (AMACs) against Vero, HeLa, and MCF7 cell lines. *Scientia Pharmaceutica, 86*(2), Article#25.

Winter, E., Chiaradia, L. D., Silva, A. H., Nunes, R. J., Yunes, R. A., & Creczynski-Pasa, T. B. (2014). Involvement of extrinsic and intrinsic apoptotic pathways together with endoplasmic reticulum stress in cell death induced by naphthylchalcones in a leukemic cell line: advantages of multi-target action. *Toxicology In Vitro, 28*(5), 769-777.

Wong, C. K. H., Lam, C. L. K., Poon, J. T. C., McGhee, S. M., Law, W.-L., Kwong, D. L. W., Tsang, J., & Chan, P. (2012). Direct medical costs of care for Chinese patients with colorectal neoplasia: a health care service provider perspective. *Journal of Evaluation in Clinical Practice, 18*(6), 1203-1210.

Wu, D., Zhao, D. W., Li, Y. Q., Shi, W. G., Yin, Q. L., Tu, Z. K., Yu, Y. Y., Zhong, B. H., Yu, H., & Bao, W. G. (2018). Antitumor potential of a novel camptothecin derivative, ZBH-ZM-06. *Oncology Reports, 39*(2), 871-879.

Wu, H., Sun, T., Li, K., Liu, B., Kou, F., Jia, F., Yuan, J., & Bai, Y. (2012). Synthesis, crystal structure, and DNA-binding studies of a nickel(II) complex with the bis(2-benzimidazolymethyl)amine ligand. *Bioinorganic Chemistry and Applications, 2012*, Article#609796.

Wuana, R. A., & Okieimen, F. E. (2011). Heavy metals in contaminated soils: a review of sources, chemistry, risks and best available strategies for remediation. *ISRN Ecology, 2011*, Article#402647.

Xia, T., Sun, H., Huang, H., Bi, H., Pu, R., Zhang, L., Zhang, Y., Liu, Y., Xu, J., Onwuka, J. U., Liu, Y., Cui, B., & Zhao, Y. (2019). Androgen receptor gene methylation related to colorectal cancer risk. *Endocrine Connections, 8*(7), 979-987.

Xu, X., Su, J., Bizzarri, A., Cannistraro, S., Liu, M., Zeng, Y., Chen, W., & Wang, C. (2013). Detection of persistent organic pollutants binding modes with androgen receptor ligand binding domain by docking and molecular dynamics. *BMC Structural Biology, 13*(1), Article#16.

Yeginer, G., Gulcan, M., Isik, S., Urut, G. O., Ozdemir, S., & Kurtoglu, M. (2017). Transition metal (II) complexes with a novel azo-azomethine Schiff base ligand: synthesis, structural and spectroscopic characterization, thermal properties and biological applications. *Journal of Fluorescence, 27*(6), 2239-2251.

Zamai, L., Canonico, B., Luchetti, F., Ferri, P., Melloni, E., Guidotti, L., Cappellini, A., Cutroneo, G., Vitale, M., & Papa, S. (2001). Supravital exposure to propidium iodide identifies apoptosis on adherent cells. *Cytometry, 44*(1), 57-64.

Zamora, A., Rodriguez, V., Cutillas, N., Yellol, G. S., Espinosa, A., Samper, K. G., Capdevila, M., Palacios, O., & Ruiz, J. (2013). New steroidal 7-azaindole platinum(II) antitumor complexes. *Journal of Inorganic Biochemistry, 128*, 48-56.

Zavodszky, M. I., Rohatgi, A., Van Voorst, J. R., Yan, H., & Kuhn, L. A. (2009). Scoring ligand similarity in structure-based virtual screening. *Journal of Molecular Recognition, 22*(4), 280-292.

Zeglis, B. M., & Barton, J. K. (2007). DNA base mismatch detection with bulky rhodium intercalators: synthesis and applications. *Nature Protocols, 2*(2), 357-371.

Zeglis, B. M., Pierre, V. C., & Barton, J. K. (2007). Metallo-intercalators and metallo-insertors. *Chemical Communications (Camb),* (44), 4565-4579.

Zhang, F.-L., Wang, P., Liu, Y.-H., Liu, L.-b., Liu, X.-B., Li, Z., & Xue, Y.-X. (2013). Topoisomerase I inhibitors, shikonin and topotecan, inhibit growth and induce apoptosis of glioma cells and glioma stem cells. *PLoS One, 8*(11), Article#e81815.

Zhang, Z., Feng, Y., Li, Z.-Y., & Cao, X.-Z. (2019). Antiproliferative and apoptotic activity of glycyrrhizinic acid in MCF-7 human breast cancer cells and evaluation of its effect on cell cycle, cell migration and m-TOR/PI3K/Akt signalling pathway. *Archives of medical science : AMS, 15*(1), 174-182.

Zhong, X., Yi, J., Sun, J., Wei, H. L., Liu, W. S., & Yu, K. B. (2006). Synthesis and crystal structure of some transition metal complexes with a novel bis-Schiff base ligand and their antitumor activities. *European Journal of Medicinal Chemistry, 41*(9), 1090-1092.

Zhu, T., Wang, Y., Ding, W., Xu, J., Chen, R., Xie, J., Zhu, W., Jia, L., & Ma, T. (2015). Anticancer activity and DNA-binding investigations of the Cu(II) and Ni(II) complexes with coumarin derivative. *Chemical Biology & Drug Design, 85*(3), 385-393.

LIST OF PUBLICATIONS AND PAPERS PRESENTED

PUBLICATIONS

1) **Heng, M.P.**, Tan, C.H., Saad, H.M., Sim, K.S., & Tan, K.W. (2020) Mitochondria-dependent apoptosis inducer: Testosterone-N^4-ethylthiosemicarbazonate and its metal complexes with selective cytotoxicity towards human colorectal carcinoma cell line (HCT 116). *Inorganica Chimica Acta, 507,* Article#119581.

2) **Heng, M.P.**, Sim, K.S., & Tan, K.W. (2020) Nickel and zinc complexes of testosterone-N^4-substituted thiosemicarbazone: Selective cytotoxicity towards human colorectal carcinoma cell line HCT 116 and their cell death mechanisms. *Journal of Inorganic Biochemistry, 208,* Article#111097.

PAPER PRESENTED

1) **Heng, M.P.**, Tan, K.W., Ng, S.W., & Sim, K.S. *Biological properties of a nickel(II) complex with testosterone Schiff Base*. Poster presented at 2018 International Conference on Biochemistry, Molecular Biology and Biotechnology, 15-16 August 2018, Kuala Lumpur, Malaysia.